Monitoring and Characterising Grain Scale Fluvial Bed-load Transport Behaviour Using Passive and Active Sensors

A thesis submitted to the School of Environmental Sciences of the University of East Anglia in partial fulfilment of the requirements for the degree of Doctor of Philosophy

Miles Clark

January 2023

Abstract

Bedload transport is a fundamental process by which coarse sediment is transferred through landscapes by river networks. Understanding how individual grains move within fluvial systems is essential for accurately modelling and predicting sediment fluxes and the evolution of sedimentary environments. Large wood is a major component of many forested rivers and to date, the impact of the presence of in stream wood on grain-scale bedload transport has not been well studied. In this thesis, passive (RFID) and active tracers (smart stones) are used to investigate and model the influence of wood on grain-scale bedload transport during long term deployment. In addition, this research examines the effectiveness of novel, Internet of Things (IoT) enabled smart stones for monitoring bedload transport.

First, 957 RFID tracers were inserted into a wood-loaded stream in Colorado and monitored over three years. Statistical modelling revealed a significant influence of wood on transport behaviour, where a reduction in entrainment likelihood, shorter transport distances, and premature deposition were recorded in tracers interacting with wood pieces. Next, a smart stone was designed embedded with 9-axis IMU sensors, integrated into an IoT network with Long Range Wide Area Network (LoRaWAN) capabilities. Laboratory experiments were conducted with the smart stones to replicate typical bedload movement behaviour, building unique IMU signatures associated with specific movement types. Smart stones were subsequently deployed at a range of field sites for remote real-time monitoring of transport behaviour. 57% of deployed tracers captured IMU data for tracer movement events, including one entrainment event captured by LoRaWAN, though the limited interaction between in stream wood and tracers precluded analysis of wood-sediment interaction. Overall, this research highlights the role of wood in altering the transport distances and entrainment likelihood of sediments. Furthermore, it demonstrates the potential for an integration of LoRaWAN networks and smart stones for remotely monitoring fluvial bedload dynamics.

Table of Contents

List of Figures

Page

List of Tables

Page

Acknowledgements

I would like to begin by expressing my deep gratitude to my primary supervisors, Georgie Bennett and Aldina Franco, for their invaluable guidance and support throughout the process of researching and writing this thesis. Their insight and expertise have been instrumental in helping me to shape my ideas and bringing this project to fruition.

I am also deeply grateful to my external supervisor, David Sear, for his valuable feedback and support throughout my PhD, both through aiding in formulating concepts for my work, and by reviewing paper manuscripts. Additionally, I would like to thank my external supervisor Sandra Ryan-Burkett for her support during field work in Colorado, and her dedication in helping me during the first few years of my research.

I am also indebted to Benedetta Dini who generously took the time to initially help me understand and use the tracking tags. I also wish to thank the wider team at the SENSUM project, particularly Martina Egedusevic, Kyle Roskilly and Alessandro Sgarabotto for their continued support during field work and in the laboratory while working with the smart stones. I also express my appreciation to Gareth Flowerdew, whose support in the workshop made producing the smart stones possible.

I would also like to extend my thanks to Banning Starr and Doug McClain at the US Forest Service Fraser Experimental Headquarters, who provided not only logistical support during our fieldwork, but also valuable technical assistance with electronic equipment. I am also grateful to Sara Rathburn for her kind hospitality and intermediate accommodation during our travels to the field site.

Finally, I am grateful to my family and friends for their unwavering support and encouragement throughout this journey and to Heather, for love and support over the last four years.

CHAPTER 1

1 Introduction

1.1 The Importance Sediment Transport in Fluvial Environments

Fluvial sediment transport is a crucial process in controlling the morphology of rivers (Best, 1988), maintaining ecological habitats (Greig et al., 2005), transporting nutrients (Walling et al., 2001), and is essential for the health and long-term stability of channels. Concurrently, the morphology of rivers is an intrinsic control on subsequent transport behaviour. Therefore, understanding and quantifying sediment transport is essential for a comprehensive interpretation of fluvial systems and is of primary importance in river engineering and management (Apitz & White, 2003; Wang et al., 2015).

Despite decades of flume and field research attempting to characterise and estimate sediment transport, challenges remain in accurately quantifying the transport behaviour of sediments. This derives from the complexities involved when accounting for the multivariate factors influencing transport. These range from physical sediment properties (Fenton & Abbott 1977), the formation of bedforms (Bridge & Best, 1988), hydraulic conditions (Nelson et al., 1995), and a range of chemical (Packman & Jerolmack 2004) and biological factors (Ryan et al., 2014). These complexities explain why, despite early research investigating sediment transport (e.g., du Boys, 1879, Gilbert & Murphy, 1914), researchers are still tackling this problem today (e.g., Hodge et al., 2011; Maniatis et al., 2017).

1.2 Transport as Bedload and Suspended Load

Fluvial sediments can be divided into suspended load and bedload (Figure 1.1) based on the mechanics of their transport (Sear et al., 2004). The bedload subdivision of transport may be defined as sediment that travels within a few grain diameters from the bed surface (Einstein, 1950), and

involves particles directly interacting with the bed. During bedload transport, if lift forces acting on grains only marginally exceed those necessary to initiate motion, then sediments will be transported as a part of the traction carpet (Allen, 2012). Traction carpet transport is limited to sliding, jostling, and rolling along the bed, with regular contact with the bed's surface. If lift forces increase, then sediments may begin to leave the traction carpet and begin bouncing on the bed in the process of saltation (Wiberg and Smith, 1985).

The suspended sediment subdivision of transport typically comprises of finer material, such as clays, silts, and sands, typically < 0.2 mm in diameter (Gomez and Church 1989). Material is transported suspended in flow as turbulent eddies outweigh the settling forces of particles (Parsons et al., 2015).

This research focuses on the bedload subdivision of fluvial sediment transport, and the movement of individual coarse-sized clasts (e.g., gravels, pebbles, and cobbles), investigating incipient movement, subsequent transport behaviour, and depositional characteristics.

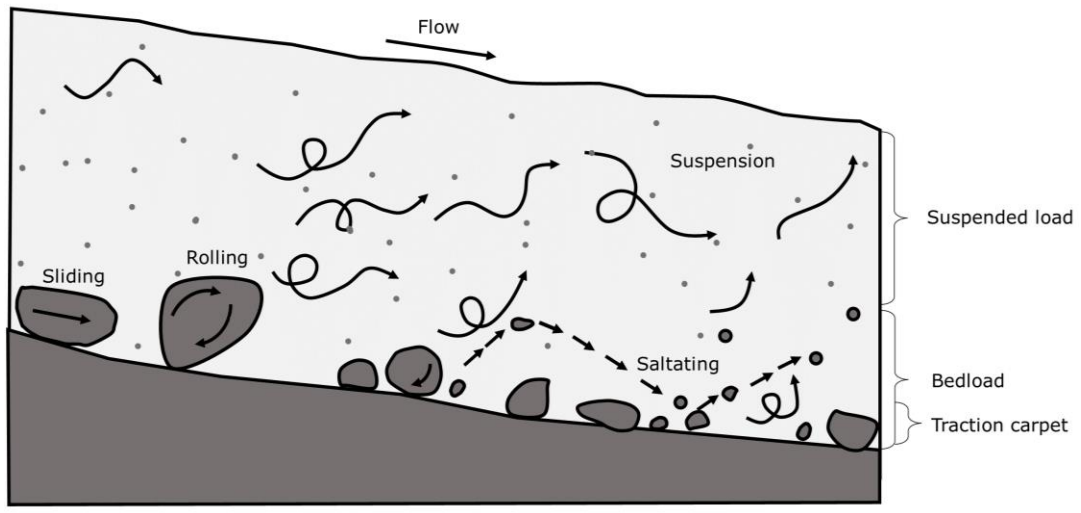

Figure 1.1: *The different modes of fluvial sediment transport demonstrating rolling, sliding, and saltating movement behaviour within bedload transport, and particles being transported in suspension within the suspended load after entrainment.*

1.3 Estimations of Incipient Motion

In principle, all formulae created to describe bedload transport are based on the premise that specific relationships exist between sedimentological parameters, hydraulic variables, and transport rates (Gomez 1991). These are typically developed either by deriving theoretical relations based on known physical principles or by using experimental data to derive empirical relationships.

Historically, analysis of particle transport on riverbeds has been described deterministically. This is where a critical threshold of shear stress is reached, which then initiates the movement of sediments of a specific size (e.g., Gilbert and Murphy, 1914; Shields, 1936; Yalin, 1963; Wiberg and Smith, 1987; Dey, 1999). The primary example of this approach in the literature is the shields' parameter $\tau*$ which is given by:

$$\tau* = \frac{\tau}{(\rho_s - \rho)gD_s}$$

Where τ is the hydrodynamic shear stress exerted on the bed, ρ_s and ρ are the densities of the sediments and the water, respectively, g is gravitational acceleration and D_s is the mean diameter of the particles.

This parameter is the foundation of many deterministic approaches in calculating a threshold for the incipient motion of sediments (Miller et al., 1977; Wiberg & Smith, 1987), although determining precisely when the threshold of sediment movement has been achieved is rather subjective (Komar and Miller, 1973). Furthermore, subsequent research has shown significant variability in the value of this criterion (Lavelle & Mofjeld 1977; Buffington & Montgomery, 1997), partially relating to its inability to account for turbulent fluctuations in fluvial systems which have nonuniform topography or roughness elements (Nelson et al., 1995). Modifications to this threshold approach incorporate the fluctuating nature of turbulent flow processes, with more recent research addressing shortcomings by considering the duration of turbulent impulses acting upon grains (e.g., Diplas et al. 2008; Valyrakis et al., 2010). While research continues towards deterministic approximations of a critical threshold value,

stochastic estimations may be more appropriate for characterising sediment transport (e.g., Niño & García 1998).

Unlike deterministic calculations, individual grain transport was first described as intermittent and probabilistic by Einstein (1937). This was in recognition of the difficulties involved when measuring the deterministic forces driving the movement of individual particles. This stochastic approach uses a probability function and a transport rate equation, where bedload transport occurs as a series of steps, resulting from turbulent fluctuations when hydrodynamic lift forces are greater than a particle's weight. Consequently, bedload transport of coarse-grained sediments is not continuous. Particles predominantly remain at rest, even when fluid stress is above the threshold of movement, with the sum of particle steps representing the total travel distance of sediments. These stochastic descriptions of motion likely better capture the turbulent forces acting upon sediments during bedload transport (e.g., Hubbell and Sayre 1964; Yang and Sayre, 1971; Papanicolaou et al., 2002; Ancey, et al., 2008; Bradley, et al., 2010; Ancey and Bohorquez, 2018). Despite this, geomorphic complexity in natural fluvial systems further complicates estimates of incipient motion, where variables, such as the presence of large wood, can have a major influence on transport processes (Wohl & Scott 2017).

To assist in the development of estimations of incipient motion (both deterministic and probabilistic) and for accurate predictions of transport behaviour, measurements accurately quantifying sediment transport should be taken. These would facilitate the verification of assumptions and test the performance of existing bedload transport models (Pähtz et al., 2020). Suitable methodologies and technologies are also required to test theoretical predictions. These need to be applied in a range of environments, with differing geomorphic features, across various sediment sizes. Historically, a wide variety of techniques are used to capture sediment transport, each with their own advantages and disadvantages and suitability for laboratory and field settings.

1.4 Bedload Transport Measurements

Methodologies for bedload measurements can be categorised into direct and indirect approaches (Gomez 1991; Sear et al., 2000a). Direct methods consist of sampling bed material, capturing sediments during transport. Indirect methods typically involve the use of tracers to monitor individual particles, or by detecting bulk sediment transport remotely, with the choice of the technique being situationally based.

Direct methods include samplers installed into the bed, such as pit and trough samplers, and manual portable samplers (e.g., Hubbell & Sayre 1964; Helley & Smith 1971; Milhous, 1973; Batalla et al., 2010). While these have relatively low operational costs and are cheap to install, they risk influencing their surrounding environment. This can result in anthropogenic distortions to transport data. Furthermore, the ability of trap-type samplers to accurately estimate total transport is hindered by variability in sampler efficiencies and the oscillatory behaviour of bedload discharge. Therefore, single short-term measurements from samplers can produce unrepresentative mean values of bedload discharge (Hubbell, 1964). While attempts to account for instrument errors through calibration have been made (e.g., Hubbell et al., 1985; Sear et al., 2000b; Bunte et al., 2010), uncertainties remain in accounting for the deviations observed.

To overcome these limitations, researchers have developed indirect methods of measuring bedload. These include bulk bedload sensing methodologies, such as the use of seismometers (Hsu et al., 2011; Krein et al., 2016; Anthony et al., 2018) and geophones (Rickenmann et al., 2012; Tsakiris et al., 2014), the use of tracers to track the movement of individual particles. Different tracer methodologies include the painting of rocks (Keller, 1970; Laronne & Carson, 1976; Petit et al., 2005), radio transmitters (Habersack, 2001; McNamara & Borden, 2004), and the use of magnetic clasts (Hassan et al., 1991; Schmidt & Ergenzinger, 1992; Ferguson & Wathen, 1998). Indirect tracer methods can have a range of disadvantages, including difficulties recognising individual clasts, loss of sediments due to burial, and anthropogenic interference, and the impact of tracer mixing time (Ferguson & Hoey, 2002). See Gray et al., (2010) for

a summary of the range of modern indirect monitoring techniques in use today by researchers, their respective reliability, and ease of use.

1.5 RFID Tracer Studies

Tracers in sedimentological research have become progressively more sophisticated over the last 50 years, with radio frequency identification (RFID) tracer technology becoming the most favoured technique for tracking coarse grained particles (see Table 1.1 for an extensive list of recent RFID tracer studies).

The technology enabling RFID tagging has been available since the mid-20th century. It has been applied in a range of environmental science applications, from bio tracking (Floyd, 2015), wood tracking (Schenk et al., 2013), and studying soil erosion (Parsons, 2014). It provides the ability to remotely identify individual items of interest, as ID codes are associated with individually tagged objects. This makes it ideal for studying the movement of individual clasts during bedload transport, as radio signals can penetrate riverbed surfaces, reducing tracer loss from burial (see section 2.1 for an explanation of sediment loss to burial during tracer experiments). Furthermore, unique IDs associated with individual sediments prevents misinterpreting signals from conflicting sources, as observed from magnetic clasts (Hassan et al., 1991).

The technology relies primarily on two pieces of hardware: a passive integrated transponder (PIT tag), which is used to mark an object of interest, and a reader (or antenna) which acts as a transmitter and a receiver. The PIT tag is comprised of a semiconductor chip, a capacitor, and an internal antenna. These are responsible for the storage of the ID, powering the tag, and sending transmissions respectively. The tags have resonant circuits which are energised by the electromagnetic field produced by an external reader. This provides power to the transponder allowing the return ID signal to be broadcast. In this way, the tags are passive, and are powered by the battery within the external reader. The lack of an internal battery provides tags with extended lifespans and a

compact size. With tracers currently down to 8 mm x 1.4 mm in size. This functionality makes RFID tagging ideal for long term fluvial research, with life span estimates of tags of > 50 years (Allan, 2006).

The earliest examples of its use in fluvial transport research are from Nichols (2004) and Lamarre et al., (2005). Their research covers the specific implementation and fundamentals of the technology for particle tracking in detail. Briefly, the process involves embedding RFID tags into existing sediments, or by placing artificial tracers with tags in fluvial environments. Initially, accurate recordings of deployment positions are made, with subsequent resurveys updating tracer locations after regular time intervals (often annually), or after specific events of interest (e.g., floods).

***Table 1.1**: The range of published RFID tracer experiments both in fluvial and coastal environments since the technique's inception*.

Author	Year	Setting
Nichols	2004	Fluvial
Lamarre et al.	2005	Fluvial
Allan et al.	2006	Beach
Lamarre & Roy	2008	Fluvial
Benelli et al.	2009	Beach
Schneider et al.	2010	Fluvial
Miller et al.	2011	Beach
MacVicar & Roy	2011	Fluvial
Bradley & Tucker	2012	Fluvial
Liébault et al.	2012	Fluvial
Benelli et al.	2012	Beach
Phillips et al.	2013	Fluvial
Arnaud et al.	2015	Fluvial
Chapuis et al.	2015	Fluvial
Olinde & Johnson	2015	Fluvial
Dolphin et al.	2016	Beach
Bradley	2017	Fluvial
Cassel et al.	2017	Fluvial
MacVicar & Papangelakis	2022	Fluvial
Clark et al.	2022	Fluvial

1.5.2 Advantages and Disadvantages of Passive Tracers

In addition to the compact size and extended lifespan, the ability for RFID radio waves to penetrate the subsurface allows the detection of sediments, even when buried (estimated depth detection of 0.5 m, Bradley & Tucker, 2012). This improves recovery rates compared to previous tracing techniques (e.g., painting clasts). Additionally, the low costs of PIT tags (typically < £2), allows large scale deployment with 100s – 1000s of tagged particles. Large sample sizes provide robust statistical analysis of bedload transport data. Moreover, using RFID tracers removes the need to disturb tracer cobbles from their natural bed position, reducing anthropogenic interference during surveys.

While there are many benefits to deploying RFID tracers, the detailed movement behaviour of individual particles is difficult to monitor using a passive approach. It is laborious and time consuming to manually relocate all clasts, especially with large scale deployments (e.g., Bradley & Tucker, 2012; Olinde & Johnson, 2015; Clark et al., 2022). Consequently, resurveys of particle positions are infrequent, with the technique only providing a snapshot of movement, giving the total particle step lengths since the previous survey only. Therefore, the number of unique periods of entrainment and deposition are unknown. Additionally, estimating particle rest times in between periods of transport is difficult. Furthermore, from infrequent surveys it is not possible to determine detailed transport characteristics of particles (e.g., rolling, sliding, or saltating), which can be directly recorded in flume settings (e.g., Lee et al., 2002).

Additionally, the use of RFID tracing is constrained by the minimum size requirements of clasts, where only coarse sediment particles can be effectively embedded. Despite the reduction in PIT size from 32 mm (Bradley & Tucker, 2012) to 12 mm (Cain & MacVicar, 2020) in recent years, and the availability of 8 mm tags (Oregon RFID, 2021), the need for drilling natural sediments limits their use to cobble and pebble sized sediments. To circumvent this, researchers have produced synthetic sediments which house the tags (e.g., Papangelakis et al., 2019), although these incur additional production costs and require artificial weights to replicate natural sediments.

1.6 Active "Smart" Tracers

With recent technological developments, it has become possible to directly monitor the step and rest behaviour of sediments with embedded inertial measurement unit (IMU) sensors and integrated wireless technology, (Olinde and Johnson, 2015). Advances in monitoring technology and micro-electro-mechanical systems, or MEMS, over the last couple of decades have resulted in "smart" active sediment tracers being developed. The distinguishing characteristic of active tags is the requirement for a

built-in power supply, usually in the form of commercially available batteries. Active tracers monitor the dynamics of individual sediments using internal IMU sensors enclosed within an artificial casing. These are designed to directly monitor the forces experienced by sediments, and in some cases, relay positional information using a combination of gyroscopes and magnetometers (Kok et al., 2017).

Early examples of this approach include Spazzapan et al. (2004) which used accelerometers embedded within a brass sphere and Kularatna et al. (2006) which used both accelerometers and gyroscopes to track movement. This allowed both linear acceleration and angular motion to be measured in six degrees of freedom. Smart sediment tracer development has rapidly evolved with multiple examples in recent years (e.g., Akeila et al., 2010; Abeywardana et al., 2012; Šolc et al., 2012; Frank et al., 2015; Olinde and Johnson, 2015; Gronz et al., 2016; Gimbert et al., 2019; Dost et al., 2020; Ravindra et al., 2020; Maniatis et al., 2020; Xie et al., 2023). Devices are enclosed in a variety of grain shaped containers made from brass to plastic, all of which aim to replicate natural sediments. Additionally, IMU smart tracking devices are being deployed to monitor other geomorphic features in fluvial systems, such as large woody debris (Spreitzer et al., 2019), to track sediments in coastal environments (Frank, et al., 2015), and to monitor boulder movement on landslides (Dini et al. 2021).

1.6.2 Smart Sediments Potential and Current Limitations

Data derived from IMU's could, in theory, allow calculations of grain velocity through the integration of acceleration data, and subsequently dead reckoning estimations of tracer positions after transport, provided the precise deployment location and the subsequent reference frame is known and integrated accurately (Grewal et al., 2007). However, IMU sensor data contains various sources of uncertainty, for example, even minor misalignment of device axes will accumulate into significant errors given a long enough recording period without verification. In addition,

signal noise and inherent bias in sensors mean devices are not suitable for applications requiring perfect dead reckoning calculations. This is highlighted in the pioneering smart sediment work of Akeila et al. (2010), where validations of their calculated trajectories from IMU devices show significant inaccuracies.

Despite the limitations highlighted above, the potential for real time monitoring of tracer movements using smart sediments presents an opportunity to further our understanding of incipient motion, interactions between flow and transport, and the impact of geomorphic variables where direct comparisons between flow rates, moment of entrainment, and subsequent tracer transport behaviour can be evaluated. In addition, recognising known IMU signals produced during specific transport behaviours in laboratory environments may help inform future field deployments with the devices. IMU data may ultimately be used to infer transport behaviour, even when tracers cannot be directly observed (e.g., during flood events). Although, similar to RFID tagging, with current battery and device size requirements its applicability is constrained to coarse grain particle tracing. However, with advances in compact IMU designs and more power efficient sensors, the space requirements will likely decrease over time as the technology matures.

1.6.3 Integrating Smart Sediments with LoRaWAN

While many recent studies using smart stones have been undertaken, they are often based in laboratory settings (e.g., Gimbert et al., 2019; Dost et al., 2020) or deployed only for a short time in field settings (e.g., Maniatis et al., 2020). This limits their applications in long term studies, which require monitoring of natural processes which may occur rarely and unpredictably (Wolman & Miller, 1960).

In this research, smart stones are developed alongside the UKRI-funded SENSUM project (NE/V003402/1) and are believed to be unique in their capability for long term deployment, with remote active monitoring across multiple sites. This is possible due to their integrated ultra-low powered

IMU sensors, provided by the software engineering firm, Miromico, and the LoRaWAN functionality of the devices.

LoRaWAN is a Long Range, Low Power, Wide Area Networking protocol which is integrated with the increasing diversity of IOT (internet of things) enabled devices (Augustin et al., 2016; Khutsoane et al., 2017). LoRa is a radio modulation technique. It manipulates radio waves to encode information using a chirped multi-symbol format. This conversion allows the transfer of data packets over large distances with minimal bandwidth and energy requirements, making it ideal for remote environmental science solutions. Encoded data is transferred over the unlicensed ISM radio spectrum, which is typically used for industrial, scientific, and medical purposes. Data produced by sensor devices is received by a single, or series of gateways, which can subsequently transmit data via the GSM mobile network to online servers.

LoRaWAN is a networking protocol built on top of the LoRa radio modulation technique. It provides point-to-multipoint communication across multiple devices, gateways, and network servers (Ibrahim 2019). This allows a range of sensors with two-way communication to be controlled by a single end user after deployment, using a network of gateways (Figure 1.2).

The functionality of the LoRaWAN network allows smart stones, and other sensors on the network, to transmit data in real time, without the need for human oversight. Furthermore, this network approach allows the monitoring of multiple devices over a large area, with estimates of the operational range of LoRa of up to 15 km (Petajajarvi et al., 2015; Adelantado et al., 2017). In addition, LoRa gateways have been shown to function reliably even in conditions with poor line of site up to 2 km (Harris & Curry, 2018). Therefore, LoRa could offer significantly higher detection ranges for tracer surveys compared to traditional wireless technologies, such as Bluetooth (e.g., Grottoli et al., 2019). This extended range allows the natural mobilisation of sediments to be captured across a wide catchment area in a variety of flow conditions, in addition to allowing the continuous monitoring of tracers after downstream transport. Additionally,

the storage of data on an external server removes the risk of reaching on device data capacity (e.g., Akeila et al. 2010; Šolc et al., 2012; Dost et al., 2020) allowing analysis to be performed across multiple months of monitoring provided transmission of sensor data to gateways remains greater than collection rates over time.

In addition to tracers, other LoRaWAN enabled devices can connect to existing gateways and transmit real time environmental information. In this way, a series of environmental sensors become integrated into a large IoT node network all monitoring a single site. For instance, flow meters at field sites can provide real time discharge information that can be directly correlated with movement events captured with tracers, all of which can be accessed via a single online database of sensors.

Using sensor networks is essential for producing accurate Digital Twins of fluvial environments (e.g., Spreitzer et al., 2022), in addition to a range of monitored environments. These digital twins and progressive advances in monitoring and computational technology will lead to an overall improved understanding of fluvial systems. Developing smart stone tracers with the means to accurately monitor sediment transport behaviour, whilst being integrated into an array of IoT devices, is an important first step towards building digital environments.

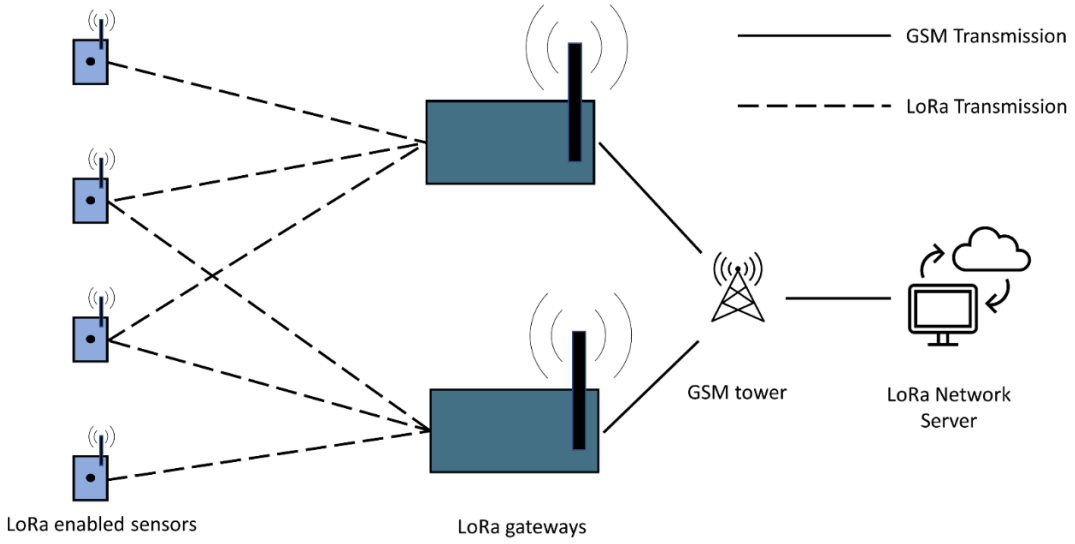

Figure 1.2: *LoRaWAN network architecture demonstrating point-to-multipoint communication across multiple LoRa enabled sensor devices, LoRa gateways, transfer over the GSM network, and end user servers. Note that communication between devices is bilateral, enabling both send and receive data packets for over the air programming.*

1.7 Large Woody Debris Influence of Transport

One of the main aims of this research is to apply modern tracing techniques (RFID and MEMS embedded smart tracers) in wood loaded rivers. This will help to better understand and model the dispersion of sediment pulses through fluvial systems that are geomorphically complex. Research with tracer sediments is often carried out in controlled environments, such as flume laboratories, or simple natural channels. This is intended to constrain variables but can result in difficulties replicating results when investigating complex natural environments with diverse morphologies and sediment sizes.

The presence of wood is a common variable in fluvial systems and adds significant geomorphic complexity to rivers and their sediments (Montgomery et al., 2003). Wood can result in the formation of log steps, altering channel gradients, increasing bedload retention, and can influence grain sorting (Thompson, 1995; Faustini & Jones, 2003; Ryan et al., 2014).

Furthermore, wood is known to alter hydraulic flow regimes (Gippel, 1996; Slater et al., 2015), and increase sediment retention in stream (Keller & Tally, 1979; Megahan, 1982; Sullivan et. al., 1987). A more detailed discussion of the influence of wood is covered in Chapter 2 of this thesis.

For a complete understanding of bedload transport, research in environments impacted by the presence of wood is necessary. This is becoming increasingly relevant as natural flood management practices (NFM) are seeing a rise in popularity for managing fluvial systems (e.g., Grabowski et al., 2019; Short et al., 2019; Black et al., 2021; Deane et al., 2021). For example, the Department for Environment Food and Rural Affairs in the UK allocated £5.2 billion in 2021 in a 6-year flood and coastal defence investment programme (Defra, 2021), which integrates NFM practices ranging from the reintroduction of beavers as ecosystem engineers (Puttock et al., 2018), to the anthropogenic addition of large wood into fluvial systems (Woodland Trust, 2016). While the reduction in flood risk from the use of woody debris in NFM is well documented (e.g., Short et al., 2019), alongside its ecological impacts (Dodd et al., 2016), there is limited research into the consequences of its implementation on the grain scale transport of sediments. Therefore, with the advances in both passive and active sediment monitoring techniques, there is an opportunity to use modern tracing technology to evaluate its impact and help inform future installations of large wood for NFM.

1.8 Key Research Aims

In this thesis, modern sediment tracing techniques are developed and used to assist in evaluating and quantifying fluvial bedload transport at the individual grain scale. Understanding how individual grains move within fluvial systems is essential for accurately modelling and predicting sediment fluxes and the evolution of sedimentary environments (Ancey, 2020). This is of particular importance in areas where data are lacking (e.g., wood loaded rivers). Therefore, both passive radio frequency identification tracer studies and LoRaWAN capable smart stones are

deployed across a range of fluvial environments, with the techniques being applied in the context of investigating the influence of large woody debris on transport behaviour.

The key objectives of this thesis are to:

1. Demonstrate the impact large wood has on the bedload transport behaviour of coarse-grained particles at the individual grain-scale, using statistical modelling to determine the relative influence of wood in comparison to other known variables.

2. Develop an "active" smart stone tracer which captures a range of transport behaviours from its embedded IMU. Using advances in low powered long range wireless transmission capabilities of modern MEMS to automatically transfer movement data in real time during long term deployment.

3. Use laboratory and field data derived from smart stones to identify specific movement characteristic during deployment (e.g., entrainment, rolling, shaking in-situ) to attempt to estimate fluvial conditions remotely.

4. Determine the capabilities and limitations of active tracer devices. To better integrate and inform their use as a part of wider sensor networks within the growing range of IoT devices in environmental science research.

5. Integrate and combine both passive and active tracer data to assess the impact of large wood on bedload transport of sediments in fluvial environments.

References

Abeywardana, D. K., Hu, A. P. and Kularatna, N., (2012) IPT charged wireless sensor module for river sedimentation detection, *IEEE Sensors Applications Symposium Proceedings,* 1-5, doi: 10.1109/SAS.2012.6166324.

Adelantado, F., Vilajosana, X., Tuset-Peiro, P., Martinez, B., Melia-Segui, J., & Watteyne, T. (2017). Understanding the limits of LoRaWAN. *IEEE Communications magazine*, *55*(9), 34-40.

Akeila, E., Salcic, Z. and Swain, A. (2010) Smart pebble for monitoring riverbed sediment transport, *IEEE Sensors Journal*, 10, 1705–1717.

Allan, J. C., Hart, R., & Tranquili, J. V. (2006). The use of Passive Integrated Transponder (PIT) tags to trace cobble transport in a mixed sand-and-gravel beach on the high-energy Oregon coast, USA. *Marine Geology*, 232(1-2), 63-86.

Allen, J. (2012). *Principles of physical sedimentology*. Springer Science & Business Media.

Ancey, C. & Bohorquez, P. (2018) Stochastic streams bedload transport in mountain, *E3S Web of Conferences,* 40, 05046.

Ancey, C. (2020). Bedload transport: a walk between randomness and determinism. Part 1. The state of the art. *Journal of Hydraulic Research*, *58*(1), 1-17.

Ancey, C., Davison, A., Bohm, T., Jodeau, M., Frey, P. (2008) Entrainment and motion of coarse particles in a shallow water stream down a steep slope, *Journal of Fluid Mechanics*, 595, 83–114.

Anthony, R. E., Aster, R. C., Ryan, S., Rathburn, S., & Baker, M. G. (2018). Measuring mountain river discharge using seismographs emplaced within the hyporheic zone. *Journal of Geophysical Research: Earth Surface*, *123*(2), 210-228.

Apitz, S., & White, S. (2003). A conceptual framework for river-basin-scale sediment management. *Journal of Soils and Sediments*, *3*(3), 132-138.

Augustin, A., Yi, J., Clausen, T., & Townsley, W. M. (2016). A study of LoRa: Long range & low power networks for the internet of things. *Sensors*, *16*(9), 1466.

Batalla, R. J., Vericat, D., Gibbins, C. N., & Garcia, C. (2010). Incipient bed-material motion in a gravel-bed river: Field observations and measurements. *US Geol. Surv. Sci. Investig. Rep*, *5091*, 15.

Best, J. L. (1988). Sediment transport and bed morphology at river channel confluences. Sedimentology, 35(3), 481-498.

Black, A., Peskett, L., MacDonald, A., Young, A., Spray, C., Ball, T., Thomas, H. and Werritty, A., (2021). Natural flood management, lag time and catchment scale: Results from an empirical nested catchment study. *Journal of Flood Risk Management*, *14*(3).

Bradley, D.N., Tucker, G.E. and Benson, D.A., (2010) Fractional dispersion in a sand bed river. *Journal of Geophysical Research: Earth Surface*, 115(F1).

Bradley, N. & Tucker, G. (2012) Measuring gravel transport and dispersion in a mountain river using passive radio tracers, *Earth Surface Processes and Landforms,* 37(10), 1034-1045.

Bridge, J. S., & Best, J. L. (1988). Flow, sediment transport and bedform dynamics over the transition from dunes to upper-stage plane beds: implications for the formation of planar laminae. *Sedimentology*, *35*(5), 753-763.

Buffington, J. M., & Montgomery, D. R. (1997). A systematic analysis of eight decades of incipient motion studies, with special reference to gravel-bedded rivers. *Water resources research*, 33(8), 1993-2029.

Bunte, K., Swingle, K.W. and Abt, S.R., (2010) Necessity and Difficulties of Field Calibrating Signals from Surrogate Techniques in Gravel-Bed Streams: Possibilities for Bedload Trap Samplers. *U.S. Geological Survey Scientific Investigations Report,* 2010-5091. Available from: http://pubs.usgs.gov/sir/2010/5091/papers/

Cain, A., & MacVicar, B. (2020). Field tests of an improved sediment tracer including non-intrusive measurement of burial depth. *Earth Surface Processes and Landforms*, *45*(14), 3488-3495.

Clark, M. J., Bennett, G. L., Ryan-Burkett, S. E., Sear, D. A., & Franco, A. M. (2022). Untangling the controls on bedload transport in a wood-loaded river with RFID tracers and linear mixed modelling. *Earth Surface Processes and Landforms*. 47(9), 2283-2298.

Deane, A., Norrey, J., Coulthard, E., McKendry, D. C., & Dean, A. P. (2021). Riverine large woody debris introduced for natural flood management leads to rapid improvement in aquatic macroinvertebrate diversity. *Ecological Engineering*, *163*, 106197.

Department for Environment Food and Rural Affairs. (2021) *Flood and coastal erosion risk management. An investment plan for 2021 to 2027.* Available from: https://assets.publishing.service.gov.uk/government/uploads/system/uploads/attachment_data/file/1006447/Flood_coastal_erosion_investment_plan_2021.pdf

Dey, S. (1999) Sediment threshold, *Applied Mathematical Modelling*, 23, 399–417.

Dini, B., Bennett, G., Franco, A., Whitworth, M., Cook, K., Senn, A., Reynolds, J., (2021) Development of smart boulders to monitor *mass movements via the Internet of Things: A pilot study in Nepal, Earth* Surface Dynamics, *Earth Surface Dynamics*, 9, 295–315,

Diplas, P., Dancey, C. L., Celik, A. O., Valyrakis, M., Greer, K., & Akar, T. (2008). The role of impulse on the initiation of particle movement under turbulent flow conditions. Science, 322(5902), 717-720.

Dodd, J.A., Newton, M & Adams, C.E. (2016) The effect of natural flood management in-stream wood placements on fish movement in Scotland, CD2015_02. Available online crew.ac.uk/publications

Dost, B., Gronz, O., Casper, M., Krein, A. (2020) The Potential of Smartstone Probes in Landslide Experiments: How to Read Motion Data.

Natural Hazards and Earth System Sciences. 20, 3501–3519, https://doi.org/10.5194/nhess-20-3501-2020.

du Boys, P. (1879). Le Rhône et les rivières à lit affouillable – Étude du régime du Rhône et de l'action exercée par les eaux sur un lit à fond de graviers indéfiniment affouillable. *Annales des Ponts et Chaussées,* 49, 141–195.

Einstein, H. A. (1950). *The bed-load function for sediment transportation in open channel flows* (No. 1026). US Department of Agriculture.

Einstein, H., (1937) Bedload transport as a probability problem, Ph.D. thesis, Mitt. Versuchsanst. Wasserbau Eidg. Tech. Hochsch, Zürich.

Faustini, J. M., & Jones, J. A. (2003). Influence of large woody debris on channel morphology and dynamics in steep, boulder-rich mountain streams, western Cascades, Oregon. *Geomorphology*, 51(1-3), 187-205.

Fenton, J. D., & Abbott, J. E. (1977). Initial movement of grains on a stream bed: The effect of relative protrusion. *Proceedings of the Royal Society of London. A. Mathematical and Physical Sciences*, *352*(1671), 523-537.

Ferguson, R. I., & Hoey, T. B. (2002). Long-term slowdown of river tracer pebbles: Generic models and implications for interpreting short-term tracer studies. Water Resources Research, 38(8), 17-1.

Ferguson, R. & Wathen, S. (1998) Tracer-pebble movement along a concave river profile: virtual velocity in relation to grain size and shear stress. *Water Resources Research,* 34, 2031–2038.

Floyd, R.E. (2015) RFID in Animal-Tracking Applications, *IEEE,* 5, 32-33.

Frank, D., Foster, D., Sou, I. M., Calantoni, J., & Chou, P. (2015). Lagrangian measurements of incipient motion in oscillatory flows. Journal of Geophysical Research: Oceans, 120(1), 244-256.

Gilbert, G. K. and Murphy, E. C., (1914) The transportation of debris by running water, *US Government Printing Office*, Washington, D.C., USA, 86.

Gimbert, F., Fuller, B. M., Lamb, M. P., Tsai, V. C., & Johnson, J. P. (2019). Particle transport mechanics and induced seismic noise in steep flume experiments with accelerometer-embedded tracers. *Earth Surface Processes and Landforms*, *44*(1), 219-241.

Gippel C.J., O'Neill I.C., Finlayson B.L., Schnatz I. (1996) Hydraulic guidelines for the re-introduction and management of large woody debris in lowland rivers, *Regulated Rivers: Research & Management,* 12, 223–236.

Gomez, B. (1991). Bedload transport. *Earth-Science Reviews*, 31(2), 89-132.

Gomez, B., & Church, M. (1989). An assessment of bed load sediment transport formulae for gravel bed rivers. *Water Resources Research*, *25*(6), 1161-1186.

Grabowski, R., Gurnell, A., Burgess-gamble, L., England, J., Holland, D., Klaar, M., Morrissey, I., Uttley, C., Wharton, G. (2019) The current state of the use of large wood in river restoration and management. *Water and Environment Journal.* 33(3), 366-377.

Gray, J. R., Laronne, J. B., & Marr, J. D. (2010). Bedload-surrogate monitoring technologies (p. 37). US Department of the Interior, US Geological Survey.

Greig, S. M., Sear, D. A., & Carling, P. A. (2005). The impact of fine sediment accumulation on the survival of incubating salmon progeny: implications for sediment management. *Science of the total environment*, *344*(1-3), 241-258.

Grewal, M. S., Weill, L. R., & Andrews, A. P. (2007). *Global positioning systems, inertial navigation, and integration*. John Wiley & Sons.

Gronz, O., Hiller, P. H., Wirtz, S., Becker, K., Iserloh, T., Seeger, M., ... & Ries, J. B. (2016). Smartstones: A small 9-axis sensor implanted in stones to track their movements. *Catena*, 142, 245-251.

Grottoli, E., Bertoni, D., Pozzebon, A., & Ciavola, P. (2019). Influence of particle shape on pebble transport in a mixed sand and gravel beach during

low energy conditions: Implications for nourishment projects. *Ocean & Coastal Management*, *169*, 171-181.

Habersack, H. (2001) Radio-tracking gravel particles in a large braided river in New Zealand: a field test of the stochastic theory of bed load transport proposed by Einstein. *Hydrological Processes* 15, 377–391.

Harris, N., & Curry, J. (2018). Development and range testing of a LoRaWAN system in an urban environment. *International Journal of Electronics and Communication Engineering*, *12*(1).

Hassan, M.A., Church, M. & Schick, A.P. (1991) Distance of movement of coarse particles in gravel bed streams*. Water Resources Research*, 27, 503–511.

Helley, E. J., & Smith, W. (1971). *Development and calibration of a pressure-difference bedload sampler*. US Department of the Interior, Geological Survey, Water Resources Division.

Hodge, R. A., Hoey, T. B., & Sklar, L. S. (2011). Bed load transport in bedrock rivers: The role of sediment cover in grain entrainment, translation, and deposition. *Journal of Geophysical Research: Earth Surface*, *116*(F4).

Hsu, L., Finnegan, N. J., & Brodsky, E. E. (2011). A seismic signature of river bedload transport during storm events. *Geophysical Research Letters*, *38*(13).

Hubbell D. and Sayre W., (1964) Sand transport studies with radioactive tracers. *Journal of the Hydraulics Division*, American Society of Civil Engineers 90, 39–68.

Hubbell, D. W. (1964) Apparatus and Techniques for Measuring Bedload. U.S. Geological Survey, *Water Supply Paper,* 1748.

Hubbell, D. W., Stevens Jr, H. H., Skinner, J. V., & Beverage, J. P. (1985). New approach to calibrating bed load samplers. *Journal of Hydraulic Engineering*, 111(4), 677-694.

Ibrahim, D. M. (2019). Internet of Things technology based on LoRaWAN revolution. In *2019 10th International Conference on Information and Communication Systems (ICICS)* (pp. 234-237). IEEE.

Keller, E. A., & Tally, T. (1979). Effects of large organic debris on channel form and fluvial processes in the coastal redwood environment. In *Adjustments of the fluvial system* (pp. 169-197). Routledge.

Keller, E.A. (1970) Bedload movement experiments, Dry Creek, California. *Journal of Sedimentary Petrology*, 40, 1339-1344.

Khutsoane, O., Isong, B., & Abu-Mahfouz, A. M. (2017). IoT devices and applications based on LoRa/LoRaWAN. In *IECON 2017-43rd Annual Conference of the IEEE Industrial Electronics Society* (pp. 6107-6112). IEEE.

Kok, M., Hol, J. D., & Schön, T. B. (2017). Using inertial sensors for position and orientation estimation. *arXiv preprint arXiv:1704.06053*.

Komar, P. D., & Miller, M. C. (1973). The threshold of sediment movement under oscillatory water waves. *Journal of Sedimentary Research*, *43*(4).

Krein, A., Schenkluhn, R., Kurtenbach, A., Bierl, R., & Barrière, J. (2016). Listen to the sound of moving sediment in a small gravel-bed river. *International Journal of Sediment Research*, *31*(3), 271-278.

Kularatna, N., Melville, B. & Kularatna, D. (2006). Implementation aspects and offline digital signal processing of a smart pebble for river bed sediment transport monitoring. *In Proceedings of Sensors*, 2006 IEEE, EXCO, Daegu, Korea, October 22-25, 1093-1098, Washington, DC, USA: IEEE.

Lamarre, H., MacVicar, B. and Roy, A.G., 2005. Using passive integrated transponder (PIT) tags to investigate sediment transport in gravel-bed rivers. Journal of Sedimentary Research, 75(4), pp.736-741.

Laronne, J. & Carson, M. (1976) Interrelationships between bed morphology and bed-material transport for a small, gravel-bed channel. *Sedimentology*, 23, 67–85.

Lavelle, J. W., & Mofjeld, H. O. (1987). Do critical stresses for incipient motion and erosion really exist?. *Journal of Hydraulic Engineering*, *113*(3), 370-385.

Lee, H. Y., You, J. Y., & Lin, Y. T. (2002). Continuous saltating process of multiple sediment particles. *Journal of hydraulic engineering*, *128*(4), 443-450.

MacVicar, B. J., & Papangelakis, E. (2022). Lost and found: Maximizing the information from a series of bedload tracer surveys. *Earth Surface Processes and Landforms*, *47*(2), 399-408.

Maniatis, G., Hoey, T. B., Hassan, M. A., Sventek, J., Hodge, R., Drysdale, T., & Valyrakis, M. (2017). Calculating the explicit probability of entrainment based on inertial acceleration measurements. *Journal of Hydraulic Engineering*, *143*(4), 04016097.

Maniatis, G., Hoey, T., Hodge, R., Rickenmann, D., & Badoux, A. (2020). Inertial drag and lift forces for coarse grains on rough alluvial beds measured using in-grain accelerometers. Earth Surface Dynamics, 8(4), 1067-1099.

McNamara, J. P., & Borden, C. (2004). Observations on the movement of coarse gravel using implanted motion-sensing radio transmitters. Hydrological Processes, 18(10), 1871-1884.

Megahan, W. F. (1982). Channel Sediment Storage Behind Obstructions in Forested Drainage Basins. *Sediment budgets and routing in forested drainage basins*, *141*, 114.

Milhous, R.T., 1973. Sediment Transport in a Gravel-Bottomed Stream. PhD Thesis, Oregon State University, Corvallis, Oregon, 232 pp.

Miller, M. C., McCave, I. N., & Komar, P. (1977). Threshold of sediment motion under unidirectional currents. *Sedimentology*, *24*(4), 507-527.

Montgomery, D., Collins, B., Buffington, J., Abbe, T. (2003) Geomorphic effects of wood in rivers. *The Ecology and Management of Wood in World Rivers, Symposium.* 37, 21-47.

Nelson, J. M., Shreve, R. L., McLean, S. R., & Drake, T. G. (1995). Role of near-bed turbulence structure in bed load transport and bed form mechanics. *Water resources research*, *31*(8), 2071-2086.

Nichols, M.H., 2004. A radio frequency identification system for monitoring coarse sediment particle displacement. Applied engineering in agriculture, 20(6), p.783.

Niño, Y., & García, M. (1998). Using Lagrangian particle saltation observations for bedload sediment transport modelling. *Hydrological Processes*, *12*(8), 1197-1218.

Olinde, L., & Johnson, J. P. (2015). Using RFID and accelerometer-embedded tracers to measure probabilities of bed load transport, step lengths, and rest times in a mountain stream. *Water Resources Research*, *51*(9), 7572-7589.

Oregon RFID, 2021, "Oregon RFID: Fish and Wildlife Tracking PIT Tags" https://www.oregonrfid.com/products/hdx-long-range-readers/mobile-reader-kit/

Packman, A. I., & Jerolmack, D. (2004). The role of physicochemical processes in controlling sediment transport and deposition in turbidity currents. *Marine Geology*, *204*(1-2), 1-9.

Pähtz, T., Clark, A. H., Valyrakis, M., & Durán, O. (2020). The physics of sediment transport initiation, cessation, and entrainment across aeolian and fluvial environments. *Reviews of Geophysics*, *58*(1), e2019RG000679.

Papangelakis, E., Muirhead, C., Schneider, A., & MacVicar, B. (2019). Synthetic radio frequency identification tracer stones with weighted inner ball for burial depth estimation. *Journal of Hydraulic Engineering*, *145*(12).

Papanicolaou, A. N., Diplas, P., Evaggelopoulos, N., and Fotopoulos, S. (2002). Stochastic incipient motion criterion for spheres under various bed packing conditions. *Journal of Hydraulic Engineering*, *128* (4), 369-380.

Parsons, A. J., Cooper, J., & Wainwright, J. (2015). What is suspended sediment?. *Earth Surface Processes and Landforms*, 40(10), 1417-1420.

Parsons, A. J., Onda, Y., Noguchi, T., Patin, J., Cooper, J., Wainwright, J., & Sakai, N. (2014). The use of RFID in soil-erosion research. *Earth Surface Processes and Landforms*, *39*(12), 1693-1696.

Petajajarvi, J., Mikhaylov, K., Roivainen, A., Hanninen, T., & Pettissalo, M. (2015, December). On the coverage of LPWANs: range evaluation and channel attenuation model for LoRa technology. In *2015 14th international conference on its telecommunications (itst)* (pp. 55-59). IEEE.

Petit, F., Gob, F., Houbrechts, G. and Assani, A.A., 2005. Critical specific stream power in gravel-bed rivers. Geomorphology, 69(1-4), 92-101.

Puttock, A., Graham, H. A., Carless, D., & Brazier, R. E. (2018). Sediment and nutrient storage in a beaver engineered wetland. *Earth Surface Processes and Landforms*, *43*(11), 2358-2370.

Ravindra, G. H., Gronz, O., Dost, J. B., & Sigtryggsdóttir, F. G. (2020). Description of failure mechanism in placed riprap on steep slope with unsupported toe using smartstone probes. Engineering Structures, 221, 111038.

Rickenmann, D., Turowski, J. M., Fritschi, B., Klaiber, A., & Ludwig, A. (2012). Bedload transport measurements at the Erlenbach stream with geophones and automated basket samplers. *Earth Surface Processes and Landforms*, *37*(9), 1000-1011.

Ryan, S., Bishop, E.L., Daniels, J.M. (2014) Influence of large wood on channel morphology and sediment storage in headwater mountain streams, Fraser Experimental Forest, Colorado, *Geomorphology*, 217, 73-88.

Schenk, E. R., Moulin, B., Hupp C. R. Richte, J.M. (2013) Large wood budget and transport dynamics on a large river using radio telemetry, *Earth Surface Processes and Landforms.* 39 (4), 487-498.

Schmidt, K. H., & Ergenzinger, P. (1992). Bedload entrainment, travel lengths, step lengths, rest periods—studied with passive (iron, magnetic) and active (radio) tracer techniques. *Earth surface processes and landforms*, *17*(2), 147-165.

Sear, D. A., Damon, W., Booker, D. J., & Anderson, D. G. (2000b). A load cell based continuous recording bedload trap. *Earth Surface Processes and Landforms*, *25*(6), 659-672.

Sear, D. A., Lee, M. E., Oakey, R. J., Carling, P. A., & Collins, M. B. (2000a). Coarse sediment tracing technology in littoral and fluvial environments: a review. In *Tracers in geomorphology* (pp. 21-55).

Sear, D.A., Thorne, C.R. and Newson, M.D. (2004) *Guidebook of applied fluvial geomorphology: Defra/Environment Agency Flood and Coastal Defence R&D Programme* (R&D Technical Report, FD1914), London. Defra Flood Management Division, 256pp.

Shields, A., (1936) Application of similarity principles and turbulence research to bed-load movement, *Hydraulic Engineering Reports*, Soil Conservation Service, Pasadena, California.

Short, C., Clarke, L., Carnelli, F., Uttley, C., & Smith, B. (2019). Capturing the multiple benefits associated with nature-based solutions: Lessons from a natural flood management project in the Cotswolds, UK. *Land degradation & development*, *30*(3), 241-252.

Slater, L. J., Singer, M. B., Kirchner, J. W. (2015) Hydrologic versus geomorphic drivers of trends in flood hazard. *Geophysical Research Letters,* 42, 370-376.

Šolc, T., A. Stefanovska, T. Hoey, and M. Mikoš (2012), Application of an instrumented tracer in an abrasion mill for rock abrasion studies, Strojniški vestnik- *Journal of Mechanical Engineering*, 58(4), 263–270.

Spazzapan, M., Petrovčič, J., and Mikoš, M., (2004) New tracer for monitoring dynamics of sediment transport in turbulent flows, *Acta Hydrotech*, 22, 135–148.

Spreitzer, G., Schalko, I., Boes, R. M., & Weitbrecht, V. (2022). Towards a non-intrusive method employing digital twin models for the assessment of complex large wood accumulations in fluvial environments. *Journal of Hydrology*, *614*, 128505.

Spreitzer, G., Schalko, I., Boes, R. M., & Weitbrecht, V. (2022). Towards a non-intrusive method employing digital twin models for the assessment of complex large wood accumulations in fluvial environments. *Journal of Hydrology*, *614*, 128505.

Sullivan, K., Lisle, T. E., Dolloff, C. A., Grant, G. E., & Reid, L. M. (1987). Stream channels: the link between forests and fishes. In *Chapter Three, In: Ernest O. Salo and Terrance W. Cundy (eds.), Streamside Management: Forestry and Fishery Interactions, Proceedings of a Symposium held at University of Washington, 12-14 February 1986. Contribution no. 57, Institute of Forest Resources, Seattle, Washington. p. 39-97.*.

Thompson, D.M., 1995. The effects of large organic debris on sediment processes and stream morphology in Vermont. Geomorphology, 11, 235-244.

Tsakiris, A. G., Papanicolaou, A. T. N., & Lauth, T. J. (2014). Signature of bedload particle transport mode in the acoustic signal of a geophone. *Journal of Hydraulic Research*, 52(2), 185-204.

Valyrakis, M., Diplas, P., Dancey, C. L., Greer, K., & Celik, A. O. (2010). Role of instantaneous force magnitude and duration on particle entrainment. *Journal of Geophysical Research: Earth Surface*, *115*(F2). Niño, Y., & García, M. (1998). Using Lagrangian particle saltation observations for bedload sediment transport modelling. *Hydrological Processes*, *12*(8), 1197-1218.

Walling, D. E., Russell, M. A., & Webb, B. W. (2001). Controls on the nutrient content of suspended sediment transported by British rivers. Science of the Total Environment, 266(1-3), 113-123.

Wang, S., Fu, B., Piao, S., Lü, Y., Ciais, P., Feng, X., & Wang, Y. (2016). Reduced sediment transport in the Yellow River due to anthropogenic changes. *Nature Geoscience*, *9*(1), 38-41.

Wiberg, P. L., & Smith, J. D. (1985). A theoretical model for saltating grains in water. *Journal of Geophysical Research: Oceans*, *90*(C4), 7341-7354.

Wiberg, P. L., & Smith, J. D. (1987). Calculations of the critical shear stress for motion of uniform and heterogeneous sediments. *Water resources research*, *23*(8), 1471-1480.

Wohl, E., Scott, D. (2017). Wood and sediment storage and dynamics in river corridors. *Earth Surface Processes and Landforms.* 42, 5-23.

Wolman, M. G., & Miller, J. P. (1960). Magnitude and frequency of forces in geomorphic processes. *The Journal of Geology*, *68*(1), 54-74.

Woodland Trust, W. (2016). Natural flood management guidance: Woody dams, deflectors and diverters.

Xie, Y., Melville, B. W., Shamseldin, A. Y., Whittaker, C. N., & Yang, Y. (2023). Smart Sediment Particle: A novel approach to investigating fluvial bed entrainment using instrumented sensors. *International Journal of Sediment Research*, *38*(1), 66-82.

Yalin, M. S., (1963) An expression for bed-load transportation, *Journal of the Hydraulics Division* 89, 221–250.

Yang C., and Sayre W., (1971) Stochastic model for sand dispersion, *Journal of the Hydraulics Division*, 97, 265–288.

CHAPTER 2

2 Untangling the Controls on Bedload Transport in a Wood-Loaded River With RFID Tracers and Linear Mixed Modelling

Content in this chapter is partially derived from the published paper: Clark, M. J., Bennett, G. L., Ryan-Burkett, S. E., Sear, D. A., & Franco, A. M. (2022). Untangling the controls on bedload transport in a wood-loaded river with RFID tracers and linear mixed modelling. Earth Surface Processes and Landforms. 47(9), 2283-2298, but has been updated and integrated here.

2.0.1 Chapter Overview

This chapter describes a three-year fluvial RFID tracer study investigating the impact of large woody debris on bedload transport in an alpine stream. Measurements of tracer-step length of tracers were determined each year, following from methodologies applied in previous tracer studies in wood free fluvial systems. The relative influence of in-stream wood on both the entrainment likelihood and subsequent transport distance of sediments is investigated using linear mixed modelling, alongside the impact of other variables known to influence sediment transport. Furthermore, the impact wood has on the deposition location of tracer sediments is determined. In addition, the dispersion characteristics of tracers is analysed to determine the diffusion behaviour of sediments at the site.

2.0.2 Study Abstract

Bedload transport is a fundamental process by which coarse sediment is transferred through landscapes by river networks and may be well described stochastically by distributions of grain step length and rest time obtained through tracer studies. To date, none of these published tracer studies have specifically investigated the influence of large wood in the river channel on sediment transport dynamics, limiting the applicability of stochastic sediment transport models in these settings. Large wood is a major component of many forested rivers and is increasing due to anthropogenic 'Natural Flood Management' (NFM) practices. This study aims to investigate and model the influence of large wood on grain-scale bedload transport.

We tagged 957 cobble – pebble sized particles (D_{50} = 73 mm) and 28 pieces of large wood (> 1 m in length) with RFID tracers in an alpine mountain stream. We monitored the transport distance of tracers annually over three years, building distributions of tracer transport distances with which to compare with published distributions from wood free settings. We also applied linear mixed modelling (LMM), to isolate the influence of wood from other controls on likelihood of entrainment, deposition, and the transport distances of sediments.

Tracer sediments accumulated both up and downstream of large wood pieces, with LMM analysis confirming a reduction in the probability of entrainment of tracers closer to wood in all three years. Upon remobilisation, tracers entrained from positions closer to large wood had shorter subsequent transport distances in each year. In 2019, large wood also had a trapping effect, significantly reducing the transport distances of tracer particles entrained from upstream, i.e. forcing premature deposition of tracers. This study demonstrates the role of large wood in influencing bedload transport in alpine stream environments, with implications for both natural and anthropogenic addition of wood debris in fluvial environments.

2.1 The Influence of Large Wood on Fluvial Systems

Large wood (defined as pieces > 1 m length and 0.1 m diameter, Wohl *et al.* 2010), is a major component of many forested rivers and can increase following disturbances such as wildfire (Bendix & Cowell, 2010), insect infestations (Ryan *et al*., 2014), mass movements, bank erosion (Steeb *et al.,* 2017), and the anthropogenic addition of wood as part of Natural Flood Management (NFM) (Grabowski *et al*., 2019). The latter has seen an increase in popularity to help regulate flow regimes, alter sediment dynamics, and support ecological habitats (e.g., Gippel *et al*., 1996; Klaar *et al*., 2011; Langford *et al.,* 2012; Dixon & Sear, 2017; Dadson *et al*., 2017). The presence of wood in a fluvial system has a major influence on sediment storage with Gregory *et al.* (1994) and Wohl and Scott (2017) finding a greater residual pool volume associated with increasing large wood loads. Large wood has also been observed to reduce overall sediment transport rates (Montgomery *et al*., 2003), significantly altering the geomorphological characteristics of streams through the formation of log steps (Ryan *et al*., 2014), in addition to strengthening channel-hillslope coupling (Golly *et al*., 2019) and adding geomorphic complexity to streams. However, there has been a lack of research into the influence of large wood on stochastic grain-scale sediment transport, which is fundamental for understanding and modelling the dispersion of sediment pulses through the fluvial system.

Pulses of sediment may enter fluvial systems through a range of anthropogenic processes, including mining (Pickup *et al*., 1983; Ferguson *et al*., 2015), dam removal (East *et al*., 2015), and road runoff (Lane and Sheridan, 2002), in addition to natural processes, including logjam break up (Umazano & Melchor, 2020), landsliding (Sutherland *et al.,* 2002) and the cyclic erosion of bedforms (Dhont and Ancey, 2018). These pulses have a range of impacts on the fluvial system as they disperse or translate downstream. They can cause changes in channel capacity, with impacts on flood hazard (e.g., Slater *et al*., 2015) and risk to people who live near or depend on fluvial environments. Furthermore, understanding both the dispersion of pulses of sediment and individual grain transport is essential

for the progression of engineering approaches and fluvial research in a range of applications, including contaminant transportation (Reneau *et al*., 2004; Malmon, 2005), fluvial sediment budgets (Kelsey, 1987; Malmon *et al*., 2003) and the restoration of rivers (Sear, 1994; Kinzel, 2009; Gaeuman *et al*., 2017).

The dispersion of a pulse of sediment can be modelled using a stochastic approach in which bedload transport is described and modelled probabilistically, in recognition that bedload transport is characterized by cyclic sequences of particle motion and rest (e.g., Cui *et al.,* 2003; Ancey *et al*., 2008; Lajeunesse, 2018). Individual grain transport was initially recognised to be intermittent and probabilistic by Einstein (1937), with the development of a probability function and a transport rate equation in which bedload transport occurs in a series of steps resulting from the turbulent fluctuations caused when hydrodynamic lift forces are greater than a particle's weight. Consequently, the transport of coarse-grained sediments is not continuous, with particles predominantly remaining at rest, even when fluid stress is above the threshold of movement.

Numerous tracer studies have characterised the stochastic behaviour of bedload transport by measuring distributions of grain step lengths and rest times of tracer particles (e.g., Bradley and Tucker, 2012; Ancey *et al*., 2014; Olinde and Johnson, 2015; Ancey and Bohorquez, 2018). Different methodologies of tracers include the painting of rocks, radio transmitters, and the use of magnetic clasts (e.g., Keller, 1970, Laronne & Carson, 1976; Hassan *et al*., 1991; Ferguson & Wathen, 1998). These methods have limitations including difficulties recognising individual clasts, loss of sediments due to burial, and anthropogenic interference. However, each approach counterbalances its limitations with corresponding advantages, such as cost-effectiveness, non-intrusiveness, and varying degrees of data accuracy. Tracer experiments have become progressively more sophisticated over the last 50 years, with radio frequency identification (RFID) tracer technology becoming the most favoured technique (Sear *et al*., 2003; Hassan & Ergenzinger, 2003; Cassel *et al.,* 2020; MacVicar & Papangelakis, 2022).

Previous studies evaluating bedload sediment transport and its dispersion characteristics with tracers of various kinds have found step length frequency distributions to most closely fit an exponential or gamma distribution (e.g., Habersack, 2001; McNamara and Borden, 2004; Bradley and Tucker, 2012), where the majority of particles have small step lengths and progressively fewer have longer displacement distances. Additionally, the diffusion of bedload sediments is determined by the tail character of the exceedance probability plots, and are typically seen to be heavy or thin, which is indicative of anomalous diffusion (e.g., Olinde and Johnson, 2015; Bradley, 2017). This type of diffusion is determined by the probability distributions of the step scaling, step lengths, and resting times. Where distributions, in combination, control the migration of particles, and the variance of displacement increases more rapidly or slowly with time than in non-linear diffusion and is therefore anomalous rather than Fickian (Martin *et al*., 2012). This can be expressed by $\sigma^2 \sim t^{\gamma}$, with $\gamma > 1$ and $\gamma < 1$ representing superdiffusion and subdiffusion respectively (Weeks & Swinney, 1998). This can be observed where particles moving with superdiffision experience more rapid and irregular displacement and particles moving with subdiffusion move more slowly than during typical diffusion. A detailed explanation of the dispersion characteristics of bedload is found within Nikora (2002), which covers particles in motion through sliding, rolling, and saltation but not total suspension.

In environments with high wood loading, the influence of large wood pieces on rock step lengths, rest times, and subsequent dispersion characteristics is currently unknown, limiting the applicability of stochastic sediment transport models in these settings. It is theorised that the presence of large wood increases bed surface roughness (e.g., Buffington & Montgomery, 1999), subsequently reducing the mean shear stress on the riverbed and subsequent sediment transport distances. Furthermore, geomorphic features formed due to woods presence, such as scour pool structures, can increase particle burial rates (e.g., Wohl & Scott, 2017) in addition to wood physically blocking sediment movement.

In this study, we aimed to evaluate the impact of large wood on grain-scale stochastic bedload transport dynamics. We undertook a sediment tracer study at a wood-loaded reach using passive RFID tags embedded in individual clasts to quantify sediment transport distances, and investigate their distribution over a three-year period with respect to wood loading, allowing comparisons with previous studies in wood-free fluvial settings (e.g., Bradley, 2017).

Additionally, we applied linear mixed modelling (LMM) to tease out the influence of wood on sediment transport dynamics from the myriad of other controls. This technique is commonly used in ecological and biological research to determine the controls on animal behaviour (e.g., McDermott-Long et al., 2017; Dunnink et al., 2019) and while this approach is novel in earth sciences, the principle of treating tracers as individuals within a larger population with varying but similar influencing variables is analogous to individual animals within a population of a species in ecological sciences. Specifically, we used LMM to untangle the influence of wood on the probability of tracer entrainment, deposition and transport distance, from other controls including tracer size and location relative to the thalweg, boulders and steps.

Our findings have implications for predicting bedload sediment transport and downstream deposition. Additionally, field data assists in determining the effectiveness and potential side effects of introducing engineered log jams in river management schemes (Bennett *et al*., 2015), as well as providing information for their installation. Finally, we demonstrate the potential of the LMM technique for tracer studies attempting to untangle the multiple controls on bedload transport.

2.2 Study Site

The study site is St. Louis Creek, Colorado, USA (Figure 2.1), a gravel bed subalpine stream characterised primarily by a step pool morphology with small sections of pool riffle at the upstream segment of the investigated area. The bed grain-size distributions has D_{16}, D_{50}, and D_{84} of 30, 53, and

77 mm respectively measured from the bed surface. Steps are primarily formed from a combination of boulders and pieces of wood incorporated into the bed (Figure 2.2). The subsection of the reach investigated is 220 m in length and has an average slope of 0.046. There are 4 log and 10 boulder steps present along the study area in addition to small patches of vegetation and gravel bars. The site is located within the Fraser Experimental Forest (FEF), Colorado. The FEF is located approximately 80 km northwest of Denver with an elevation above ~2700 m, and is an experimental area managed by the U.S. Forest Service. Its watershed is underlain mostly by granite, gneiss, and schist bedrock (Green, 1992).

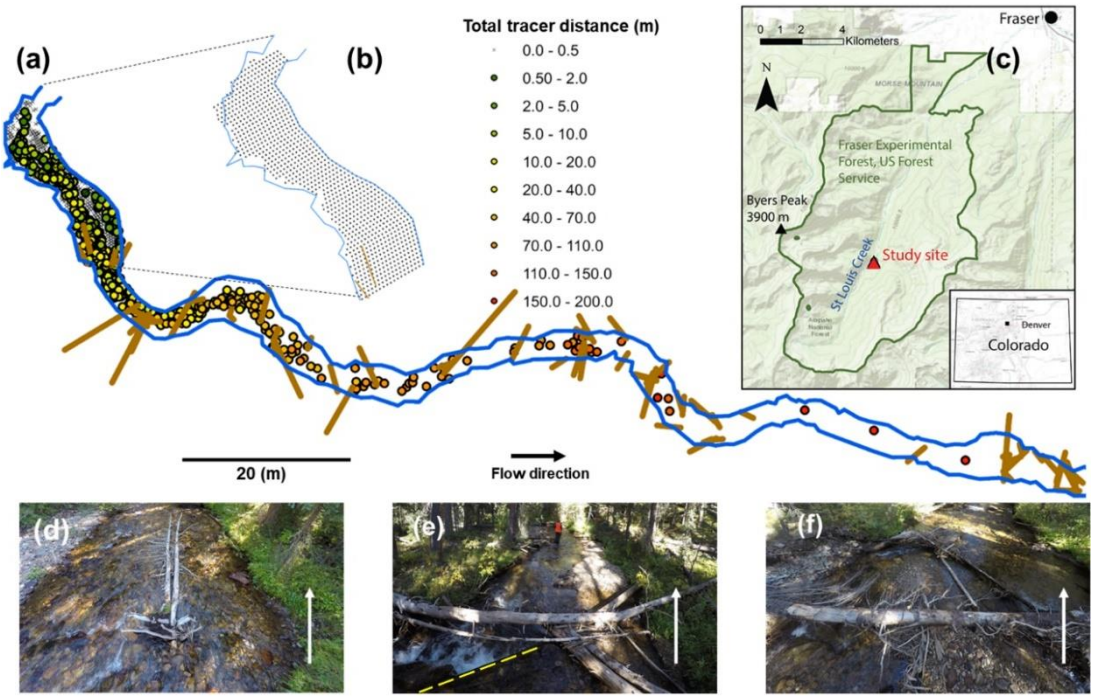

Figure 2.1: *Overview of St Louis Creek with: (a) ArcMap spatial representation of study site with final (2019) locations of tracer sediments, with colour representing cumulative total tracer transport distance since the study began demonstrated by total cobble distance moved, and the location of large wood pieces that are interacting with bedload transport; (b) original seed locations of tracer sediments in 2016, known as the 'seeded reach' (seed locations appearing to overlapping channel bank are a result of bank overhang); (c) location of study site within the Fraser Experimental Forest; (d) image representing area within seeded reach, which includes a wood piece that fell into the stream between 2016 and 2017; (e) buried wood (dashed yellow line) forming a log step and log jam approximately 100 m downstream of seeded reach; (f) a build-up of sediments behind large wood located just beyond the final tracer position. (Flow direction is approximately north in (c) and is represented by the white arrows on images).*

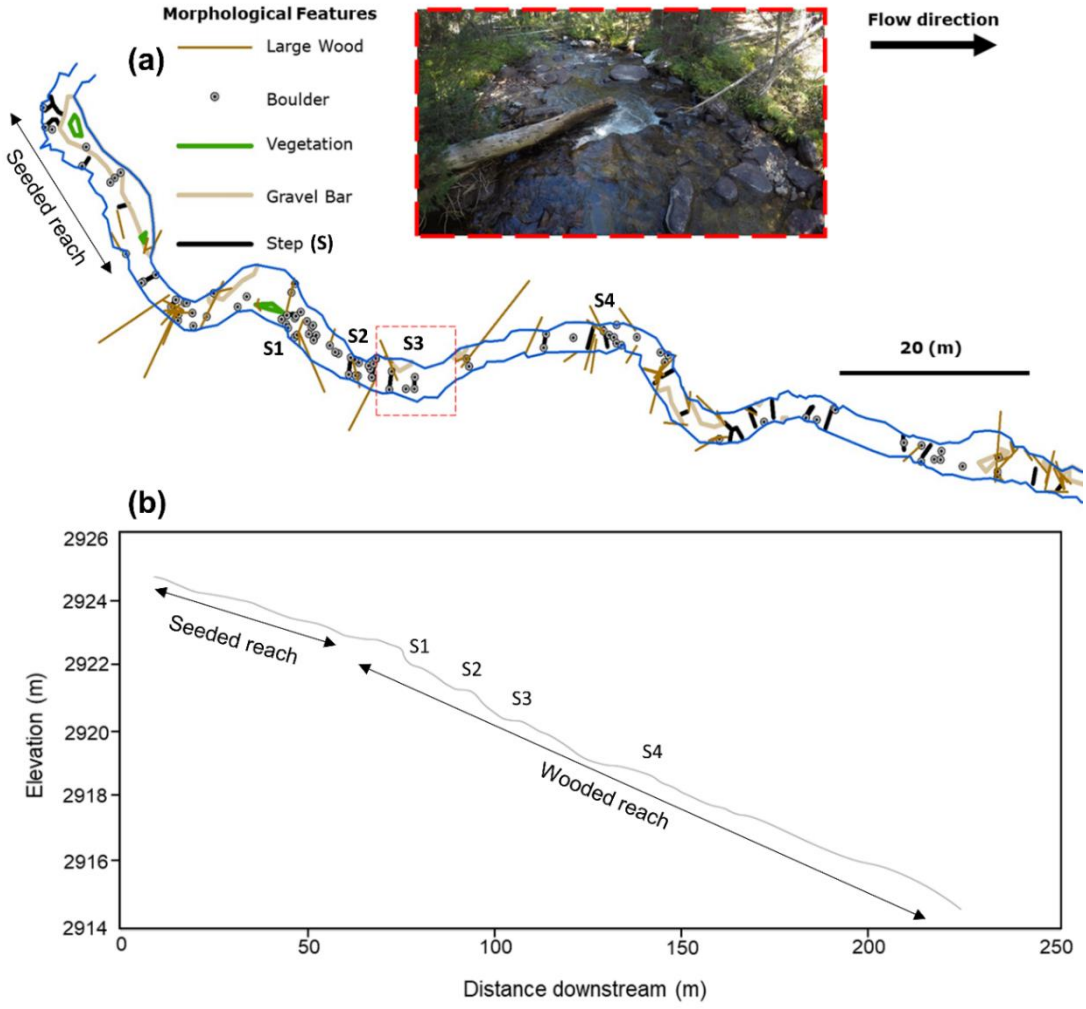

Figure 2.2: *(a) Morphological features surveyed at St Louis Creek including large wood, boulders, vegetation, gravel bars, and locations of steps. Area highlighted in dashed line as an image displays a typical section of the study area beyond the seeded reach with an example of a typical boulder step and large wood piece observable. (b) Longitudinal profile of reach derived from tracer cobble elevations, with steps of interest labelled on feature map and profile (e.g., Supporting Information Table A.1). Note the change to a steeper gradient slope from the end of the seeded reach into the wooded reach, with the seeded and wooded reach having slopes of 0.0328 and 0.0502 respectively.*

St. Louis Creek is a second order stream, with a flow regime characterised by snowmelt run off, with flow rates generally beginning to rise during April, typically peaking throughout May, June, and July and returning to base flow in late summer (Figure 2.3). Because of this, the field season surveys took place during late summer, when water levels are low enough for particle relocation and the winter snows have yet to begin restricting access to the site.

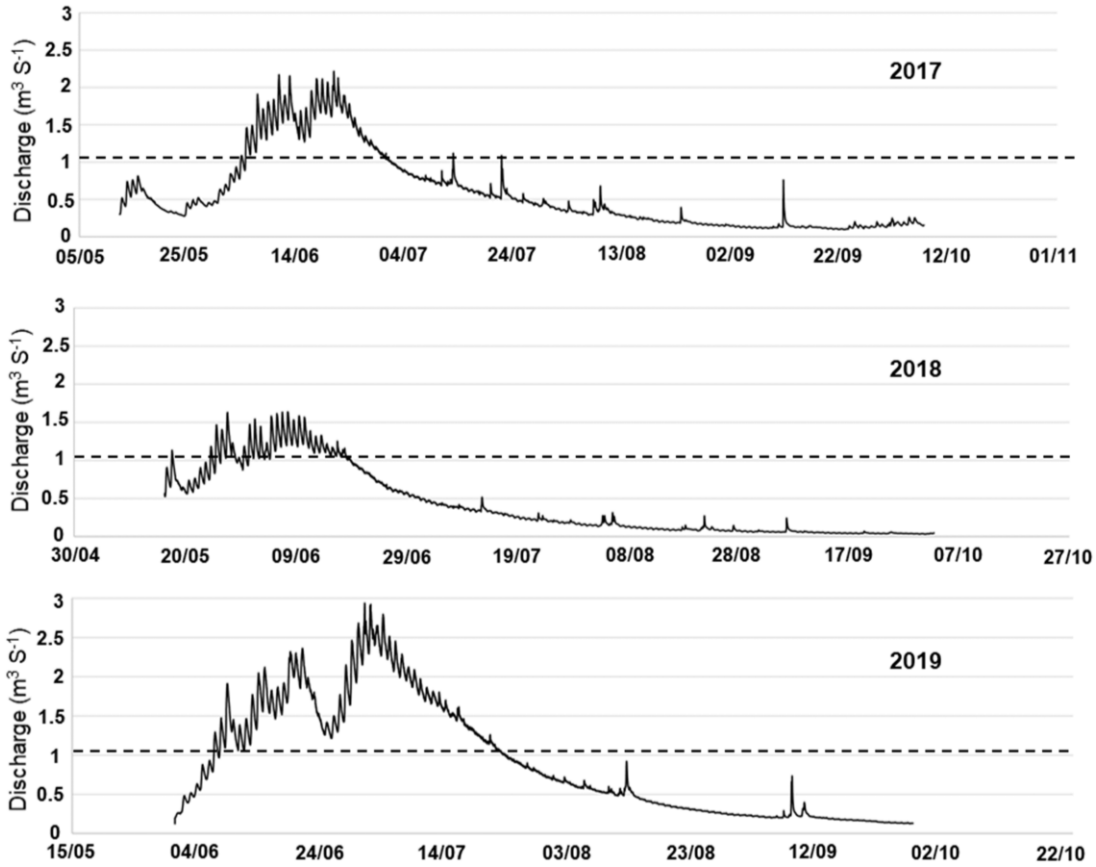

Figure 2.3: *Annual discharge data from St Louis Creek for 2017–2019 during periods of discharge gauge deployment upstream of study reach. Dashed line represents calculated discharge value of 1.02 m^3 s^{-1} required to exceed estimated critical threshold (Ferguson, 2005). Note the oscillation from June to August likely represent periods of snowmelt and associated increases in runoff.*

The site is ideal for studying the influence of large wood on sediment transportation as it is undergoing an increase in wood loading due to the death of the majority of the old growth Lodgepole pine (*P. contorta*),

resulting from infestations of the mountain pine beetle (*Dendroctonus ponderosae*) (Raffa *et al*., 2008). The site therefore acts as a natural case study for the impact of wood loading, its influence on geomorphic change, and sediment transport. Wood at the site is present in the form of log steps, ramps, bridges, and incorporated jams (Wohl *et al*., 2010), with > 75 % of surveyed pieces attached or incorporated into the banks.

The study area is subdivided into two main reaches, distinguished by morphology and channel slope (Figure 2.2b). Firstly, the "seeded" reach which covers the area of initial instillation of tracer sediments (Figure 2.1b). It extends 35 m downstream streamwise, with channel widths ranging from 3 to 10 m (average 6.8 m) and has a slope of 0.0328. Morphology here is less complex than further downstream, with small gravel bars and pool riffle sequences. The channel here is unconfined. Secondly, the "wooded" reach is downstream of the seeded reach and has significant wood loading. It extends 185 m downstream streamwise, with channel widths ranging from 3.2 to 9.7 m (average 5 m) and a slope of 0.0502. Morphology here is more complex with pools and steps formed from a combination of boulders and wood pieces (e.g., Figure 2.1e). Downstream sections of the reach become confined due to the narrowing of the river channel by adjacent slopes.

2.3 Methods

RFID is a wireless identification system with a variety of applications in environmental science (e.g., biotracking (Floyd, 2015), wood tracking (Schenk *et al*., 2014), and sediment transport (Nichols, 2004; Lamarre *et al.,* 2005). It provides the ability to remotely identify individual items of interest, making it ideal for studying individual clasts during bedload transport. The technology relies primarily on two pieces of hardware: a passive integrated transponder (PIT tag), which is used to mark objects of interest, and a reader (or antenna) which acts as a transmitter and a receiver. This study used a long-range Oregon RFID mobile reader kit (Oregon RFID, 2021), with 32 x 3.65 mm PIT tags weighing 0.8 g each, which can be embedded into clasts with a b-axis as small as 47 mm with

minimal effect on shape and density of clasts. See Nichols (2004) for detailed description of RFID particle tracking methodology.

Initially, 957 cobble to pebble sized clasts were selected, due to their similarity in composition and size to bed materials, in addition to their suitability for tagging. Clast weight and axes size were recorded (Table 2.1), and the selected clasts were drilled to allow space for the implanting of the passive RFID PIT tags. Once tags were inserted, silicone was used to seal the tags within the clasts, producing tracer sediments that appeared unchanged compared to the natural sediments of the study site. As a failsafe in case of tag failure, and initial identification of tracers, the corresponding RFID identification numbers were written on the surface of tagged clasts.

Table 2.1: Key size and weight statistics of sediments selected for RFID tagging.

	Weight (g)	**B - axis (mm)**
Mean	636.1	74.2
Median (range)	605.5 (201.1 - 1483.3)	74.0 (47.0 - 110.0)
Mode	465.7	78
Standard deviation (σ)	208.7	10.3

In addition to sediments, pieces of large wood (typically trunks from adjacent riparian areas) were tagged and measured, and an inventory of their defining characteristics, including length, diameter and structural associations, was collected based on agreed definitions (Wohl *et al*., 2010) and are available in supplementary information (A.1). While many pieces of large wood classified as bridges were characterised and tagged, they were not included in subsequent sediment transport analysis due to their current lack of interaction with the bed, even during high flow. Finally, the US Forest Service installed a discharge gauge at the upstream end of the study site. This gauge collected flow data from May to October between

2017 and 2019. It used the depth and width of the channel, in addition to internal calibrations, to calculate the flow rate. There are no substantial tributaries located along the study reach, therefore flow rates characterize the whole site. Flow rates recorded in St. Louis Creek (Figure 2.3) match well with another gaged river, Bobtail Creek (see appendix A.2), whose record extends from 1986 – 2019, facilitating estimation of the recurrence interval of transporting flows within the study stream, assuming the flows have always been analogous due to proximity, similar forest cover, aspect and altitude of sites. We calculated related stream power using surveyed bed slope, channel width, and discharge (Petit et al., 2005). The discharge gauge was installed and discontinued in the spring and autumn, respectively, due to the environmental conditions over the winter period potentially damaging the device.

Tracer clasts were seeded in summer 2016, in a 0.5 m grid across the channel from bank to bank. This channel segment is referred to as the "seeded" reach (Figure 2.1b) that extended from the location of the discharge gauge to ~ 35 m downstream. Deployment of tracers was on the surface of the bed, resulting in tracers beginning in highly mobile positions (e.g., Bradley and Tucker, 2012), analogous to the most mobile surface grains of the pre-existing bed surface (i.e., existing sediments protruding from the bed surface). Spatial locations of tracer sediments were recorded to an estimated accuracy of < 50 mm using a Leica total station with a known GPS location and a reflector placed above tracer sediment locations. It has been established that both clustering and orientation of transponders can add uncertainty to detection ranges (Chapuis *et al.,* 2014; Arnaud *et al.,* 2015). However, we conducted burial experiments of the tagged clasts and established that tracer identifiers (IDs) could be read from ~0.70 m, with minimum interference from water or surrounding and overlying sediments.

Tracer sediments and wood locations were resurveyed on an annual basis after annual snowmelt in 2017, 2018 and 2019 using an Oregon RFID mobile reader setup. This included a backpack, antenna, and mobile reader. Tracers were considered mobile, and their new deposition location recorded if transport was > 1 m to account for the potential variation in

detection distances each year. Wood debris was classified as significant and surveyed if it is at least 10 cm in diameter and > 1 m in length following the parameters suggested by Wohl *et al*. *(*2010). Additional characteristics such as size, classification (e.g., ramp or bridge type), and state of decay was recorded annually to determine if these characteristics impacted interaction with sediment transport or subsequent wood transport (e.g., Dixon & Sear, 2016). Additionally, other geomorphic features within the study site were surveyed, such as the location of banks, steps, and boulders. All spatial data was recorded in ArcGIS10, alongside supplementary information (e.g., size or defining characteristics of wood pieces) producing a spatially accurate map of the area which was updated every year (e.g., Figure 2.1a). Annual spatial locations of tracers are available in supplementary information (A.3).

To produce accurate tracer transport data, cartesian GPS locations of tracers were converted into a channel-based coordinate system, as the spatial referencing of river channels is complicated by bending. Coordinates were converted following the methods of Legleiter & Kyriakidis (2006), which consider the channel centre line as the streamwise axis (i.e. relative distance downstream), allowing travel distances to be corrected for channel curvature.

Annually resurveying tracer locations after high flow conditions during snowmelt resulted in a dataset spanning 3 years of tracer transport distances. This was used to investigate and evaluate any disruption to "typical" transport behaviour introduced by the presence of large wood.

2.3.2 Burial Experiments

For the successful communication of the RFID tags, sufficient power is required to charge the device capacitor to allow transmission of the ID (Finkenzeller, 2010). The distance that the minimum power requirements of the tags are met is effectively the device read range. This is primarily governed by direct linear distance, as the emitted strength of the reader decays by a factor of the inverse cube of the distance between the tag and

the power source (Lehpamer, 2012). We wished to investigate the influence of other variables, such as burial, submersion in water, and the angle of the reader on read range, to determine how resurveying may be affected.

To test the maximum range of the antenna, a RFID tagged cobble was initially used on the surface of the bed. The maximum scanning distance was found to be 0.7 m. This was possible at multiple angles with only slight variations in scanning distance (< 0.05 m). This was repeated underwater (approximately 0.4 m submerged) with no effect on scanning distance identified. These detection distances were slightly improved from previous research estimates of 0.5 m (Lamarre et al., 2005; Schneider et al., 2010).

Next, upstream of the seeded reach, a hole was dug in the gravel bed of approximately 0.3 m. Both large cobbles, gravel, and sand was removed until the water table was reached, preventing the further removal of material. The RFID tagged cobble was placed at the base of the hole and removed material was used to infill the space, making sure to follow its original stratigraphic composition (Figure 2.4). Additionally, pieces of woody material and large cobbles were placed on top of the hole to further bury the tag.

Again, the antennas maximum read range was approximately 0.7 m, suggesting that burial, at least out of water, does not affect read range at these depths. This suggested that the burial would not prevent successful resurveys of tracer sediments up to these depths.

Figure 2.4: *RFID read range experiments, showing successful detection of tracers buried at depths of up to 0.7 m under sediments, water, and woody debris. This indicates that tracer burial has minimal impact on detection.*

2.3.3 Statistical Analysis and Modelling

Quantifying and modelling tracer-step length and rest time distributions allows accurate predictions to be made of bedload transport in fluvial environments using established statistical estimation methods of previous tracer studies (e.g., Hassan, *et al*., 2013; Olinde and Johnson, 2015). The length of our study of 3 years precluded analysis of particle rest time but we are able to plot tracer transport distance distributions for comparison with published studies in wood-free settings. Exponential and gamma distributions were fitted to the tracer transport distance frequency data (Figure 2.5). In order to identify the likely type of sediment diffusion (super or sub diffusive), we quantified the exponent on the tail of the exceedance probability distribution of tracer transport distances. This was conducted in MATLAB (R2018B) by fitting a power-law distribution model to the tail of the distribution following the methods of Clauset *et al*. (2009), where

$x_{\min}$ for 2017, 2018, and 2019 was calculated to be 33.45, 5.77, and 41.06 respectively.

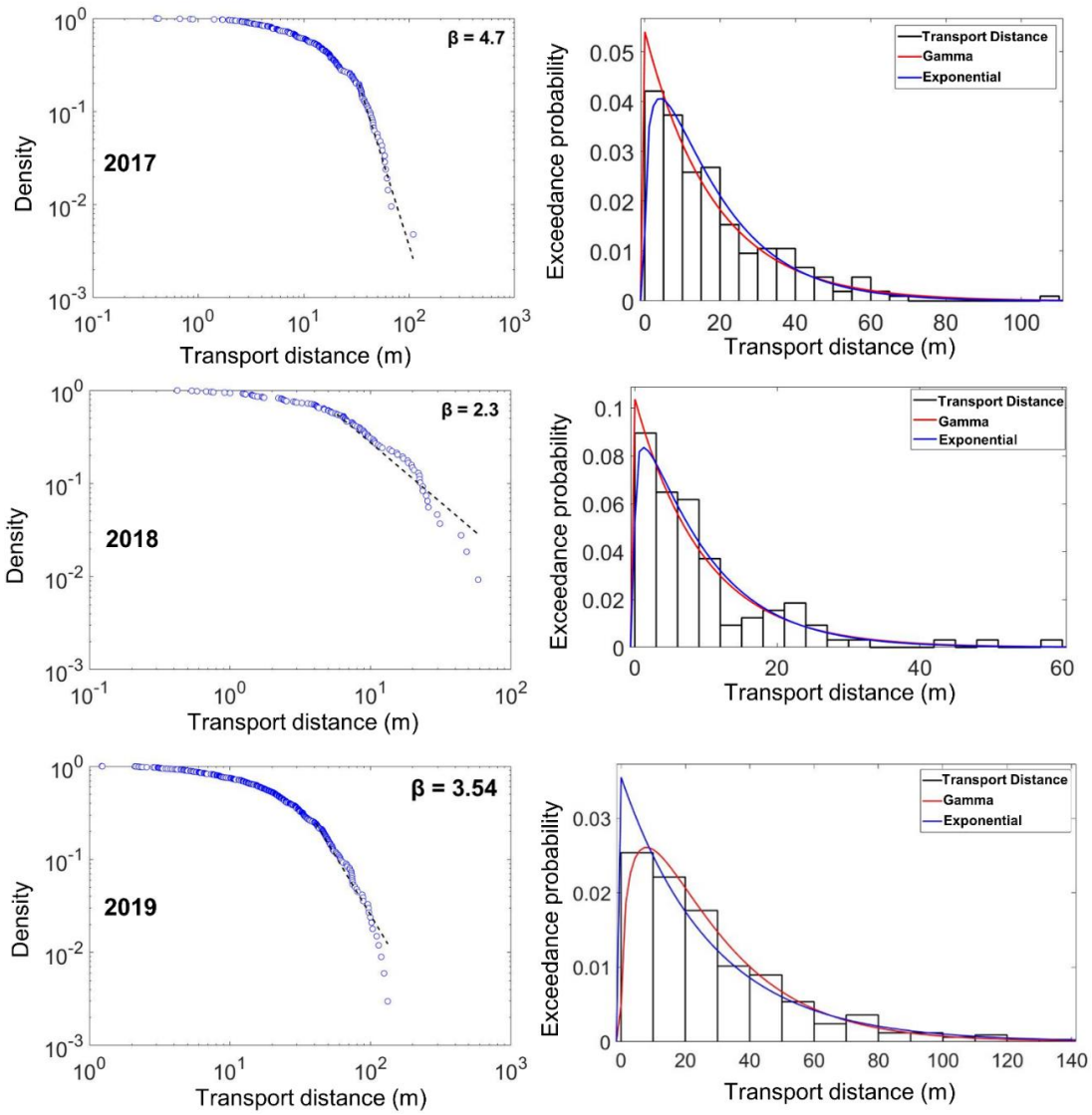

Figure 2.5: *Probability density functions of tracer transport distances, with overlain exponential (blue) and gamma (red) curves. Additionally, the annual exceedance probability graphs are displayed, fitted with a power law exponent line and a β value, representing the tail character of the data.*

Linear mixed modelling was used for determining the influence that individual variables (e.g., proximity to large wood) have, on a continuous dependent variable (e.g., transport distance of tracers) or a binary dependent variable (e.g., entrainment or deposition of tracers). This approach was implemented as it can account for the characteristics of a given population (e.g., weight, size, location of tracers in channel, etc…) and determine if their levels of influence on sediment transport are significant. Furthermore, interactions between variables and their level of significance can also be determined.

Investigating the influence that large wood has on tracer entrainment, deposition, and transport distances required an analysis of all the potential variables that influence transport behaviour, as well as producing a testable variable for the influence of wood. The distance of tracer sediments to large wood in both their deposition and entrainment positions was determined in ArcGIS 10.6.1 using the Near (Analysis) proximity toolset, by mapping all mobile tracers to their nearest piece of large wood using their GPS locations for each annual dataset. This generated an inventory of spatial data that was used to determine the relative influence of distance to wood on sediment transport. Other key variables considered and determined were distance to channel thalweg (calculated using the same approach of distance to wood), distance to boulders and non-wood steps, and tracer sediment size (represented by b-axis length). The influence of differing river discharge year on year was not included directly in the LMM analysis, with each year being considered separately to isolate the effect of variables such as wood from annual changes in hydrology. Analysis of yearly LMM results is subsequently discussed in the context of associated flow rates, estimates of stream power, and degree to which critical thresholds are exceeded.

The relative influence of other geomorphic features, including the spatial location of boulders and non-wood steps, were found to not be significant using LMM analysis and therefore were not included in subsequent analysis. Insignificant LMM results are available in supplementary information (A.4).

To isolate the influence of large wood pieces and remove anthropogenic bias from initial 'hypermobility' seen in previous tracer studies (e.g., Bradley and Tucker, 2012), tracers were selected for LMM analysis if their deposition location was downstream from the seeded reach after each year of the study from 2017. This area of the reach was also selected due to the abundance of large wood providing greater interaction with transported sediments. Finally, wood pieces classified as bridges were not included in the LMM analysis due to their lack of interaction with the bed.

The lme4 package in R (Bates et al, 2015) was used for LMM analysis. We used a binomial LMM model to investigate the relative influence of variables on the likelihood of entrainment and deposition of tracer sediments, and a gamma model to investigate a given variable's influence on tracer transport distance.

2.4 Results

The discharge data for 2017 – 2019 show peak flow to be occurring during the summer months of May, June, and July (Figure 2.3). 2017 flow rates initially rise in late May from a base level of ~ 0.5 m^3 s^{-1}, to peak conditions of 1.4 – 2.2 m^3 s^{-1} over June, followed by a continuous return to base flow during July. 2018 flow rates were consistently the lowest of the three years surveyed, with flow rising from the base rate of ~ 0.5 m^3 s^{-1} in May to peak conditions ranging from 1.1 - 1.6 m^3 s^{-1} over June before again dropping to base conditions. 2019 flow rates were substantially higher, with two distinctive periods of increasing and lowering flow rates over June and July, peaking at 2.9 m^3 s^{-1}. The recurrence interval for the peak flow rates recorded in 2019 at the analogous stream Bobtail Creek are 1.9 years based on annual maxima of historical flow rates, suggesting even our highest measured flow rates are relatively common.

Stream power at annual peak flow was calculated for the average channel width of 5.5 m and average channel slope of 0.046 and was found to be 180.5, 131.3, and 237.9 W m^{-2} for 2017, 2018, and 2019 respectively. Stream power exceeded the estimated critical threshold (Ferguson 2005)

for the D_{50} of tracer sediments of 83.93 W m^{-2} in all years surveyed, where a discharge value exceeding 1.02 m^3 s^{-1} was required to initiate movement. Thresholds were therefore exceeded for approximately 26, 24, and 45 days in 2017, 2018, 2019 respectively (Figure 2.3). When subdividing the reach, the gentler sloping and wider seeded reach critical threshold (88.90 W m^{-2}) is still exceeded by estimated stream power in 2017 and 2019 (104.10 W m^{-2} and 137.22 W m^{-2}), although the 2018 stream power (75.70 W m^{-2}) is slightly lower than estimated from the threshold. Despite this, tracers were still entrained and transported within the seeded reach, although at a lower rate and shorter transport distances than other survey years.

Discharge each year showed an expected correlation with the mean transport distance of tracer sediments and the likelihood of tracer movement (Table 2.2), with 2019 and 2018 having the highest and lowest percentage of tracers transported respectively, and the highest and lowest maximum transport distances respectively. However, estimating the direct influence of flow rate on the likelihood of movement and distance moved is cautioned as retrieval rates differed between years, meaning the total population of tracer sediments is not accounted for. Furthermore, in 2017, sediments have the potential to be hypermobile, as they were artificially placed on the bed surface without replacement of original sediments and are therefore not fully incorporated into the bed.

Table 2.2: *Key statistics of tracer sediment movement, showing annual and cumulative results of transported sediments.*

Year	Retrieval Rates (%)	Cobbles Moved (%)	Median B-Axis and range (m)	Maximum Transport Distance (m)	Peak river discharge (m^3 s^{-1})	Mean Transport Distance (m)
2017	88	22	73 (50 – 110)	109	2.217	29.96
2018	75	11	73 (51 – 110)	58	1.634	9.63
2019	80	35	73 (48 – 102)	133	2.938	28.14
Total	**81***	**49**	N/A	**193**	N/A	

* = Mean retrieval rates

Observed changes to the overall geomorphology of the reaches are minimal over the 3 years of study. There was, however, an accumulation of sediments, including our tracers, around pieces of large wood (e.g., Figure 2.1d) and some reworking of gravel bars observed. Wood transport was limited to only one tagged piece falling into the channel and moving downstream 25 m. No additional wood was recruited after the 2017 study year. This demonstrates that the majority of sediment-wood interaction over the three years of the study was related to immobile wood and therefore, wood classification had no observable impact on wood transport during our study.

Tracer retrieval rates were comparable to previous studies (Hassan and Bradley, 2017), between 75% in 2018 and 88% in 2017 (Table 2.2). The tracer population has a grain size distribution range of 47 – 110 mm with a median b axis diameter of 73 mm. This is larger than the D_{50} (53 mm) of the bed surface material, giving the majority of tracer sediments a Di / D_{50} of > 1 relative to bed material.

Maximum tracer transport distances in 2017, 2018, and 2019 were 109, 58, and 133 m respectively, with one clast travelling a cumulative 193 m downstream over the study period (Table 2.2). Of the 49% of cobbles that became mobile during our study 73% of these travelled beyond the seeded reach. The tracer transport distance probability density functions in 2017 and 2019 fit a gamma distribution, although the data from 2018 show a weaker gamma distribution fit that is interrupted between tracer transport distances of ~ 15 – 25 m (Figure 2.5). The associated power law exponent, β, is > 2 for all three years, representing superdiffusive behaviour, although the 2018 β value of 2.3 is close to the threshold of β = 2 for this characterisation, matching with the interruption seen in the gamma distribution fit. This is suspected to be caused by a clustering of tracers around a piece of large wood (the fallen tree) that entered the seeded reach in 2017 (Figure 2.6). This wood piece was initially transported downstream 20 m to its deposition location and was subsequently incorporated into the bed with increasing burial occurring every year. The increased density of tracer deposition in close proximity to this wood piece

gives an initial indication of the impact of large wood on bedload transport. This is further investigated using LMM analysis.

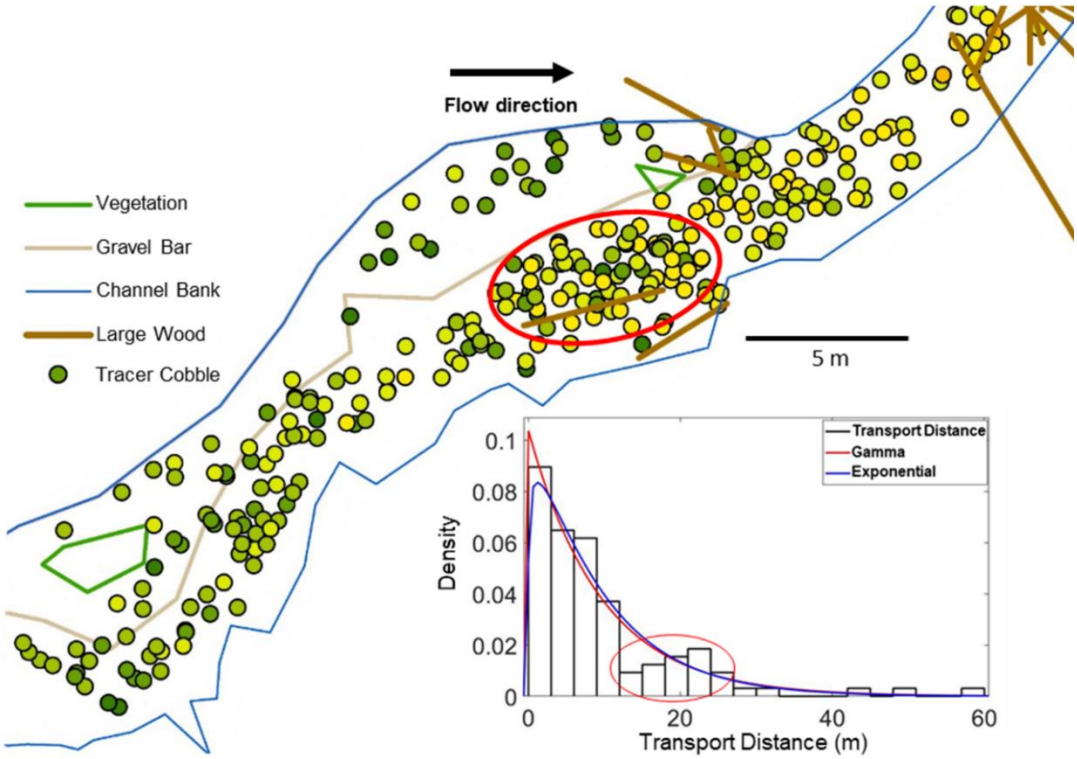

Figure 2.6: *Clustering of tracer sediments from 2018 data around a large wood piece within the seeded reach (as shown in Figure 2.1d). Note that the reversal of the trend in the probability density function calculated for 2018 (Figure 2.5) appears to match location of large wood piece (e.g., 15 – 25 m).*

2.4.2 Linear Mixed Modelling of Influence of Wood and Other Variables on Tracer Transport

Probability of Tracer Entrainment

Linear mixed modelling (LMM) provides a statistical assessment of the influence of large wood on sediment transport. LMM of sediment entrainment likelihood in relation to distance to wood of tracer entrainment location across all years is significant to at least a 99% level of confidence using the binomial modelling approach, with 2018 and 2019 reaching > 99.9% levels of confidence (Table 2.3). This confirms that proximity to wood pieces has a significant influence on entrainment likelihood, where tracers closer to wood pieces are less likely to be entrained. Clasts residing at > 5 m from wood are 37.5% more likely to be entrained than those < 1 m on average over the study (Figure 2.7).

The tracer b-axis and relative distance to channel thalweg were also investigated for their influence on entrainment likelihood. The influence of b-axis on entrainment likelihood was found to be significant in 2018 and 2019 with smaller tracers more likely to be entrained. Distance to channel thalweg was found to be significant in 2017 and 2019 with tracers closer to the channel thalweg more likely to be entrained. Clasts found at > 3 m from the thalweg are at least 55% and 27% less likely to move in 2017 and 2019 respectively (Table 2.3, Figure 2.7).

Table 2.3: *Linear mixed model output data for the likelihood of tracer sediment entrainment within the wooded reach, including the coefficient, standard error, z-value and p-value for all variables. P values indicated with a *, **, and *** represent a 95%, 99%, and 99.9% level of confidence respectively.*

2017 Binomial	**Coefficient**	**Standard Error**	**Z**	**P**
Distance to thalweg	-0.574	0.221	-2.603	0.0093**
Distance to wood	0.533	0.163	3.261	0.0111**
B – Axis	-0.015	0.015	-0.954	0.3398
2018 Binomial				
Distance to thalweg	-0.056	0.233	-0.240	0.81019
Distance to wood	0.664	0.155	4.293	<0.001***
B – Axis	-0.034	0.017	-2.012	0.0442*
2019 Binomial				
Distance to thalweg	-0.321	0.144	-2.227	0.026*
Distance to wood	0.458	0.012	3.950	<0.001***
B – Axis	-0.035	0.011	-3.313	0.0017**

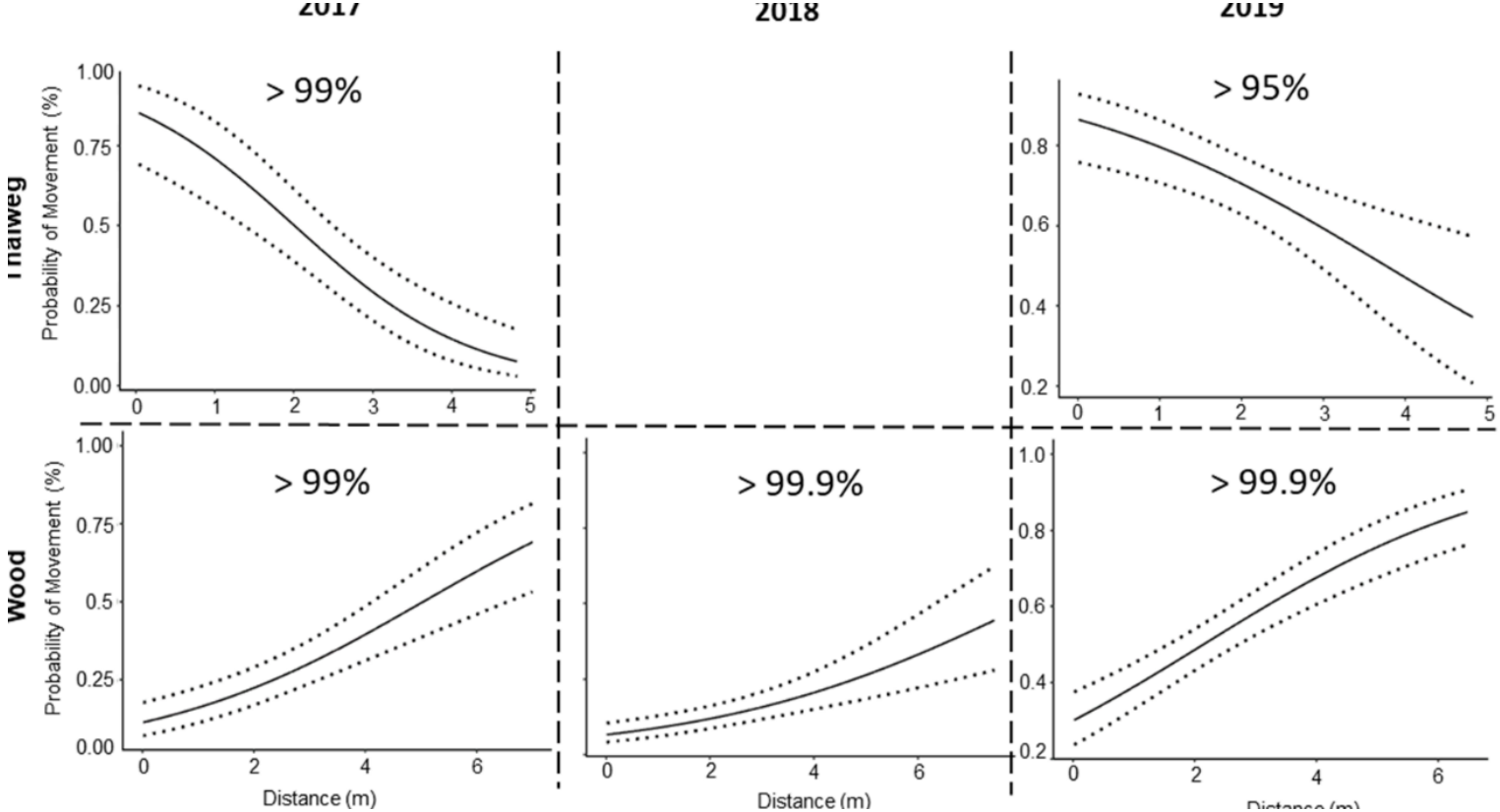

Figure 2.7: *Relative influence of distance to thalweg at point of tracer entrainment (top), and distance to wood at point of tracer entrainment (bottom) on probability of tracer movement each year based on the binomial LMM prediction frame, with upper and lower bounds represented by dotted lines. Significant (> 95%) relationships between probability of movement and wood distances, or probability of movement and thalweg distances are plotted. Relationships below a 95% level of confidence are omitted (e.g., 2018 thalweg).*

Influence of Entrainment Location on Tracer Transport Distance

A first LMM gamma model investigated the relationship between entrainment location variables and subsequent tracer transport distances. The influence of proximity to wood on tracer transport distance is significant to at least a 95% level of confidence in each year, with 2017 and 2018 reaching 99.9% levels of confidence (Table 2.4, Figure 2.8). The closer a tracer is located to wood when it is entrained, the shorter its subsequent transport distance. Unsurprisingly, shorter distances from the channel thalweg were also significant for longer rock transport distances in 2018 and 2019 with at least a 99% level of significance. The b-axis of tracers was significant every year to at least a 95% level of significance, where shorter b-axis size resulted in longer transport distances of tracers (Table 2.4).

Table 2.4: *Linear mixed model output data for the influence of distance to wood, thalweg, and b-axis on the transport distance of tracer sediments at the point of entrainment within the wooded reach, including the coefficient, standard error, z-value and p-value for all variables. P values indicated with a *, **, and *** represent a 95%, 99%, and 99.9% level of confidence respectively.*

2017 Entrainment	**Coefficient**	**Standard Error**	**Z**	**P**
Distance to thalweg	-0.100	0.058	-1.721	0.00878
Distance to wood	0.034	0.008	3.799	0.0002***
B – Axis	-0.019	0.007	-2.890	0.0046**
2018 Entrainment				
Distance to thalweg	-0.323	0.091	-3.633	<0.001***
Distance to wood	0.074	0.014	5.387	<0.001***
B – Axis	-0.020	0.009	-2.132	0.0369*
2019 Entrainment				
Distance to thalweg	-0.118	0.044	-2.720	0.0067**
Distance to wood	0.016	0.007	2.241	0.0258*
B – Axis	-0.021	0.004	-4.686	<0.001***

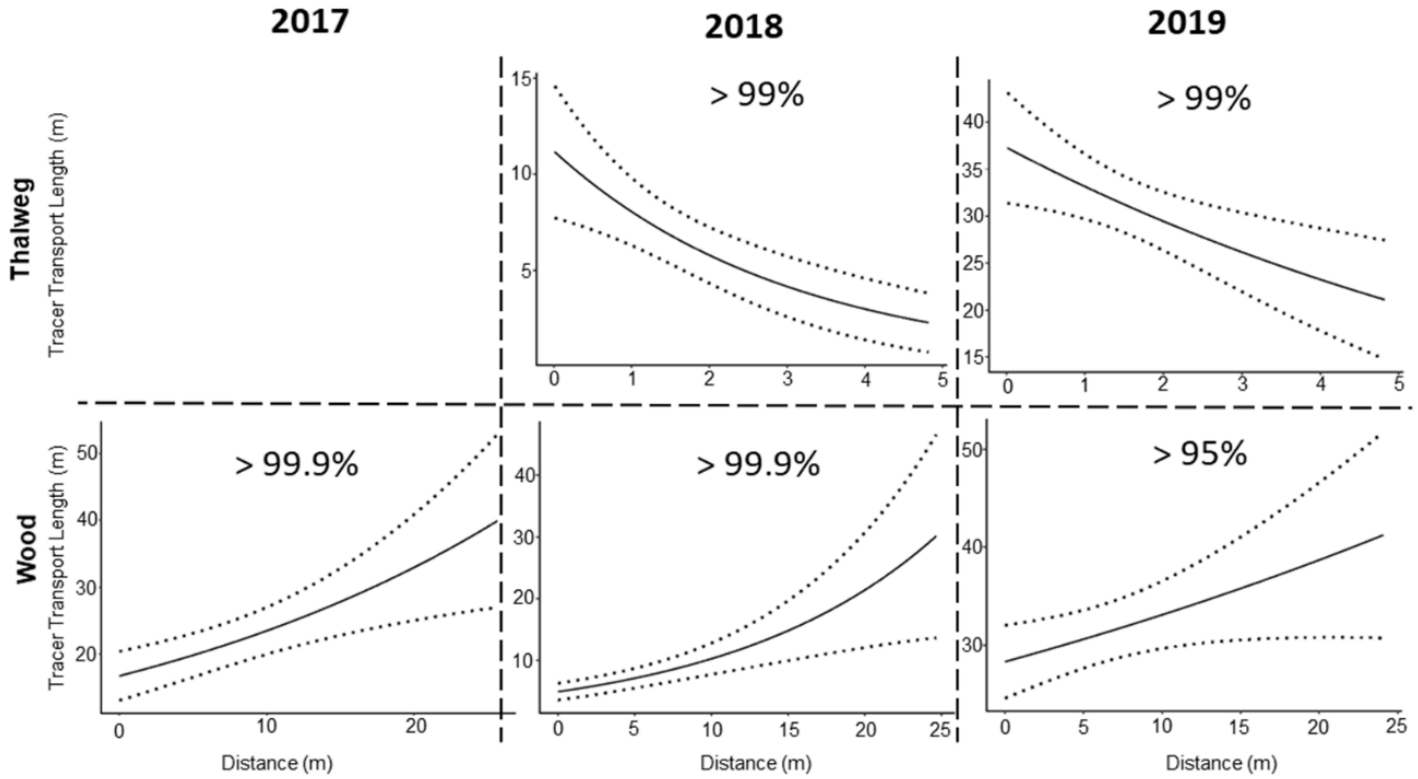

Figure 2.8: *Relative influence of distance to thalweg at point of tracer entrainment (top), and distance to wood at point of tracer entrainment (bottom) on tracer transport length each year based on the gamma LMM prediction frame, with upper and lower bounds represented by dotted lines. Significant (> 95%) years relationships between tracer transport length and wood distances, or tracer transport length and thalweg distances are plotted, whilst relationships below a 95% level of confidence are omitted (e.g., 2017 thalweg).*

Downstream Factors Influencing Rock Transport Distance

A final LMM gamma model investigated the relationships between location in which tracers were deposited and tracer transport distance prior to deposition. This analysis reveals a trapping influence of wood on sediment when comparing rock transport distance with depositional proximity to large wood (i.e., large wood is associated with a shortening in transport distance). This is significant in 2019 at a 95% level of significance (Table 2.5, Figure 2.9) The same relationship occurs in 2017 and 2018, though is not significant above a 95% level of confidence. Clasts deposited closest to the thalweg had the longest transport distances, with at least a 95% level of significance. Finally, the b-axis of tracers was significant every year to at least a 95% level of significance, with the largest clasts having shorter transport distances.

*Table 2.5: Linear mixed model output data for the influence of distance to wood, thalweg, and b-axis on the transport distance of tracer sediments at the point of deposition within the wooded reach, including the coefficient, standard error, z-value and p-value for all variables. P values indicated with a *, **, and *** represent a 95%, 99%, and 99.9% level of confidence respectively.*

2017 Deposition	**Coefficient**	**Standard Error**	**Z**	**P**
Distance to thalweg	-0.112	0.066	-1.752	0.0823
Distance to wood	-0.115	0.059	-1.936	0.0552
B – Axis	-0.018	0.007	-2.723	0.0074**
2018 Deposition				
Distance to thalweg	-0.220	0.105	-2.105	0.039*
Distance to wood	-0.130	0.104	-1.245	0.2177
B – Axis	-0.023	0.011	-2.013	0.0485*
2019 Deposition				
Distance to thalweg	-0.191	0.052	-3.690	<0.001***
Distance to wood	0.073	0.031	2.400	0.017*
B – Axis	-0.002	0.004	-4.149	<0.001***

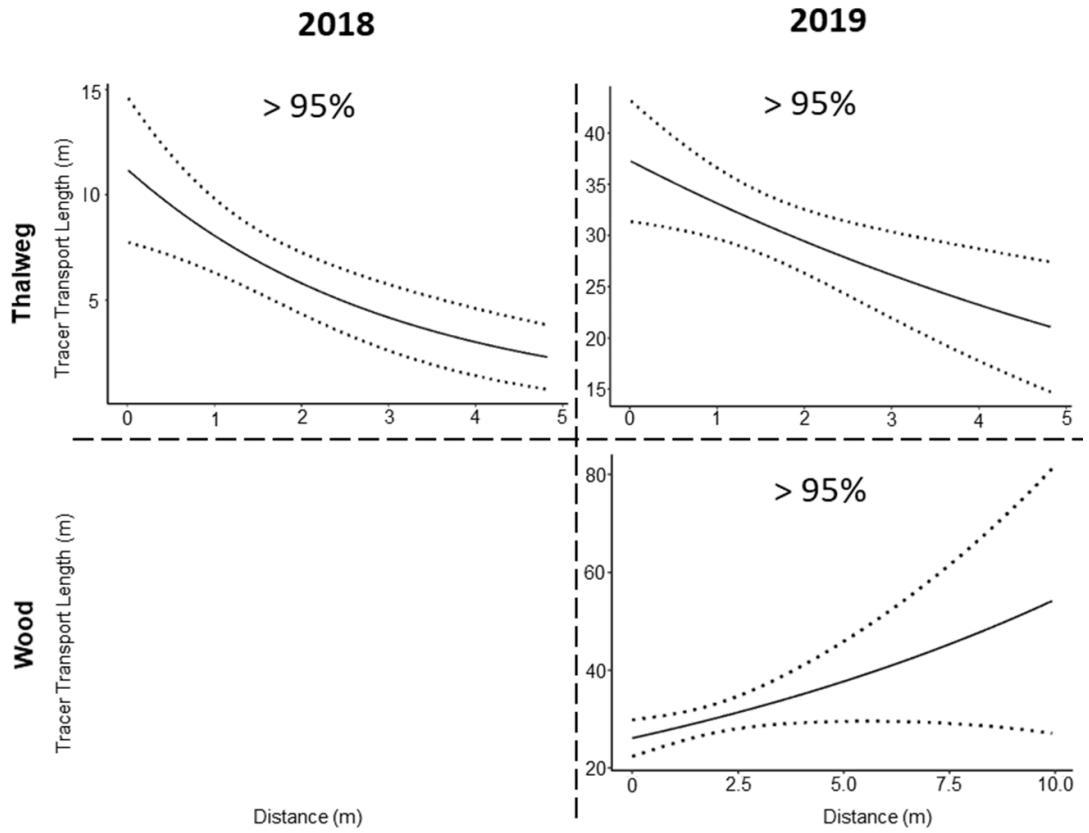

Figure 2.9: *Relative influence of distance to thalweg upon tracer deposition (top), and distance to wood upon tracer deposition (bottom) on tracer transport length each year based on the gamma LMM prediction frame, with upper and lower bounds represented by dotted lines. Significant (> 95%) years relationships between tracer transport length and wood distances, or tracer transport length and thalweg distances are plotted, whilst relationships below a 95% level of confidence are omitted (e.g., insignificant relationships in 2017).*

2.4.3 Making Predictions of Sediment Transport from Linear Mixed Models

Figure 2.8 displays the positive relationship between increased tracer transport distance and greater distances of tracers entrainment positions from wood for all years based on the gamma LMM output. This approach can be used to estimate a tracer's transport distance based on its initial distance from large wood before entrainment. For instance, in 2019, a clast

located approximately 5 m from a large wood piece will move downstream approximately 30 m streamwise on average, with transport distance increasing the further a tracer is entrained from large wood. Conversely, Figure 2.8 displays the inverse relationship between increasing tracer transport distance and increased tracer distance from channel thalweg at entrainment position. Additionally, Figure 2.7 displays the relatively negative correlation between the distance of the tracer from the thalweg and probability of entrainment. These models can both be used to estimate a tracer's transport distance and movement likelihood in relation to this variable. For example, a tracer 2 m from thalweg is predicted to have a transport distance of 6 m on average from its entrainment position.

While these estimations can give an approximate transport distance or probability of movement based on the single variable dataset, direct extrapolation from the graphs does not include the influence of other variables, limiting the applicability outside of the general correlation and relative influence of each variable. However, they do provide a clear indication that proximity to large wood, distance from channel thalweg, and sediments b-axis all play an influential role on transport behaviour.

2.5 Discussion

2.5.1 Influence of Wood on Stochastic Sediment Transport Dynamics

Stochastic sediment transport dynamics may be described with a combination of tracer transport distances and rest time distributions. We were unable to return to the field site to resurvey in 2020 due to Covid 19 restrictions on travel for two years, hence are limited to 3 years of resurvey data of the planned 5. In addition, implementation of active tracers (smart stones) with embedded accelerometers, gyroscope, and magnetometers (Gronz et al., 2016; Dost, 2020; Maniatis, 2020; Dini et al., 2021) was interrupted. Therefore, data was insufficient to build a distribution of particle rest times and thus fully characterize sediment transport behaviour. However, we have been able to build distributions of tracer

transport distances for the three resurvey years and observed deviations in these distributions as a result of wood-loading.

Qualitatively, large wood appears to alter the spatial deposition of sediments. One example observed was a dead tree that fell from the bank during runoff in 2017, floating roughly 20 m and being deposited in the downstream end of the seeded reach. Sediments were subsequently observed accumulating around the wood piece, with ramping of sediments up the root wad in 2018 (Figure 2.1d) and progressively incorporating the wood further into the bed by 2019. Additionally, our RFID tracer sediments were deposited more densely in close proximity to the wood piece in 2018 and 2019 comparatively to the rest of the seeded reach (Figure 2.7), which displays otherwise similar morphological characteristics. In addition, tracers were observed to accumulate in the pools of log steps (e.g., Figure 2.1e), supporting Wohl and Scott's (2017) finding that rivers with wood see an increase in pool sediment volume, alongside accumulating behind log steps forming a ramp (e.g., Figure 2.1f).

The tracer transport distance probability density functions for 2017 and 2019 in Figure 2.5 appear to match well with the overlain expected gamma distribution (Bradley and Tucker, 2012). Additionally, the associated exceedance probability displays the expected super diffusive behaviour (e.g., $\beta > 2$), although the 2018 plot breaks from this trend, and its β value of 2.3 is closer to the super - sub diffusive threshold of $\beta = 2$. This change could suggest a quantifiable influence of wood is observable, at least in 2018, where lower shear stress due to a more moderate flow year (Figure 2.3) increases wood's impact on tracer movement as the blocking effect is more difficult to overcome. However, these changes could be attributed to alterations in the vertical mixing of sediments (Hassan *et al.,* 2013). While channel morphology's impact on transport distributions could offer another explanation (e.g., Pyrce and Ashmore, 2003), the visual and recorded observations of clustering sediments around the large wood piece located within the seeded reach (Figure 2.6) supports wood as a particularly important factor for the disruption in transport distributions.

Whilst the influence of wood on the distribution of tracer transport distance is not definitive, LMM modelling helped to demonstrate the trapping influence of wood more clearly. LMM modelling in 2019 (Table 2.5, Figure 2.9) showed that tracers deposited closer to wood had shortened transport distances prior to being deposited, suggesting a trapping effect. The cause of trapping and reduced transport distances is likely related to wood loading increasing roughness within the fluvial system (Buffington and Montgomery, 1999) and its impact on local hydraulic conditions (Matheson et al., 2017). This agrees with other sediment transport investigations where roughness was found to be a key influencing factor on reducing transport distances of sediments (e.g., Roth *et al*., 2020).

The lack of statistical significance for the influence of wood on shortening rock transport distances in 2017 and 2018 is potentially related to the lack of wood found in the areas 1 to 10 m downstream of the seeded reach (Figure 2.1), where the majority of tracers were deposited during the first two years of the study. By 2019 the number of tracers deposited within the wooded reach is greatly increased, alongside more tracers interacting with wood throughout the length of the study area as seen in Figure 2.1a. This resulted in a population of tracers large enough to demonstrate a significant interaction, and positive correlation (e.g., Figure 2.9), between deposition location of tracers in relation to wood and transport distance of tracers.

Results from the binomial LMM analysis demonstrate how the presence of wood in St. Louis Creek is reducing entrainment likelihood of sediment (Table 2.3, Figure 2.7). This result is significant every year, however there is a slight decrease in significance in 2019. We suspect that the higher proportion of tracer sediments moved in 2019, resulting from the higher flow rates and subsequent stream power, could lessen the impact wood has on entrainment, where higher shear stress from stronger flows negates the limiting effect wood has on sediment entrainment likelihood. In addition, many immobile clasts from previous years were entrained by reworking of the bed during higher flow rates, independent of the spatial location of wood pieces. Despite this, these results agree with the findings of previous studies that an abundance of wood causes fluvial systems to

retain a greater proportion of sediment in storage, in addition to reducing overall sediment transport rates (Buffington & Montgomery, 1999; Montgomery *et al*., 2003; Wohl and Scott, 2017).

The LMM gamma model showed that the influence of distance to wood on subsequent tracer transport distance is significant for all years (Table 2.4, Figure 2.7), with a 99.9% degree of certainty in 2017 and 2018, dropping to 95% in 2019. This reduction in statistical significance is likely related to the proposed reduction of the influence of large wood in 2019 due to greater flow rates, where wood has reduced impact on tracers due to higher water levels causing tracers to more easily pass over wood pieces. Additionally, the accumulation of sediments along the upstream side of pre-existing large wood may have resulted in an easier passage of logs by 2019. Finally, it is possible for large wood to float during higher periods of runoff (Wohl and Scott, 2017), which may have allowed a larger proportion of particles to pass underneath in 2019 given the relatively higher flow rates that year.

Additional data would be needed to further assess the influence of wood on transport distance distributions, but this initial data indicates that wood is having a disruptive effect (Figure 2.6). The potential for prediction of sediment transport distance and entrainment likelihood shown in Figure 2.8 and Figure 2.9 is an example of how linear mixed modelling could be used to predict sediment transport in such settings. This study exemplifies how distances to wood from either depositional, or entrainment location can be used to predict sediment transport distances with a large enough population of tracers, while accounting for other influential variables such as distance to thalweg, and size of surveyed tracers.

2.5.2 Other Controls on Particle Entrainment

Key variables identified to significantly influence particle entrainment with the binomial LMM approach included particle size (represented by b-axis in this study). This agreed with conventional understanding of the correlation between sediment size and entrainment likelihood (e.g.,

Ashworth and Ferguson, 1989; Wilcock and Crowe, 2003), with smaller grain sizes having a greater probability of entrainment. This suggests, in our study area, that the role of protrusion on entrainment likelihood (e.g., Fenton & Abbott 1977; Hodge *et al*., 2020) is minimal, assuming that smaller grain sizes protrude less but yet were more likely to be entrained in our sample of pebble – cobble sized tracer sediments. Additionally, the distance of tracer sediments to channel thalweg has an influential role on entrainment likelihood, with sediments with closer proximity to channel thalweg having higher entrainment likelihoods, due to increased shear in the thalweg (Petit *et al*., 1987).

While b-axis size was found to be significant in influencing entrainment likelihood in 2018 and 2019, the results from the 2017 output were not significant (Table 2.4). This is potentially related to the 'hypermobility' of sediments in the first year of the study, where sediments are not naturally incorporated into the channel bed (Bradley and Tucker, 2012). A caveat to b-axis tracer results would be that the D_{50} value of the tracer sediments (73 mm) is larger than that of the bed material (53 mm), where the $D_{50\ tracer} / D_{50\ bed} = 1.38$, potentially making them unrepresentative of the total sediment population of the stream. The larger D_{50} of tracer sediments were unavoidable due to the size of the embedded RFID tags requiring clasts large enough to drill. However, results likely well characterise the pebble – cobble proportion of sediments transport behaviour in gravel bed streams.

2.5.3 Limitations and Future Work

While multiple researchers have used RFID technology in tagging coarse particle transport, there is a lack of a consistency in the methodologies applied (e.g., standard procedures for tagging and detection methods). This may lead to differences in retrieval rates and detection location accuracy due to experimental setup, rather than environmental conditions. Therefore, future research should adopt a standardized approach in the use of RFID equipment, the depth of tag embedding, and the placement of tracers in order to reduce operational interference.

Retrieval rates of tracers consistently stayed above 75% every year and even increased from 2018 to 2019, demonstrating the success and longevity of the approach, even in complex environments such as wood loaded rivers. For instance, Liébault *et al.* (2012) and Olinde & Johnson's (2015) recovery rates decreased annually over their studies from 78%, 45%, 25% and 83%, 50% respectively, with burial being highlighted as a particular issue. This highlights the effectiveness of the RFID scanning technique implemented, as multiple tracers which were buried without visual confirmation were subsequently identified and located.

While these studies suggest a poor recovery rate, the technique is still relatively new, with developments in the technology ongoing. The use of ultra-high frequency tags (Cassel *et al*., 2017; Brousse et al., 2020; Cassel et al., 2021) are overcoming many of the limitations with traditional (low frequency) PIT tags, such as difficulties separating signals and short detection ranges (e.g., Lamarre *et al*., 2005). This may allow tracer studies to occur in previously inaccessible environments, such as wide braided rivers.

Including stream power directly in the LMM analysis for individual clasts was beyond the scope of this study due to uncertainties in subdividing the reach into multiple distinct sections with justifiable stream power estimates. Only including clasts that have entered the wooded reach in the LMM accounts for the change in average slope and channel width between the two reaches, but future work would require more detailed measures of driving force to accurately assess forces acting on individual clasts. Despite this, we were still able to determine the influence of large wood on tracer transport, probably because the critical stream power threshold was exceeded throughout the study reach. Any relatively small changes in stream power between clasts within the wooded reach were unable to mask the impact of wood on sediment transport dynamics.

Deploying subsequently developed smart stone tracers could have helped determine relationships between flow rate and entrainment thresholds. Although unfortunately this was not possible due to travel restrictions

surrounding the covid-19 pandemic from 2020 onwards, preventing further visits to the field site.

2.6 Conclusions

We conducted a RFID tracer study in a wood-loaded, alpine stream in Colorado USA over three years to investigate the influence of large wood on stochastic sediment transport dynamics. We investigated the influence of wood on aspects of sediment transport, including transport distance and entrainment probability, and used the novel approach of linear mixed modelling to untangle the influence of wood from other controls and build predictive models of sediment transport. Over three years, the tracer transport distance frequency distributions of tracers were found to match previous tracer research, with an expected gamma distribution and dispersion characteristics of sediments remaining superdiffusive, as indicated by a power law exponent on the tail of the distribution, $\beta > 2$ (e.g., Bradley and Tucker, 2012). However, flattening of the power law tail of the transport distance distribution in 2018 (Figure 2.6), is suspected to result from the interception of tracers by a large wood piece during lower flows, bringing it closer to more subdiffusive behaviour, i.e. with a $\beta < 2$. The LMM results support this clustering effect. It was found that large wood trapped sediments and forced premature deposition and reduced transport distances. Furthermore, tracers with a closer proximity to large wood had a significantly reduced likelihood of entrainment, in addition to smaller transport distances, compared to tracers entrained from wood free areas. Meanwhile, as expected, LMM found that both tracer transport distance and entrainment likelihood both decrease with increasing distance of tracers from the channel thalweg. Additionally, LMM found that smaller b-axis resulted in greater likelihood of entrainment and subsequent transport distances. These results indicate that streams undergoing increased wood loading would experience a significant reduction in entrainment and subsequent transport distances of cobble – pebble sized clasts in alpine environments.

The approaches implemented in this research can help inform future river management schemes by providing a methodology to determine the effectiveness, and potential side effects, of introducing engineered large wood structures (e.g., log jams) in NFM practices. The collection of additional data sets, with different volumes and configurations of large wood under a broader range of grain size and discharge regimes, is necessary to determine if the observations reported in this study are consistent. This would allow for a further understanding of grain-scale bedload transport behaviour in wooded reaches.

References

Ancey, C. & Bohorquez, P. (2018) Stochastic streams bedload transport in mountain, *E3S Web of Conferences,* 40, 05046.

Ancey, C., Bohorquez, P., Bardou, E. (2014) Sediment Transport in Mountain Rivers, *ERCOFTAC Bulletin,* 100, 37-52.

Ancey, C., Davison, A., Bohm, T., Jodeau, M., Frey, P. (2008) Entrainment and motion of coarse particles in a shallow water stream down a steep slope, *Journal of Fluid Mechanics*., 595, 83–114.

Arnaud, F., Piégay, H., Vaudor, L., Bultingaire, L. and Fantino, G., 2015. Technical specifications of low-frequency radio identification bedload tracking from field experiments: Differences in antennas, tags and operators. *Geomorphology*, 238, 37-46.

Ashworth, P.J., Ferguson, R.I. (1989) Size-selective entrainment of bed load in gravel bed streams. *Water resources Research.* 25(4), 627-634.

Bates, D., Mächler, M., Bolker, B., & Walker, S. (2015). Fitting Linear Mixed-Effects Models Using lme4*. Journal of Statistical Software*, 67(1). doi:10.18637/jss.v067.i01

Bendix J. and Cowell, M. (2010) Fire, floods and woody debris: Interactions between biotic and geomorphic processes, *Geomorphology*, 116(3-4), 297-304.

Bennett, S. J., Ghaneeizad, S. M., Gallisdorfer, M. S., Cai, D., Atkinson, J. F., Simon, A., Langendon, E. J. (2015) Flow, turbulence, and drag associated with engineered log jams in a fixed-bed experimental channel, *Geomorphology*, 248 1, 172-184.

Bradley, N. & Tucker, G. (2012) Measuring gravel transport and dispersion in a mountain river using passive radio tracers, *Earth Surface Processes and Landforms,* 37(10), 1034-1045.

Bradley, N. (2017) Direct Observation of Heavy-Tailed Storage Times of Bed Load Tracer Particles Causing Anomalous Superdiffusion, *Geophysical Research Letters,* 44(24), 12,227-12,235.

Brousse, G., Arnaud-Fassetta, G., Liébault, F., Bertrand, M., Melun, G., Loire, R., & Borgniet, L. (2020). Channel response to sediment replenishment in a large gravel-bed river: The case of the Saint-Sauveur dam in the Buëch River (Southern Alps, France). *River Research and Applications*, *36*(6), 880-893.

Buffington, J. M., Montgomery, D. R. (1999) Effects of sediment supply on surface textures of gravel-bed rivers, *Water Resources Research,* 35, 3523 – 3530.

Cassel, M., Navratil, O., Perret, F., & Piégay, H. (2021). The e-RFIDuino: An Arduino-based RFID environmental station to monitor mobile tags. *HardwareX*, 10.

Cassel, M., Piégay, H., Fantino, G., Lejot, J., Bultingaire, L., Michel, K., Perret, F. (2020) Comparison of ground-based and UAV a-UHF artificial tracer mobility monitoring methods on a braided river, *Earth Surface Processes and Landforms,* 45, 1123 – 1140.

Chapuis, M., Bright, C.J., Hufnagel, J. and MacVicar, B., 2014. Detection ranges and uncertainty of passive Radio Frequency Identification (RFID) transponders for sediment tracking in gravel rivers and coastal environments. *Earth Surface Processes and Landforms*, 39(15), 2109-2120.

Clauset, A., Shalizi, C., Newman, M.E.J. (2009) Power-law distributions in empirical data, *SIAM Review*, 51(4), 661-703.

Cui, Y., Parker, G., Lisle, T. E., Gott, J., Hansler-Ball, M. E., Pizzuto, J. E., Allmendingern N. E., & Reed, J. M. (2003).

Sediment pulses in mountain rivers: 1. Experiments. *Water Resources Research*, 39(9).Dhont, B., and Ancey, C. (2018) Are Bedload Transport Pulses in Gravel Bed Rivers Created by Bar Migration or Sediment Waves?. *Geophysical Research Letters.* 45(11). 5501-5508.

Dini, B., Bennett, G., Franco, A., Whitworth, M., Cook, K., Senn, A., Reynolds, J., (2021) Development of smart boulders to monitor *mass*

movements via the Internet of Things: A pilot study in Nepal, Earth Surface Dynamics, *Earth Surface Dynamics*, 9, 295–315,

Dost, B., Gronz, O., Casper, M., Krein, A. (2020) The Potential of Smartstone Probes in Landslide Experiments: How to Read Motion Data. *Natural Hazards and Earth System Sciences.* 20, 3501–3519, https://doi.org/10.5194/nhess-20-3501-2020.

Dunnink, J., Hartley, R., Rutina, L., Alves, J., & Franco, A. (2019) A socio-ecological landscape analysis of human–wildlife conflict in northern Botswana. *Oryx,* 1-9. doi:10.1017/S0030605318001394

East, A.E., Pess, G.R., Bountry, J.A., Magirl, C.S., Ritchie, A.C., Logan, J.B., Randle, T.J., Mastin, M.C., Minear, J.T., Duda, J.J., Liermann, M.C., McHenry, M.L., Beechie, T.J., Shafroth, P.B. (2015) Large-scale dam removal on the Elwha River, Washington, USA: River channel and floodplain geomorphic change. *Geomorphology* 228, 765–786.

Fenton, J. D., & Abbott, J. E. (1977). Initial movement of grains on a stream bed: The effect of relative protrusion. *Proceedings of the Royal Society of London. A. Mathematical and Physical Sciences*, *352*(1671), 523-537.

Ferguson, R. & Wathen, S. (1998) Tracer-pebble movement along a concave river profile: virtual velocity in relation to grain size and shear stress. *Water Resources Research,* 34, 2031–2038.

Ferguson, R., Church, M., Rennie, C., Venditti, G. (2015) Reconstructing a sediment pulse: Modeling the effect of placer mining on Fraser River, Canada*. Journal of Geophysical Research: Earth Surface*, 120, 1436–1454.

Ferguson, R.I., (2005). Estimating critical stream power for bedload transport calculations in gravel-bed rivers. Geomorphology, 70(1-2), 33-41.

Finkenzeller, K. (2010). RFID handbook: fundamentals and applications in contactless smart cards, radio frequency identification and near-field communication. John wiley & sons.

Floyd, R.E. (2015) RFID in Animal-Tracking Applications, *IEEE,* 5, 32-33.

Gaeuman, D., Stewart, R., Schmandt, B., Pryor, C. (2017) Geomorphic Response to Gravel Augmentation and High-Flow Dam Release in the Trinity River*. Earth Surface Processes and Landforms.* 42(15), 2523–2540.

Gippel C.J., O'Neill I.C., Finlayson B.L., Schnatz I. (1996) Hydraulic guidelines for the re-introduction and management of large woody debris in lowland rivers, *Regulated Rivers: Research & Management,* 12, 223–236.

Golly A., Turowski J.M., Badoux A., Hovius N. (2019) Testing models of step formation against observations of channel steps in a steep mountain stream, *Earth Surface Processes and Landforms,* 44, 1390-1406.

Grabowski, R., Gurnell, A., Burgess-gamble, L., England, J., Holland, D., Klaar, M., Morrissey, I., Uttley, C., Wharton, G. (2019) The current state of the use of large wood in river restoration and management. *Water and Environment Journal.* 33(3), 366-377.

Green, G.N. (1992) The Digital Geologic Map of Colorado in ARC/INFO Format. Open-File Report 92-0507, U.S. Geol Sur, Denver, CO. available on-line (04/08/2020): http://pubs.usgs.gov/of/1992/ofr-92-0507/.

Gronz, O., Hiller, H., Wirtz, S., Becker, K., Iserloh, T., Seeger, M., Brings, C., Aberle, J., Casper, M., Ries, J. (2016) Smartstones: A small 9-axis sensor implanted in stones to track their movements. *CATENA* 142, 245-251.

Habersack, H. (2001) Radio-tracking gravel particles in a large braided river in New Zealand: a field test of the stochastic theory of bed load transport proposed by Einstein. *Hydrological Processes* 15, 377–391.

Hassan, M. A. and D. N. Bradley (2017). Geomorphic controls on tracer particle dispersion in gravel-bed rivers. Gravel-Bed Rivers: Process and Disasters: 159-184.

Hassan, M.A. & Ergenzinger, P. (2003) Use of tracers in fluvial geomorphology. In Tools in Fluvial Geomorphology, Kondolf GM, Piégay H (eds). John Wiley & Sons: Chichester, 397–423.

Hassan, M.A., Church, M. & Schick, A.P. (1991) Distance of movement of coarse particles in gravel bed streams*. Water Resources Research*, 27, 503–511.

Hassan, M.A., Voepel, H., Schumer, R., Parker, G., Fraccarollo, L. (2013) Displacement characteristics of coarse fluvial bed sediment. Journal of Geophysical Research: Earth Surface, 118, 155-165.

Helley, E. J., & Smith, W. (1971) Development and Calibration of a Pressure-Difference Bedload Sampler. Open-File, USGS, *Water Resources Division*, Menlo Park, California.

Hodge, R., Voepel, H., Leyland, J., Sear, D., Ahmed, S. (2020) X-ray computed tomography reveals that grain protrusion controls critical shear stress for entrainment of fluvial gravels, *Geology,* 48(2): 149–153.

https://doi.org/10.5194/esurf-9-295-2021

Hubbell, D. W. (1964) Apparatus and Techniques for Measuring Bedload. U.S. Geological Survey, *Water Supply Paper,* 1748.

Keller, E.A. (1970) Bedload movement experiments, Dry Creek, California. *Journal of Sedimentary Petrology*, 40, 1339-1344.

Kelsey, H, Lamberson R, Madej M. (1987) Stochastic model for the long-term transport of stored sediment in a river channel. *Water Resources Research.* 23. 1738–1750.

Kinzel, P. (2009) *Channel Morphology and Bed Sediment Characteristics Before and After Habitat Enhancement Activities in the Uridil Property, Platte River, Nebraska, Water Years 2005–2008*, USGS Open-File Report 2009–1147.

Klaar, M.J., Hill, D.F., Maddock, I., Milner, A.M. (2011) Interactions between instream wood and hydrogeomorphic development within recently deglaciated streams in Glacier Bay National Park, Alaska. *Geomorphology* 130, 208–220.

Lajeunesse, E., Devauchelle, O. & James, F. (2018) Advection and dispersion of bed load tracers. *Earth Surface Dynamics*, **6**(2), 389–399.

Lamarre, H., MacVicar, B. and Roy, A.G., 2005. Using passive integrated transponder (PIT) tags to investigate sediment transport in gravel-bed rivers. *Journal of Sedimentary Research*, 75(4), 736-741.

Lane, P. and Sheridan, G. (2002) Impact of an unsealed forest road stream crossing: waterquality and sediment sources. *Hydrological Processes.* 16, 2599 –2612.

Langford T., Langford J., Hawkins S. (2012) Conflicting effects of woody debris on stream fish populations: implications for management. *Freshwater Biology,* 57, 1096–1111.

Laronne, J. & Carson, M. (1976) Interrelationships between bed morphology and bed-material transport for a small, gravel-bed channel. *Sedimentology*, 23, 67–85.

Legleiter, J.C. & Kyriakidis, P.C. (2006) Forward and Inverse Transformations between Cartesian and Channel-fitted Coordinate Systems for Meandering Rivers, *Mathematical Geology,* 38(8), 927-958.

Lehpamer, H. (2012). RFID Design Principles (2nd ed.). Norwood, MA: Artech House.

Liébault, F., Bellot, H., Chapuis, M., Klotz, S., Deschâtres, M. (2011) Bedload tracing in a high-sediment-load mountain stream. *Earth Surface Processes and Landforms*. 37 (4), 385-399.

MacVicar, B. J. and Papangelakis, E., (2022) Lost and found: Maximizing the information from a series of bedload tracer surveys. *Earth Surface Processes and Landforms*, 47(2), 399-408.

Malmon D. V. (2005) Influence of sediment storage on downstream delivery of contaminated sediment. *Water Resources Research*. 41.

Malmon, D. V., Dunne, T., & Reneau, S. (2003) Stochastic theory of particle trajectories through alluvial valley floors. *The Journal of Geology*, 111(5), 525–542.

Maniatis, G., Hoey, T., Hodge, H., Rickenmann, D., Badoux, A. (2020) Inertial drag and lift forces for coarse grains on rough alluvial beds

measured using in-grain accelerometers. *Earth Surface Dynamics.* 8, 1067–1099.

Matheson, A., Thoms, M., & Reid, M. (2017). Does reintroducing large wood influence the hydraulic landscape of a lowland river system?. Geomorphology, 292, 128-141.

Martin, R. L ., Jerolmack, D. J., Schumer, R. (2012) The physical basis for anomalous diffusion in bed load transport. *Journal of Geophysical Research Earth Surface*. 117.

McDermott Long, O., Warren, R., Price, J., Brereton, T.M., Botham, M.S. and Franco, A.M., (2017) Sensitivity of UK butterflies to local climatic extremes: which life stages are most at risk?. *Journal of Animal Ecology*, 86(1), 108-116.

McNamara, J.P., Borden, C. (2004) Observations on the movement of coarse gravel using implanted motion-sensing radio transmitters. *Hydrological Processes* 18, 1871–1884.

Montgomery, D., Collins, B., Buffington, J., Abbe, T. (2003) Geomorphic effects of wood in rivers. *The Ecology and Management of Wood in World Rivers, Symposium.* 37, 21-47.

Nichols, M. H., (2004) A radio frequency identification system for monitoring coarse sediment particle displacement. *Applied Engineering Agriculture* 20, 783–787.

Nikora, V., H. Habersack, T. Huber and I. McEwan (2002). "On bed particle diffusion in gravel bed flows under weak bed load transport." Water Resources Research 38(6): 17-11-17-19.

Olinde, L. & Johnson, J. (2015) Using RFID and accelerometer-embedded tracers to measure probabilities of bed load transport, step lengths, and rest times in a mountain stream, Water Resources Research, 51, 7572-7589.

Oregon RFID, 2021, "Oregon RFID: Fish and Wildlife Tracking PIT Tags" https://www.oregonrfid.com/products/hdx-long-range-readers/mobile-reader-kit/

Petit, F. (1987) The relationship between shear stress and the shaping of the bed of a pebble-Ioaded river (La Rulles-Ardenne). Catena 14(5), 453-468.

Petit, F., Gob, F., Houbrechts, G. and Assani, A.A., 2005. Critical specific stream power in gravel-bed rivers. Geomorphology, 69(1-4), 92-101.

Pickup, G., Higgins, R., Grant I. (1983) Modelling sediment transport as a moving wave — The transfer and deposition of mining waste. *Journal of Hydrology.* 60(1–4), 281-301.

Powell, J.A., Logan, J.A. (2005) Insect seasonality: circle map analysis of temperature- driven life cycles. *Theoretical Population Biology*, 67, 161–179.

Pyrce, R. S. and P. E. Ashmore (2003). "Particle path length distributions in meandering gravel-bed streams: Results from physical models." Earth Surface Processes and Landforms 28(9): 951-966.

Raffa, K.F, Aukema, B.H, Bentz, B.J, Carroll, A.L, Hicke, J. A, Turner, M.G, Romme, W.H. (2008) Cross-scale Drivers of Natural Disturbances Prone to Anthropogenic Amplification: The Dynamics of Bark Beetle Eruptions, *BioScience,* 56(6), 501-517.

Reneau, S. L., Drakos, P. G., Katzman, D., Malmon, D. V., McDonald, E. V., & Ryti, R. T. (2004) Geomorphic controls on contaminant distribution along an ephemeral stream. *Earth Surface Processes and Landforms*, 29, 1209–1223.

Roth, D. L., Doane, T. H., Roering, J. J., Furbish, D. J. and Zettler-Mann, A. (2020). Particle motion on burned and vegetated hillslopes. *PNAS*. 117(41). 25335-25343.

Ryan, S., Bishop, E.L., Daniels, J.M. (2014) Influence of large wood on channel morphology and sediment storage in headwater mountain streams, Fraser Experimental Forest, Colorado, *Geomorphology*, 217, 73-88.

Schenk, E. R., Moulin, B., Hupp C. R. Richte, J.M. (2013) Large wood budget and transport dynamics on a large river using radio telemetry, *Earth Surface Processes and Landforms.* 39 (4), 487-498.

Schneider, J., Hegglin, R., Meier, S., Turowski, J. M., Nitsche, M., & Rickenmann, D. (2010). Studying sediment transport in mountain rivers by mobile and stationary RFID antennas. *River flow 2010*, 1723-1730.

Sear, D. A. (1994). River restoration and geomorphology. *Aquatic Conservation: Marine and Freshwater Ecosystems*, *4*(2), 169-177.

Sear, D. A., Lee, M. W. E., Carling, P. A., Oakey, R. J., & Collins, M. B. (2003). An assessment of the accuracy of the Spatial Integration Method (SIM) for estimating coarse bed load transport in gravel-bedded streams using tracers. *Iahs Publication*, 164-171.

Slater, L. J., Singer, M. B., Kirchner, J. W. (2015) Hydrologic versus geomorphic drivers of trends in flood hazard. *Geophysical Research Letters,* 42, 370-376.

Steeb, N., Rickenmann, D., Badoux, A., Rickli, C. and Waldner, P., 2017. Large wood recruitment processes and transported volumes in Swiss mountain streams during the extreme flood of August 2005. *Geomorphology,* 279, 112-127.

Sutherland, D., Ball, M., Hilton, S., Lisle, T. (2002) Evolution of a landslide-induced sediment wave in the Navarro River, California. *Geological Society of America Bulletin*, 114(8), 1036–1048.

Umazano, A., Melchor, R. (2020) Volcaniclastic sedimentation influenced by logjam breakups? An example from the Blanco River, Chile. *Journal of South American Earth Sciences.* 98.

Weeks, E., Swinney, H. (1998) Anomalous diffusion resulting from strongly asymmetric random walks. *Physical Review E,* 57(5), 4915–4920.

Wilcock, P. R., & Crowe, J. C. (2003). Surface-based transport model for mixed-size sediment. Journal of hydraulic engineering, 129(2), 120-128.

Wohl, E., Cenderelli, D.A., Dwire, K.A., Ryan-Burkett, S.E., Young, M.K., Fausch, K.D. (2010) Large in-stream wood studies: a call for common metrics. Earth Surface Processes and Landforms. 35, 618–625.

Wohl, E., Scott, D. (2017). Wood and sediment storage and dynamics in river corridors. *Earth Surface Processes and Landforms.* 42, 5-23.

CHAPTER 3

3 Production and Development of LoRaWAN Smart Stones

3.0.1 Chapter Overview

The development of a smart autonomous observing system was an integral aspect of this research as funding was provided by the NEXUSS CDT, which prioritised novel technological approaches to environmental science challenges. Therefore, this chapter describes the process of designing, producing, and the initial stress testing of the LoRaWAN enabled smart stone tracers. It covers the manufacture of artificial sediment housing, from silicone moulding of existing sediments, to concrete production and design. It also covers the capabilities of the Miromico sensor module embedded in the smart stones, alongside the development and optimisations of device firmware over time. Furthermore, the results from battery longevity experiments and gateway range testing are also described.

3.1 Introduction

Using passive RFID tracers, it was possible to quantify the relative influence of the proximity to wood on entrainment, deposition likelihoods, and tracer step lengths. This is pivotal in furthering our understanding of the consequences of large woody debris in rivers, helping to inform its installation as a part of NFM techniques. The work described in chapter 2 built upon a growing literature investigating grain scale transport characteristics in fluvial systems (e.g., Nichols 2004; Bradley & Tucker 2012; MacVicar & Papangelakis, 2022). However, the requirement for manual relocation of tagged sediments limited data collection to once per annum at St. Louis Creek. Therefore, calculating the precise rest times of sediments, and capturing detailed transport behaviour was not possible. Furthermore, flow rates and entrainment likelihood could only be compared using the recorded peak flow values, with the exact timing of incipient motion of sediments remaining unknown.

To better characterise the bed load transport of sediments, and the role of wood in influencing movement, real-time data collection is required. With advances in MEMS, active IMU tracers (e.g., Gronz et al., 2016), and the integration of Internet of Things technological approaches in environmental science (Hart & Martinez 2015), I aimed to develop smart stone tracers which could monitor transport in real time remotely. It was hoped that these LoRaWAN enabled smart stones would overcome the limitations of infrequent data collection observed in RFID studies, and by integrating the devices into a wider network of environmental sensors, fluvial conditions at deployment sites could be continuously monitored. This would facilitate a greater understanding of the relationships between individual grain motions and environmental conditions, providing valuable datasets for both researchers interested in the grain-scale dynamics of sediment transport, and for informing hazard risk monitoring.

3.1.2 The SENSUM Project

The smart SENSing of landscapes Undergoing hazardous hydrogeologic Movement, or SENSUM, is a UKRI funded project under the Constructing a Digital Environment programme (NE/V003402/1) (Roskilly *et al.,* 2022). The project involves the use of integrated technological approaches to tackle challenges related to monitoring natural hazards. SENSUM is taking advantage of advances in wireless sensor networks, and the development of Internet of Things technologies, as well as the ability to embed microelectronic devices within the natural environment. Hazards from landslides and flooding are the primary focus of the SENSUM project, with smart tracking devices being used to monitor large woody debris and boulders at high-risk sites. Sensor networks are also being tested for their feasibility as early warning systems.

My research, focused on tracing the bedload transport of fluvial sediments, was a natural fit for collaboration alongside the SENSUM project. As many of the technological approaches applied, such as continuous long-term monitoring using wireless LoRaWAN networks, also showed great promise for advancing sediment tracing techniques. Furthermore, many of the fluvial sites planned for hazard monitoring within the SENSUM project had flow conditions not dissimilar to St. Louis Creek, with coarse-grained transport of sediments being observed (pebble – cobble). Therefore, active tracer sediments, or smart stones, were developed in tandem with the SENSUM project, to evaluate the feasibility of using LoRaWAN networks alongside the active tracing of sediments. In this way, similar technological approaches were applied to track sediment transport to those implemented to monitor hazards, with eventual goal of integrating smart stones into wider hazard monitoring solutions.

3.2 Production of Smart Stone Tracers

Typically, during tracer surveys existing sediments are drilled, and tracing devices are embedded (e.g., Bradley & Tucker, 2012; Olinde & Johnson, 2015; Clark et al., 2022). This approach is not feasible with smart stones

during long term deployment (> 2 months) due to the battery size requirements (e.g., C cell). Drilling pebble to cobble sized sediments with a bit diameter wide enough to fit device components (~ 35 mm) often caused sediments to shatter.

To circumvent this, a design for an artificial sediment, or purpose-built SENSUM smart stone, was produced. The design involved moulding an existing natural cobble, matching its size and shape, and included a predesignated cavity to contain the device components. This removes the need for drilling existing sediments, preventing the risk of shattering tracers, and allowed the most efficient use of space within the cobble.

To most closely match natural sediments during deployment, concrete was used as the construction material for the replica sediments. Other materials were evaluated, such as silicone, and brass, but these did not sufficiently reproduce the characteristics of natural sediments (e.g., density, shape, texture, strength, etc…). Concrete also has the advantage of being relatively cheap, simple to use, and easy to produce at scale. This allowed multiple artificial sediments to be produced for testing and deployment for a range of laboratory and field settings.

3.2.2 Silicone Mould Production

For the artificial sediment mould, one of the tracers from St. Louis Creek was used as the base. This clast was chosen as its size (90 mm b-axis) represented the coarse-grained portion of bedload, in addition to its subrounded shape matching the majority of tracers used in previous research. In addition, the artificial sediment would be large enough to contain the tracking device and have a battery with sufficient capacity for long term monitoring. The original intension was to deploy the smart stones in St. Louis Creek in order to build rest time distributions of tracers at the site, although this was not possible. However, the use of a mould based on sediments that had been previously investigated facilitated comparisons between previous research utilizing RFID tags and deployments in the UK.

To produce the mould, a Polycraft GP 3481-F general purpose RTV silicone rubber kit was used. The kit comprised of liquid silicone, materials for mixing, and a catalysis to harden the material. The silicone had both high strength and high elasticity, which allowed the easy removal of the original clast once the mould was fully set.

For production, a container was chosen that was slightly larger than the selected sediment, which allowed for efficient use of material (Figure 3.1a). The silicone was mixed with the catalyst and added to the container, surrounding the sediment (Figure 3.1b), The poured silicone was left to cure in a fume cupboard for 24 hours. Once fully cured, the sediment was removed from the hardened silicone using a retractable utility knife, preserving the shape and texture of the original sediment in the mould. The resulting cavity was therefore identical to the original sediment and was subsequently filled with concrete to replicate the original clast. This process was repeated twice, producing two identical moulds of the original sediment (Figure 3.1c).

3.2.3 Concrete Production

Concrete was produced by mixing blue circle general-purpose cement and building sand at a 1:1 ratio. This ratio was used after strength testing determined that a lower sand-to-cement concentrations provided the most robust sediments. These withstood the greatest impacts tested, ensuring durability during deployment. Furthermore, the increased density from a higher cement ratio resulted in an increased overall weight of the concrete casing. This helped achieve an overall density more closely replicating natural sediments, without altering the fundamental properties of the artificial sediment. This additionally allowed the finished tracers to more closely match pre-existing tracers deployed in hardness, providing longevity during deployment.

Before pouring concrete, the silicone mould was sealed with tape to prevent leaks (Figure 3.1d). To ensure space within the sediment to embed the IMU sensor board and battery, a purpose-built iron plug was designed

and produced by the technicians at the University of East Anglia. This matched the size requirements for the sensor housing, which included all device components, in addition to a cylindrical C-cell battery (35 x 70 mm). The plug was wrapped in clingfilm before use and lubricated to prevent concrete sticking to the plug. This was lowered into the freshly poured concrete, displacing excess material (Figure 3.1e). This plug allowed concrete to be partially formed around it before removal. After approximately 24 hours of curing, the plug was removed leaving the artificial sediment to finish curing.

With the iron plug removed and the concrete partially cured, the tape and silicone mould were carefully peeled away from the concrete. At this stage, any imperfections were cleaned from the surface, with the artificial sediment resembling the original sediment (Figure 3.1f). The concrete was left to cure for at least two weeks to ensure the artificial sediments reached their maximum strength. After this time, they could be used in laboratory testing or for field deployment.

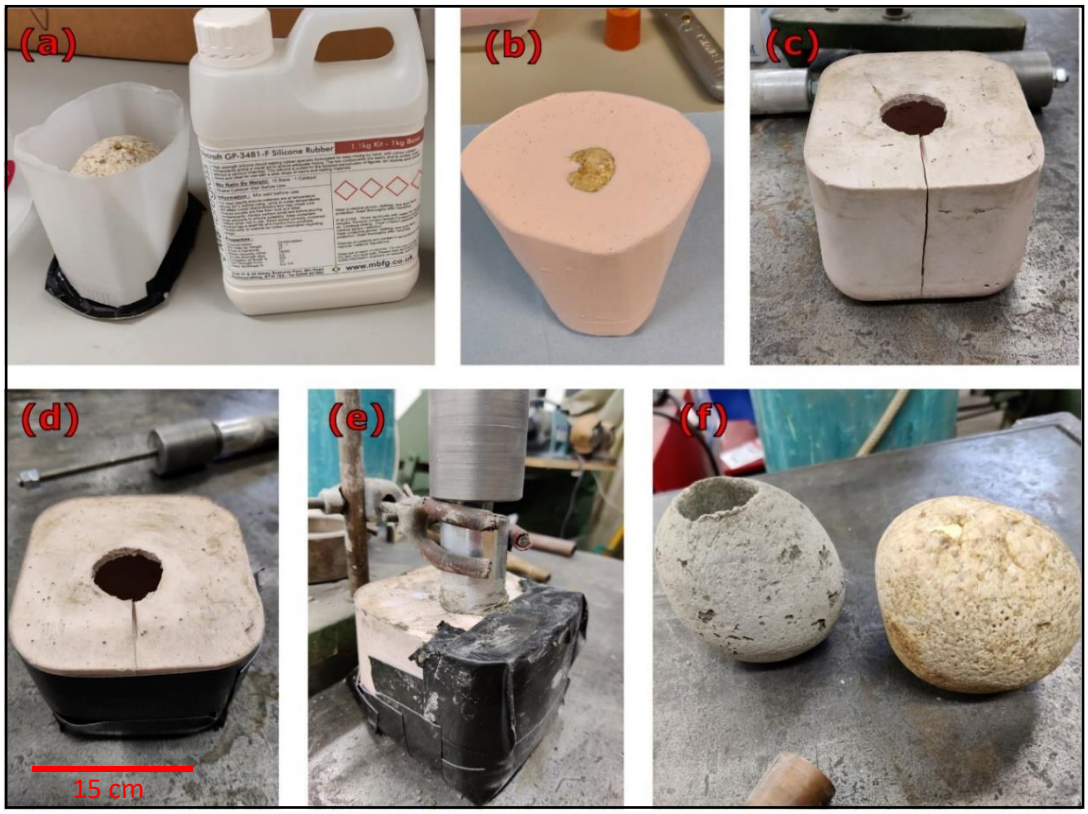

Figure 3.1: *Production process for the artificial sediments, from silicone moulding of original sediment to concrete fabrication displaying: (a) the Polycraft general purpose silicone rubber kit used; (b) the hardened silicone surrounding the original cobble forming sediment shape; (c) the finished mould after sediment extraction; (d) the sealed silicone mould ready for concrete production; (e) the metal plug displacing concrete to produce cavity for device components and; (f) finished concrete cobble beside original sediment.*

3.2.4 Case Production

Typically, environmental sensors in fluvial research are protected by a housing made from bulky metal or PVC components. Due to size limitations when embedding sensors inside artificial sediments, the sensor case design needed to be as small as possible, while still being sufficiently robust to protect the electronics. Additionally, the case needed to be lightweight, so that the density of the completed smart stone was not significantly affected. It also needed to enable easy access to the device for manually uploading data. Furthermore, if smart stones are to be deployed across multiple sites, the cost to produce individual tracers needed to be relatively low, so production could be cost effective at scale.

With these criteria in mind, a custom case was designed and was produced to store all device components and a C-cell battery.

3D printing of case materials was initially attempted, following previous examples during smart stone enclosure development (e.g., Maniatis et al., 2013). Unfortunately, unreliable production quality and associated material costs resulted in a shift from a custom 3D printed design, to a design with prefabricated components which could be ordered in mass.

The cases comprised of an ultra-thin MoCap tube container, resized to fit all components efficiently (32 x 65 mm). After fixing components in place, the tubes were padded with foam to prevent the movement of device components within the container, limiting experimental noise caused by the rattling of loose items. The cases were plugged with matching MoCap caps, sealing components within the cases. During deployment, containers were additionally sealed with PTFE tape to further minimise the risk of moisture leakage as a failsafe in the case of a leak inside the sediment housing. Additionally, containers within smart stones that were deployed for extended periods of time (> 24 hours) were sealed using black epoxy.

The embedded IMU sensor board was positioned as close as possible to the centre of mass of the artificial sediment, whilst still providing access to the device. This was to facilitate more accurate measurements of the forces acting upon the grain from all angles (Maniatis et al., 2020). It should be noted that due to imperfections during the manufacturing process of tracer cobbles, there will be slight deviations between sensor board positions within individual cobbles.

3.2.5 Finalised Smart Stone Prototype

A scaled structure from motion model of the finalised smart stone prototype is displayed in Figure 3.2. Accounting for all components making up the artificial sediment (e.g., concrete, case, battery, and IMU module) the total weight of the prototype smart stone was 673.14 g. There are likely minor deviations between subsequently produced sediments, but materials and process remained consistent across all replicas produced. The sediments have an estimated density of 2169 kg/m^3. This is less dense

when compared to expected sedimentary material in streams (e.g., density of quartz = 2650 kg/m^3, and density of shale = shale 2430 kg/m^3). However, density more closely represents surrounding sediments after deployment in the field due to saturation of the concrete with water. This increases estimated density to approximately 2313 kg/m^3 based on data from soaking experiments of finished artificial sediments.

In total, 22 artificial sediments, with their associated sensor cases, were produced over the course of the research. These were distributed for both laboratory testing, field deployment, and for use by researchers on the SENSUM project at the University of Plymouth.

Figure 3.2: *3D structure from motion model stills of smart stone sediment, demonstrating sediment size and cavity space within concrete housing for embedding the battery and sensor module.*

3.3 Prototype Stress Testing

Upon the production of a prototype, stress testing of artificial sediments was undertaken. This was intended to evaluate if the design could withstand impacts typical of those experienced during deployment in the field and laboratory. Stress testing consisted of dragging artificial sediments along various concrete surfaces, colliding with other sediments,

and drop testing. The prototypes were monitored for damage throughout testing.

Across all stress testing activities, sediments retained their structural integrity, with no sediments shattering or cracking. During drop testing, sediments were dropped from progressively increasing heights onto a concrete surface in intervals of 0.25 m, up to a maximum height of 1.5 m. Even at the maximum heights tested, damage observed was minimal, with only minor scratches on the surface of the sediments. As impacts in the laboratory and during deployment were unlikely to reach levels withstood during stress testing, it was concluded that the design was fit for purpose.

In addition to impact testing, underwater experiments evaluated the ability of the prototypes to withstand submersion. Multiple sediments were submerged in water depths of 0.5 m for > 48 hours before retrieval. The interior of all cases remained dry, suggesting that water could not penetrate the device housing.

3.4 LoRaWAN®-RF-Module Tracking Devices

The sensor module (Nomad, https://miromico.ch/miro-nomad) used for tracking movement within the artificial sediments was initially developed by Miromico AG in collaboration with the Movetech Telemetry project. Their first use case was to study animal movement behaviour (e.g., Soriano-Redondo et al., 2021; Acácio et al., 2022), using known movement patterns and geographical location to understand animal behaviour. The devices are based on standard FMLR LoRaWAN®-RF-Modules produced by Miromico, but are adapted to fit ongoing research needs. Identical hardware is used across multiple research projects and is adapted to fit specific environmental conditions through firmware alterations.

The devices are low powered and compact, with the circuit board module measuring 23 x 13 x 1 mm, and weighing 1.3 g (Figure 3.3a). The module contains a range of sensors including a GPS, a barometer, a thermometer, an internal clock, an ultra-low powered accelerometer, and a 9-DOF IMU

sensor. They are also equipped with flexible GNSS and LoRa antennas for communication with GPS and LoRa gateway networks.

Collected sensor data can be stored on the device's 16MBit FLASH memory, which can contain > 10,000 payloads (data package containing all sensor data) of sensor information. Additionally, data can be transmitted wirelessly from devices using LoRa. They have the capability to transmit data on the 868 Mhz band in near real time to any LoRaWAN gateways (Figure 3.3b). LoRa gateways (e.g., Multitech IP67) can connect to internet service providers either through ethernet, Wi-Fi, or mobile GSM networks. Additionally, they can be powered through direct mains supply or by using integrated batteries, providing functionality in a range of environments.

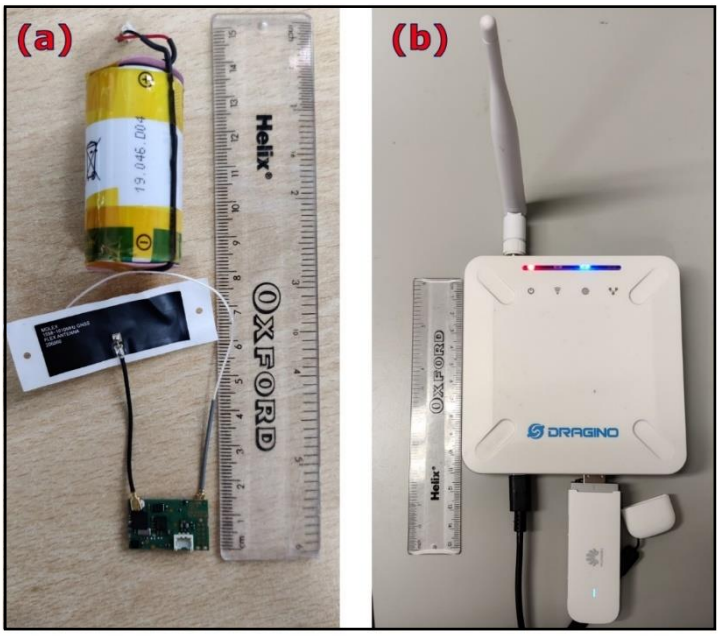

Figure 3.3: *(a) Miromico Nomad LoRaWAN®-RF-Module with Molex Flexible GNSS Antenna and Omni Directional LoRa antenna with example C cell battery used during deployment; (b) LoRaWAN gateway with USB type C power connector, LoRa antenna and USB GSM dongle.*

Gateways are programmed to send device payloads via GSM to the LoRaWAN network server provider LORIOT®. LORIOT® is a third-party network operator which hosts a range of IOT applications. From the LoRa server, data packets are exported to a local server (e.g., Movetech Telemetry server) which decodes the data back into a readable format for end user analysis (Figure 3.3). Maximum communication ranges of LoRa

devices are estimated to be over 15 km, with only minor data packet loss at these distances (Petajajarvi et al., 2015). Dini et al. (2021) had real world deployment ranges of over 800 m, with deployment inside boulders, and noted that the upper limit of communication range was likely not reached.

In addition to sensor data, devices can transmit descriptive information on battery level, and hardware status. This supports ongoing maintenance and monitoring of deployed devices. Transmitted data packets also contain a server time stamp, and an internal time stamp. This indicates any differences between data collection being triggered and the time of data upload. This is essential for determining data transfer speeds during hazard monitoring applications. The internal device time stamps also support the synchronisation of data with other IoT enabled devices on the wider network (e.g., river flow gauges).

3.4.2 Device Programming

The devices are programmable via a USB cable with any serial terminal software, with a wide variety of commands to alter device behaviour and optimize performance. Miromico have installed a rudimentary text-based interface to assist in programming devices but have planned for an updated graphical UI for future applications.

The ability to change sensor module behaviour allows further customisation of the devices to adapt to a variety of use cases.

Notable device settings which can be altered include:

- Individual sensor activation
- Data collection frequency
- IMU data ranges
- Triggering thresholds for data collection
- Start and stop conditions during data collection
- Rate of status messages
- LoRa connectivity and upload settings

A full list of settings implemented for both the laboratory experiments and field deployments is included in the appendices (Appendix B.1).

These settings allow devices to adapt to a range of deployment and laboratory environments. For instance, to isolate specific movements (e.g., rolling), it is possible to limit data collection to occur only after a threshold of angular velocity change or linear acceleration is exceeded. Furthermore, it is possible to activate and deactivate individual components of the sensors when data trimming is preferred.

With LoRa capabilities activated, the devices also have two-way connectivity and can be programmed remotely using over the air downlinks through the LoRa network. This provides further adaptability after deployment, to respond to changing experimental or environmental conditions, and for device maintenance. Additionally, stored data on the devices can be exported via a serial USB connection. This can be advantageous when attempting to retrieve thousands of data packets over a short time period (e.g., during laboratory experiments), as to not be limited by the slower wireless upload speeds of LoRaWAN when not necessary.

3.4.3 Inertial Measurement Unit for Tracking Sediment Movement

The IMU is a combination of sensors that measure orientation and motion with respect to an inertial reference frame. The Miromico device uses a LSM9DS1 9-degree of freedom (DOF) IMU module, which comprises an accelerometer, gyroscope, and magnetometer, each with 3 axes.

The accelerometer converts accelerational forces impacting the device into measurable quantities along the X, Y and Z axis. It achieves this as piezoelectric materials within the device create an electrical charge that is proportional to the force exerted upon it. As the mass of this material remains constant, it is possible to infer the acceleration applied from the electrical charge to calculate linear acceleration. It should be noted that due to the accelerational force of gravity on earth (9.81 m/s^{-2}), if the device is stationary, a reading of 1 g across the direction of gravitational

force will be recorded by the sensor. The accelerometer measures accelerations within the range of ± 16 g (1 g = 9.81 m s^{-2}) at up to a sampling rate of 238 Hz.

The gyroscope measures the degree of rotational change experienced by the device. It measures angular velocity within the range of ± 2000 ° s^{-1}, again at a sampling rate of up to 238 Hz. Gyroscope measurements are often referred to as pitch, roll and yaw in previous literature, but will be referred in terms of X, Y, and Z for continuity with the accelerometer henceforth.

The magnetometer measures orientation with respect to magnetic north by detecting fluctuations in the Earth's magnetic field strength along its X, Y, and Z axes. Specifically, the Y-axis corresponds to changes relative to magnetic north, the X-axis to magnetic east, and the Z-axis to magnetic up, pointing away from the Earth's core. This stands in contrast to the gyroscope's coordinate system, which is body-fixed and relies on the initial position of the device for its measurements. Therefore, any subsequent references to the X, Y, and Z axes in the context of the magnetometer pertain to these magnetic coordinates. A schematic demonstrating the differences between the three sensors X, Y, Z axis is included in appendix B.2 The magnetometer has a range of 16 G (1 G = 10^{-4} T), and a sampling rate of up to 40 Hz.

The device also makes use of an ultra-low power accelerometer (LIS2DH), used previously in landslide research (Dini et al., 2021) and in ecological research (Acácio et al., 2022). This component can collect lower frequency accelerometer data (2 Hz). In this research high frequency, 9-DOF data sets are required, therefore, the LIS2DH is only used to trigger data collection while the device is in power saving mode.

Devices have an active mode and a low power mode to maximise efficiency. In low power mode, the devices are programmed to check for connectivity and send a routine status payload every hour if movement has not been detected. The status payload contains date, time, GPS, and battery information. This informs the user that the devices are working correctly and are within gateway range. The LSMDS1 9-DOF IMU sensor

remains in hibernation until triggered. The active mode is triggered upon movement detection with the LIS2DH accelerometer above a specified threshold (e.g., 0.2 g), where full IMU data is subsequently collected. Only activating the more power intensive sensors on the IMU board when movement is initially detected extends the potential deployment length of the devices.

After data collection is complete, the device will attempt to establish gateway connectivity. If successful, it will continuously send payloads until all data is uploaded, and then return to low power mode. If gateway connectivity is not available, then data is stored on the 16 MBit flash drive, and the device will return to low power mode. The devices can be programmed to check for gateway connectivity at a specified frequency, with a 1-hour time span being used for the smart stones. When the gateway is in range again, any data stored is then transferred to the LoRa server, and the device storage is cleared.

While data collection is triggered using the LIS2DH accelerometer, the behaviour of the device can be modified to suit specific data collection modes. For instance, during all laboratory and field testing the device was programmed to collect data continuously until movement was stopped in this research. However, it is possible to alter the device settings to collect data for specified periods of time after triggering (collect data for five minutes after triggering event) or periodically activate over a certain frequency (i.e., active every hour for one minute of data collection). These modes of data collection could be potentially beneficial in instances where movement is common and snap shots of transport behaviour over long periods of time are preferable to save both battery life and data bandwidth.

It should be noted that the storage of the IMU data is split across two data packets, which are encoded for LoRa transmission separately. The first contains the accelerometer and gyroscope data and has priority during LoRa transmission. The second contains the magnetometer data and is transferred after all accelerometer and gyroscope data is successfully uploaded. This can cause problems if large amounts of movement data are transferred in a single instance, as the magnetometer data can be delayed

significantly, or even interrupted if gateway connectivity fails during transfer.

3.4.5 Firmware Development

The devices were actively being developed in collaboration with Miromico AG during the research. Consequently, multiple iterations of the devices were available for testing at different stages of laboratory work and during field deployment. The device capabilities described above are from the final firmware version, used during most laboratory experimentation and field deployment in 2022.

Hardware remained unchanged throughout the research, but device functionality was altered multiple times in response to the needs of the SENSUM project, the requirements of the smart stones, and as a result of user feedback. For instance, the initial firmware tested, and that installed on devices during research by Dini et al. (2021), was limited to data collection using the LIS2DH accelerometer only. This capped acceleration data collection frequency to 2 Hz and did not have gyroscope and magnetometer functionality. This lacked the movement information desired when tracking tracer sediments, preventing the capture of specific movement behaviours seen during bedload transport.

Subsequent iterations of device firmware brought new functionality, but also changed device behaviour, often in unintended ways. This resulted in the need for repeated verification of device functionality, to confirm usability for laboratory testing and field deployment. Furthermore, firmware bugs occasionally lead to unexplained data loss, so a period of bug fixing would be required after each update. See appendix C.1 for timeline of firmware updates in relation to research activities.

In January 2021, a firmware update allowed the activation of the device LSM9DS1 IMU sensor. Functionality was limited to the gyroscope and the high frequency accelerometer, giving only 6-DOF IMU data. Additionally, the maximum capacity of the gyroscope and accelerometer was limited to 245 ° s^{-1} and 2 g respectively. Regardless, initial laboratory testing was

conducted, with experiments at the University of Plymouth dry granular slope using this firmware version (see chapter 4).

In August 2021, a further firmware update introduced the functionality of the magnetometer. Additionally, the caps on capacity were removed, allowing data collection of up to ± 2000 ° s^{-1} and ± 16 g for the gyroscope and accelerometer. Deployment of smart stones at the Tebay field site in November 2021 used this firmware version (see Chapter 4). However, firmware bugs were subsequently discovered, preventing data collection across some deployed devices.

In February 2022, a firmware update resolved many of the issues causing loss of data in the previous version, in addition to adding various improvements regarding the programming of devices.

Whilst there have been further updates to firmware, devices throughout the remaining research in this thesis use the February 2022 firmware. This is to allow comparisons across laboratory experimentation and field deployment using an identical setup. This should prevent differences in firmware potentially altering data outcomes. This does risk newly discovered bugs in the February firmware, and limits further development of device capabilities, but for data continuity, and relative stability, the device firmware remained unchanged for the remained of work.

3.5 Battery Optimisation

Various battery setups were tested for feasibility with the sensor modules. A balance had to be established between battery capacity and physical size. While much smaller batteries (e.g., AA) had the advantage of requiring less space within the sediments, their limited capacity (e.g., LS 14500 = 2.45 Ah) raised concerns regarding their longevity during extended deployment in the field. Furthermore, as the physical size of the circuit board is larger than an AA battery, the compact size is less relevant at these sizes.

High-capacity D cells (e.g., LS 33600 = 17.0Ah) were considered, although the size of the cavity required to contain the battery and device components was excessive for desired tracer size. Artificial sediments would have to be produced significantly larger than the D_{50} grain size of most field sites, so a smaller battery was selected.

A compromise between physical size and capacity resulted in the Saft LS 26500 high energy density C cell being used during field deployment. The battery has dimensions of 50 x 35 mm, weighs 48.2 g, and has a capacity of 7.7Ah. For laboratory testing, a RS PRO 3.7 V (2.0 Ah) rechargeable battery was used, allowing extended short-term use.

Testing of C cell longevity was undertaken by installing a device with typical deployment settings and leaving the device for > 1 month. Additionally, the device was periodically moved to trigger data collection over this time, this simulated periods of movement expected during deployment. The device continued to function throughout testing, with cell voltage remaining consistent. This matched the manufacturers expected power discharge profiles given known device power requirements and confirmed C cell batteries to be appropriate for long term deployment. Subsequent deployment of smart stones at field sites (Chapter 5) have proven the potential battery life of the C cells in the devices to be at least 5 months. However, the lifespan of an individual device is contingent upon the frequency and intensity of usage during deployment, where frequent activation of the IMU will more rapidly drain battery voltage. Multiple deployment periods in a range of conditions are necessary to estimate an overall average, and site-specific averages of C cell lifespans. This will additionally help constrain the impact of changing temperatures on battery life.

3.6 LoRaWAN Gateway Experiments

The Miromico devices embedded within the smart stones are connected to the wider sensor network via LoRaWAN gateways. Before deployment at field sites, the capabilities of these gateways needed to be evaluated for

their suitability in forested fluvial environments. To simulate a gateway located at a typical vantage point over a fluvial catchment area, gateways were installed on the roof of the University of East Anglia Environmental Science Building. Following this, range, line of site, and submersion experiments were undertaken (Figure 3.4). This was intended to replicate potential environmental interruptions encountered in the field, and to test the limits of device transmission.

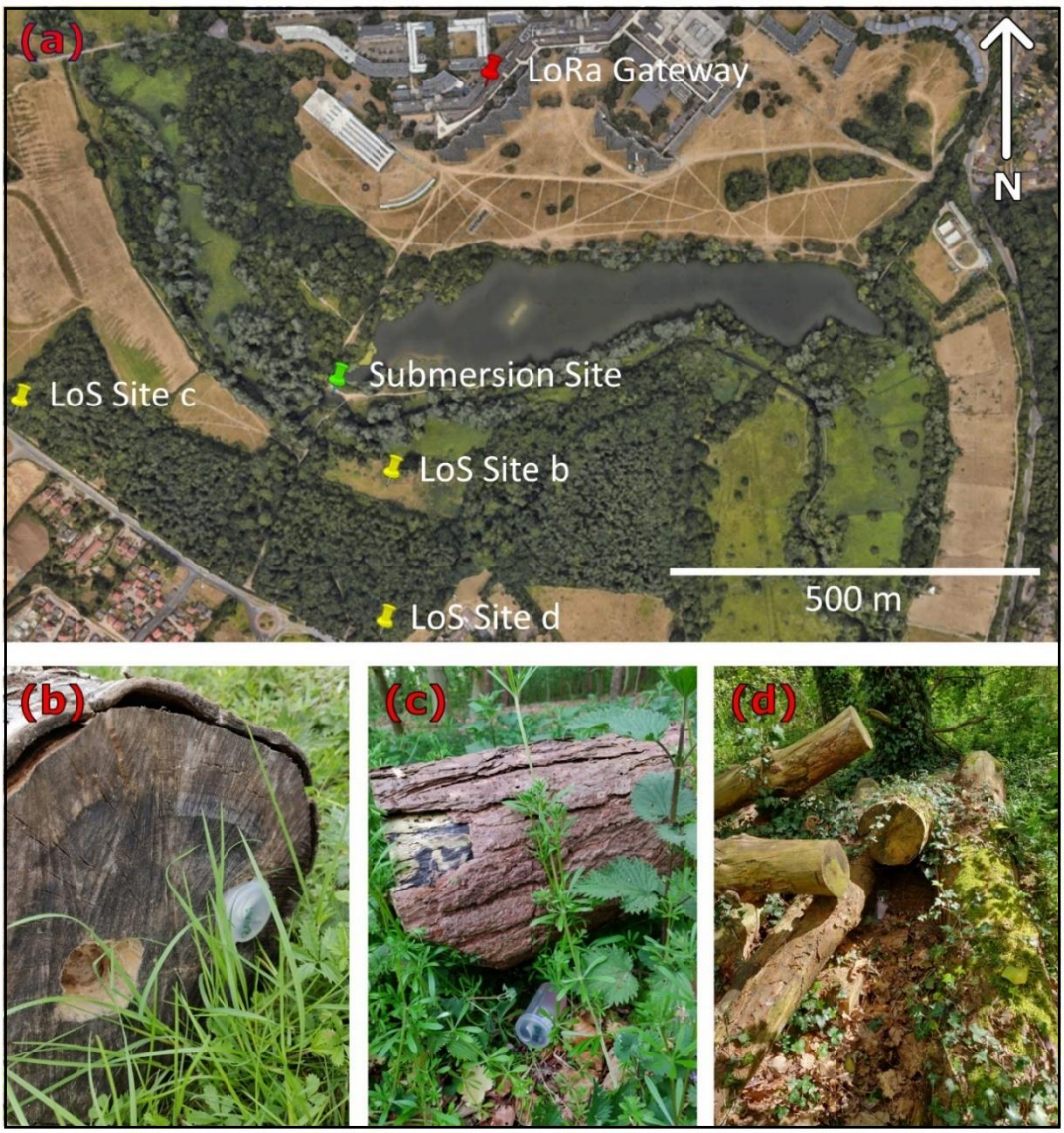

Figure 3.4: *LoRaWAN gateway experiments investigating the impact of Line-of-Sight (LoS) interruptions and submersion in water on transmission range with: (a) map of the LoRaWAN gateway and deployment locations of devices across the University of East Anglia Campus; (b) deployment of device in woodland clearing providing good LoS; (c) deployment site with poor LoS under forest canopy and placement under large wood piece; (d) additional poor LoS deployment site with placement under multiple wood debris pieces.*

The University of East Anglia campus is ideally suited for these experiments as the campus contains a large, forested area 500 - 900 m from the gateway location. Additionally, the nearby River Yare provides an opportunity for submersion testing at a range of depths.

For the initial range experiments, devices were transported > 800 m from the gateway, into a densely forested area on the university campus. Three

deployment sites were chosen. Two in forested areas, to test differing angles and canopy densities impact on gateway transmission (Figure 3.4c, 3.4d), and one in a clearing with limited canopy cover (Figure 3.4b). At all locations, devices were tucked under or placed inside wood pieces, to further simulate line of site interruptions expected in the field. At all sites, gateway communication was uninterrupted, and devices successfully transmitted data in real time.

The impact of different depths of water submersion on device connectivity was also tested. The River Yare provides an ideal site to test connectivity as there is a reasonable line of site to the rooftop gateway. This isolates the variable of water submersion on connectivity. The test site was located ~ 500 m from the gateway. The device was sealed in a waterproof casing ready for submersion experiments.

Initially, connectivity was established to be of high quality above the water's surface, with direct line of site to the gateway. Following this, the device was lowered at 5 cm intervals. Communication with the gateway was evaluated at each depth, by comparing server upload time stamps with internal device time. Connectivity and data transfer speeds remained high until depths of 15 cm, when connectivity became intermittent, but communication was still possible. At depths of > 30 cm connectivity became problematic, with devices unreliably sending data.

Analysis of the submersion experiments demonstrated that devices could transmit underwater, but become unreliable at depths greater than 30 cm. This suggests that in deep water devices could struggle to transmit movement information in real time. Devices would still function and continue to collect movement data until they are positioned closer to the water's surface, when saved data would be transmitted. This may be analogous to tracers storing movement data during high flows over winter and subsequently transmitting during drier summer months.

However, the GPS accuracy of the submerged devices was consistently > 10 m. While unfortunate, the result was not surprising due to known difficulties with radio signals propagating underwater accurately (Taraldsen et al., 2011). Furthermore, the unreliability of tag GPS

embedded in boulders previously (Dini et al., 2021) suggested poor performance with limited line of sight to satellites. Consequently, the GNSS sensor was disabled in subsequent deployments underwater, as the additional drain on the battery could not be justified.

These results demonstrate the success of using the smart stone devices in a range of environmental conditions. Although, the gateway being located at a high location on top of a building potentially has an advantageous vantage point in comparison to those expected in the field. Additionally, gateway to server connectivity through GSM service is likely to be more reliable at the university site, although gateways are installed with large antennas to compensate for decreased mobile coverage in remote areas.

3.7 Summary

With the successful completion of the smart stone prototypes, stress testing of the sediment design, and the completion of battery longevity and gateway range experiments, the production of multiple smart stones could begin. These would initially be applied in laboratory experiments, capturing movement data in controlled environments (Chapter 4), but later be deployed at multiple field sites across the UK once COVID-19 Pandemic related travel restrictions had lifted (Chapter 5). Additionally, many devices would be, and continue to be, used for concurrent research alongside the SENSUM project.

References

Acácio, M., Catry, I., Soriano-Redondo, A., Silva, J. P., Atkinson, P. W., & Franco, A. (2022). Timing is critical: consequences of asynchronous migration for the performance and destination of a long-distance migrant. Movement Ecology, 10(1), 1-16.

Bradley, N. & Tucker, G. (2012) Measuring gravel transport and dispersion in a mountain river using passive radio tracers, *Earth Surface Processes and Landforms,* 37(10), 1034-1045.

Bradley, N. & Tucker, G. (2012) Measuring gravel transport and dispersion in a mountain river using passive radio tracers, *Earth Surface Processes and Landforms,* 37(10), 1034-1045.

Clark, M. J., Bennett, G. L., Ryan-Burkett, S. E., Sear, D. A., & Franco, A. M. (2022). Untangling the controls on bedload transport in a wood-loaded river with RFID tracers and linear mixed modelling. *Earth Surface Processes and Landforms*. 47(9), 2283-2298.

Dini, B., Bennett, G. L., Franco, A., Whitworth, M. R., Cook, K. L., Senn, A., & Reynolds, J. M. (2021). Development of smart boulders to monitor mass movements via the Internet of Things: a pilot study in Nepal. *Earth Surface Dynamics*, *9*(2), 295-315.

Dini, B., Bennett, G., Franco, A., Whitworth, M., Cook, K., Senn, A., Reynolds, J., (2021) Development of smart boulders to monitor *mass movements via the Internet of Things: A pilot study in Nepal, Earth* Surface Dynamics, *Earth Surface Dynamics*, 9, 295–315,

Gronz, O., Hiller, P. H., Wirtz, S., Becker, K., Iserloh, T., Seeger, M., ... & Ries, J. B. (2016). Smartstones: A small 9-axis sensor implanted in stones to track their movements. *Catena*, 142, 245-251.

Hart, J. K., & Martinez, K. (2015). Toward an environmental Internet of Things. *Earth and Space Science*, *2*(5), 194-200.

MacVicar, B. J., & Papangelakis, E. (2022). Lost and found: Maximizing the information from a series of bedload tracer surveys. *Earth Surface Processes and Landforms*, *47*(2), 399-408.

Maniatis, G., Hoey, T., & Sventek, J. (2013). A New Method for Rapid Prototyping of Purpose-Specific Sensor Enclosures: Example Application and Implications for Data Coherence. *Journal of Sensor and Actuator Networks*, *2*(4), 761-779.

Maniatis, G., Hoey, T., Hodge, R., Rickenmann, D., & Badoux, A. (2020). Inertial drag and lift forces for coarse grains on rough alluvial beds measured using in-grain accelerometers. Earth Surface Dynamics, 8(4), 1067-1099.

Nichols, M.H., 2004. A radio frequency identification system for monitoring coarse sediment particle displacement. Applied engineering in agriculture, 20(6), p.783.

Olinde, L., & Johnson, J. P. (2015). Using RFID and accelerometer-embedded tracers to measure probabilities of bed load transport, step lengths, and rest times in a mountain stream. *Water Resources Research*, *51*(9), 7572-7589.

Petajajarvi, J., Mikhaylov, K., Roivainen, A., Hanninen, T., & Pettissalo, M. (2015, December). On the coverage of LPWANs: range evaluation and channel attenuation model for LoRa technology. In *2015 14th international conference on its telecommunications (itst)* (pp. 55-59). IEEE.

Roskilly, K., Bennett, G., Curtis, R., Egedusevic, M., Jones, J., Whitworth, M., Dini, B., Luo, C., Manzella, I. and Franco, A., (2022). *SENSUM project, Smart SENSing of landscapes Undergoing hazardous hydrogeomorphic Movement* (No. EGU22-10289). Copernicus Meetings.

Soriano-Redondo, A., Franco, A. M., Acácio, M., Martins, B. H., Moreira, F., & Catry, I. (2021). Flying the extra mile pays-off: Foraging on anthropogenic waste as a time and energy-saving strategy in a generalist bird. *Science of The Total Environment*, *782*, 146843.

Taraldsen, G., Reinen, T. A., & Berg, T. (2011). The underwater GPS problem. In *OCEANS 2011 IEEE-Spain* (pp. 1-8). IEEE.

CHAPTER 4

4 Characterising Transport Behaviour Using Smart Stones in the Laboratory

4.0 Chapter Overview

This chapter describes the application of the LoRaWAN enabled smart stones in laboratory settings. First, it covers initial laboratory experimentation, where the capabilities of the devices are determined, and the ideal firmware settings for capturing sediment movement are established for future deployments (e.g., frequency of data collection). Second, the experiments undertaken at the University of Plymouth's dry granular slope are described, attempting to match high speed video recordings to motion captured through the IMU module within the smart stones. These experiments also helped to identify improvements still required in the sensor firmware. Finally, experiments with updated firmware are undertaken to replicate typical transport behaviour. These are used to build an inventory of known "expected" movement data, for comparison and verification of subsequent field data in Chapter 5.

4.1 Introduction

Smart stones have the potential to significantly enhance our understanding of sediment transport behaviour and its controlling factors. Sediment transport theory is covered in Chapter 1 of this thesis, with Figure 1.1 showing the different modes of behaviour (shaking, sliding, saltating, and rolling). With existing technologies it remains challenging to detect the point of entrainment of individual grains (Dey & Ali, 2017), and even with advances in embedded IMU tracers, calculating precise trajectories of tracer sediments remains difficult (e.g., Gronz et al., 2016; Dost et al., 2020). Therefore, the ultimate aim of the rest of this thesis is to use the smart stone described in Chapter 3 to broadly characterize bedload transport in the field and detect the point of entrainment of grains. The next step towards this aim is to characterise different bedload behaviours in the laboratory.

This chapter aims to use experiments replicating typical transport behaviour to build a library of known "expected" movement data, for comparison and verification of subsequent field data obtained in Chapter 5. It was hypothesised that specific movement modes would produce unique signatures within the IMU data. Once these signatures were known, they could be recognised, and interpreted within field data to infer the movement behaviour of deployed sediments, without direct observation. For instance, data captured from a tracer experiencing a rolling motion would have specific identifiers within its accelerometer, gyroscope, and magnetometer data. This would be distinct from, for example, a tracer sliding along the bed surface during transport, or simply shaking on the bed in-situ pre-entrainment. These unique signatures could then be used to infer sediment transport behaviour at the field sites in Chapter 5 and compare these to hydraulic condition over time, potentially helping to establish approximate threshold discharge for entrainment at the sites.

The following chapter details a range of experiments which correspond to the development of the LoRa enabled smart stone, from initial laboratory experimentation with each new firmware update (section 4.2 & 4.4), the optimisation of device settings for capturing transport behaviour (section

4.5), the testing of the capabilities of the smart stones (section 4.3, 4.7) and finally covering the characterisation of specific movement behaviours using IMU data (section 4.9).

4.2 Initial Laboratory Movement Experiments

With the smart stones produced, and confirmed to be functional in Chapter three, initial laboratory experiments were carried out to improve the understanding of the device's response to basic motions within the IMU data. This would establish a foundation for recognizing movement signatures in field deployments (as outlined in Chapter 5).

First, simple rotational movements along each directional axis were completed, with the relationship between motion, rotational speed, and data output being determined. Additionally, progressive impact tests were undertaken to test the capabilities of the device, where the maximum force needed to exceed IMU read range were determined.

At the time of these initial experimental runs, the devices were running an earlier firmware version (January 2021). This update already provided improvements from the sensors used in Dini et al. (2021) by activating the accelerometer and gyroscope on the LSM9DS1 IMU sensor. This firmware version enabled data collection ranges of up to 2 g and 245 ° s^{-1} for the accelerometer and gyroscope respectively. This restricted interpretations of data sets produced by movements with accelerational forces and angular velocities above these threshold values (e.g., Figure 4.1) in these initial experiments and the subsequent dry lab experiments (section 4.3). Additionally, it was not possible to enable the magnetometer, limiting orientation tracking of the smart stones. These experiments are still described here as they were pivotal in informing future firmware modifications, developing experimental setups, and understanding the expected behaviour of the smart stones during various transport modes.

Following IMU response experiments, initial runs of specific movement behaviours (rolling, shaking, sliding) were carried out. These were feasibility experiments to determine if data output was quantitatively distinct during different movement modes. Additionally, these experimental runs established uniform laboratory methodologies across all future firmware updates, which considered the ideal device settings and limitations in the laboratory.

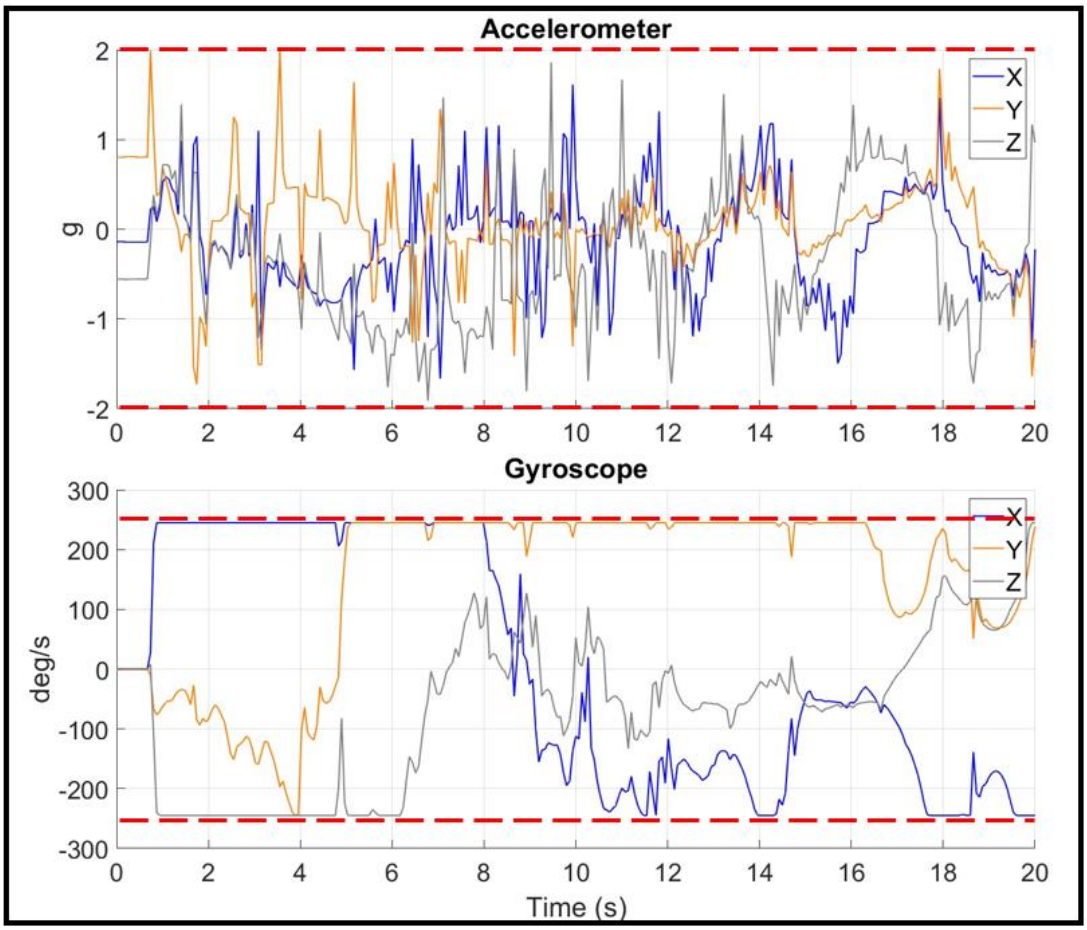

Figure 4.1: *Example data collection using original device firmware (January, 2021), with dashed lines representing upper limit of recording capabilities at the time (2 g and 245 ° s^{-1}, for the accelerometer and gyroscope respectively).*

One of the key end-user functionalities of the Nomad devices is the flexibility to alter device settings. For instance, the minimum accelerational forces needed or the degree of rotation required to exceed the triggering threshold of data collection can be set (e.g., 0.2 g, 10 ° s^{-1}). This prevents

unwanted activation of the device between experiments, or isolates data capture from only significant movement events (e.g. Dini et al., 2021). Similarly, the duration of data collection, IMU sensor range, and data collection frequency were adjusted to fit the needs of the experiments. The devices were originally designed to capture animal movement and therefore default movement detection settings needed to be adapted to capture the transport dynamics of sediments.

The ability to modify device behaviour was beneficial when formulating experimental design, although a large portion of time during these initial experiments was dedicated to refining settings to enable the devices to capture and send the signature of movement accurately. This process needed to be repeated after future firmware updates, to account for changes in device behaviour (see appendix C.1 for timeline of firmware update availability). Once device behaviour, settings, and expected data outputs were better understood and reliably being captured by the devices, smart stones were used in a controlled laboratory environment.

4.3 Dry Granular Slope Experiments: University of Plymouth

It was not possible to place smart stones in available flumes as water velocities are insufficient to move cobble sized sediment. However, in July 2021, the smart stones were tested at the University of Plymouth dry slope laboratory in collaboration with members of the SENSUM team. The goal was to capture rolling and sliding sequences down a slope in a more controlled laboratory setting. The laboratory was comprised of a fully adjustable granular flow experimental slope (Figure 4.2). The angle of the slope could be altered through a winch system, producing different transport conditions for the smart stones. Furthermore, a manual release mechanism was synchronised with multiple high frequency video recording surrounding the slope, allowing the initiation of motion to be matched with tracer transport footage.

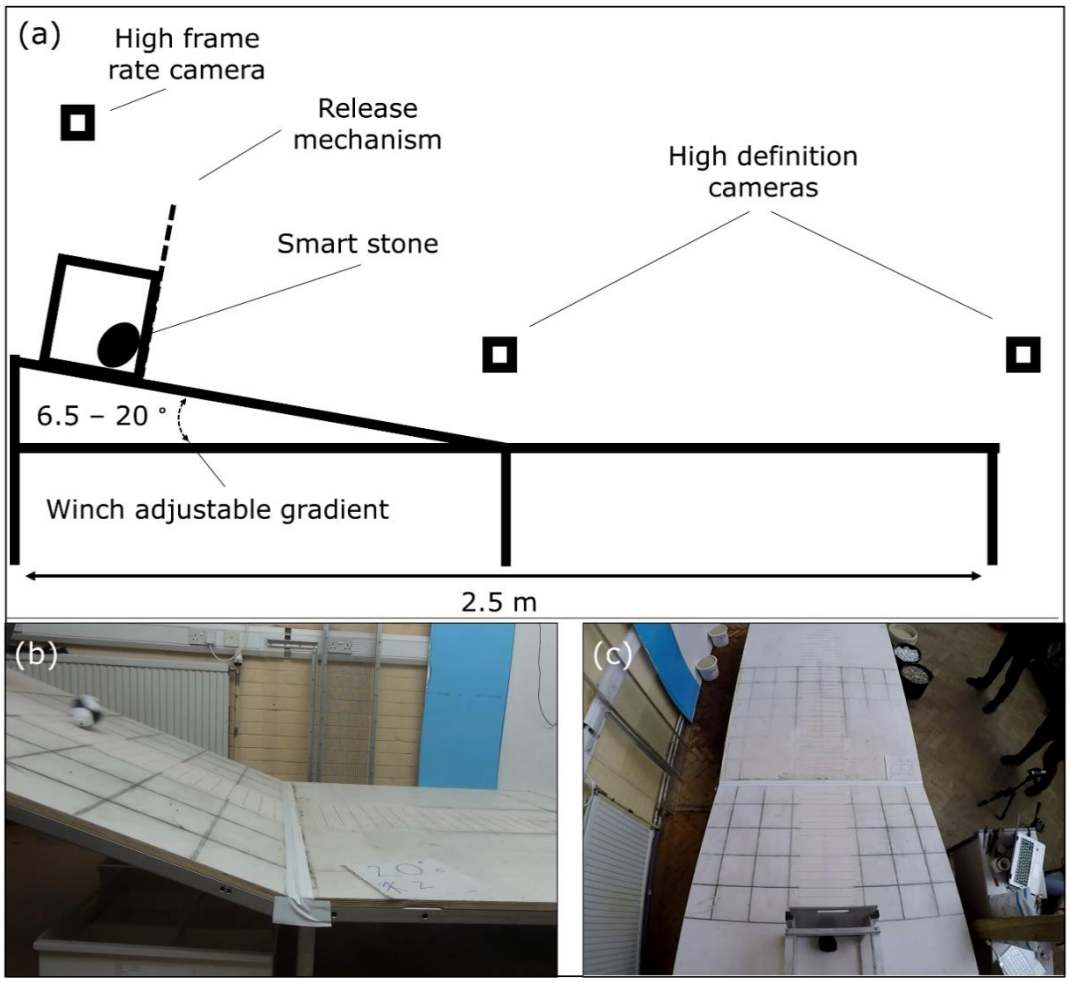

Figure 4.2: *University of Plymouth Dry Granular Slope with: (a) a simplified sketch of the adjustable slope, demonstrating the winch system, camera setup, and release mechanism in the laboratory; (b) lateral view from high-definition camera; (c) birds eye view from high frame rate camera, displaying the ruled surface for calculating transport velocity.*

Recordings were taken with a triple camera setup. Two high definition (1920 x 1080 pixels) cameras captured movement from the front and side of the slope, with a high frame rate camera (120 frames per second) capturing transport from above the slope. This facilitated the verification of motion data, by tracking tracer movement and enabling comparison with the IMU data output. To support this, the slope surface was ruled, which allowed precise transport speed estimations.

In the laboratory, a range of rolling experiments were undertaken with slope angles of 6.5, 10, 15, and 20 degrees. This replicated the movement

behaviour expected at the point of entrainment and during subsequent transport within the smart stones. At each change in gradient, multiple experimental runs provided a range of movement behaviours. Rolling was observed to be qualitatively distinctive across all gradients. With transport speeds being positively correlated with increased gradient. As expected, increases in slope angle also resulted in greater angular velocity and acceleration values recorded by the gyroscope and accelerometer. However, due to the device range limitations, maximum capacity values were exceeded in all cases, with the rate of change, and duration of missed data being longer for higher slope gradients (Figure 4.3).

As gyroscope and accelerometer values experienced were greater than the firmware limits of 245 ° s^{-1} and 2 g respectively, it was not possible to accurately determine a relationship between the IMU data collected and the video footage of sediment transport above these thresholds. Therefore, it was unfeasible to distinguish between the forces experienced by the smart stones during movement, as the extent of the angular velocity and linear acceleration experienced by the smart stones could not be interpreted. This highlighted the need for an expanded sensor range, as forces regularly exceeded the maximum detectable capacity of the accelerometer and gyroscope.

Collision experiments between multiple smart stones were also undertaken at the Plymouth laboratory. These experiments expanded upon previous experimental runs by adding smart stones that collected IMU data at the base of the slope, in addition to the stones that were rolling. These attempted to replicate impact forces experienced by sediments associated with grain-to-grain collisions during transport, or while resting on the bed surface. Impacts from other sediments, or interruptions to transport by objects such as wood, or large grains, were simulated. Similar to rolling experiments, these involved a range of slope gradients, but with smart stones positioned at the base and top of the slope. Sediments were intermittently released, and the resultant forces experienced during impact between the two tracer groups were calculated from both the rolling and stationary sediments.

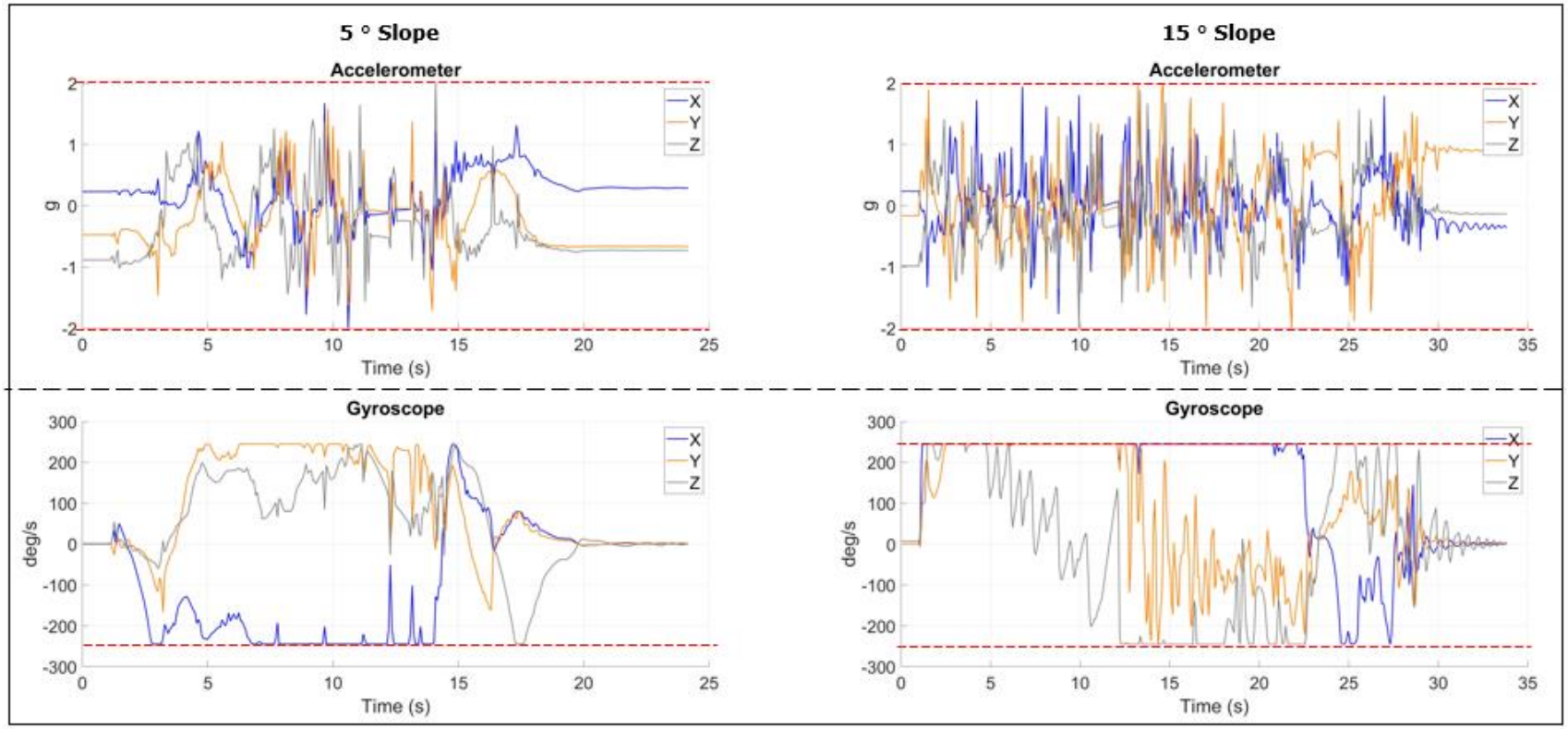

Figure 4.3: *Example accelerometer and gyroscope data outputs from 5 ° and 15 ° slope gradients at the University of Plymouth's dry granular slope. The figure demonstrates the extent of missing data due to linear acceleration and angular velocity exceeding threshold values of 2 g and 245 ° s^{-1} and the relative rate of change difference between the slope gradients. Threshold values are indicated by red dashed lines.*

Again, it was not possible to accurately infer a relationship between smart stone movement captured from video footage and that recorded by the IMU devices as maximum threshold values for the accelerometer and gyroscope were exceeded. However, the timing of impact events could be established from the data by observing the rapid increase and decrease in linear acceleration surrounding the event, although the peak values reached remained unknown. This could be achieved both within the transported tracers, where a distinctive spike in linear acceleration was captured, and within the stationary smart stones, where both gyroscope and accelerometer briefly exceed the measurement thresholds immediately following impact.

Overall, experiments undertaken at the Plymouth laboratory had mixed success. Video footage of the granular flow slope could not be used to directly compare to IMU data sets, primarily due to firmware capacity limitations. However, the runs were helpful to inform future laboratory work by establishing experimental procedures (e.g., section 4.7). They also highlighted the need for an upgraded sensor range. Continued laboratory work was put on hold due limitations in sensor capacity, until new firmware extending the device capacity became available.

4.4 Updated Firmware

The updated version of the Miromico firmware was available in August 2021. Updates included the enabling of the magnetometer, increasing the range of the accelerometer, gyroscope, and magnetometer to 16 g, 2000 ° s^{-1}, and 16 G (Gauss) respectively, in addition to various software bug fixes. As with all new firmware updates, experiments were undertaken to test the capabilities of the tags, verify that previous settings continued to function correctly, and gain experience with the magnetometer. The impact and rotation experiments outlined in section 4.2 were successfully replicated and verified consistent device behaviour. This ensured that data collection remained unchanged between the firmware versions. Subsequently, given the enhancement of the sensor capabilities, a series of experiments were conducted to determine the optimal settings for data

collection. The primary objective of these experiments was to identify the configuration that would yield the highest level of detail in terms of data collection, whilst remaining functional during deployment.

4.5 Data Collection Frequency Experiments

The IMU can collect data at a range of frequencies. This allowed devices to adapt to different environmental and laboratory conditions. When monitoring detailed movement behaviour, high frequency data collection is required, although this needs to be balanced with storage requirements. At higher frequencies, the smart stones are limited to shorter collection periods before reaching maximum flash memory space. Conversely, low frequency data collection may not fully characterise movement behaviour and could miss important events, such as the precise timings of impacts or the moment of tracer entrainment. High-frequency data collection also results in large quantities of data, requiring longer upload times via the LoRa network. This is often impractical for many applications, such as laboratory testing and early warning of movement in the field. This was an important consideration when accounting for the objectives of the SENSUM project, as rapid response times are needed for hazard management.

Therefore, different frequency settings were evaluated for the IMU sensors. The magnetometer can collect data at seven frequencies (0.625, 1.25, 2.5, 5, 10, 20, and 40 Hz), while the gyroscope and accelerometer can collect data at four frequencies (14.9, 59.5, 119, and 238 Hz) in unison. The ideal collection frequency setting would balance providing comprehensive interpretations of motion, while collecting the minimal amount of data to do so. High frequency data collection using smart tracers has been achieved previously. For instance, Šolc et al. (2012) and Valyrakis et al. (2010), collected accelerometer data at frequencies of 2832 and 500 Hz respectively during their smart tracer experiments. However, there are limited advantages in increasing data collection frequency to these high values, demonstrated by Maniatis et al., (2020) where lower frequencies (50 Hz) were found to be adequate for capturing the dynamics of particle movements. Higher frequencies are only beneficial in instances

of rapid movement where events occur over short time periods (e.g. < 10 ms). However, most movements in natural environments rarely reach speeds that require this level of detail to capture movement (e.g. Drake et al., 1988).

To evaluate the ideal frequency settings to implement in the smart stones to capture bedload transport behaviour, experiments were undertaken to test the level of detail each frequency setting could achieve. A movement arc, transporting the device 180 degrees and 30 cm along the same axis, was initially used as an easily identifiable signal within the IMU data. By repeating an identical movement pattern (the movement arc), at altering data collection frequencies, differences between the level of detail of data captured could be easily compared (as demonstrated in Figure 4.4).

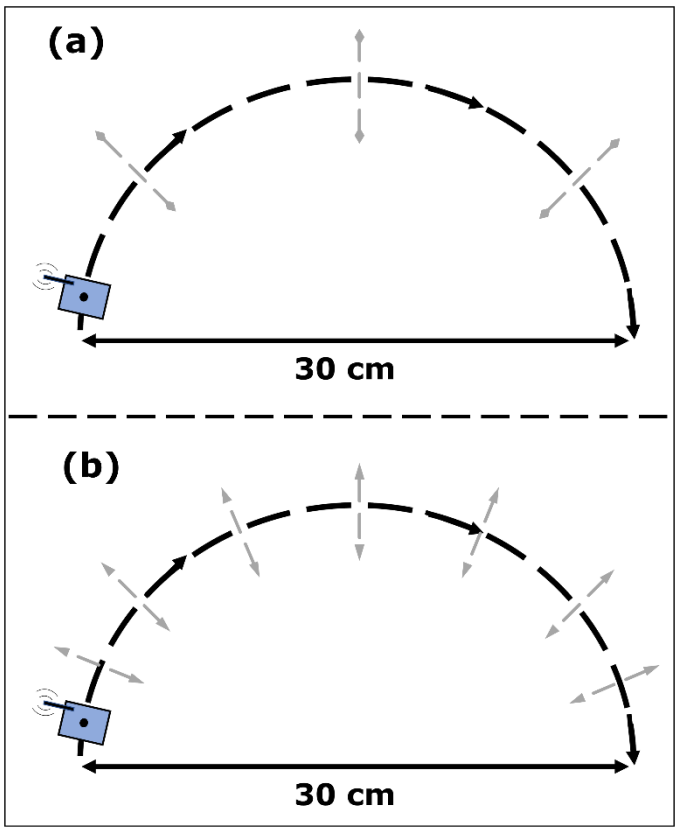

Figure 4.4: *180-degree arc used during data frequency experiments to distinguish between level of detail captured during movements with: (a) example low frequency data collection, with minimal movement detail captured; (b) example higher frequency data collection, with greater movement detail captured. (See figure 4.5 and 4.6 for example data outputs).*

For the gyroscope and accelerometer, 14.9 Hz was determined to be ideal. Increasing to higher collection frequencies (e.g., 59 Hz or 119 Hz) provided limited additional insight into device trajectory (Figure 4.5). Rather, it increased experimental noise, and at 238 Hz erroneous values emerged in the gyroscope data. While there may be advantages to collecting data above 14.9 Hz in complex high velocity events, the reduced storage capacity, and increased LoRa upload time, did not support its increase in the context of bedload transport during extended field deployment periods.

For the magnetometer 5 Hz was found to be ideal. This frequency allowed a sufficient understanding of the device position relative to magnetic north. Increasing above 5 Hz added additional experimental noise and did not provide further insight into positional information. Frequency settings below 5 Hz (e.g., 2.5 and 1.25 and 0.625 Hz) did not fully capture movement (Figure 4.6), missing the timing of the initiation of movement events during data collection.

Similarly, basic movements (e.g., rolling, sliding, shaking) were also evaluated at a range of collection frequencies, to determine if frequency settings matched level of detail requirements. Based on the analysis conducted, it was determined that for optimal data collection, devices should be configured to acquire data at 14.9 Hz for the accelerometer and gyroscope and 5 Hz for the magnetometer. This frequency was determined to be the optimal balance between capturing sufficient detail and maintaining efficient storage capacity within the device. These settings were applied for all subsequent laboratory experiments and during field deployments of smart stones.

Figure 4.5: *IMU frequency experimental results, demonstrating the range of data outputs recorded using an identical movement at differing collection frequencies. Data output supports the assessment of ideal collection settings which balance level of detail and available device storage. With (a) and (b) showcasing collection frequencies for the gyroscope and accelerometer respectively. Minimal improvements in level of detail are obtained increasing above 14.9 Hz on repeated experiments, suggesting increasing collection frequency further is not required.*

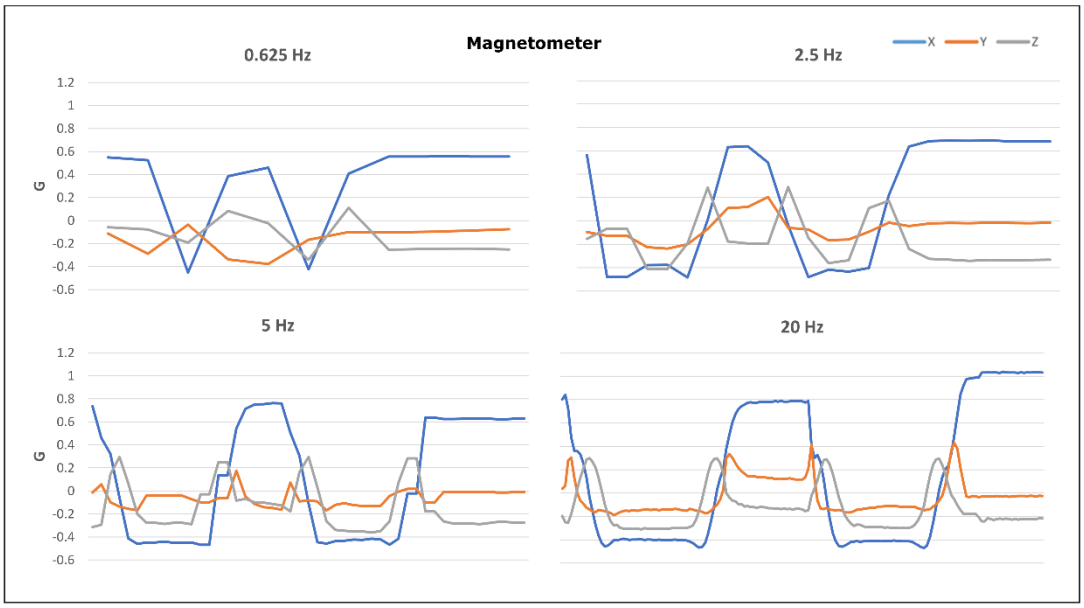

Figure 4.6: *IMU frequency experimental results for the magnetometer, demonstrating the range of data outputs recorded using an identical movement at differing collection frequencies. Output supports the assessment of ideal collection settings which balance level of detail and available device storage. 5 Hz was found to collect sufficient level of detail while requiring minimal storage space. Note the poor detail captured at 0.625 and 2.5 Hz, missing the initiation of movement, and the minimal improvement seen when increasing to 20 Hz.*

4.6 IMU Drift and Noise

For an accurate interpretation of data, an understanding of the baseline behaviour and any irregularities of the devices needed to be evaluated. All IMU sensors experience some degree of drift (Zhao, 2018). Small miscalculations during the measurement of linear acceleration and angular velocity can accumulate into larger errors, as measurements recorded are relative to those previously calculated (Kok et al., 2017). Therefore, it was imperative to quantify to what extend this was occurring within the Nomad IMU sensors. This could then inform the likely degree of uncertainty during interpretations of movement data.

Baseline IMU data (no activity) was needed to evaluate the extent of drift measured by the smart stones. To produce this, data collection was

triggered, and devices were programmed to continuously record for ≥ 30 seconds. After triggering, data was collected without subsequent movement. This captured any internal deviations recorded by the device, unrelated to movement. This provided examples of background IMU values and allowed gyroscope drift from 0 ° s^{-1} to be estimated.

Averaging deviations from baseline, gyroscope drift was found to be minimal. Drift typically was within ± 3 ° s^{-1} across all test runs. This suggested that gyroscope data interpreted during laboratory experiments, or data derived from field deployment, can be assumed to be roughly within 3 ° s^{-1} of true rotational values. Therefore, drift was likely negligible when interpreting sediment movement, where associated changes in angular velocity were usually an order of magnitude larger than 3 ° s^{-1}.

Additionally, magnetometer drift was analysed. Recorded deviations from baseline were also found to be minimal (± 0.0232 G). While sensor drift is unlikely to be a significant source of error within the magnetometer, objects containing ferrous metal, in the laboratory, or environment, could potentially distort data (McFee et al., 1994). At the field deployment sites, there is little that can be done regarding eliminating ferrous materials, although in the laboratory, experiments are conducted away from magnetic objects to preserve magnetometer accuracy.

Due to the natural gravitational forces experienced by the accelerometer when stationary, baseline linear acceleration values consistently display readings of approximately 1 g across the device axes. The primary axis experiencing this is dependent on the position of the device relative to the direction of gravitational force. These results suggest when interpreting laboratory and field data, and the absolute position of the device is not known, it must be assumed that any raw data values < 1 g could be resulting from gravitational force, rather than resulting from changes in linear acceleration. Filtering this gravitational effect is theoretically possible, if alignment relative to gravity is known. Unfortunately, when dealing with long term deployments in the field, without direct observations, absolute estimations of device positions become unfeasible. As a result, it becomes difficult to continuously correct the acceleration

values. Therefore, when interpreting linear acceleration data sets, a 1 g threshold must be considered.

4.7 LoRa Data Transfer

Data transfer from the Nomad sensor board can be achieved through two main methodologies. Direct upload from the device, using a USB serial connector, or data transfer wirelessly, using LoRaWAN transmission. Within the laboratory, multiple gateways were available for testing the capability of LoRaWAN transmission, and the relative speed of data transfer. This provided an opportunity to compare wirelessly uploading data to transferring data directly via the USB serial cable.

Each transfer approach was evaluated for its effectiveness in a laboratory environment, with the unique advantages and disadvantages of both methods being determined. Using LoRaWAN removes the need for device extraction from the smart stone case between tests, as both data transfer and setting alterations can be performed over the air. Furthermore, real time data retrieval via LoRa allowed device performance to be instantly evaluated, as time stamps are embedded within collected IMU data. These conditions also most similarly matched the methodology planned during long term deployment in the field.

Despite this, LoRaWAN was found to have an increased risk of erroneous data during testing, as there is the potential for data corruption during payload transfer. Although, this appears to be minimal with the most up to date version of the firmware. Additionally, data transfer speeds are significantly slower, particularly when using high frequency data collection. While this is not problematic during field deployment, it can be detrimental when in a time constrained laboratory setting. For instance, single experimental runs, with less than one minute of movement activity, can take multiple hours to fully upload.

Transferring data via the USB serial cable is comparatively faster, only requiring 2 – 10 seconds to upload the contents of the device’s memory. In addition, there is no risk of data corruption. However, between

experimental runs, additional time is needed for setup, as the module must be removed from the smart stone before connecting the serial cable. This can also cause unwanted triggering of data collection, with experimental noise being captured by the devices when removing the smart stone housing. Therefore, transferring data via USB requires more time during analysis to filter movement not associated with experimental runs, and any problems with the devices or data are only discovered after upload.

With both approaches being evaluated in the laboratory, the USB serial cable approach became the standard method, primarily due to time constraints. LoRaWAN transfer is applicable in field environments, as movement is often sporadic, with long static periods allowing time for data transfer. This contrasts with the needs of laboratory experimentation, where multiple individual movement events needed to be triggered and recorded over short time periods.

Difficulties in isolating experimental runs from background setup noise within the data were resolved using a known rotational signal performed immediately prior to and following each experimental run (Figure 4.7). This double rotation is distinct from the surrounding experimental noise and laboratory data and was effective for indicating the initiation and end of the data collection.

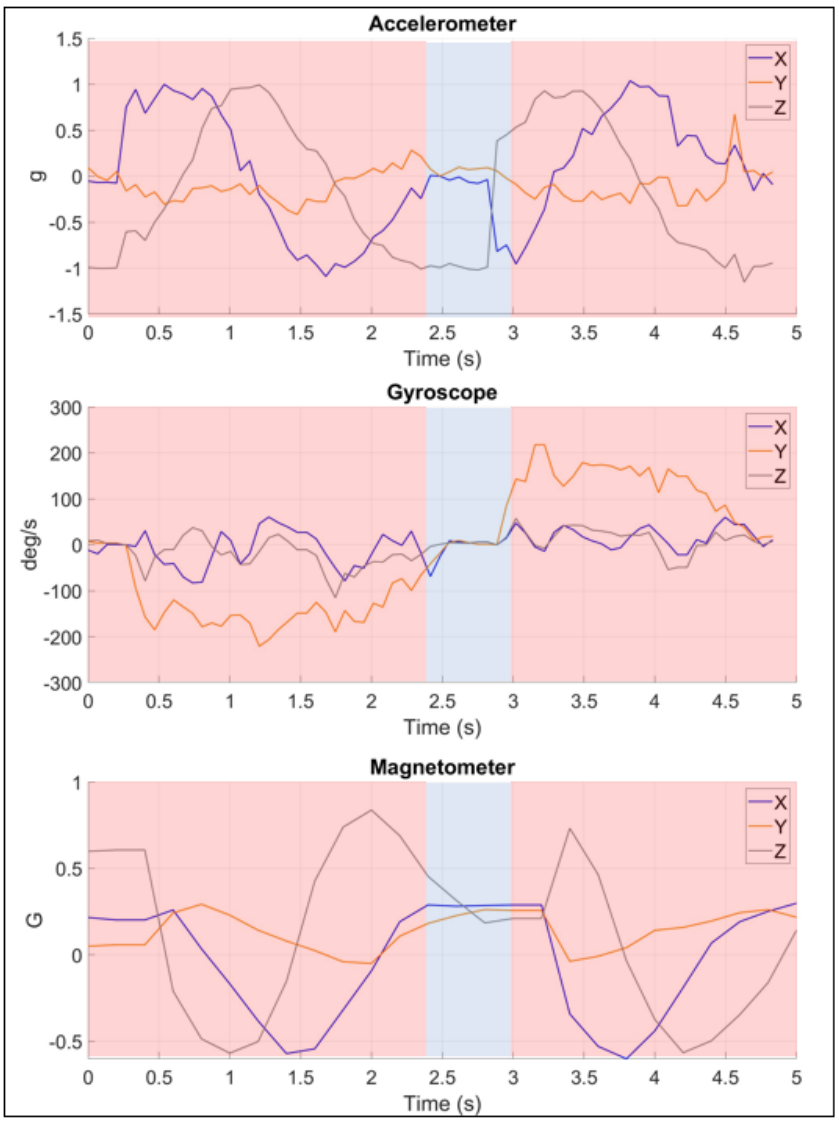

Figure 4.7: *Double rotational signal used to indicate the beginning and end of individual experiments, with the distinctive double peak in the accelerometer data and the associated changes in the gyroscope and magnetometer. Periods of rotation highlighted in red with transition to second rotation highlighted in blue.*

4.8 Revised Laboratory Experimentation

Once device settings were optimised, the LoRa gateways tested, and an understanding of sensor baseline behaviour was established, drop tests and high velocity rolling experiments were completed. These were used to assess if the expanded range of the devices (16 g and 2000 ° s^{-1}) would capture all movement smart stones would potentially experience in the

field. Across all experiments, the extended maximum ranges were not exceeded, with maximum angular velocity and linear acceleration recorded being 1217 ° s^{-1} and 12.12 g respectively.

The behaviour of the updated magnetometer was also investigated. Rotational experiments along a single axis were used to determine the relative response of the magnetometer. Following this, rolling experiments were used to achieve values closer to those expected during deployment. Once these initial feasibility tests were completed, the experiments characterising individual transport behaviours could begin.

4.9 Transport Behaviour Replication in the Laboratory

The rationale behind laboratory experiments was to build an IMU data inventory of specific movement types, typical of coarse-grained sediments in natural fluvial environments. These ranged from the simple shaking of sediments, i.e. replicating protruding clasts in flow conditions prior to entrainment, to transport conditions after incipient motion, via rolling or sliding. These data sets are intended to inform the analysis of field data, providing a greater understanding of tracer movements captured during deployment.

To simulate high velocity movement events where sediments are abruptly interrupted, e.g., by a stationary object, drop and collision experiments were carried out. These were designed to emulate the conditions of a tracers clashing with other coarse-grained particles, or by being interrupted during transport by large wood pieces. In addition, dropping motions experienced by smart stones in the laboratory were intended to simulate the deposition of tracers into scour pools, where tracers were dropped from a range of heights from 15 – 30 cm.

Shaking experiments were used to simulate environmental conditions before entrainment where individual grains will shake in the bed pocket as they approach the energy required to initiate entrainment (e.g., Garcia et al., 2007). This was achieved either with individual sediments being

manually vibrated, or through a collection of sediments being vibrated at a set frequency in a container.

To simulate the conditions of a tracer being transported along a bed surface through rolling, a similar setup to the Plymouth experiments was used. A slope was designed and constructed with an adjustable height, and a high frame rate camera was set up to capture transport. This allowed a range of rolling speeds to be captured by altering the slope gradient, emulating different fluvial conditions. Velocities of transported tracers ranged from 0.6 - 0.9 m s^{-1} across all experiments. Additionally, barriers were implemented to impede sediment movement and confine rolling to simulate bed conditions.

The transport of sediments via a sliding motion was also investigated. This was replicated through dragging smart stones across a simulated bed surface with consistent contact with the ground, maintaining the original orientation of the sediment by pulling the tracer via a taped string attached to the face of the smart stone.

Across all laboratory experiments, qualitative descriptions of the data output from the IMU sensors were beneficial for identifying distinct responses to movement events within the smart stones. i.e. the qualitative description of overall shape, length, and distinct peaks within recorded data can be used to initially understand tracer movements and interpret transport mode. Furthermore, the rate and magnitude of change in each individual sensor can be unique to specific movement behaviours (e.g., continuous oscillations within the magnetometer indicating rotation). These initial interpretations are further supported by quantitative data (e.g., linear accelerational values recorded during shaking are less than those recorded during sediment collisions). By combining qualitative and quantitative information derived during laboratory experimentation, unique signatures can be produced for each movement mode experienced by the smart stones.

4.10 Laboratory Methodology

4.10.1 Impact Experiments

In total, 30 impact events were recorded and evaluated. Collision forces were replicated by allowing smart stones to drop under gravitational force from a range of heights. Events were categorised into medium impacts, simulated by dropping tracers at a height of 15 cm, and high impacts, which were simulated with drop heights of 30 cm.

All events were captured using video recordings, which provided a direct comparison between observed tracer movement and IMU data, allowing verification. All resultant forces, from free fall, impact, and subsequent motion were recorded until the cessation of movement, with the moment of collision observed to be distinct within the data.

4.10.2 Rolling Simulation Experiments

Rolling experiments were designed to replicate typical bedload transport conditions experienced by the smart stones, immediately following entrainment. They also provided a direct comparison to the granular slope experiments undertaken at the University of Plymouth (section 4.3), but with updated device firmware capable of capturing the full range of forces experienced by the smart stones.

Each experimental run on the UEA laboratory slope was recorded using a stationary high-definition camera, recording at 60 frames per second. This was located at the base of the slope and captured all transport within its field of view. Barriers were installed along the perimeter of the slope, ensuring sediments would be transported down its full length. In total, the slope had a length of 1.2 m and a gradient of 10 ° was used during all recorded experiments.

4.10.3 In-Situ Shaking Experiments

Shaking experiments emulated environmental conditions before the initiation of entrainment, from minor vibrations caused from low flow conditions to forces experienced immediately prior to incipient motion. To simulate these, different experimental setups had varying intensity levels of shaking, categorised into low, moderate, and high, based on the vibrational force applied during each experimental run. Where, increasing intensities of shaking intended to simulate sediments in conditions progressively closer to the threshold of entrainment.

4.10.4 Sliding Experiments

Transport without particles pivoting can occur when drag force from streamflow is applied to particles uniformly (Dey and Ali, 2017). Sliding experiments were designed to simulate the transport of individual sediments without a rotational component, where constant contact between the bed surface and smart stones remains throughout movement.

4.11 Experimental Results

4.11.1 Impact Results

A rapid spike, or cluster of activity, from the accelerometer are a prominent feature seen during collision response (Figure 4.8). These are observable immediately after tracer freefall, which is identified by 0 g being recorded across all accelerometer axes. At impact, accelerational forces of > 2 g were recorded during every collision and are followed by a rapid return to baseline values. These spikes of activity are also replicated within the gyroscope data, where background values rapidly increase to over 200 ° s^{-1} followed by a return to base line (Figure 4.8). The relative size of these spikes differs on average between the medium and high impact events, where tracers dropped from greater heights have distinctly larger peaks. In contrast, magnetometer data is not an ideal indicator of impacts, as the relative position of tracers are not consistent between individual experiments following impact.

Peak accelerometer and gyroscope values recorded were 4.24 g and 510.79 ° s^{-1} respectively (Table 4.1). As expected, these values were produced during one of the high impact experiments. In each case, a change from baseline, to peak values occurred in < 500 ms, with the rapid rate of change being indicative of the point of impact. Not every axis experienced a rapid increase in recorded values during impact (i.e., across X, Y, and Z). Although at least one axis experienced a rapid increase in both the gyroscope and accelerometer during every collision. Additionally, on average, gyroscope peak values were greater during the high impact experiments for every axis. Whereas the accelerometer peak values were greater in the X and the Y axis (Table 4.1).

Changes in the magnetometer values lack a distinctive signature during impact experiments, as their values represent orientation relative to magnetic north, rather than a change from a baseline value. Despite this, the moment of impact can often be interpreted from a rapid change of > 1 G in at least two of the magnetometer axes. This often resulted from the smart stone rotating immediately after a collision, but this effect was not consistent across all impact events.

Table 4.1: *Peak and mean values recorded during impact experiments, displaying maximum and average values for the X, Y, and Z axis, separated into 15 and 30 cm experimental sets. N.B. Overall maximum forces measured boldened, and mean values adjusted for negative results.*

	Axis	**ACC** (g)	**GYRO** (° s^{-1})
Max (15 cm)	X	-4.18	-232.6
	Y	-4.26	-329.84
	Z	4.16	-285.25
Max (30 cm)	X	3.13	447.93
	Y	**-4.37**	**510.79**
	Z	4.15	-429.87
Mean (15 cm)	X	1.36	158.93
	Y	1.53	193.62
	Z	1.68	153.11
Mean (30 cm)	X	1.40	265.85
	Y	1.68	243.35
	Z	1.59	187.05

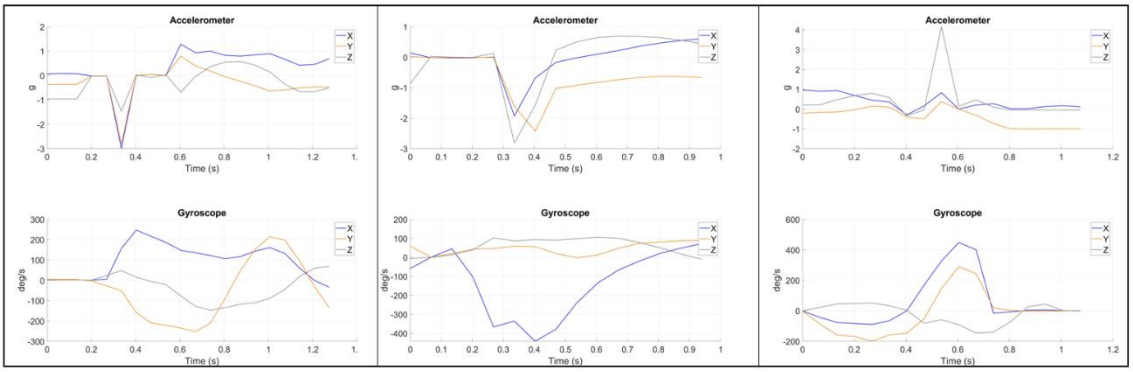

Figure 4.8: *Resultant data output from smart stone impact experiments, highlighting the rapid spike in the accelerometer of > 2 g at moment of impact and its associated gyroscope activity. (a) and (b) represent examples of medium impacts (15 cm free fall), and (c) represents an example of high impact (30 cm free fall). Note the 0 g readings in the X, Y, and Z axis of the accelerometer prior to impact resulting from the lack of gravitational force readings on the accelerometer during freefall.*

4.11.2 Rolling Results

All three sensor components of the IMU device provided distinctive signals during rolling experiments. Gyroscope measurements were unique due to the progressive increase in collected values, stabilisation, and return to baseline (Figure 4.9). This represents the relative acceleration immediately after entrainment, reaching a peak transport velocity, followed by a gradual deceleration at the base of the slope. As the gyroscope measures relative change in angular velocity, these single large peaks are indicative of constant movement, and therefore can be used to infer full tracer step length.

The magnetometer results were equally distinctive, as the rapid shifting of values in an oscillatory pattern matches the relative position of the tracer as it rotated down the slope. The rate of positional change, as demonstrated by the magnetometer, is unique to transport via rolling. For example, magnetometer alone can be used to estimate the number of rotations experienced by the tracer. This is achieved by observing the number of peaks and troughs along a single axis in the data sets. This was verified from observations from video recordings of the rolling events. For

example, the seven main peaks recorded in the Y axis (Figure 4.9) align with seven full rotations experienced by the smart stone as it was transported downslope.

The data output from the accelerometer during rolling was also distinctive. Linear acceleration was the highest recorded across all movement behaviours replicated in the laboratory. Relative size of individual accelerometer peaks matched gyroscope intensity, with a rapid increase at the initiation of entrainment, followed by a progressive decrease as transport speeds reduce.

Peak accelerometer values recorded throughout rolling experiments all exceed 4.5 g in at least one axis during transport (Table 4.2). Similarly, recorded peak gyroscope values all exceed 1000 ° s^{-1} on at least one axis (Table 4.2). While rolling was initiated from identical positions at the top of the slope, the preferred axis of rotation deviated after each experimental run. This is reflected in both the gyroscope and accelerometer data, where the primary axis with the highest recorded values alternates each run. For example, the gyroscope data during run 2 and run 5, $X_g > Y_g, Z_g$, and in the accelerometer during run 3 and run 6 $X_a > Y_a, Z_a$. Although, in run 1 the Z axis dominates across both the gyroscope and accelerometer. This suggests a diversity in rolling behaviour, where tracers are unlikely to always be transported along the same axis.

Table 4.2: *Maximum accelerometer and gyroscope values recorded during each rolling experiment.*

	X_g (°/s)	Y_g (°/s)	Z_g (°/s)	X_a (g)	Y_a (g)	Z_a (g)
Run 1	1202.25	711.34	1331.68	3.73	-4.39	4.83
Run 2	1325.94	-758.45	1099.42	10.55	-5.39	-9.24
Run 3	-621.67	1246.91	1217.79	11.81	-4.95	-4.66
Run 4	1062.60	830.34	-916.79	-5.50	-6.90	8.57
Run 5	1580.74	743.33	374.50	3.18	-3.60	5.40
Run 6	-1058.61	903.42	1434.72	7.99	6.19	5.60

**X_g and X_a indicate X axis gyroscope and X axis accelerometer respectively*

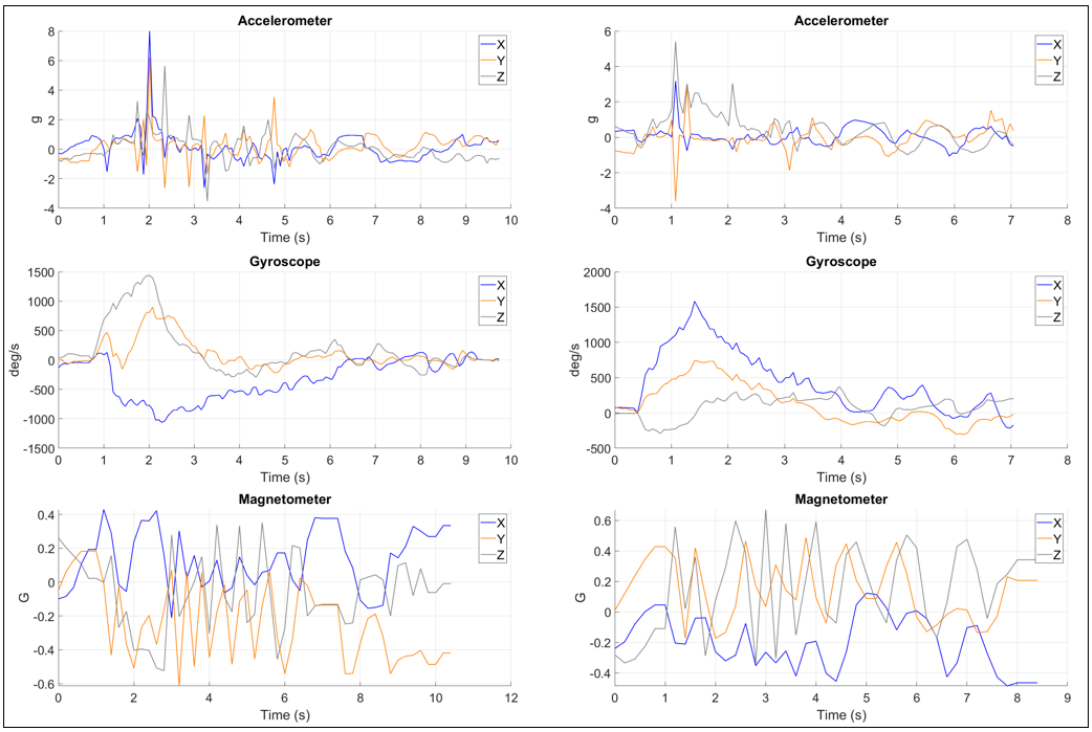

Figure 4.9: *Example data outputs of rolling experiments demonstrating key distinctive features of movement behaviour. With a single large peak in gyroscope representing continuous rolling, with gradual increase, stabilisation, and progressive return to original values, peak accelerometer values matching maximum transport speeds, and oscillatory pattern within*

the magnetometer data matching the position of the tracer rotating down the slope.

4.11.3 Shaking Results

The accelerometer, gyroscope, and magnetometer all displayed distinctive characteristics during the shaking experiments. Particularly, the gyroscope and accelerometer sensors produced repeated spikes from data baseline. These matched the frequency of the shaking experienced by the smart stones and aligned with video recordings. Additionally, the peak values measured were positively correlated with the intensity of the shaking experienced by the smart stones. A clear, rapid, oscillation pattern is observed within the plotted data, this repeated sequence is distinct to tracer shaking behaviour (Figure 4.10).

The magnetometer is ideal for identifying shaking without entrainment, as values recorded remain relatively constant, as orientation change is limited. This is a distinctive feature compared to other movement behaviours replicated in the laboratory.

These characteristic signals within the IMU data, in combination, produced a unique signature of shaking. This suggested it was possible to determine if a tracer is remaining stationary on a riverbed pre-entrainment, with only minor vibrations being experienced, and without rotation occurring.

Peak accelerometer and gyroscope values recorded during shaking are typically lower than other movement types recorded. During these experiments accelerometer and gyroscope values do not exceed 3.50 g and 175 ° s^{-1} across all experimental runs. As expected, the maximum accelerometer and gyroscope values of 3.31 g and 163.87 ° s^{-1} were recorded during the higher intensity shaking experiments (Table 4.3). Similarly, the lowest intensity shaking experiments had peak values as low as -0.61 g and -15.4 ° s^{-1}, demonstrating the distinction between shaking intensity levels observed in the data.

The magnetometer data during shaking does not deviate significantly (< 0.2 G) from original baseline values. This, alongside other characteristics described, appears to be the ideal identifier for this type of movement.

Table 4.3: *Maximum values recorded during each shaking experiment, demonstrating the relative relationship between shaking intensity and accelerometer values.*

	X_g (° s^{-1})	Y_g (° s^{-1})	Z_g (° s^{-1})	X_a (° s^{-1})	Y_a (° s^{-1})	Z_a (° s^{-1})	**Intensity**
Run 1	50.40	76.16	34.23	1.50	-1.80	-3.1	Moderate
Run 2	-40.25	114.17	-60.83	0.81	-1.30	-1.8	Moderate
Run 3	44.87	-58.31	35.49	0.70	-1.20	-2.4	Moderate
Run 4	101.22	145.74	163.87	-1.90	3.31	-2.9	Intense
Run 5	-156.38	60.20	85.75	-0.90	0.37	-1.0	Light
Run 6	7.14	-15.40	10.78	-0.60	0.66	-0.7	Light

**X_g and X_a indicate X axis gyroscope and X axis accelerometer respectively*

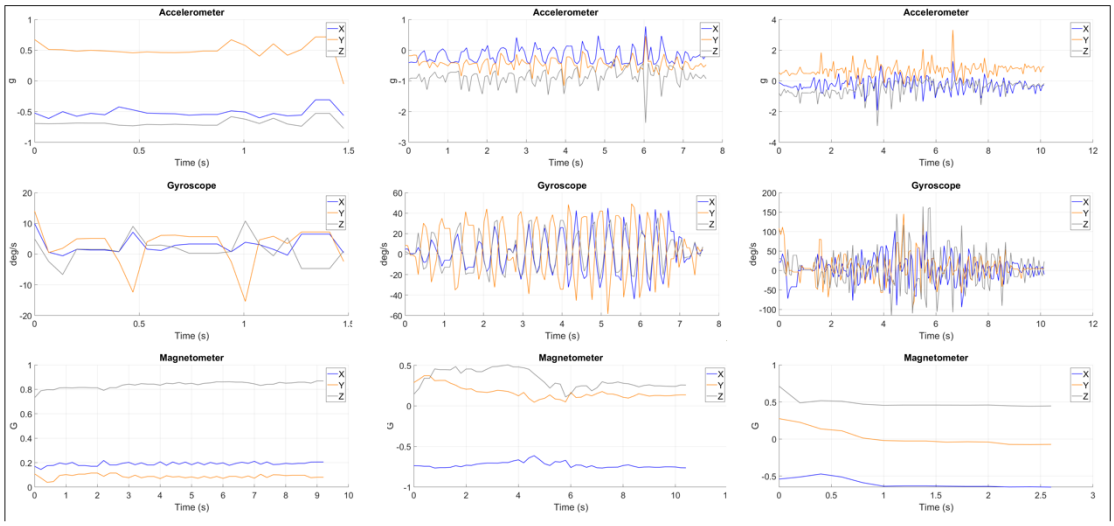

Figure 4.10: *Accelerometer, gyroscope, and magnetometer response during shaking experiments with varying intensities of shaking. With clear oscillating patterns observed in gyroscope and accelerometer data and distinctive lack of change in magnetometer values. (a), (b), and (c) represent light, moderate, and intensive shaking respectively.*

4.11.4 Sliding Results

Transport of the smart stone across the experimental surface was not continuous and smooth, where changes in friction between the tracer and surface periodically increased and decreased transport velocity. This was reflected within the gyroscope and accelerometer data sets, where periodic

spikes of activity matched moments of trapping and release observed during transport (Figure 4.11).

Similar to shaking experiments, magnetometer measurements were relatively stable, with only minor deviations in orientation over time. This clearly distinguishes this form of transport from rolling, where orientation change is a primary indicator.

Linear acceleration and angular velocity remained relatively low throughout sliding experiments, with peak gyroscope and accelerometer values recorded reaching 271 ° s^{-1} and 2.88 g respectively.

Magnetometer data during sliding did not deviate significantly from pre-entrainment values, with < 0.2 G change typical during most transport periods, although limited orientation change is observed during some experiments (Figure 4.11).

Minimal magnetometer activity, in addition to relatively low linear acceleration and angular velocity values recorded during transport, appeared to be the ideal identifier for this mode of movement. With the smaller range of values captured specifically distinguishing sliding from rolling behaviour.

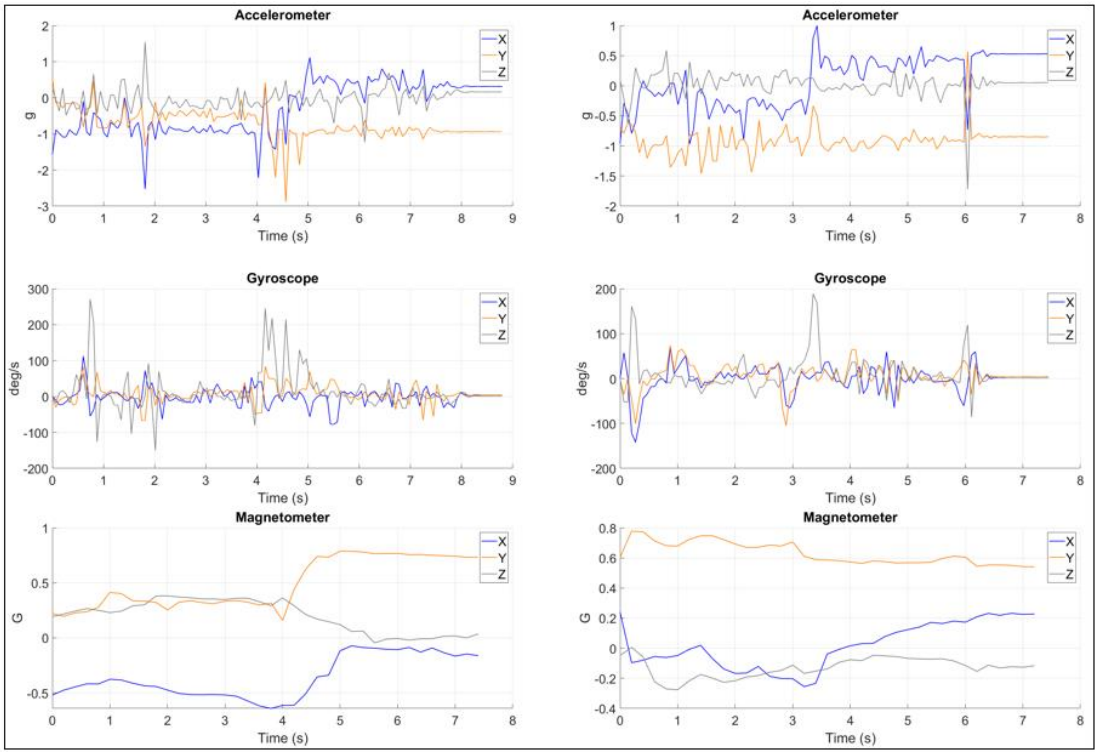

Figure 4.11: *Resultant data output from a selection of sliding experiments, highlighting the distinctive lack of change within the magnetometer, and the periodic trapping and release observed during transport being reflected as spikes of activity in both the gyroscope and accelerometer.*

4.12 Summary Characteristics and Unique Movement Signatures

Distinctive responses from the IMU sensor could be characterised and linked to specific transport behaviour of the smart stones (Table 4.4). Unique signals within the accelerometer, gyroscope, and magnetometer, either individually, or in combination, was indicative of all movement modes investigated (e.g., Rolling, sliding, shaking, and impacts). Both qualitative interpretations from data, (e.g., patterns in device response), in addition to quantitative evaluations (e.g., range of values, rate of change, and thresholds) were used to initially identify and categorise movement. Subsequent experimental runs verified these IMU signatures and built an inventory of data sets available for comparisons to field deployment data.

Table 4.4: *Distinctive characteristics of IMU data output, derived from laboratory experiments of specific movement types.*

	ACC	**GYRO**	**MAG**
Collision	Rapid spike at impact (0 – 4.37 g in < 0.5 s)	Rapid spike at impact (0 – 510.79 °/s in < 0.5 s)	Not distinctive
Shaking	Oscillating peaks and troughs (max = 3.3 g)	Oscillating peaks and troughs (max = 156 °/s)	Typical change in value (< 0.2 G)
Rolling	Multiple high value peaks during motion (max = 11.81 g)	Single large GYRO peak (max = 1580.74 °/s)	Rapid continuous oscillations
Sliding	Low peak values (max = 2.88 g)	Low peak values (max = 271 °/s)	Typical change in value (< 0.2 G)

Comparative analysis between data sets simulating tracer transport, and those replicating pre-entrainment conditions were typically differentiated by the range of accelerational and rotational forces experienced (Figure 4.12). Furthermore, rapid changes in orientation interpreted by the magnetometer were highly indictive of transport events. Although, transport by sliding retained tracer orientation, but exceeded the typical accelerational values expected from a stationary sediment (e.g., during shaking).

These laboratory experiments suggested that it should be possible to review data sets obtained from the field and interpret the likely movement mode without direct observations. Particularly, data collection caused by pre-entrainment conditions (shaking) appears to be unique compared to other transport conditions, supporting the estimation of the timing of incipient motion for IMU data. While it is possible for smart stones to experience collision forces while stationary, the signature within the

gyroscope and accelerometer is always short-lived and can be distinguished from data derived from transport.

Threshold values could be determined for the gyroscope and accelerometer to distinguish between movement categorised as entrainment via rolling and other movement modes (e.g., 6 g and 600 ° s^{-1}, Figure 4.12). However, its applicability to data derived from field deployment may be limited due to the differences in the laboratory setting and natural environments.

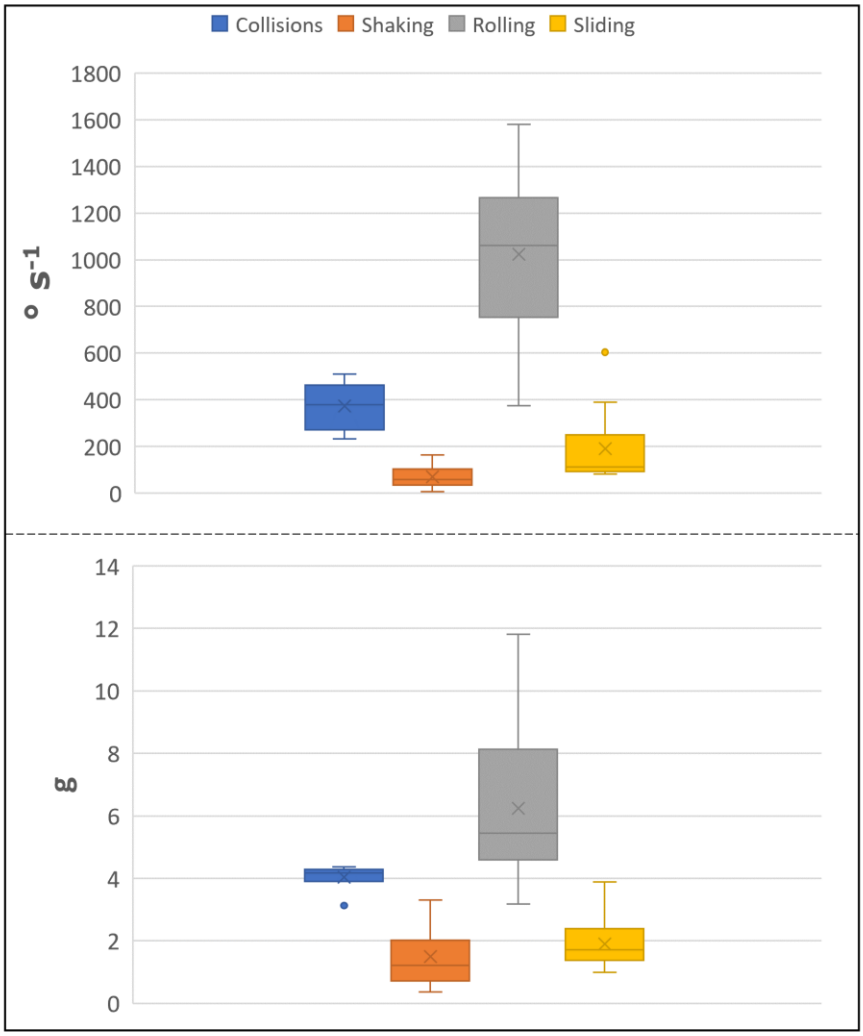

Figure 4.12: *Range of gyroscope and accelerometer data experienced in the laboratory for each movement mode investigated, demonstrating the divide between transport and non-transport movement modes. N.B. values have been adjusted for negative values to allow full comparison all data collected (absolute values have been used).*

4.13 Limitations of Laboratory Experimentation

Simulating expected modes of transport, and the associated accelerational and rotational forces experienced by the smart stones, can only approximate natural environments. Data sets derived from laboratory experimentation only provide analogous information to those obtained during field deployment (Recking, 2012). It was not possible to replicate all variables expected, primarily the forces associated with the natural mobilisation of sediments, and the influence of water on transport behaviour. Additionally, the impact of transport over natural bed material, the process of sediments saltating, and the full range of flow conditions could not be accurately reproduced in a laboratory environment. This highlighted the need for smart stone deployment in the field. Despite this, by accumulating an inventory of data sets associated with specific movement modes of the smart stones, interpreting field data without direct observation becomes potentially possible.

References

Dey, S., & Ali, S. Z. (2017). Mechanics of sediment transport: Particle scale of entrainment to continuum scale of bedload flux. *Journal of Engineering Mechanics*, *143*(11), 04017127.

Drake, T. G., Shreve, R. L., Dietrich, W. E., Whiting, P. J., and Leopold, L. B.: Bedload transport of fine gravel observed by motion-picture photography, J. Fluid Mech., 192, 193–217, 1988.

Garcia, C., Cohen, H., Reid, I., Rovira, A., Úbeda, X., & Laronne, J. B. (2007). Processes of initiation of motion leading to bedload transport in gravel-bed rivers. *Geophysical research letters*, 34(6).

Kok, M., Hol, J. D., & Schön, T. B. (2017). Using inertial sensors for position and orientation estimation. *arXiv preprint arXiv:1704.06053*.

Maniatis, G., Hoey, T., Hodge, R., Rickenmann, D., & Badoux, A. (2020). Inertial drag and lift forces for coarse grains on rough alluvial beds measured using in-grain accelerometers. *Earth Surface Dynamics*, 8(4), 1067-1099.

McFee, J. E., Ellingson, R. O., & Das, Y. (1994). A total-field magnetometer system for location and identification of compact ferrous objects. *IEEE transactions on instrumentation and measurement*, *43*(4), 613-619.

Recking, A. (2012). *Bedload transport in rivers: from the flume to the field* (Doctoral dissertation, HDR mécanique, Université de Grenoble).

Šolc, T., A. Stefanovska, T. Hoey, and M. Mikoš (2012), Application of an instrumented tracer in an abrasion mill for rock abrasion studies, Strojniški vestnik- *Journal of Mechanical Engineering*, 58(4), 263–270.

Valyrakis, M., Diplas, P., Dancey, C. L., Greer, K., & Celik, A. O. (2010). Role of instantaneous force magnitude and duration on particle entrainment. *Journal of Geophysical Research: Earth Surface*, *115*(F2).

Zhao, J. (2018, September). A review of wearable IMU (inertial-measurement-unit)-based pose estimation and drift reduction technologies. In *Journal of Physics: Conference Series* (Vol. 1087, No. 4, p. 042003). IOP Publishing.

CHAPTER 5

5 Deployment of Smart Stones at UK Field Sites

5.0 Chapter Overview

This chapter describes the deployment of the smart stone tracers at three UK field sites, the data obtained during deployment, the challenges and limitations encountered, and comparisons to the dry laboratory library of data sets discussed in chapter 4. Firstly, short term experimentation at the "controlled" field site, Branscombe Beach, is covered. Where the natural mobilisation of tracers is achieved and recorded in a wood free environment, replicating dry laboratory transport experiments in a non-simulated setting. Secondly, the long-term deployment of smart stones at a Natural Flood Management (NFM) research site with anthropogenically placed woody debris (Tebay Gill) during the winter of 2021 – 2022. Finally, I present the long-term deployment of LoRaWAN-enabled smart stones at Yarner Woods throughout 2022, allowing for monitoring of natural woody debris in combination with the smart stones. This final site is also used to assess the functionality of real time continuous monitoring of tracer movement behaviour relative to flow conditions throughout the year.

5.1 Introduction

The smart stone dry laboratory experiments described in chapter 4 yielded an inventory of tracer movements, each with unique identifying characteristics within the IMU data. These characteristics represented specific movement types; shaking, rolling, sliding, and collisions. This was an essential first step in understanding how smart stones could help characterise typical bedload transport behaviour and detect the point of entrainment of grains. However, these findings need to be verified with data from the transport of tracers in natural flows, as forces experienced in geomorphologically complex environments may not be apparent in the laboratory. Therefore, this chapter covers a range of deployment sites that were selected for their varying environmental conditions. These sites include those with natural woody debris (section 5.6), anthropogenically placed woody debris (section 5.4), and a wood-free site (section 5.2) for controlled natural transport experiments (Figure 5.1). By studying these differing sites, it is possible to gain a more complete understanding of the effects of different types of woody debris on the transport of grains. This is critical for developing effective strategies for managing bedload transport using NFM techniques across a range of environments.

To validate laboratory data sets, smart stones were initially deployed at Branscombe Beach, a wood-free site chosen to replicate controlled laboratory conditions but with natural flows over short-term deployment periods. This allowed for a direct comparison between the laboratory data and the field data, providing a means of verifying the accuracy and reliability of the laboratory results. By conducting experiments at a wood-free site, it was possible to isolate the effects of the natural flow conditions on the movement of the tracer particles, without the complicating factors introduced by the presence of woody debris. This provided a useful control for the subsequent deployment at sites with varying amounts and types of woody debris.

For the second field experiments, the smart stones had long term deployment at two different sites and compared two different data storage methods: one using LoRaWAN-enabled smart stones, and the other using

direct storage of data on the devices. At the first site, Tebay Gill, the smart stones were configured to store data directly on the devices, rather than transmitting it wirelessly. At the second site, the smart stones were equipped with LoRaWAN technology, which allowed for the wireless transmission of data to a central server. This enabled real-time monitoring and analysis of the tracer particle movements, and allowed for rapid detection of any changes in flow conditions. Both methods had their advantages and encountered specific challenges, which are described in this chapter.

The findings within this chapter contribute to a better understanding of the use of smart stone devices within an integrated IoT LoRaWAN network, and have implications for their successful implementation in early warning systems in remote environments. By studying the performance of these devices under different conditions, it is possible to identify key factors that affect their reliability and accuracy. This information can be used to optimize the design and deployment of smart stone networks, improving their effectiveness at tracking movement behaviour and as early warning systems in remote environments.

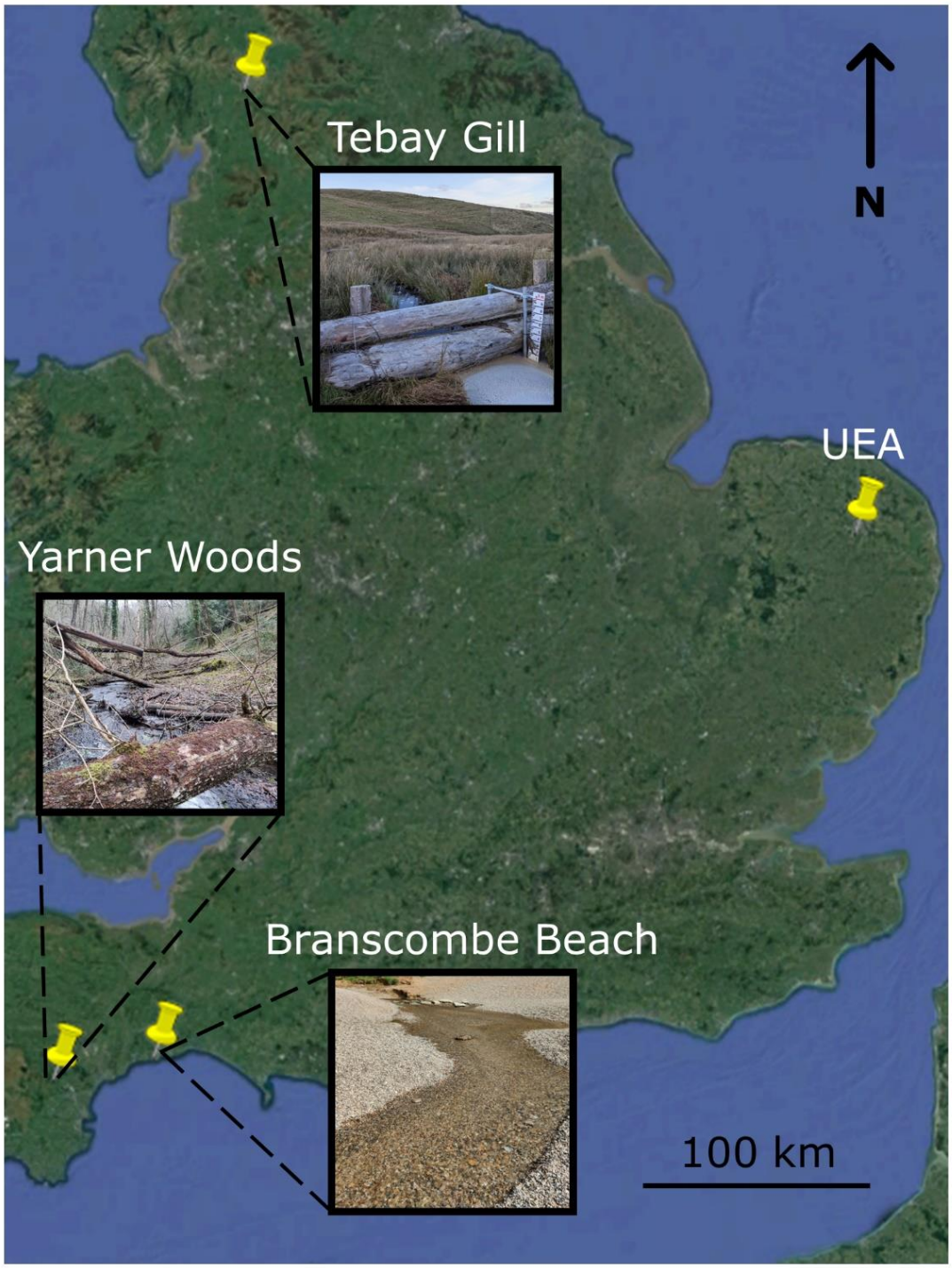

Figure 5.1: *Location of the three UK smart stone sites, from the wood free Branscombe Beach, to the natural woody debris site Yarner woods, and the anthropogenic wood site Tebay Gill. Examples of deployment streams segments are embedded onto the map.*

5.2 Branscombe Beach, South Devon

5.2.1 Site Overview

The Branscombe Beach deployment site was selected to test the capabilities of the smart stones in a controlled natural environment. The site, located approximately 30 km southeast of Exeter, is an incised stony beach intersected by a stream that flows through 20 - 25 m of pebble-cobble sized grain material before reaching the ocean (see Figure 5.1). By deploying the smart stones at this site, it is possible to gain a better understanding of their capabilities and limitations in a natural environment.

The morphology of the stream changes over time in response to tides and current flow rates. However, it was consistently observed that particles of a similar size range to the smart stones (pebble - cobble) were transported downstream. This natural flume is therefore an ideal laboratory for testing the smart stones in a controlled environment where deployment, transport, and recovery can be completed over a short period. This allows for the study of the movement of the tracer particles under a range of flow conditions, without the need for complex and time-consuming experiments. The controlled conditions of the natural flume make it a useful tool for studying bedload transport and the performance of smart stone devices in natural flows.

The data obtained from the Branscombe experiments built upon the knowledge gained from dry laboratory experiments by allowing correlations between IMU data and specific movement characteristics observed at the site. Compared to dry laboratory experiments, the Branscombe site has several advantages. For example, it is difficult to replicate the effects of water resistance and lift forces on tracer sediments in the laboratory, or to study how LoRa connectivity will perform in an uncontrolled environment. Additionally, the site allows for the study of non-anthropogenically produced step-and-rest transport behaviour. These factors make the Branscombe site a valuable resource for expanding our

understanding of bedload transport and the use of smart stone devices in natural flows.

5.2.2 Methodology

Device settings applied to smart stones deployed at Branscombe Beach were identical to those used during subsequent field deployments (e.g., Yarner Woods). This facilitated direct comparisons of data between all deployment sites. The full list of settings applied is provided in the appendices (B.1).

To establish the feasibility of using the smart stones at the deployment site, a portable gateway was deployed to establish LoRa connectivity to the study area. The smart stones were activated, and data collection was triggered on the devices to confirm that they would capture movement data and that mobile coverage was sufficient for data transfer and upload. Additionally, the smart stones were initially added to the stream to confirm that flow rates were sufficient for the natural mobilization of the tracer sediments.

Once these initial tests were completed, a segment of the stream was selected for smart stone deployment, providing a potential transport distance of more than 20 m between the starting location and the ocean. The smart stones were positioned at their deployment locations and cleared of data in preparation for the first experiment. Each experimental run involved securing the tracer in place prior to recording, then simultaneously initiating recording and releasing the smart stone into the flow.

High definition (1920 x 1080) footage of transport was taken using a Oneplus AC2003 camera, recording at 60 frames per second. The movement of the tracers was continuously monitored and recorded until movement stopped naturally, or until manual interruption of transport was required to prevent tracer loss to the ocean.

Due to the step-and-rest behaviour of sediments during bedload transport, movement was considered the end of the experimental run if transport did not occur for more than 1 minute. The smart stone was again secured in place at its final depositional location, preventing further data collection from being triggered that was not associated with recorded movements. After securing the smart stones, they were allowed sufficient time between runs for data upload via the LoRaWAN network. Once the IMU data had been transmitted to the server, a command downlink was sent to reset and clear the smart stone of data, preparing the device for subsequent experimental runs. This process was repeated for all the smart stones deployed at Branscombe. In time-constrained circumstances, where LoRa upload was not feasible (e.g., the final run of a day), data was extracted from the smart stones using a USB serial cable.

Aligning the retrieved IMU data from the smart stones with the video recordings was possible by matching the moment of the initiation of movement, the length of the run, and the frequency of data collection. This was supported by verification with time stamps embedded within the IMU data and camera. This allowed specific movement patterns observed (e.g., rolling, steps, and rests) to be matched with their associated response within the data.

The site was visited on three occasions in 2022 (February, May, and October), repeating experimental runs in different flow conditions. Consistent methodologies were employed during each visit, with individual movement events being recorded by a single smart stone, before resetting the device upstream for the next movement event. However, on the final visit, the methodology for data transfer deviated due to limitations in data transfer speeds (see section 5.2.7).

5.2.3 February Site Visit

The field site was first visited on February 28, 2022. This initial visit allowed for the evaluation of the stream, determining its feasibility for use in smart stone transport experiments and as an analogous natural laboratory for

comparison to the dry slope experiments. Entrainment and transport of sediments larger than the smart stones were observed in the current flow conditions, supporting the decision to deploy smart stones at the site. Sediments were observed exhibiting step-and-rest behaviour, with transport primarily by rolling along the bed surface, although smaller pebble-sized sediments were observed saltating along the bed.

On this initial visit, the LoRa gateway had intermittent mobile coverage dropouts and unreliable connectivity with the smart stones. It was later determined that the connectivity issues were a result of a faulty mobile gateway, although this was not understood at the time. Despite these challenges, multiple experimental runs were attempted to test the feasibility of deploying at the site. Although the connectivity issues limited the success of the experiments.

Deploying the smart stones into the flow did result in entrainment and transport, with some transport events lasting more than 15 m. The tracers primarily rolled downstream along a single axis, while also displaying step-and-rest behaviour. However, the smart stones only successfully transmitted data packets infrequently, making it difficult to match the recordings of transport with the data packets. It is likely that the failure of data transfer was due to the gateway connectivity problems experienced, making it impossible to interpret the data obtained as a specific movement behaviour.

Despite the difficulties faced during the initial experimental runs, these experiments confirmed that the site was ideal for further investigation. The bed conditions and flow rates were sufficient to transport the smart stones, and the sediments displayed a range of movement characteristics that were difficult to replicate in the dry laboratory (e.g., step-rest movements, saltation). Additionally, the deployment methodology did not damage the devices, confirming that the smart stones could withstand the environmental conditions likely to be encountered during field deployment. These findings supported the decision to continue with the experiments at the site, in order to gain a better understanding of the capabilities and limitations of the smart stones in a natural environment.

Data derived from experiments in February appears to be erroneous. Only 27 lines of gyroscope and accelerometer data were successfully uploaded to the online server for extraction. The data that was transferred displays minimal movement, covering only a few seconds of transport and does not reflect any recognizable movement modes. It is assumed that the faulty gateway either resulted in data packets being received but not uploaded to the storage server, or that the smart stones could not transmit due to an internal fault with the gateway. The connection between the gateway and the online servers is assumed to be the point of failure, as no data was left available on the tags for cable upload following the experimental runs. Mobile coverage was independently verified to be sufficient with other devices in the area, so a return to the site with a new gateway was necessary to repeat the experiments. These issues highlighted the importance of reliable GSM connectivity in the field, as potential data loss is possible in the case of connection failure partway through data transfer.

5.2.4 May Site Visit

On the 6th of May 2022, the Branscombe Beach site was again used for natural mobilisation experiments using the smart stone tracers. At the site, gateway connectivity was established, mobile coverage was confirmed, and initial testing demonstrated that data was successfully being transmitted to the online server. This confirmed that the gateway issues encountered during the previous visit were resolved. This allowed the experiments to proceed without interruptions, ensuring that data was collected and transmitted reliably, and allowing for more accurate and meaningful analysis of the transport data obtained.

Flows were still entraining pebble to cobble size particles. Initial test runs without data collection successfully confirmed that the flow rates were sufficient to transport the smart stones.

In total, three experimental runs were conducted at the site. The first and second runs utilized LoRaWAN transmission for data transfer, while the final run was time-limited and therefore data was completed using the

cable upload approach in combination with LoRa. LoRaWAN transfer speeds at the site were slower than expected, dropping to as low as one data packet per minute at times. Since the magnetometer stores data in a separate packet for transmission to the gyroscope and accelerometer, and the sensors had recording frequencies of 5 Hz and 14.9 Hz, it became clear that the upload times of the experimental runs would become extensive with transport distances of up to 20 m. Furthermore, as magnetometer data is only transferred after gyroscope and accelerometer data transmission is complete, there is a risk of magnetometer data loss given limited transfer times.

Consequently, the downstream length of tracer transport was capped at 3 m in the second and third experimental runs. Despite this, some data was lost at the end of the experimental runs at Branscombe due to the slow transfer speeds. However, enough data was obtained to characterise specific movement behaviour of the tracers during transport.

5.2.5 Qualitative Descriptions of Experiments

During the first experimental run, the total transport time was 55 seconds. The run was primarily characterised by rapid transport and rolling downstream. Approximately 3 seconds after deployment, the tracer became trapped and rested on the bed for 10 seconds before being nudged to return to the flow. The sediment was then transported without interruptions until reaching its final resting position approximately 20 m downstream.

Due to concerns regarding the lengthy upload times and ease of data interpretation (see section 5.2.7), the subsequent experimental runs were interrupted approximately 3 meters downstream of their deployment locations. The second run lasted for 8 seconds and had a relatively slower transport rate. The movement was characterised by rolling with intermittent steps and rests. Notably, the sediment collided with, and rolled over, a large cobble at approximately 6 seconds, with a high impact observed. After reaching 3 meters, the cobble was held in place for 30

seconds to prevent further data collection. This indicated the end of the experimental run in the data.

The third and final run was undertaken on the same stream segment as the previous run. In total, the run lasted 8 seconds, with the first 3 seconds representing the movement of the smart stone into the flow. The run is characterised by moderate transport speeds, with the tracer sediment rolling up and over small cobble-sized clasts. The sediment was again interrupted and held for 30 seconds to indicate the end of the run within the data.

5.2.6 May Experimental Results

Run 1

Due to the limited transfer speeds, only gyroscope and accelerometer data were successfully uploaded to the online server via LoRa. The data that was uploaded was interpreted as the rolling motion of the smart stone surrounding the trapping event observed three seconds after deployment. As recorded in laboratory experiments, rapid oscillations are observed in the accelerometer data, with maximum peak values of 2.30 g observed in the Z axis during transport. Additionally, large smooth peaks of up to 703 °/s are recorded from the gyroscope, representing a rolling motion primarily along a single axis (Figure 5.2). A reduction of gyroscope values to close to 0 °/s is observed halfway through the dataset. This likely represents the period of trapping, which is supported by the flatlining of the accelerometer data over the same period, suggesting that accelerational forces have stopped. This suggested that step and rest behaviour can be interpreted from accelerometer and gyroscope data outputs.

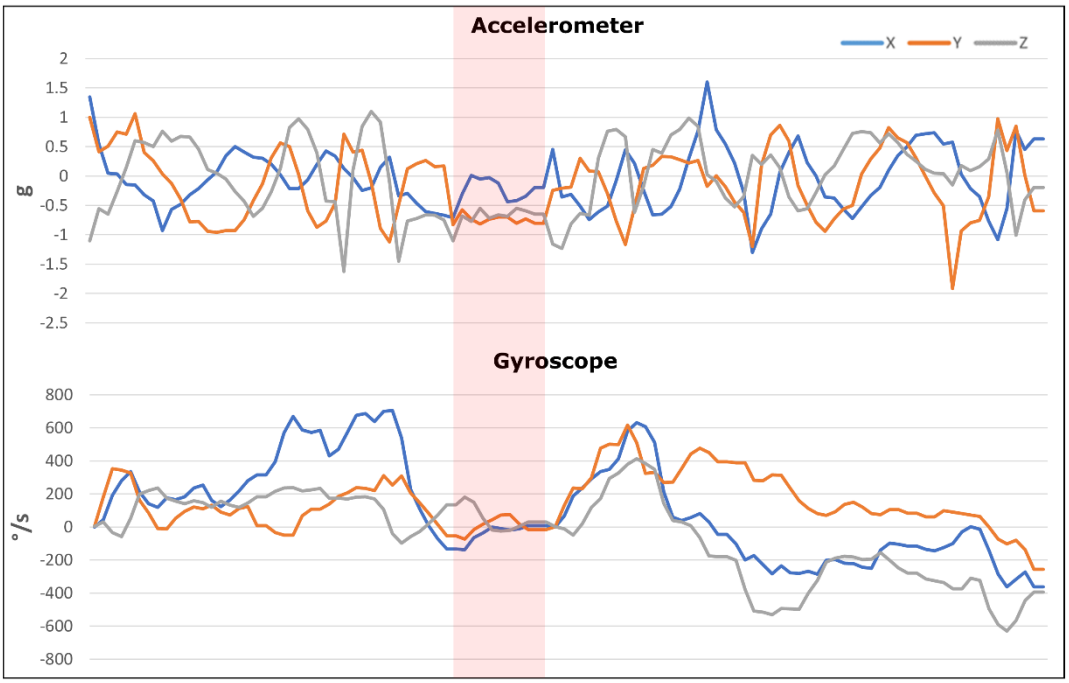

Figure 5.2: *Accelerometer and gyroscope data output during run 1 (May) at Branscombe beach, with two large peaks in gyroscope data indicating continuous movement and rapid oscillating accelerometer data indicating rotational movement downstream. Note the period of reduced activity approximately halfway through the data set (highlighted in red), representing the trapping of the tracer observed during the run.*

Run 2

Again, limited transfer speeds resulted in only gyroscope and accelerometer data being available, as magnetometer data was not successfully uploaded via LoRa in time. Figure 5.3 shows a peak accelerometer value of 3.3 g towards the end of the data collection period. This spike in acceleration is interpreted as the large impact that was qualitatively observed during the run. It matches the typical acceleration values from laboratory collision experiments and is distinct from the surrounding dataset. Rotation of the smart stone primarily occurred along the X axis, with consistently elevated values peaking at 606 ° s^{-1}, indicating continued rotation.

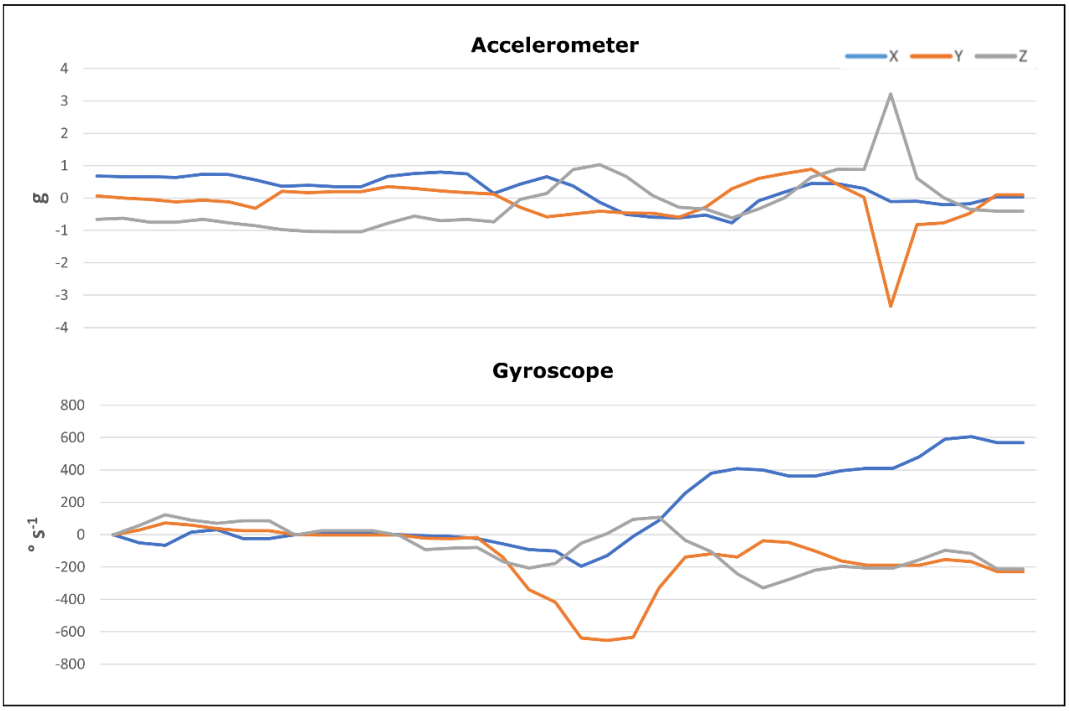

Figure 5.3: *Accelerometer and gyroscope data output during run 2 (May) at Branscombe beach, with accelerometer spike of 3.3 g interpreted as impact observed during the run.*

Run 3

Due to time constraints in the field, only 29 packets of gyroscope and accelerometer data were successfully uploaded via LoRa during the final experimental run. This only represents a few seconds of data collection. Significant gyroscope activity only included a single peak of 348 ° s^{-1}, with peak value of 0.8 g in the accelerometer. This likely only represents the initiation of movement of the smart stone immediately following data collection triggering. However, the limited dataset makes it difficult to make confident interpretations of transport conditions.

It was hoped that the remaining data could be retrieved through a cable upload. Unfortunately, the cable data only included measurements recorded after transport had ended. This was determined because the first 750 data packets (approximately 50 seconds) displayed little to no movement. It is assumed that the missing movement data was converted to a LoRa payload but did not upload in time. Since the devices were

subsequently disconnected from the LoRa gateway, the later stages of the experimental run data were lost.

5.2.7 May Data Summary

The May experimental runs further highlighted the limitations of using LoRa for data transfer over limited time periods, as 1-2 hours of upload time was insufficient to transfer all movement data collected during the runs. As a result, it was not possible to fully match the data with video recordings for the entire length of the experiments. However, specific movement events (e.g., step and rest behaviour of tracers) were captured in both the data and video (see appendix D5 for examples of step and rest behaviour). This suggested calculating step length and rest times of smart stones should be possible (e.g., Olinde & Johnson, 2015), improving upon what was achieved using RFID tags at St. Louis Creek (Chapter 2). Based on these results, it was determined that a final site visit would be necessary, with deployment not relying on LoRa gateways for short-term data transfer.

5.2.8 October Site Visit

On October 10th, 2022, the site was revisited. However, due to the lack of recent precipitation, flows onto Branscombe Beach had been severely reduced, with the stream traveling below the surface of the beach, rather than the beach being incised by the flow. This removed the segment previously used for experimental runs. As a result, another suitable site was located further upstream where flow could produce incipient motion of the smart stones.

The experimental design was replicated from previous visits to the field site, but without using a LoRaWAN gateway. This allowed for faster experimental runs and did not risk data loss during transmission. In total, five movement experiments were undertaken and recorded directly onto

the device memory storage. Flows were lower than during the previous runs, resulting in a reduced variety of movement behaviours.

Of the five experimental runs, all were characterised primarily by rolling behaviour. During the first and second runs, the smart stones travelled 2.1 and 1.7 m downstream, respectively, while the latter three runs were deposited in the same location, with transport at approximately 3.5 m. While transport velocities were generally consistent, some variation was observed. In particular, run four had variable transport rates, and run two had significantly slower transport rates overall (Table 5.1).

5.2.9 October Experimental Results

Complete sets of accelerometer, gyroscope, and magnetometer data were available for all five experimental runs, with clearly defined start and end times for movement caused by natural mobilization in the stream. This improved the precision of interpreting and matching specific movements observed qualitatively with the data, compared to previous experiments at Branscombe. For a summary of the peak linear acceleration and angular velocity with respect to transport speed for the October runs, see Table 5.1.

Table 5.1: *Experimental results for the 5 runs at Branscombe in October, showing measured peak values for angular velocity, peak linear acceleration, and estimated transport speed of smart stones.*

Experiment Number	Angular Velocity (° s^{-1})	Peak Linear Acceleration (g)	Estimated Transport Speed* (m s^{-1})
1	501	4.68	0.33
2	588	2.1	0.28
3	764	6.3	0.38
4	524	6.3	0.30
5	639	3.6	0.34

** Transport speeds were estimated using the total time of data collection from entrainment to deposition, and the step length of tracers*

Run 1

Data recorded during the first run is representative of typical rolling behaviour previously simulated in the dry laboratory. With oscillating accelerometer data (maximum peak of 4.68 g), large smooth peaks in the gyroscope (maximum peak of 501 ° s^{-1}) and oscillating magnetometer values (Figure 5.4). The magnetometer data reveals five distinct full rotational movements during the 6.1 seconds of transport time, as indicated by the five peaks in each axis. These rotations can be corroborated by matching the data with observations of transport. Furthermore, the gyroscope data shows a transition from rotational movement primarily on the Y-axis to the X-axis, which is consistent with qualitative observations from the video.

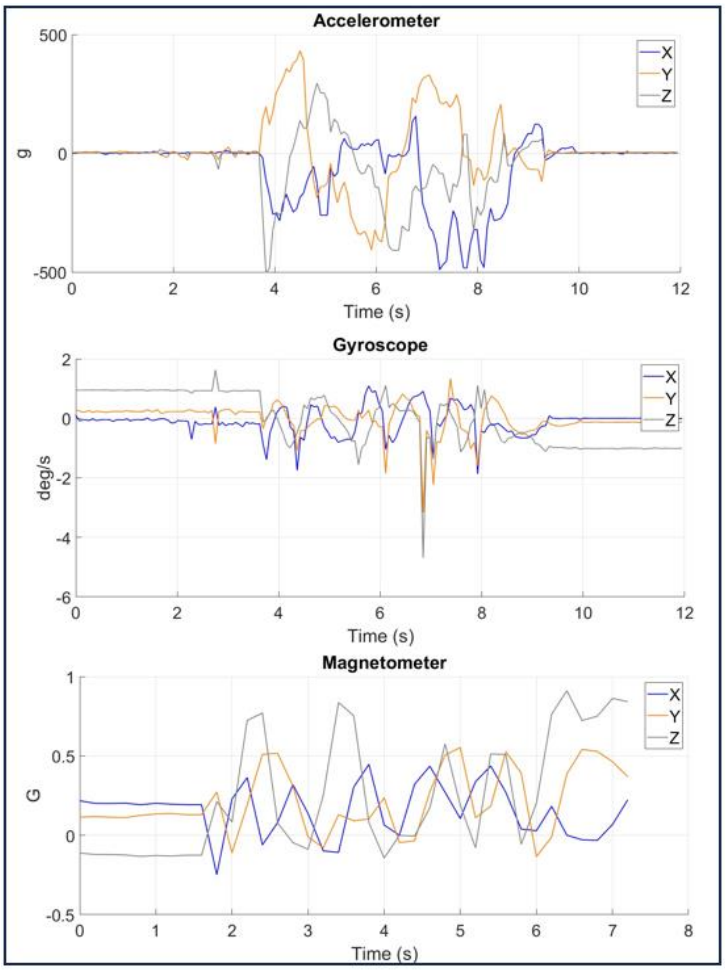

Figure 5.4: *Full IMU data output during Branscombe natural mobilisation (run 1). Typical rolling data observed, with large peaks produced from the gyroscope and spikes in activity from the accelerometer. Note the 5 peaks in the Z axis of the magnetometer match the number of rotations observed during the run.*

Run 2

Run 2 yielded IMU data consistent with the results of the rolling experiments and previous runs (Figure 5.5). The peak accelerometer value recorded during this run was 2.1 g, lower than those observed in previous runs, likely due to the slower transport rate, which reduced the accelerational forces acting on the sediment. The peak rotational acceleration measured was 588 ° s^{-1}.

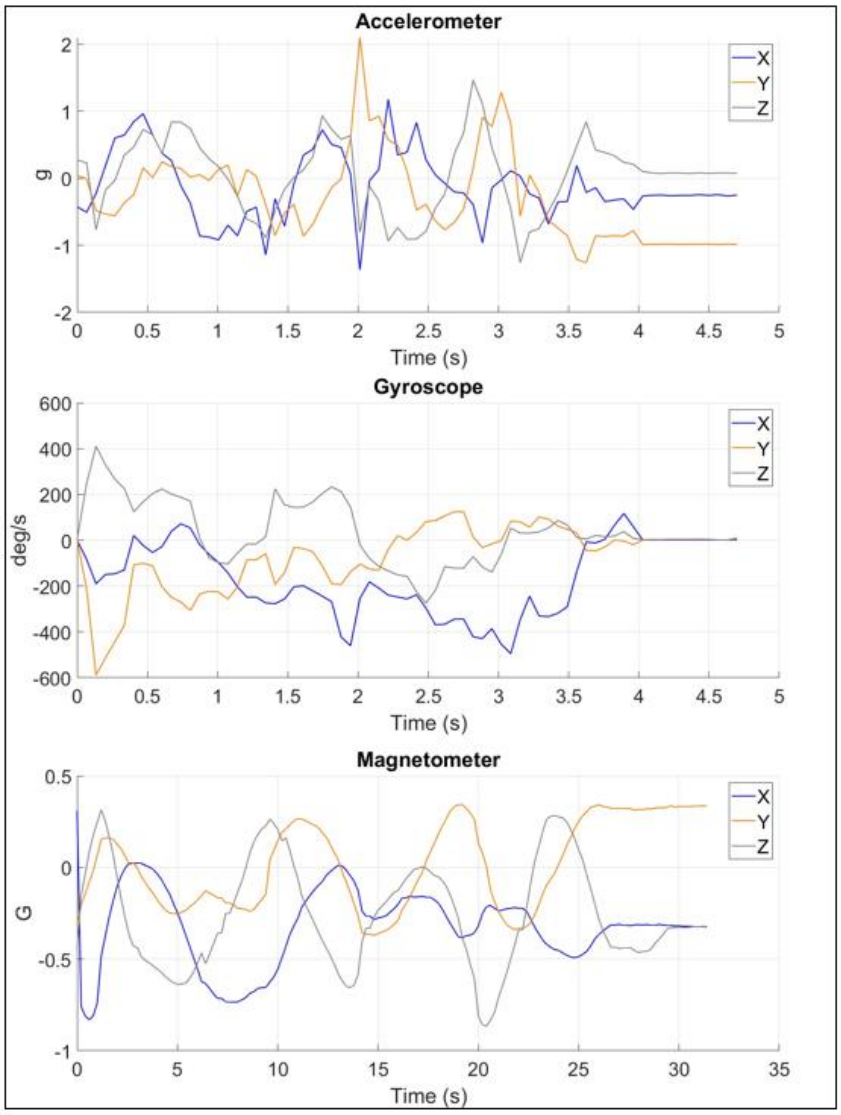

Figure 5.5: *Full IMU data output during Branscombe natural mobilisation (run 2)*

Run 3

The IMU data from the third experimental run was consistent with the results of the rolling experiments and previous runs (Figure 5.6). The longer transport distance and extended data collection period are reflected in the longer recording time of the accelerometer and gyroscope. The higher transport rate of 0.38 $m.s^{-1}$ is also evident in the increased peak values recorded by the accelerometer (6.3 g) and gyroscope (764 ° s^{-1}). However, the magnetometer data does not appear to be synchronized with the other sensors, suggesting a possible delay in the triggering of data collection in this sensor. The cause of this discrepancy is unknown and has not been observed in previous or subsequent experiments or deployments.

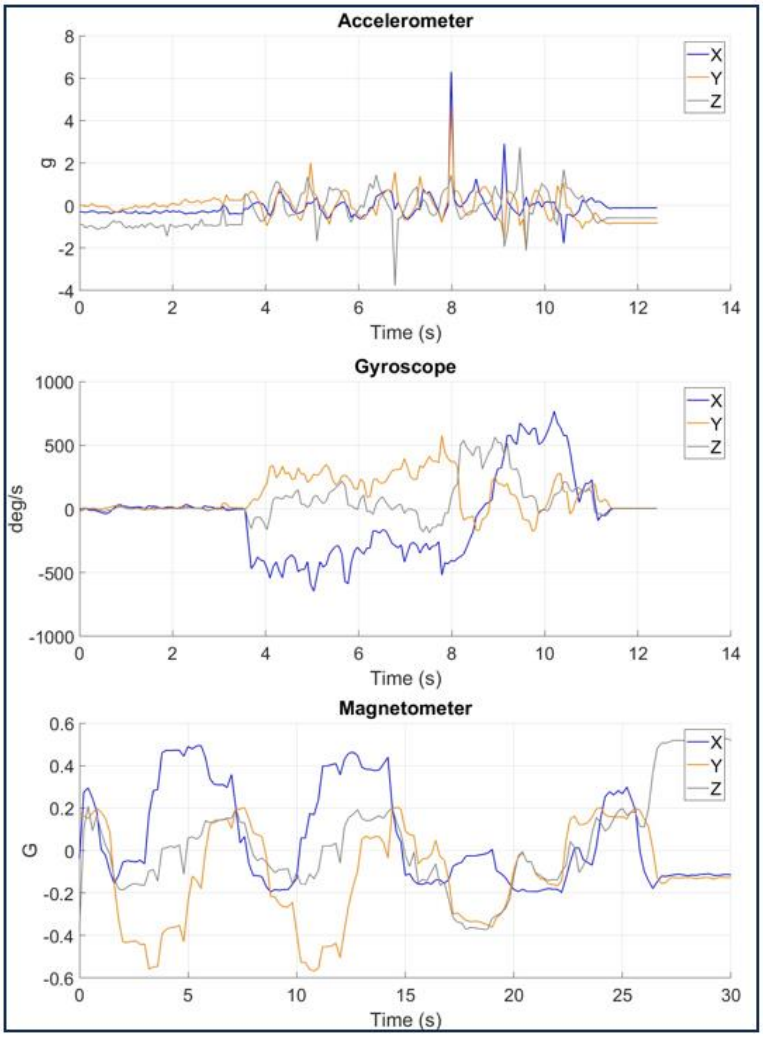

Figure 5.6: *Full IMU data output during Branscombe natural mobilisation (run 3). Note the misalignment of the magnetometer data collection period, suggesting a delay in data collection of this sensor.*

Run 4

Again, IMU data is consistent with the rolling experiments, and from previous experimental runs. Unique to this run, tracer speed reduces for approximately 5 seconds post-entrainment for two seconds before returning to the previous velocities. The change is evident in the magnetometer data, where the frequency of rotational oscillations decreases, and the wavelength of these oscillations increases (Figure 5.7). It is also possible to match the individual peaks in the magnetometer data to observed rotations, with the smart stone fully rotating 8 times before deposition. Relative to the other runs, peak accelerometer and gyroscope values are moderate, at 6.3 g and 524 ° s^{-1} respectively. This matches with the moderate sediment transport speeds observed during this run.

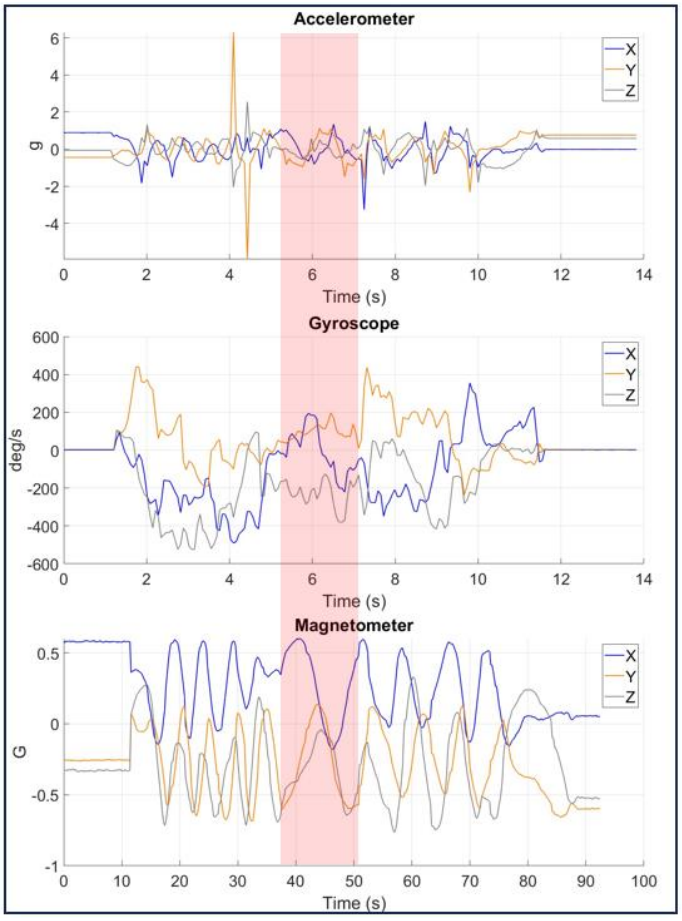

Figure 5.7: *Full IMU data output during Branscombe natural mobilisation (run 4). Notably, the oscillation frequency of the magnetometer reduces approximately halfway through the data collection period (highlighted in red). This represents the reduction in transport speeds of the smart stone tracer.*

Run 5

The full set of IMU data was collected and is generally consistent with that observed in the rolling experiments and previous runs. However, the magnetometer data does not exhibit the smooth oscillatory waves seen in earlier runs (Figure 5.8), potentially due to rotations along different axes or at a higher rate. The run had moderate gyroscope and accelerometer max values of 639 ° s^{-1} and 3.6 g respectively.

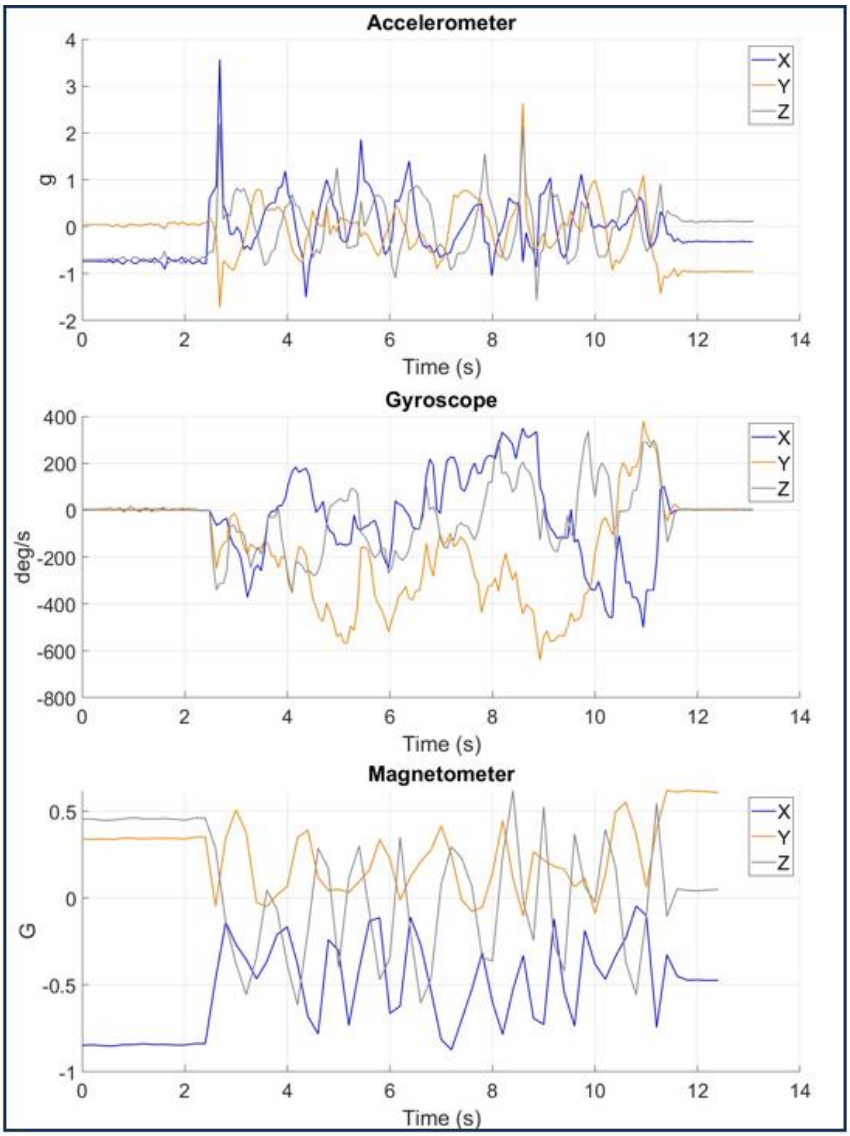

***Figure 5.8**: Full IMU data output during Branscombe natural mobilisation (run 5)*

5.3 Branscombe Experiments Summary

The Branscombe field site is an effective natural laboratory, allowing for direct comparisons to data from dry lab experiments. However, some aspects of the experiments needed refining, particularly the use of LoRaWAN to retrieve data from the tracers, which led to data loss due to slow transfer speeds during the first two visits to the field site.

By the field visit in October, the refined methodology was successfully capturing detailed movement. However, time restrictions resulted in this being the last visit possible to the location. Issues surrounding LoRa connectivity and transmission time during the first two visits make it difficult to precisely match movement with sensor data. Despite this, these provided a foundation for future experimentation once problems had been resolved. Additionally, these initial field experiments helped field deployment at the Yarner Woods site, with sources of errors being known. They helped inform appropriate changes to the device settings before remote deployment in the field.

The success of the data sets retrieved using the cable upload method demonstrates that movement can be captured in controlled field settings using the smart stones. This shows the capability of the devices to capture detailed transport behaviour and serves as a case study for the type of data that can be expected during long-term field deployment. However, the lower flow conditions at the time of the experiment resulted in minimal variation in the movement behaviours observed. Multiple examples of transport via rolling were captured, but the step rest sequences and saltating behaviours seen during earlier site visits (e.g., Figure 5.2) were not repeated in the data. However, rolling captured during field experiments matched those produced in the laboratory environment (e.g., Figure 4.9) across all three IMU sensors. This suggested data obtained during long term deployment should be recognisable as behaviours previously replicated in the laboratory.

Regardless, unique observations can be interpreted from the data, with the entrainment and deposition of sediments easily identifiable. Furthermore, it was possible to precisely match individual rotations

observed to the sensor data (Figure 5.4). In addition to observations of positive correlations between higher accelerometer values and generally faster transport rates (Table 5.1).

5.4 Tebay Catchment, Cumbria

5.4.1 Site Overview

The Tebay Catchment is one of the key SENSUM field sites and the location of previous research monitoring NFM techniques using woody debris (Chappell et al., 2017). The catchment area is approximately 5 km^2 and receives an average annual rainfall of 1600 mm. The main river, Tebay Gill, is located at the eastern edge of the Lake District National Park (Figure 5.1), and was the chosen location for smart stone deployment.

Flow rates at the site are monitored using a combination of a water level gauge staff and a camera trap. The camera takes photos every 5 minutes, and water height is used to accurately estimate flow rates in cubic meters per second (cumecs).

As part of a previous NERC-funded project that aimed to quantify the potential benefits of nature-based flood mitigation measures across large catchments (Chappell et al., 2017), 77 engineered log dams were installed in the main channel of the Tebay catchment site by November 28, 2020. However, during the initial site visit in late 2021, it was observed that some of the installed dams had already been damaged, likely due to high flow events during the winter months.

The debris dams are typically made up of imported single or stacked logs that span the width of the river (Figure 5.9a). The logs are secured to the sides of the channel by cables wrapped around posts embedded into the banks. The leaky design of the dams at the site allows for space between the riverbed and the base of the wood pieces ranging from 50 to 300 mm, which facilitates the bedload transport of sediment and reduces the accumulation of sediments at the base of the barriers. In addition, the flow of water is maintained through the dam, and during high flow events, water can flow around and over the dams.

This site was chosen for smart stone deployment as a case study in evaluating the impacts of woody debris on bedload transport. Specifically, the site was picked to investigate if more engineered natural flood management approaches caused observable changes in the typical transport behaviour of sediments. This could then be compared to more natural NFM techniques at Yarner Woods (Section 5.6) and sediment transport in wood free environments (e.g., section 5.2).

Figure 5.9: *Tebay Gill deployment site with: (a) example of the leaky debris dams installed as a of part natural flood management effectiveness monitoring, with its associated water height gauge; and (b) deployment of smart stones at the site, in November 2021*

5.4.2 Smart Stone Deployment at Tebay

Smart stones were deployed in the Tebay catchment on the 3rd of November 2021 (Figure 5.9b). At the time of deployment, a LoRaWAN enabled gateway had not been installed at the site due to the need for permissions to be obtained from the land owner. Despite the lack of a LoRaWAN gateway at the site, it was decided to deploy smart stones at the location in order to capture the high flows expected during the coming winter months (December – February). Without LoRa connectivity, data was stored directly in device memory. This had the disadvantage of not

allowing for precise monitoring of the timing of movement events, as constant monitoring was not possible. However, this approach allowed for the capture of movement data during the typically higher winter flows. It also served as an initial feasibility test for the long-term deployment of the smart stones in the field, providing insight into the design, methodology, and device settings that would be most effective for future deployment.

The deployment location of the seven tracers was chosen to be 2 meters downstream of the water level gauge, allowing for accurate estimation of the flow velocity directly affecting the tracers. The smart stones were placed on top of the bed in a grid pattern, with 0.5 meter spacing between each stone and the grid centred on the channel bed.

5.4.3 Grain Size Analysis

To evaluate the relationship between the smart stones and the surrounding bed material, grain size was measured at the site. Samples of the bed material surrounding the smart stone deployment site were investigated for their range of particle sizes. To improve the randomness of grain size sample location selection, and to remove bias, a random number generator was used to select a specific section within a transect grid which covered the bed surface. A stratified random sampling approach was also implemented, dividing the chosen transect grid into sub-grids. The final transect size was 1 x 1 m, with all sediments being measured within the grid. A ruled calliper was used to take the measurements, recording the b-axis of the sediments. In the selected transect 33 sediments were sampled, with the D50 of the bed being estimated as 70 mm (D16 = 30 mm, D84 = 140 mm). This suggests that the smart stones fit well within the normal range of sediment sizes at the Tebay site with a b-axis of 80 mm. The particle grain size distribution for measured sediments within the Tebay Catchment are included in Appendix D.4.

5.4.4 Tebay Discharge Data

Discharge data covering the period of deployment from November 2021 to retrieval in June 2022 was provided by Nick A Chappell from the Q – NFM project (Appendix D.2, Chappell and Page, 2020). As expected, flows were higher during the winter months with significant peaks identified on the following dates: 19/10/21, 31/12/21, and 20/02/22 (Appendix D.1). These are associated with prolonged periods of increased flow, with the final date corresponding to the major flood event of Storm Eunice in February 2022. Although it cannot be confirmed due to the lack of an internal clock, entrainment and transport of the deployed smart stones likely occurred from November 2021 to March 2022 during these peak flow periods.

5.4.5 Smart Stone Recovery

On June 26th, 2022 (235 days after deployment), the site was visited to recover the tracer sediments and extract the collected transport data. The site's morphology remained stable, with all previous debris dams still in place with no observable damage to the structures since the initial visit to the site.

The new locations of the smart stones were surveyed using an Oregon RFID kit (see chapter 2), and through visual identification when possible. Some difficulties were encountered with the RFID tags embedded in the smart stones. Although all of the tracers were visually identified, some of the RFID tags were not detected. The reason for the failure of RFID detection is unclear, as the tags appeared to be undamaged upon recovery and the burial conditions should not have been sufficient to impede signal transmission. Despite the difficulties with RFID detection, all 7 deployed smart stones were successfully recovered, and their transport distances were accurately measured.

All tracers were found to have been transported downstream since deployment. The transport distances ranged from 2.60 m to 11.40 m, with a mean distance of 7.97 m. Furthermore, it was observed that 5 of the

smart stone tracers had passed under and interacted with at least one debris dam. For the purposes of clarity, each smart stone was assigned an ID from A to G based on the order of their recovery, and these IDs will be used throughout the remainder of this chapter to refer to the smart stone devices.

The smart stones were found to be integrated into the bed in their resting positions. Upon recovery, some of the sediments were partially buried, with tags C and G being wedged into the bank. The depositional locations of the sediments were recorded, and the smart stones were extracted from the catchment. As in the laboratory testing, a double rotation was immediately applied to indicate the end of the data collection period on the devices (see figure 4.7). After this, the seal was removed from the smart stones and the batteries were extracted from the devices to prevent further data collection.

The data was uploaded using the cable transfer method, with tags C and G containing a full array of IMU data and smart stone E containing accelerometer and gyroscope data. However, tags A, B, D, and F either collected no data or stopped functioning during deployment due to damage or unresolved firmware bugs.

It is assumed that the damage to some of the tags resulted from the inner casing cracking due to temperature changes during the winter (tags A and D had visible cracks after extraction). This appears to have allowed water to penetrate the inner casing of the devices. Some corrosion was observed on tag D, indicating that water damage had occurred. It is uncertain whether this issue is a result of a design flaw or if environmental conditions at the Tebay site (such as temperature fluctuations or high impact events) caused the cracking and subsequent water penetration. Temperatures at the site frequently dropped below freezing over the winter months, so there is potential of freeze thaw damage to the devices, although no visible damage was apparent on the cobble surface.

Devices B and F were functional but had not collected any movement data. The reason for this failure is unknown, as all of the tags had identical hardware, firmware, and settings. It is possible that undiscovered firmware

bugs at the time of deployment could explain the failure of the devices, as they were using an older iteration of the software (See appendix C.1). It is expected that more recent firmware versions will not include the same firmware bugs that were present in the version used during deployment.

5.4.6 Tebay Smart Stone Deployment Data

Since the smart stones were not connected to LoRaWAN, they did not have a calibrated internal clock, making it difficult to precisely match the timings of movement events with the IMU data. This also made it more challenging to distinguish between the movement data associated with the placement and extraction of the smart stones, and the data from natural movements during deployment.

The timing of natural movement was estimated by utilizing known stages of deployment. The data associated with device setup can be distinguished from those recorded during deployment by analysing the IMU values, which tend to spike chaotically and do not accurately represent expected movements from a natural environment. Additionally, the start and end of deployment periods were identified using a double rotation pattern, similar to the one used in dry laboratory testing. This signal can be identified within the data and indicates the beginning and end of the relevant data. Data collected outside of this period is considered experimental noise and is discarded. Furthermore, experience gained from analysing data derived from laboratory experiments and deployment at Branscombe helped inform the evaluation of field data, enabling the identification of natural sediment movement.

5.4.7 Descriptions of Tebay Data

Smart Stone C

The accelerometer data of smart stone C shows a consistent deviation from baseline throughout the collection period (Figure 5.10). Occasional spikes in activity are observed, with the maximum recorded acceleration being -

2.23 g. These spikes coincide with peak activity in the gyroscope data. Additionally, oscillations of accelerometer activity across all three axes, similar to those observed during laboratory rolling experiments are present. These may indicate periods of sediment transport. Periods of reduced activity are also recorded, with only minor changes in acceleration over time (< ± 1 g). At the end of the data collection period, a reduction in accelerometer activity is observed, suggesting that the tracer was in its final resting position. This is supported by the concurrently reduced activity in the magnetometer and gyroscope data. The minor deviation from 0 g during this period may be due to minor shaking without entrainment and/or impacts from transported sediment.

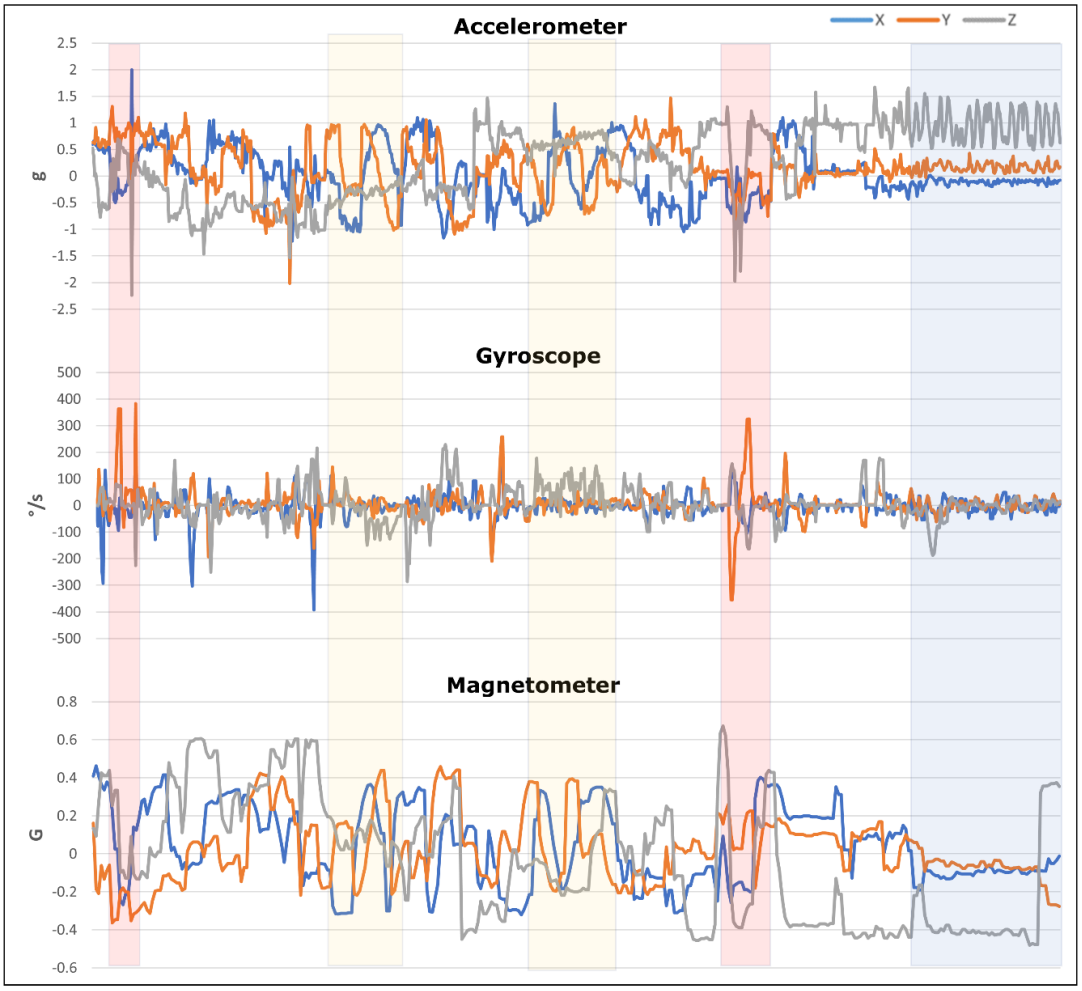

Figure 5.10: *Full IMU data output derived from Tebay smart stone C since deployment in November 2021 to extraction in June 2022. With estimated periods of movement, shaking in-situ, and resting on the bed highlighted in red, yellow, and blue respectively.*

Data derived from the gyroscope of smart stone C is characterised by short spikes in activity with varying intensities, followed by periods of reduced activity (Figure 5.10). These spikes align with the activity observed in the accelerometer. Of these movement events, the maximum gyroscope value recorded is 382° s^{-1}, with many activity periods exceeding 100° s^{-1}, indicating significant movement. The gyroscope data at the end of the collection period remained within the range of ± 50 ° s^{-1}, supporting the hypothesis that the tracer has reached its final resting position. This reduced activity is consistent with the accelerometer readings.

The magnetometer data extracted from smart stone C is characterised by consistent orientation changes after deployment, suggesting movement via rolling throughout the recorded period. The most rapid shifts in orientation correspond with data spikes within the gyroscope and accelerometer data. Towards the end of the data, the magnetometer values stabilize (as seen in Figure 5.10), indicating that movement activity has stopped, and the tracer is remaining stationary. A final rapid shift in orientation is observed at the end of the data, which is likely experimental noise resulting from tracer extraction.

Smart Stone G

The accelerometer data derived from smart stone G displays many similar characteristics to those observed from smart stone C, such as consistent deviation from 0 g for the majority of the data collection period, and a final segment of reduced activity. In comparison to smart stone C, peak accelerometer activity of up to 3.9 g is recorded, potentially indicating higher energy transport conditions. The oscillation pattern observed within the accelerometer data also suggests transport is occurring (as seen in Figure 5.11).

The gyroscope data derived from Smart stone G exhibits periods of varying intensity, with maximum values recorded at 524 ° s^{-1}. This suggests fast relative rotation, indicating faster rolling and transport behaviour compared to smart stone C. Additionally, a significant portion of the larger

spikes in gyroscope activity coincide with relatively larger spikes in the accelerometer data.

Magnetometer data recovered from smart stone G is also characterised by consistent change. Transport is inferred through the change in orientation observed within the magnetometer, which indicates a rolling motion. Again, the stabilisation of magnetometer values at the end of the data period suggests the tracer has reached its final resting position. The rapid change in orientation recorded at the end of the data collection period likely results from movement caused by tag recovery.

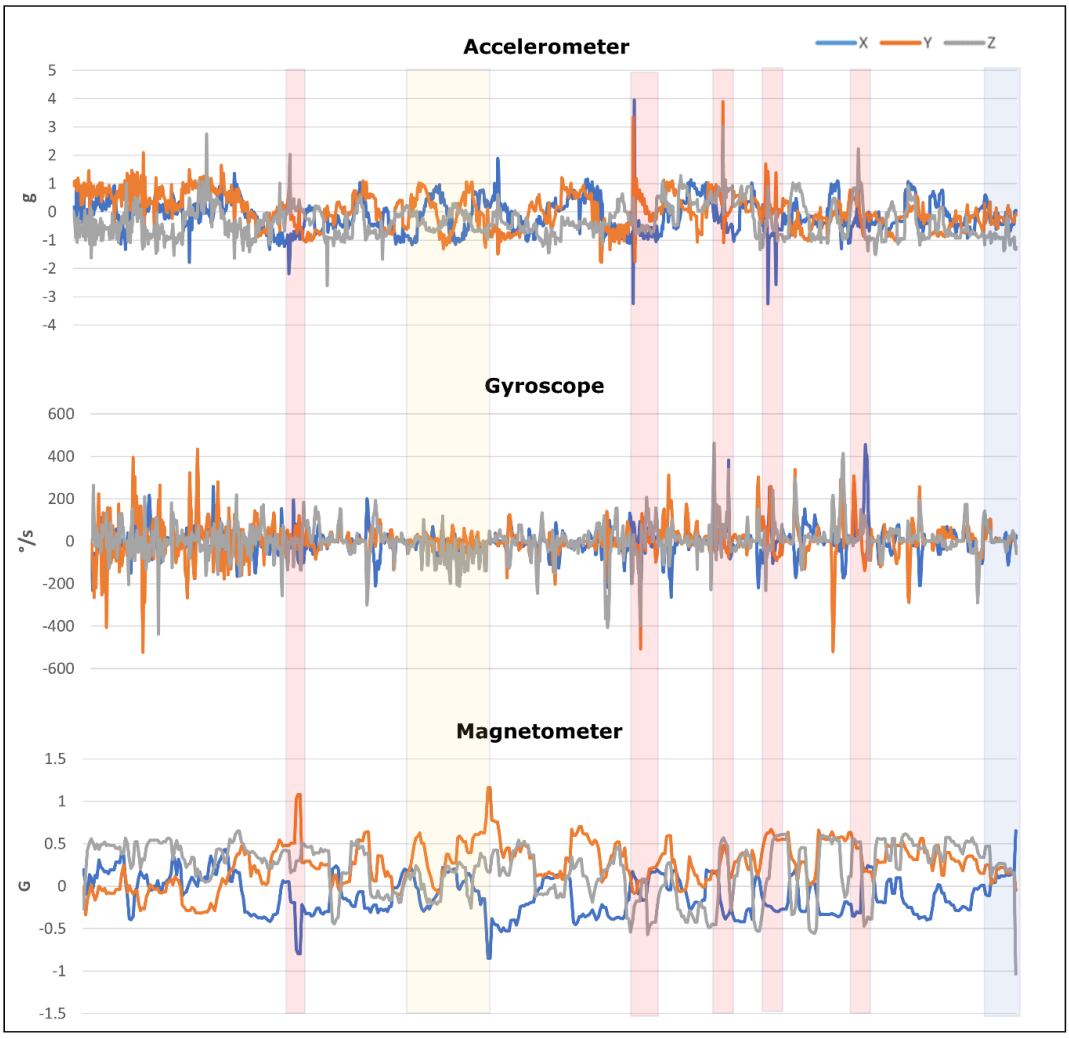

Figure 5.11: *Full IMU data output derived from Tebay smart stone G since deployment in November 2021 to extraction in June 2022. With estimated periods of movement, shaking in-situ, and resting on the bed highlighted in red, yellow, and blue respectively.*

Smart Stone E

While Smart stone E appeared to be functioning normally after retrieval, the device collected minimal data during deployment at Tebay, with only 8 lines of accelerometer and gyroscope data recorded. This suggests that an error occurred in the device firmware, causing the tag to stop collecting data after setup. As these devices were deployed in November, they are running an older firmware version known to have bugs (see appendices C.1). It is therefore assumed that one of these errors in the firmware caused the failure of data collection to occur as intended.

Despite the limited data collected, a brief spike in acceleration of -2.5 g in the Z axis is observed, which subsequently reduces to below ± 1 g for the remainder of the collection period. Additionally, the gyroscope data suggests rotation occurred, but it is limited to < 50 ° s^{-1}. However, it is difficult to draw any definitive conclusions from this data due to the lack of information regarding the time of recording, the absence of magnetometer data, and the limited number of data points collected (< 10 lines).

5.4.8 Comparisons to Laboratory Data

Smart stone C

The absence of a continuously changing single large peak within the gyroscope data, as observed in the rolling experiments, suggests that the movement from the tracer's deployment location to its resting position did not occur in a single event. Instead, it appears that the smart stone made multiple steps, with intermittent shaking in bed pockets, before reaching its final resting position on the bed. The oscillations seen in the accelerometer data match those observed in the dry lab shaking experiments (section 4.11.3), indicating that these reflect periods of non-transport, but with flows causing shaking behaviour. The simultaneous spikes in activity across all three sensors match the data observed in the rolling experiments just after the initiation of movement (Figure 5.10),

suggesting that these moments indicate entrainment and subsequent sediment transport.

The accelerometer and gyroscope recorded highs of 2.23 g and 382 ° s^{-1}, respectively, which is consistent with the lower end of values recorded during dry laboratory rolling experiments. This suggests that laboratory rolling is typically faster than that observed at the Tebay site, potentially due to differences in air and water resistance during movement, where the presence of water dampens impacts on the sediments and slows rotation. However, these values are in line with the lower peak values recorded during the Branscombe experimental runs.

The reduction in accelerometer and gyroscope activity and the stabilization of the magnetometer values are interpreted as the smart stones reaching their final resting position, wedged at the side of the channel. This parallels what is observed at the end of the rolling experiments, where both gyroscope and accelerometer values lower to near zero during the final seconds of the experiment. While the tracer sediment still exhibits some gyroscope activity (± 50 ° s^{-1}), this is likely due to the continuous impact of the flow, causing minor shaking.

Smart stone G

Many of the same comparisons to both the shaking and rolling experiments are apparent in the smart stone G data. Again, it appears that the movement from the deployment location to the final resting position did not occur in a single large event, but rather involved intermittent steps and rests, as indicated by multiple spikes in activity within the gyroscope and accelerometer followed by rapid reductions in activity. This contrasts with the single spike observed in the gyroscope data during the rolling experiments. Additionally, oscillations in the accelerometer and gyroscope data without significant changes in the magnetometer values suggest shaking within a bed pocket without transport, matching the laboratory data. Finally, the reduction in gyroscope and accelerometer values observed towards the end of data collection matches what is seen at the

end of the rolling experiments, indicating that the tracer had reached its final resting position.

The accelerometer and gyroscope recorded highs of 3.90 g and 524 ° s^{-1}, respectively, which are greater than those recorded by smart stone C and more closely resemble the average peak values observed in laboratory rolling experiments and deployment at Branscombe Beach. This further suggests that smart stone G experienced faster transport than smart stone C.

5.5 Tebay Summary

The results from the Tebay site represent the first instance of field data captured using the smart stones, featuring full IMU data captured from at least two devices over the 2021-2022 period. Although deployment occurred before many technical aspects of the device firmware had been resolved (e.g., bugs preventing data collection in some of the smart stones) and before gateway connectivity could be established at the site, it was deemed necessary to attempt to capture flows strong enough to cause transport over the winter months.

All three smart stones that collected data were transported through a debris dam at Tebay, with smart stone E being deposited just upstream of a second debris dam, indicating that its transport was interrupted. It was hypothesized that a distinctive "wood signature" may be observable in the data from Tebay, either as an impact signal or another departure from expected data output, by comparing it to the wood-free data from Branscombe. However, due to the limited number of data sets retrieved from Tebay, it is difficult to identify any specific signals that would correspond to wood impact or general interaction. Further deployment of multiple additional smart stones could potentially capture a wood-stone interaction, however resources and time were limited at the site.

Regardless, IMU data from devices C and G reflects expected transport values based on dry laboratory experiments and field experiments at Branscombe. The accelerometer and gyroscope values observed in these

devices fall within the expected ranges for entrainment and transport via rolling downstream, with step and rest behaviour interpreted. Also, periods of shaking without entrainment are identified.

It was hoped that the timing of movement of the Tebay smart stones could be estimated, despite the absence of an internal clock, by correlating peak flow values and individual movement periods in the data. However, distinguishing individual movement events in the IMU data is difficult, as transport activity is rarely clearly separated, with distinct individual peaks in flow rates not matching individual peaks in IMU activity.

The size of the smart stones (80 mm b-axis) is approximately representative of the rest of the bed material (D50 = 70 mm). However, the tracer sediments may initially be hypermobile due to the anthropogenic placement of the sediments onto the bed surface, before becoming integrated into the bed after transport. This is because greater grain protrusion from the bed is a major control on critical shear stress required for entrainment (Fenton & Abbott, 1977; Hodge et al., 2020).

5.6 Yarner Woods, Devon

5.6.1 Site Overview

Yarner Woods is a key field site for the SENSUM project. Located in the Bovey Valley within the East Dartmoor National Nature Reserve (see Figure 5.1), the site is managed by Natural England and has been used for a range of environmental science research projects (e.g., Brookes et al., 1980; Loveland & Clayden, 1987). A series of "natural" debris dams were installed in Yarner Woods in 2020 (Figure 5.12a, b). These dams are constructed from one or more logs collected from local riverbanks, or even formed from felled trees to dam the channel. This approach contrasts with the methods employed at the Tebay site (section 5.4), where larger logs were imported from off site and anchored in place using cable. Yarner Woods is therefore an ideal site for measuring the influence of more natural woody debris dams on sediment transport.

Figure 5.12: *Overview of Yarner Woods field site, with natural woody debris acting as leaky barriers with: (a) examples of SENSUM tagged wood pieces; (b) stacked logs forming natural barrier and; (c) relatively wood free segment of the field site.*

As part of the SENSUM project, debris classified as large wood at the site (Wohl et al., 2010) both in and between leaky dams was tagged with RFID and Miromico tags, similar to those used in the smart stones. These tags were installed to monitor changes in the position of the wood throughout the year and to capture any significant transport events with detailed IMU information. Additionally, a water level meter with LoRa connectivity was installed downstream of the site, providing real-time flow rate information.

Two LoRaWAN gateways were installed at the site to provide full area coverage. One was attached to the Natural England office at the entrance to the field site. This mains-powered gateway provides reliable coverage for the water level meter, as well as coverage for the lower segment of the catchment. The second gateway is located further upstream on a valley slope with reliable mobile coverage. It had a good field of view for sensor communication throughout the catchment area and was solar powered. Wildlife camera traps were also set up at the site to capture major sediment transport events or the movement of wood pieces.

The stream at the Yarner Woods site is primarily characterised by pool-riffle sequences, with pools often forming downstream of large wood pieces interrupting flow. Channel cross sections were taken at the site, with

measurements taken every 2 meters from the deployment locations of the smart stones for 20 meters downstream. The channel widths ranged from 1.1 to 3.2 meters, with an average width of 2.02 meters along the investigated area. The slope of the channel was measured to be 0.050 over the same area, corresponding to a gentle to moderate gradient of 5% (Rosgen, 1994).

5.6.2 Large Wood at Yarner Field Site

A survey of wood characteristics was conducted at the site of smart stone deployment of woody debris classified as large wood (> 1 m, Wohl et al, 2010). Of the surveyed wood, 2 pieces were associated with debris dams, 4 were at least partially buried in bed sediment, and 4 were fixed on channel banks. All surveyed wood was partially decayed, with needles, bark, and the majority of limbs absent. This suggests a significant amount of time has passed since the wood entered the channel. No new wood pieces were observed being added to the debris dams in the investigated segment of the channel throughout the deployment period of the smart stones. The large wood pieces comprising the debris dams varied in size, with lengths ranging from 1.3 to 6 m.

Further downstream, a segment of the channel lacked the presence of wood (e.g., Figure 5.12c). This provided an opportunity to directly compare sediment transport within two segments of the study site, a wood loaded segment, and a wood free segment.

5.6.3 Grain size Analysis

To estimate the smart stones' relation to the rest of the bed, the grain size of natural sediments was measured at the site. Following the methodology of sample selection at Tebay, random transects were used to select an area for sampling grain size. Again, a transect of 1 m^2 was used, with all sediments falling within the grid being sampled. Measurements were taken using a ruled calliper, with sediments B-axis being recorded. At the site

112 sediments were sampled in total, with the D50 of the bed being estimated as 53 mm based on these measurements (D16 = 6 mm, D84 = 83 mm). The b-axis grain size of the smart stone is 80 mm, therefore the D50 of sediments of the Yarner site is smaller than the grain size of our tracers.

While the tracers may not ideally fit within the medium grain size, it was not possible to produce artificial sediments smaller than 80 mm while containing a C-cell battery for long term deployment. Additionally, deposits of mobile sediments larger than the smarts stone were observed in the channel, suggesting that entrainment of smart stones was possible from the flows experienced at the site. Furthermore, within gravel bed rivers the largest grains in the bed likely control morphological stability more than the D50 portion of the bed (MacKenzie *et al.,* 2018), suggesting the artificial tracer size is appropriate for the deployment environment.

5.6.4 Smart Stone Deployment

In total, 7 smart stones were deployed at Yarner woods on the 2nd of March 2022. All devices deployed at the site had identical firmware settings (see appendix B.1) and their functionality was tested prior to use to confirm connectivity with the LoRaWAN gateways at the site. Smart stones were allocated a label from A1 – A7 corresponding to their device ID, with these values being added to the surface of the stones for rapid visual identification in the field in addition to their embedded RFID tags.

To allow comparison between the wood loaded segment of the study site and the wood free segment, sediments were separated into two groups. The control group, which included A5 and A6, was deployed further downstream in a wood free environment (Figure 5.13a). It was hoped that data derived from these devices would act as a wood free comparison to the sediments interacting with wood at the upstream segment.

Smart stones A1, A2, A3, A4, and A7 were deployed at the upstream segment of the site (Figure 5.13b). This area is dominated by woody debris in the stream, and it was hoped that smart stones would interact with wood

and be distinct from the control group. Once deployed, all devices were reset via a LoRaWAN uplink. This cleared any pre-existing movement data produced during placement onto the bed.

After deployment, data collection continued on an irregular basis, with devices sending status messages intermittently. This may have been caused by poor connectivity between the tags and the gateway, or by the gateway receiving a weak GSM signal. In some cases, multiple weeks would pass without responses from the tags before connectivity was re-established and data could be transmitted again. Considering these irregularities, a return visit to the site was planned to evaluate the field setup and assess the condition of the smart stones.

Figure 5.13: *Deployment of smart stones at Yarner Woods field site, with wood free control group (a) and wood loaded group (b) separated at the two different deployment areas.*

5.6.3 Return Field Site Visit

On May 6, 2022, a field site visit was conducted with the addition of a portable gateway. This portable gateway was designed to retrieve data from devices that were previously out of range of the two existing gateways, enabling an evaluation of sediment and wood movement since

deployment. The return visit also presented an opportunity to address connectivity issues with the existing gateways and redeploy any malfunctioning devices.

The transport of the smart stones was initially visually evaluated. All tracers were relocated, and except for tracer A3, all displayed some degree of transport or orientation change from their original deployment positions.

Smart stones that had been unresponsive for over a month at the time of the field site visit, and were not detected by the portable gateway, were removed from the channel (A1, A2, A3, A5, and A6). This was done to check for device functionality, battery life, and any signs of damage. All devices extracted from the channel appeared to function correctly when tested, with no signs of damage from deployment. Additionally, device battery life was still sufficient upon extraction, although their C cells were replaced to maximize the deployment length of the smart stones. As no problems with the devices were detected, it was concluded that the unresponsiveness of the devices was likely due to either minimal movement from April to May not triggering data collection or connectivity issues with the gateway. Extracted devices had their remaining data manually downloaded via a USB serial cable and were reset and redeployed for continued monitoring at the site.

The movement activated cameras installed at the site were also checked for evidence of wood or sediment movement captured. Unfortunately, no significant movement events were captured at the site. The camera traps were then reinstalled for subsequent monitoring.

5.6.4 Final Field Site Visit

A final visit to the field site was conducted on October 10, 2022. This allowed for a final assessment of large wood at the site, determining any transport, deposition of additional wood, and overall characterisation of wood at the site (e.g., width, length, state of decay, geomorphological relationships, etc.). No large wood pieces had been transported downstream since the deployment of the smart stones, and no additional

pieces had entered the area studied. Consequently, at the time of writing, no relevant IMU data was available for processing from the tagged wood pieces.

Additionally, the updated resting positions and condition of the smart stones were assessed, with transport distances being measured. Tracers were found resting on the surface of the bed in all cases, without incorporation into the surrounding bed sediments. Furthermore, not all tracer sediments appeared to have been transported or changed resting position since their deployment in February. Some were rotated without transport (e.g., A7), and others only transported a small distance (< 1 m).

The stationary gateway overlooking the catchment was stolen from the site in late July 2022. This was scheduled to be replaced in late November. Therefore, a portable gateway was again taken to the site to check if additional data could be collected from the devices. Particularly, the smart stones out of gateway range from July – October while the gateway was missing.

Flows during the summer months are typically lower, consequently it appeared minimal tracer movement had occurred since the site visit in May. Therefore, it was unsurprising that additional transport data was not collected via the portable gateway during this final visit.

Tracers were left in place to continuously monitor any further transport at the site. A new gateway was installed in late November, providing gateway coverage for all devices going into the autumn and winter months, when flows are likely to increase.

5.6.5 Yarner Woods Smart Stone Data

The data detailed below was obtained from the deployed smart stones at the Yarner Woods field site using the installed LoRaWAN gateways from February to October 2022. It should be noted that in May 2022, tracers (A1, A2, A3, A5, A6) had any remaining data still stored on the devices uploaded via the USB serial cable before redeployment at the site. To

distinguish differences between data derived from wireless LoRa transfer and manual cable upload, they are described separately.

5.6.6 Flow Rates

Flow rates at the site are estimated through a combination of data from a LoRa enabled water level gauge located at the downstream end of the site, and high-frequency measurements taken at an analogous stream within the catchment area (the River Bovey). This allows estimations of the timing of changes in discharge flux, supporting prediction of conditions sufficient to initiate movement. Flows at Yarner are typically higher during the winter months, particularly during the months of February and March in 2022. Flow rate peaks are succeeded by a gradual reduction in flows until subsequent peaks occur (Figure 5.14). From April 2022, peaks occurred with decreasing frequency and flow rates remained mostly stable and < 2 cumecs over the remaining recorded period.

The highest flows recorded were on the 2nd of March 2022. The timing of peak flows is associated with smart stone movement where devices A2, A5, and A6 were all triggered from the 2nd – the 6th of March 2022. Flows peaked at 14 cumecs, up from 2.5 – 3 cumecs 48 hours prior (Figure 5.14, Table 5.2). Flows remained high over this period, with an average of 6.15 cumecs and lows of 4.44 cumecs. Other peak flow rates associated with smart stone movement include 0.839 cumecs from the 7 - 9th of May and 0.997 cumecs from the 14th – 25th of May. These values are significantly lower than those observed in March, but nevertheless, are associated with triggering smart stone data collection (A1, A2, A3, A5, and A6).

The discharge gauge located downstream of the field site was activated in late February 2022, thus missing a significant portion of the peak flows that occurred during the winter months. Despite the temporal limitation, comparisons of peak flows between the Yarner Wood and River Bovey data sets revealed correlation, indicating that meaningful comparisons may still be made using the available data. The complete discharge gauge data set can be found in Appendix D.3.

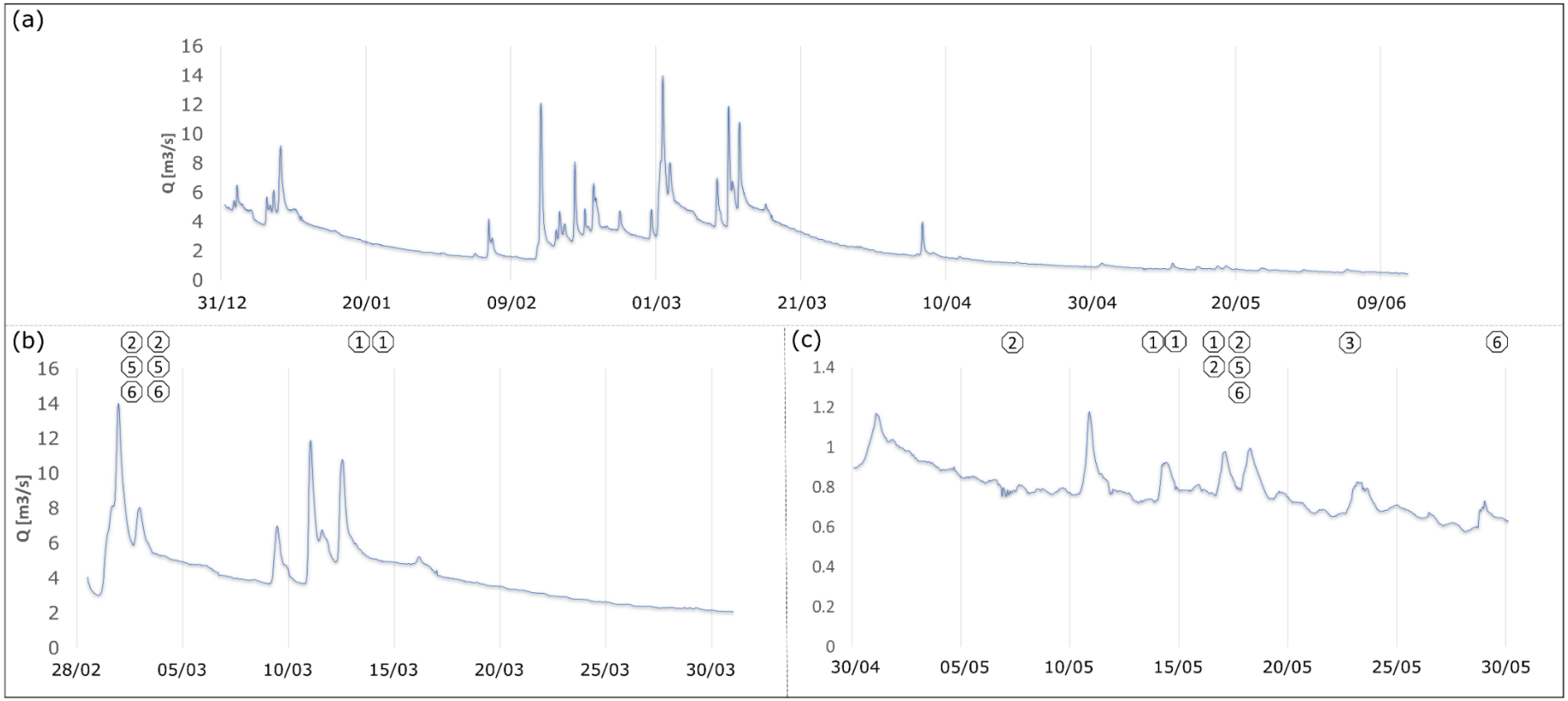

Figure 5.14: *Estimated flow rates at Yarner Woods during deployment of smart stones derived from the River Bovey flow calculations with; (a) analogous flow rates over 2022 covering smart stone deployment in February, to lower flows during summer months; (b) flow rates associated with tracer movements in March with the timing of activated smart stones identified; (c) flow rates associated with tracer movement in May with the timing of activated smart stones identified. The full list of smart stones dates associated with data collection are also highlighted in Table 5.2.*

Table 5.2: *Date of data collection of all smart stones deployed at the Yarner Woods field site.*

Movement Date	Smart Stone
3rd March	A2, A5, A6
4th March	A2, A5, A6
15th March	A1
16th March	A1
8th May	A2
14th May	A1
15th May	A1
17th May	A1, A2
18th May	A2, A5, A6
23rd May	A3
31st May	A6

5.6.7 LoRaWAN Data Descriptions

Smart stones A1, A2, and A3 all had data collection triggered by minor rotational signals throughout the month of May (Figure 5.14c). Movement was detected on the 14th, 15th, and 17th for A1, the 8th for A2, and 17th, 18th, and twice on the 23rd for A3. Gyroscope values recorded a range from 60 ° s^{-1}, as seen in A1, to 5 ° s^{-1} recorded by A3. In each case, where gyroscope data spikes are observed, there is minimal associated accelerometer and magnetometer activity (e.g., Figure 5.15). This suggests that in all cases transport is unlikely, as tracers do not display the typical accelerational forces and orientation changes expected from entrainment. While river flows at this time are lower than during the winter months, occasional increases in flow are observed throughout May (Figure 5.14c). These increases in flow rate often precede the triggering of data

collection and are potentially associated with the minor movement recorded by the smart stones.

Smart stone A5 sent a full array of IMU data on May 18th. The peak gyroscope values recorded were 86.1° s^{-1}, with a shift from ~1 to -1 g in the accelerometer Z axis and rapid changes in magnetometer orientation (Figure 5.16). These values are within the range observed during laboratory shaking experiments. Additionally, the magnetometer values returning to their original position suggest that the tracer was not entrained at this time. Like A1 - A3, small gyroscope spikes were also recorded on May 31st with minimal associated accelerometer or magnetometer activity, suggesting minor shaking.

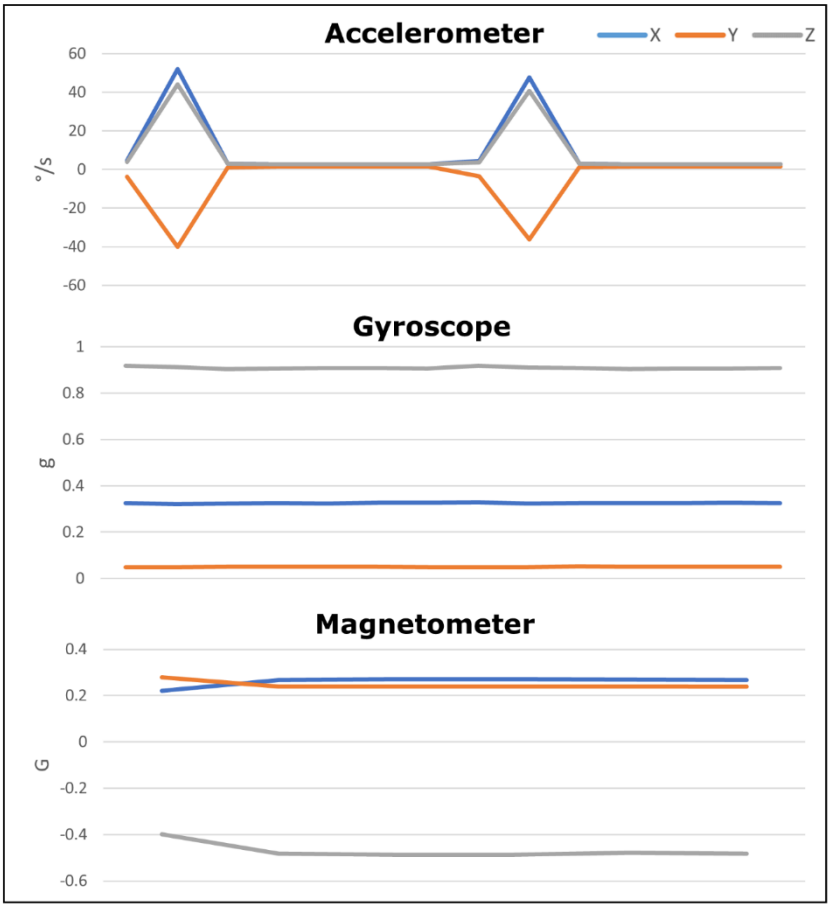

Figure 5.15: *Example IMU data transmitted via LoRa from on the 14th of May from smart stone A1, demonstrating the minor gyroscope spikes which trigged data collection with minimal associated accelerometer and magnetometer activity.*

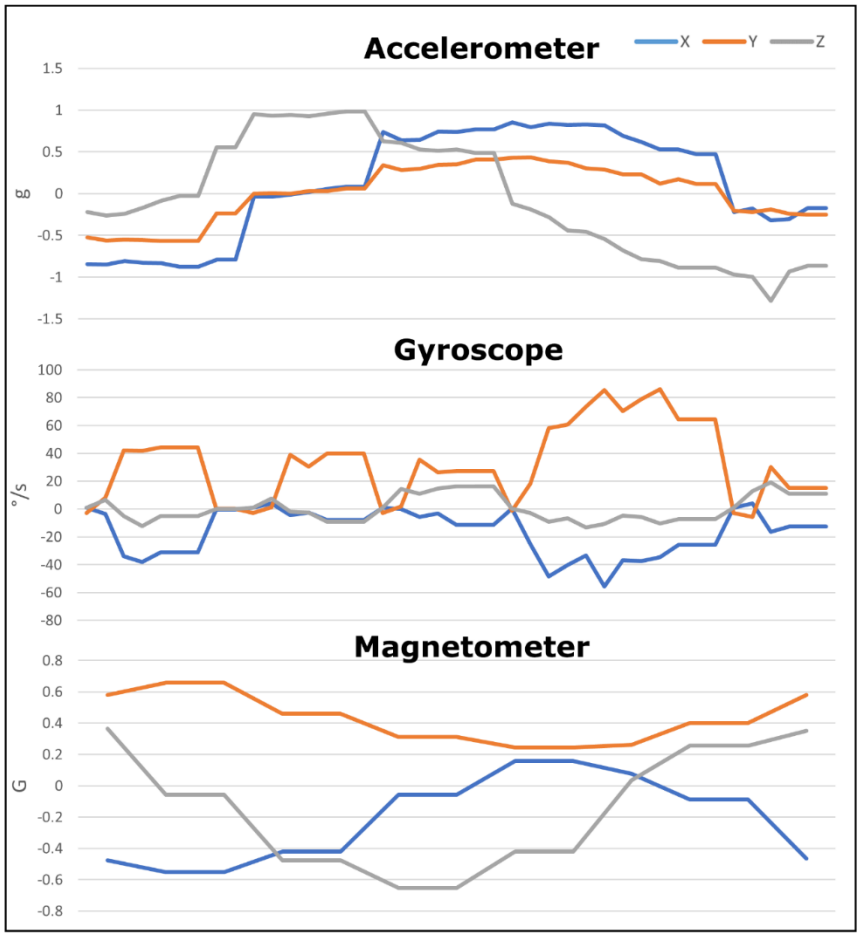

Figure 5.16: *Smart stone A5 movement data transmitted on the 18th of May with peak gyroscope values recorded of 86.1 °/s, and a shift from ~ 1 to –1 g in the accelerometer. The relatively small forces captured suggest only minor shaking was experienced by the tracer sediment.*

On the 18th of May, smart stone A6 also displayed shaking behaviour. With peak gyroscope values recorded of 83.7 ° s^{-1}, a shift from ~ 1 to –1 g in the accelerometer X axis, and changes in the orientation displayed from the magnetometer before returning to original values. Similar to A5, this event is interpreted as shaking without entrainment.

On the 31st of May, data that was indicative of entrainment and subsequent transport was transmitted by A6. The full IMU data set matched the expected values observed during experiments at Branscombe and the rolling experiments in the dry laboratory. Gyroscope data displayed a single large peak (> 1000 ° s^{-1}), with multiple oscillating spikes of up to 5.8 g in the accelerometer data (Figure 5.17). Rapid changes of

magnetometer values in an oscillating pattern are also indicative of transport via rolling downstream.

Smart stones A4 and A7 were not triggered for data collection and did not send IMU data over the deployment period. The tracers did send status messages, confirming they were active, but no movement was detected and uploaded to the online database.

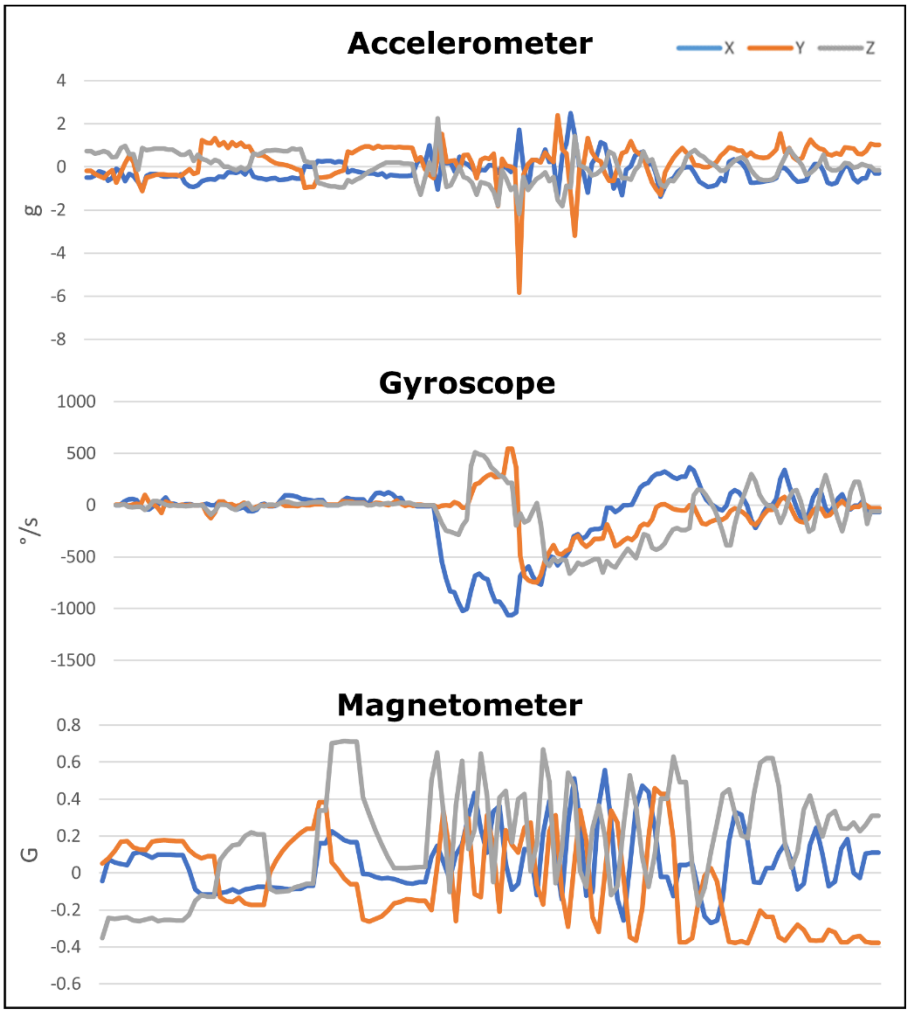

Figure 5.17: *Data output of smart stone A6 on the 31st of May at Yarner Woods, with rapid acceleration spikes, a large single peak in recoded angular velocity and the clear rotational signal in the magnetometer supporting the interpretation of entrainment and subsequent transport of the tracer.*

5.6.8 Cable Data Descriptions

Smart stones A1, A2, A3, A5 and A6 all had data collection triggered during March (Figure 5.14b), this was extracted via the USB serial cable during the initial return visit to the site. These events correlate with some of the highest estimated flow rates observed at Yarner Woods. Specifically, movement was captured in tracers A2, A5 and A6 on the 3rd and 4th, which matches with the maximum flow peaks observed since the deployment of the tracers (Figure 5.14b). Additionally, movement was captured by tracer A1 on the 15th and 16th of March which corresponds to the end of the high flow period during the month.

In all cases, small spikes and repeated pulses of gyroscope values are observed (e.g., Figure 5.18), matching those recorded from the LoRa data. These range from 35 ° s^{-1} to 10 ° s^{-1} and are associated with only minor changes in the accelerometer and magnetometer values. This suggests minimal movement, and likely only represents shaking behaviour without full entrainment.

The Smart Stone A3 lacked stored movement data on the device for cable transfer and was redeployed in the stream for continued monitoring.

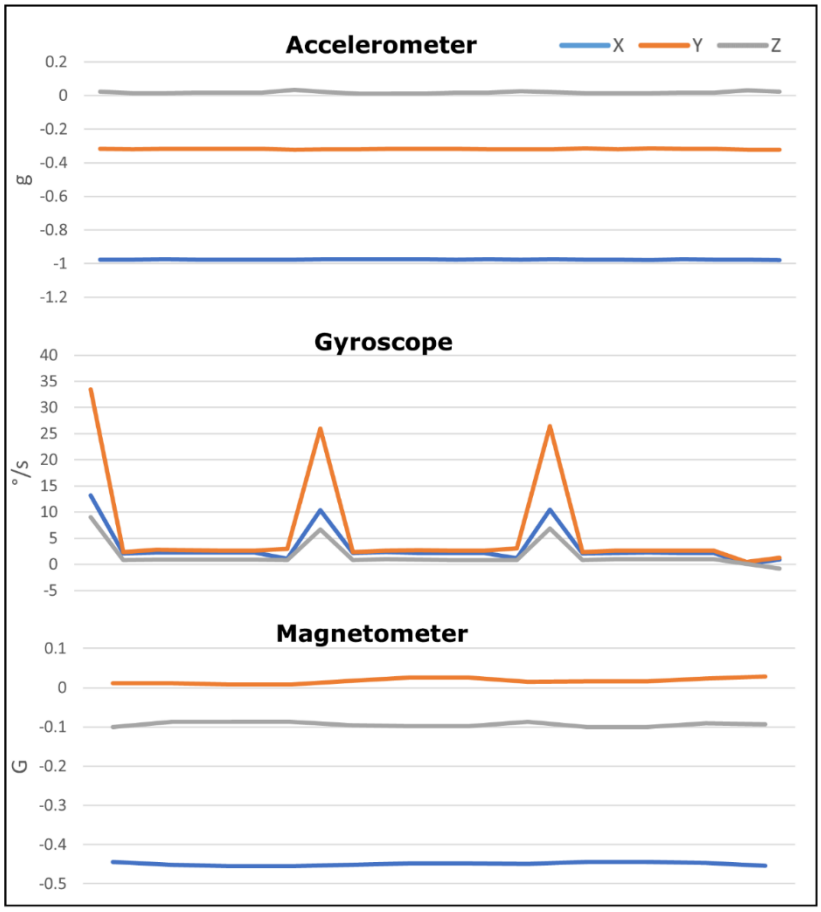

Figure 5.18: *Example of minor gyroscope spikes extracted from activity periods during the 3rd and 4th of March, matching those recorded from the LoRa data. Minimal accompany activity is recorded by the accelerometer or magnetometer.*

5.6.9 Data Summary

Data derived from the smart stones deployed at the Yarner Woods field site displayed a range of tracer movement behaviour. Except for tracers A4 and A7, all tracers recorded movements interpreted as shaking. Smart stone A6 recorded movement data which was interpreted as entrainment and subsequent transport downstream by rolling. Data collection was triggered following peak flows in March, and following periods of increased flow rate in May.

Due to the limited number of tracers which displayed full transport data, it was not possible to distinguish between the smart stones allocated to the

wood-free control group segment of the study site, and those within the wooded group. Furthermore, it is not possible to determine points of wood–sediment interaction within the data, as tracers were not transported past any large wood pieces, and no wood pieces were transported to the deployment area of the smart stones over the study period.

5.6.10 Yarner Woods Summary

Yarner Woods was the key field site investigating the effectiveness of the long-term deployment of the smart stone tracers using LoRaWAN remote data collection. It acted as a case study for the implementation of the devices, providing an opportunity to assess the potential limitations of the smart stones and to resolve any problems that arose. It also allowed the quality of data derived during long-term deployment to be evaluated. Furthermore, the site had various examples of natural woody debris in the channel, contrasting with the hard-engineered dams at the Tebay site. It was hoped that a comparison between the two deployment sites could provide insight into the impact of soft and hard-engineered natural flood management techniques on bedload sediment transport.

Deployment was a mixed success. While data from the movement of smart stones was captured, there was minimal transport of tracers over the monitored period (May – October), with only one of the deployed smart stones successfully sending full IMU values which are interpreted as entrainment and bedload transport. Other smart stones which uploaded data were not transported but displayed shaking behaviour, typically seen in flows below entrainment thresholds. The low flows during the spring and summer months are less likely to cause movement, so it is unfortunate that winter deployment in 2021 was delayed due to COVID restrictions.

Despite this, the data that was received matched well with the analogous data derived from the dry laboratory experiments, and the Branscombe field site. Furthermore, the methodology proved to be feasible over the long term, with smart stones remaining active over many months unsupervised. It is believed with greater flow rates, more typical over the

winter months, many more tracers would have been transported. This would have provided a greater selection of data sets, allowing comparisons between wood loaded and wood free environments. However, with the data sets available, it was not possible to directly compare wood loaded and wood free segments of the Yarner site. In addition, with more instances of transport being recorded, it may be possible to derive estimates for discharge entrainment thresholds at the site.

Ongoing issues with gateway connectivity appear to have limited the potential inventory of data sets retrieved at the site. Many smart stones were relocated with at least some movement visually identified, but some lacked associated movement data on the LoRaWAN server. Mobile coverage at the site had been intermittent, despite the gateway being positioned on high ground. This could have prevented the successful transfer of movement data. In addition, it may explain why some devices only transferred gyroscope and accelerometer data packets but did not successfully upload the associated magnetometer data packets for the same time period. This further highlights the need for reliable GSM coverage when deploying LoRaWAN devices for environmental science applications.

A possible future development for the Smart Stone software that could prevent data loss could involve waiting for a confirmation from the LoRaWAN network to signal a successful transfer before clearing the device's memory. This would take the form of a data packet command dispatched from the online server after a predetermined period of inactivity, i.e., not receiving data packets from the devices. However, this approach risks overloading the device's memory in cases of continuous movement and might be best suited for fluvial environments where intermittent movement is anticipated. The data that was collected is promising for the development and use of LoRaWAN smart stones. With additional time for deployment, a new gateway with better mobile coverage, and updated bug free firmware, it is thought that the devices could be implemented successfully, providing a continuous collection of bedload transport data for many months to years, depending on battery longevity.

5.7 Performance of LoRaWAN Smart Stone

Data collected from the smart stones across all sites revealed that of the 14 stones deployed for an extended period, only 3 collected transport data. Notably, 4 stones stopped functioning at the Tebay site, and 2 have appeared to have stopped functioning at the Yarner site, although these have not been extracted at the time of writing for confirmation. A combination of physical damage to the devices (water infiltration) and software issues, appears to be responsible. This resulted in a success rate of 57% for the smart stones during their long-term deployment, accounting for all devices that at least captured some movement activity. However, it is important to note that only 21% (3 out of 14) of the smart stones deployed were able to collect entrainment and transport data. This low percentage is likely due to the low flow conditions experienced after deployment at the sites, rather than a failure in device performance. Future deployments during winter months with peak flows, in conjunction with an optimized casing design to avoid damage, may enhance the tracer success rate, bringing it closer to the efficacy observed in other tracer methodologies such as magnetic and RFID tracers.

Smart stones hold significant promise for supporting the monitoring bedload transport of sediments. As advancements continue to be made in both MEMS embedded sensors and wireless data transfer technology, smart stones offer a powerful tracing tool for advancing the understanding of individual grain motions and overall sedimentary processes.

References

Brookes, P. C., Wigston, D. L., & Bourne, W. F. (1980). The dependence of Quercus robur and Q. petraea seeding on cotyledon potassium, magnesium, calcium and phosphorus during the first year of growth. *Forestry: An International Journal of Forest Research*, *53*(2), 167-177.

Chappell, N. and Page, T. 2020. Measuring NFM effectiveness. *NERC NFM programme webinar series,* 3rd December 2020, Available at: www.lancaster.ac.uk/lec/sites/qnfm/

Chappell, N., Beven, K., Lamb, R., Haygarth, P., Quinton, J., Page, T., Kretzschmar, A., Hankin, B. and McShane, G., 2017, Q-NFM : Quantifying the likely magnitude of nature-based flood mitigation effects across large catchments, Retrieved from http://www.lancaster.ac.uk/lec/sites/qnfm.

Fenton, J. D., & Abbott, J. E. (1977). Initial movement of grains on a stream bed: The effect of relative protrusion. *Proceedings of the Royal Society of London. A. Mathematical and Physical Sciences*, *352*(1671), 523-537.

Hodge, R., Voepel, H., Leyland, J., Sear, D., Ahmed, S. (2020) X-ray computed tomography reveals that grain protrusion controls critical shear stress for entrainment of fluvial gravels, *Geology,* 48(2): 149–153.

Loveland, P. J., & Clayden, B. (1987). A hardpan podzol at Yarner Wood, Devon. *Journal of soil science*, *38*(2), 357-367.

MacKenzie, L. G., Eaton, B. C., & Church, M. (2018). Breaking from the average: Why large grains matter in gravel-bed streams. Earth Surface Processes and Landforms, 43(15), 3190-3196.

Olinde, L., & Johnson, J. P. (2015). Using RFID and accelerometer-embedded tracers to measure probabilities of bed load transport, step lengths, and rest times in a mountain stream. *Water Resources Research*, *51*(9), 7572-7589.

Rosgen, D. L. (1994). A classification of natural rivers. *Catena*, *22*(3), 169-199.

Wohl, E., Cenderelli, D.A., Dwire, K.A., Ryan-Burkett, S.E., Young, M.K., Fausch, K.D. (2010) Large in-stream wood studies: a call for common metrics. Earth Surface Processes and Landforms. 35, 618–625.

CHAPTER 6

6 Conclusions, Limitations and Outlook

6.0 Chapter Overview

This chapter summarises the overall conclusions and key results covered in the previous chapters in the context of the key research aims outlined in section 1.7. The limitations of the study are discussed and potential avenues for future research are identified, along with an outlook on the potential impact and implications of the findings for research on sediment transport dynamics.

6.1 Conclusions

The aim of this thesis was to examine the feasibility of utilising contemporary sediment tracing techniques, namely embedded RFID tags and MEMS IMU embedded smart stones, to study the effect of woody debris on the grain scale dynamics of sediment transport in fluvial systems. In doing so, this thesis also evaluated the capabilities of novel LoRaWAN enabled smart stone tracers during long term deployment periods, and investigated the possibility of integrating these devices into wireless Internet of Things networks to remotely monitor sediment transport dynamics in the field with minimal human intervention.

Chapter 2 presents the first study of the impact of wood on fluvial bedload sediment transport dynamics, where > 950 Tracer sediments embedded with RFID tags were seeded into a wood-loaded alpine stream. Wood pieces were observed to alter the spatial distributions of sediments by causing localised clustering of tracers. However, the nature of the dispersion of sediments remained superdiffusive, matching wood free environments (e.g., Bradley and Tucker 2012; Phillips et al., 2013; Bradley, 2017). In addition, the distribution of travel distances were accurately described by gamma and exponential functions, in agreement

with prior research on bedload tracer movement (e.g., Hassan et al., 1991; Gintz et al., 1996). Linear Mixed Modelling was used to investigate the impact of wood relative to other controls on transport. A statistically significant reduction in both entrainment likelihood and tracer transport distances were recorded for sediments in close proximity to wood pieces. Additionally, a trapping effect of wood was observed where tracers were significantly more likely to have shorter transport steps if deposited near large wood. These statistical approaches provided quantitative data supporting the hypothesis that fluvial systems with wood have increased particle deposition rates (Wohl and Scott 2017) and may explain the observed increases in overall sediment retention rates in wood loaded rivers (Keller & Tally, 1979; Megahan, 1982; Sullivan et. al., 1987).

Chapter 3 presents the development of a new smart stone design intended for use in sediment transport experiments and field monitoring. This active tracer represents an advancement over other similar smart stones (e.g., Gronz et al., 2016; Dost et al., 2020; Maniatis et al., 2020) due to its integration of a novel ultra-low power IMU sensor and LoRaWAN wireless communication capabilities. The IMU, comprising of an accelerometer, gyroscope, and magnetometer sensors, captures detailed high-frequency movement data with low power consumption, enabling long-term field deployment at remote field sites wirelessly. This chapter focused on the testing of the sensor and the design of a concrete cobble to house the device. Not only did the development of this smart stone form the basis of subsequent laboratory and field deployment in this thesis, but it was also utilized in laboratory experiments on the SENSUM research project, in which I served as a graduate research assistant alongside my PhD studies.

Chapter 4 presents the creation of a library of IMU signatures used for categorising different modes of bedload movement during laboratory experiments at the University of East Anglia. Unique signatures were determined for rolling, sliding, collisions, and for tracers vibrating in-situ. These experiments complement work using the smart stones undertaken on the SENSUM project at the University of Plymouth, which also found that rolling can be distinguished from sliding (Sgarabotto et al., 2022). These signatures were crucial for interpreting IMU data collected from

smart stones deployed in the field without direct observations (e.g., Chapter 5), and for any future field deployments using LoRaWAN.

Chapter 5 presents data from smart stones deployed at a range of UK field sites, demonstrating the devices long-term monitoring capabilities and the collection of data representing natural entrainment events. Deployment at the Tebay field site validated the devices extended lifespan over several months of monitoring. Furthermore, the use of smart stones at the Branscombe site provided a natural transport dataset, allowing comparison with the laboratory results. Additionally, smart stones in Yarner Woods captured and transferred movement data via LoRaWAN for the first time, demonstrating their potential for remote data collection without the need for retrieval. Tracer movement was compared with discharge data where possible. Movement typically occurred within the 24 hours surrounding peak flow events, with the detection of movement being closely correlated with instances of peak flow at the site. However, the discharge data collection frequency from the gauge installed in the Yarner Woods sensor network was not frequent enough to accurately quantify threshold discharge conditions for entrainment. Additionally, the limited sample size of tracers interacting with wood precluded the analysis of woods influence on smart stone transport behaviour. Regardless, this chapter contributed to the refinement of the methodology for using smart stones equipped with LoRaWAN capabilities for tracking bedload, helping to inform future efforts of its implementation in field environments and highlighting areas where further optimisation may be required.

6.2 Limitations and Outlook

6.2.1 Sediment-Wood Interaction

Insights From Passive Sensors

Due to travel restrictions related to the COVID-19 pandemic, it was not possible to return to St Louis Creek after the 2019 field season, limiting the length of the tracer transport data sets to 3 years (2017 – 2019). This

was not sufficient to characterise distributions of particle rest times, which are needed in combination with distributions of particle transport distances to fully characterise the nature of diffusion. Typically, timeseries of several years of tracer transport data are needed to quantify rest times in between transport at a data collection frequency of 1 year (e.g. Bradley and Tucker, 2012). A return visit was intended after the pandemic to deploy smart stones in St Louis Creek, to enable the collection of rest time data to compliment the RFID step length data sets, following Olinde and Johnson (2015), but ultimately this was not feasible due to continued travel disruption. Instead, efforts were focused on investigating bedload interaction with wood in UK field settings alongside the SENSUM research project.

The analysis of passive tracer data from St Louis Creek revealed the impact of wood on transport behaviour and effectively demonstrated Linear Mixed Modelling as a technique for isolating the influence of wood on sediment transport from other key variables. However, a larger dataset spanning multiple years would have been beneficial to enhance the statistical validity and further examine specific subgroups of tracers. For instance, it would have been beneficial to analyse and compare the mobility of tracers located upstream and downstream of wood pieces, in order to evaluate the relative upstream and downstream effects of woody debris on sediment transport, taking into account different geomorphic features that tend to form, such as the upstream formation of backwater areas and downstream plunge pools (Montgomery et al., 2003; Wohl et al., 2016). Future investigations on the influence of in-stream wood could focus on determining if the position of tracer sediments relative to wood pieces influences subsequent transport behaviour.

Future studies on wood-sediment interactions could also consider channels with more mobile wood pieces. The limited amount of large wood transported in St. Louis Creek during the three years of investigation precluded the evaluation of the effects of wood movement events, such as collapse of log-jams, on sediment transport. It has been documented that log jam breakages lead to a rapid release of impounded sediment (Abbe and Montgomery, 2003), but the movement behaviours of individual clasts

during these events have not yet been investigated through tracer studies. The implementation of RFID tracer sediments, or smart stones, prior to log jam breakage could inform transport processes immediately after release.

The apparent lack of wood mobility at St. Louis Creek may be due to the relatively low flow rates observed during the study period. The recurrence interval for the peak flows experienced in 2019 was 1.9 years, indicating average to below average flow rates over the course of the study. It is possible that higher flow events in the future may mobilise key wood pieces and release tracer sediments, allowing for the tracking of post-log jam breakage sediments. Continued monitoring would have been necessary to fully assess the relationship between flow rates, wood mobility, and subsequent sediment transport at the site.

Fully characterising wood-sediment interaction is essential for evaluating the impact of the addition of woody debris in Natural Flood Management (NFM). As public perception evolves (Piégay et al., 2005), and implementation of NFM practices becomes more widespread (Cooper et al., 2021), it is crucial to fully understand the consequences at both the catchment scale (Dadson et al., 2017), and the specific sedimentological implications of introducing woody debris to fluvial systems. The successful utilization of RFID tracers in this research demonstrated the impact of large wood on grain transportation, suggesting potential future research avenues for assessing NFM's impacts prior to widespread adoption, helping to inform landowners and policy makers (Bark et al., 2021). Furthermore, the development of active smart stone tracers has the potential to automate the tracking of sediment behaviour, improving both the detail and ease of data collection.

Insights From Active Sensors

The utilisation of smart stone data in UK sites in Chapter 5 was initially envisioned as a means to gain deeper insight into the impact of large woody debris on the transport dynamics of sediments, with the aim of supplementing the findings of the RFID tracer transport study presented in Chapter 2. Unfortunately, the limited movement of the smart stones

over 2022 resulted in a scarcity of observations of wood-sediment interactions. However, data collection during this period demonstrated the potential for the capturing of modes of movement from field data using smart stones over extended deployment periods. Despite the detection of tracer movement at Yarner Woods in Dartmoor, the transport distances recorded were insufficient to reveal interaction with large woody debris. Future deployments could benefit from tagging a combination of wood pieces and smart stones in more active channels with mobile wood. This would enable the direct tracking of the interaction between log jam break up and subsequent tracer transportation upon the release of impounded sediment.

In addition, the low transport rates and small tracer sample size at Yarner Woods precluded the calculation of tracer step and rest times, which would have enabled comparisons to the St. Louis Creek data sets and other bedload studies (e.g., Olinde and Johnson, 2015; Pretzlav et al., 2021). Continued monitoring over 2022 - 2023 at Yarner Woods may produce further transport data sets enabling these calculations, provided tracers continue to function at the site over the winter months.

Future investigations into bedload transport dynamics could combine passive and active tracer deployments, to benefit from both the continuous and detailed transport data provided by smart stones and the reliability of radio transmitters. In addition, incorporating a range of LoRa enabled sensors to collect environmental data in real time could facilitate the identification of the conditions required for entrainment and transport, providing further insights into the underlying mechanisms of sediment transport behaviour and its interaction with wood.

6.2.2 Smart Stone Design

The design of the smart stone proved successful in acquiring movement data from the deployment sites at Tebay and Yarner Wood in Chapter 5. However, it should be noted that some devices sustained damage upon retrieval from the Tebay site, due to water infiltration into the inner casing

of the artificial sediments. Although the majority of tracer sediments remained operational following eight months of submersion during deployment, future versions of the smart stone design should incorporate additional redundancy measures to mitigate the risk of damage. An internal design that prioritises waterproofing and incorporates stronger internal support structures (e.g., Maniatis et al., 2013), could significantly reduce the likelihood of damage occurring during future deployments.

6.2.3 Smart Stone Laboratory Experiments

Chapter 4 focused on using smart stones to characterise signatures of different modes of movement from IMU data. The range of movement behaviours that could be differentiated within the laboratory environment was limited to collisions, shaking, rolling, and sliding of the smart stones. Further laboratory research has the potential to broaden the scope of identifiable transport behaviours within the IMU data by exploring specialised movement patterns, such as transportation in temporary suspension or via saltation. This would require a more advanced laboratory setup than that was available during this research, but it would provide a more comprehensive understanding of the full range of movement types that are possible in natural environments. In addition, scaled down flume experiments incorporating geomorphic complexity, such as simulated woody debris (e.g., Mutz et al., 2007; Davidson, 2011), could contribute to a greater understanding of the effects of these factors on sediment transport. Simulated log jam breakage experiments could also replicate conditions immediately following the release of impounded sediments. This would provide laboratory transport data in controlled environments which would more closely replicate natural deployment sites.

Prior smart stone research in the laboratory has focused on producing precise trajectory estimates of tracer movements in the process of dead-reckoning, with estimated trajectories verified using high-speed camera setups (e.g., Dost et al., 2020). Although, Maniatis (2016) highlights that, due to limitations in the accuracy of sensors and measurement noise, obtaining accurate particle trajectory estimations using sensor data from

the IMU devices is not feasible beyond a few seconds of movement. Therefore, attempts to precisely predict transport and depositional locations of tracers have resulted in deviations from true depositional positions when verified, even in highly controlled laboratory settings (e.g., Gronz et al., 2016; Dost et al., 2020). As a result, smart stone data obtained from the laboratory focused solely on characterising movement patterns in this research, given the emphasis on long-term deployment and obtaining remote measurements in the field (Chapter 5). Although, parallel experiments conducted on the SENSUM project using the smart stone produced in Chapter 3, presented by Scarabotto et al. (2022), demonstrated an approach to filter data to more precisely derive reliable values of the position, orientation, velocity and acceleration of smart stones.

6.2.4 Smart Stone Field Deployments

Deployment of the smart stones at the Branscombe field site provided the first examples of natural mobilisation data and confirmed device functionality during submersion. Despite this, deployment at the site demonstrated that the use of LoRa transmission for the transfer of high-frequency data is not optimal, given the short experimental time frames and the large quantity of IMU data required for movement characterisation. Initial attempts to capture and transmit transport data were hindered by prolonged upload times from sensors to the gateway, often resulting in data loss. Despite possible LoRaWAN transfer speeds of 2 Kbit/s (Mikhaylov et al., 2016), increasing distance and obstructions between sensors and gateways have been shown to reduce data transfer speeds to as low as 100 bits/s (Gambiroža et al., 2019). Whilst this is not an issue during longer term deployment of devices, the problems faced at the Branscombe field site suggest that the use of LoRa for time-limited applications, such as repeated laboratory experimentation, should not be implemented.

The persistent issue of intermittent communication between the smart stones, LoRa gateways, and GSM network was a consistent factor

encountered during the deployment at the Yarner Woods site, despite the distance between the gateways and sensors being < 1 km. This suggests that the claims of a 15 km read range of LoRa devices (Petajajarvi et al., 2015) is an overestimation when accounting for the range of obstacles typically encountered in remote field deployment (e.g., diverse topography, poor line of sight due to vegetation). Furthermore, the gateway GSM connectivity issues experienced reflected those encountered by Dini et al. (2021), suggesting a future emphasis on improving gateway reliability is required for successful continued long-term monitoring.

Currently, the dependence on mobile network coverage for the functioning of LoRaWAN technology impairs its ability to fully serve remote environmental science applications. However, the technology is still in its infancy, with new gateways in development likely overcoming the shortcomings of range and intermittent connectivity encountered (Manchev et al., 2019). It is estimated that by 2025, 25% of all IoT devices will be integrated with low-power wide-area networks, such as LoRaWAN (Ikpehai et al., 2018). As such, there is much potential for the further development of smart tracer devices to monitor fluvial systems, and for environmental monitoring more generally, combining advances in microelectromechanical systems and LoRa capabilities.

Despite encountering challenges, such as limited sediment transport and inconsistent gateway connectivity during the study period, the deployment of smart stones in the field served as a successful pilot study for the larger-scale implementation of tracers integrated in a LoRaWAN network, for the automatic monitoring of fluvial processes. The feasibility and effectiveness of the methodology was evaluated, with potential issues being highlighted and addressed over the course of the research, informing future deployments.

The deployment of LoRa networks with improved gateways that have a greater consistency in their GSM connectivity would facilitate more reliable comparisons of transport conditions across field sites. The integration of additional LoRa-enabled environmental sensors into future stable gateway networks would also allow for the real time collection of various data sets

(e.g., temperature, precipitation, flow rates), which could aid in the interpretation of the overall conditions influencing transport behaviour. This would provide a more comprehensive understanding of these environments, enabling a more accurate analysis of risk for decision making in instances of hazard management (Sayers et al., 2002). The implementation of such networks would reflect recent developments in the use of environmental sensors integrated into LoRa networks in both urban areas to monitor air quality (Candia et al., 2018; Howerton & Schenck, 2020) and in the agricultural sector to monitor soil health (Ma & Chen, 2018; Ramson et al., 2021).

As the technology matures, large-scale LoRa networks could provide cost-effective solutions for the remote monitoring of field sites. Ongoing expenses would primarily consist of infrequent replacement of batteries for sensor devices. Such networks could continuously provide data without incurring the costs associated with travel and labour, which are inherent in current remote manual data collection approaches.

6.3 Advancing Sediment Transport Research with Smart Stone Technology

The precise determination of entrainment thresholds has been a persistent challenge in sedimentology (Dey & Ali, 2018). The complexity of factors influencing particle entrainment, including grain protrusion (Fenton & Abbott 1977; Hodge et al., 2020), have hindered a satisfactory resolution of the problem. Smart stones, however, present a promising opportunity for providing field data to verify theoretical models, provided the limitations of the technology are considered when interpreting IMU data (Maniatis, 2021). Unfortunately, discharge data collected at Yarner Woods lacked sufficient detail to estimate an entrainment threshold for the transport event detected. Future research on the SENSUM project plans to improve the discharge gage installed in Yarner Woods to better constrain approximations of entrainment thresholds at the site.

Another advancement in the use of smart stones to enhance the understanding of sediment transport would be the automatic classification of smart stone movements from laboratory and field data using machine learning. By compiling a sufficiently large data inventory of verified smart stone movement patterns from IMU outputs, it should be possible to utilise and train machine learning algorithms to automatically recognise specific movement characteristics. This approach is similar to the characterisation of various physical activity movement types using accelerometers from commercial fitness trackers (e.g., Nunavath et al., 2021).

It is possible that, the utilisation of neural networks in conjunction with LoRa capabilities could enable the deployment of smart stones, the upload of their data to an online database, followed by the automatic characterisation of movement behaviours. This would fully automate the process of tracking bedload transport. However, this would require a high level of accuracy and success rate of characterisation, which, with the current limitations of embedded IMU's (Maniatis, 2021), has the potential risk of data misinterpretation. Regardless, this approach could offer a novel method for monitoring river sediments with minimal human oversight to enhance our understanding of fluvial systems.

By utilising an automated process, it may be feasible to integrate risk management solutions whereby the entrainment and rapid transport of multiple tracers could signal the occurrence of flood events. This could be integrated with early warning systems to alert downstream authorities, similar to approaches being developed on the SENSUM project for the monitoring of hazardous movement events such as landslides (Dini et al., 2021; Roskilly et al., 2022).

References

Abbe, T. B., & Montgomery, D. R. (2003). Patterns and processes of wood debris accumulation in the Queets river basin, Washington. *Geomorphology*, *51*(1-3), 81-107.

Bark, R. H., Martin-Ortega, J., & Waylen, K. A. (2021). Stakeholders' views on natural flood management: Implications for the nature-based solutions paradigm shift?. *Environmental Science & Policy*, *115*, 91-98.

Bradley, D. N. (2017). Direct observation of heavy-tailed storage times of bed load tracer particles causing anomalous superdiffusion. *Geophysical Research Letters*, *44*(24), 12-227.

Candia, A., Represa, S. N., Giuliani, D., Luengo, M. Á., Porta, A. A., & Marrone, L. A. (2018, November). Solutions for SmartCities: proposal of a monitoring system of air quality based on a LoRaWAN network with low-cost sensors. In *2018 Congreso Argentino de Ciencias de la Informática y Desarrollos de Investigación (CACIDI)* (pp. 1-6). IEEE.

Cooper, M. M., Patil, S. D., Nisbet, T. R., Thomas, H., Smith, A. R., & McDonald, M. A. (2021). Role of forested land for natural flood management in the UK: A review. *Wiley interdisciplinary reviews: Water*, *8*(5), e1541.

Dadson, S. J., Hall, J. W., Murgatroyd, A., Acreman, M., Bates, P., Beven, K., ... & Wilby, R. (2017). A restatement of the natural science evidence concerning catchment-based 'natural'flood management in the UK. *Proceedings of the Royal Society A: Mathematical, Physical and Engineering Sciences*, *473*(2199), 20160706.

Davidson, S. (2011). *Modelling channel morphodynamics associated with large wood in an intermediate-sized stream* (Doctoral dissertation, University of British Columbia).

Dey, S., & Ali, S. Z. (2017). Mechanics of sediment transport: Particle scale of entrainment to continuum scale of bedload flux. *Journal of Engineering Mechanics*, *143*(11), 04017127.

Dini, B., Bennett, G. L., Franco, A., Whitworth, M. R., Cook, K. L., Senn, A., & Reynolds, J. M. (2021). Development of smart boulders to monitor mass movements via the Internet of Things: a pilot study in Nepal. *Earth Surface Dynamics*, *9*(2), 295-315.

Dost, B., Gronz, O., Casper, M., Krein, A. (2020) The Potential of Smartstone Probes in Landslide Experiments: How to Read Motion Data. *Natural Hazards and Earth System Sciences.* 20, 3501–3519, https://doi.org/10.5194/nhess-20-3501-2020.

Fenton, J. D., & Abbott, J. E. (1977). Initial movement of grains on a stream bed: The effect of relative protrusion. *Proceedings of the Royal Society of London. A. Mathematical and Physical Sciences*, *352*(1671), 523-537.

Gambiroža, J. Č., Mastelić, T., Šolić, P., & Čagalj, M. (2019, June). Capacity in LoRaWAN networks: challenges and opportunities. In *2019 4th International Conference on Smart and Sustainable Technologies (SpliTech)* (pp. 1-6). IEEE.

Gintz, D., Hassan, M. A., & SCHMIDT, K. H. (1996). Frequency and magnitude of bedload transport in a mountain river. *Earth Surface Processes and Landforms*, *21*(5), 433-445.

Gronz, O., Hiller, P. H., Wirtz, S., Becker, K., Iserloh, T., Seeger, M., ... & Ries, J. B. (2016). Smartstones: A small 9-axis sensor implanted in stones to track their movements. *Catena*, 142, 245-251.

Hassan, M. A., Church, M., & Schick, A. P. (1991). Distance of movement of coarse particles in gravel bed streams. *Water Resources Research*, *27*(4), 503-511.

Howerton, J. M., & Schenck, B. L. (2020, April). The deployment of a LoRaWAN-based IoT air quality sensor network for public good. In *2020 Systems and Information Engineering Design Symposium (SIEDS)* (pp. 1-6). IEEE.

Ikpehai, A., Adebisi, B., Rabie, K. M., Anoh, K., Ande, R. E., Hammoudeh, M., ... & Mbanaso, U. M. (2018). Low-power wide area network

technologies for Internet-of-Things: A comparative review. *IEEE Internet of Things Journal*, *6*(2), 2225-2240.

Keller, E. A., & Tally, T. (1979). Effects of large organic debris on channel form and fluvial processes in the coastal redwood environment. In *Adjustments of the fluvial system* (pp. 169-197). Routledge.

Ma, Y. W., & Chen, J. L. (2018, April). Toward intelligent agriculture service platform with lora-based wireless sensor network. In *2018 IEEE International Conference on Applied System Invention (ICASI)* (pp. 204-207). IEEE.

Manchev, N. P., Angelov, K. K., Kogias, P. G., & Sadinov, S. M. (2019). Development of Multichannel LoRaWAN Gateway for Educational Applications in Low-Power Wireless Communications. In *2019 IEEE XXVIII International Scientific Conference Electronics (ET)* (pp. 1-4). IEEE.

Maniatis, G. (2016). *Eulerian-Lagrangian definition of coarse bed-load transport: theory and verification with low-cost inertial measurement units* (Doctoral dissertation, University of Glasgow).

Maniatis, G. (2021). On the use of IMU (inertial measurement unit) sensors in geomorphology. *Earth Surface Processes and Landforms*, *46*(11), 2136-2140.

Maniatis, G., Hoey, T., & Sventek, J. (2013). A New Method for Rapid Prototyping of Purpose-Specific Sensor Enclosures: Example Application and Implications for Data Coherence. *Journal of Sensor and Actuator Networks*, *2*(4), 761-779.

Megahan, W. F. (1982). Channel Sediment Storage Behind Obstructions in Forested Drainage Basins. *Sediment budgets and routing in forested drainage basins*, *141*, 114.

Mikhaylov, K., Petaejaejaervi, J., & Haenninen, T. (2016, May). Analysis of capacity and scalability of the LoRa low power wide area network technology. In *European Wireless 2016; 22th European Wireless Conference* (pp. 1-6). VDE.

Montgomery, D. R., Massong, T. M., & Hawley, S. C. (2003). Influence of debris flows and log jams on the location of pools and alluvial channel reaches, Oregon Coast Range. *Geological Society of America Bulletin*, *115*(1), 78-88.

Montgomery, D., Collins, B., Buffington, J., Abbe, T. (2003) Geomorphic effects of wood in rivers. *The Ecology and Management of Wood in World Rivers, Symposium.* 37, 21-47.

Mutz, M., Kalbus, E., & Meinecke, S. (2007). Effect of instream wood on vertical water flux in low-energy sand bed flume experiments. *Water Resources Research*, *43*(10).

Nunavath, V., Johansen, S., Johannessen, T. S., Jiao, L., Hansen, B. H., Berntsen, S., & Goodwin, M. (2021). Deep Learning for Classifying Physical Activities from Accelerometer Data. *Sensors*, *21*(16), 5564.

Olinde, L. & Johnson, J. (2015) Using RFID and accelerometer-embedded tracers to measure probabilities of bed load transport, step lengths, and rest times in a mountain stream, Water Resources Research, 51, 7572-7589.

Petajajarvi, J., Mikhaylov, K., Roivainen, A., Hanninen, T., & Pettissalo, M. (2015, December). On the coverage of LPWANs: range evaluation and channel attenuation model for LoRa technology. In *2015 14th international conference on its telecommunications (itst)* (pp. 55-59). IEEE.

Phillips, C. B., Martin, R. L., & Jerolmack, D. J. (2013). Impulse framework for unsteady flows reveals superdiffusive bed load transport. *Geophysical Research Letters*, *40*(7), 1328-1333.

Piégay, H., Gregory, K. J., Bondarev, V., Chin, A., Dahlstrom, N., Elosegi, A., ... & Zawiejska, J. (2005). Public perception as a barrier to introducing wood in rivers for restoration purposes. *Environmental Management*, *36*(5), 665-674.

Pretzlav, K. L., Johnson, J. P., & Bradley, D. N. (2021). Smartrock transport from seconds to seasons: Shear stress controls on gravel

diffusion inferred from hop and rest scaling. *Geophysical Research Letters*, *48*(9), e2020GL091991.

Ramson, S. J., León-Salas, W. D., Brecheisen, Z., Foster, E. J., Johnston, C. T., Schulze, D. G., ... & Málaga, M. P. (2021). A self-powered, real-time, LoRaWAN IoT-based soil health monitoring system. *IEEE Internet of Things Journal*, *8*(11), 9278-9293.

Roskilly, K., Bennett, G., Curtis, R., Egedusevic, M., Jones, J., Whitworth, M., Dini, B., Luo, C., Manzella, I. and Franco, A., (2022). *SENSUM project, Smart SENSing of landscapes Undergoing hazardous hydrogeomorphic Movement* (No. EGU22-10289). Copernicus Meetings.

Sayers, P. B., Hall, J. W., & Meadowcroft, I. C. (2002). Towards risk-based flood hazard management in the UK. In *Proceedings of the Institution of Civil Engineers-Civil Engineering* (Vol. 150, No. 5, pp. 36-42). Thomas Telford Ltd.

Sgarabotto, A., Manzella, I., Roskilly, K., Luo, C., Clark, M., Franco, A., Bennet, G., Raby, A. (2022, May). Investigating boulder motions with smart sensors in lab experiments. In *EGU General Assembly Conference Abstracts* (pp. EGU22-10198).

Sullivan, K., Lisle, T. E., Dolloff, C. A., Grant, G. E., & Reid, L. M. (1987). Stream channels: the link between forests and fishes. In *Chapter Three, In: Ernest O. Salo and Terrance W. Cundy (eds.), Streamside Management: Forestry and Fishery Interactions, Proceedings of a Symposium held at University of Washington, 12-14 February 1986. Contribution no. 57, Institute of Forest Resources, Seattle, Washington. p. 39-97.*

Wohl, E., Bledsoe, B. P., Fausch, K. D., Kramer, N., Bestgen, K. R., & Gooseff, M. N. (2016). Management of large wood in streams: an overview and proposed framework for hazard evaluation. *JAWRA Journal of the American Water Resources Association*, *52*(2), 315-335.

Wohl, E., Scott, D. (2017). Wood and sediment storage and dynamics in river corridors. *Earth Surface Processes and Landforms.* 42, 5-23.

Appendix A

Supplementary material for chapter two

Table A.1*: Key recorded characteristics of tagged wood at St. Louis Creek. Note that not all wood pieces tagged with metal tags were also tagged with RFID tags*

Tag	D1 (cm)	D2 (cm)	Age	Stab	R-Wad	Func	Chan.	Structure		Key/categories	
213	7	15	4	1	1	3	5	8,3			
204	9	20	4	1	1	3	5	8,2,3		**Age Class**	
201	8	29	3	1	0	3	5	8		0 Rotten	3 Limbs
203	8	29	2	1	0	3	5	8,3		1-Decayed	4 Bark
202	37	29	2	1	0	3	5	3,2		2 Bare	5 Needles
214	13	2	2	0	1	3	5	3			
215	12	9	2	1	1	3	5	38		**Stabillity**	
205	27	12	2	1	0	1	5	23		0 No ends	2 Two ends
206	18	47	1	2	1	1	5	8		1 one end	
207	36	14	0	0	1	4	5	0			
212	8	37	4	1	1	3	5	8,3			
208	11	33	2	2	1	1	5	3,8,2		**Root wad**	
211	13	31	2	1	0	1	4	8		0 no	1 Yes
209	14	27	2	1	0	1	4	8,2			
210	14	5	4	1	0	2	4	8		**Structural Association**	
216	32	50	0	1	0	3	4	8		1 Debris Jam	6 Bedrock
217	43	55	4	1	0	3	4	8		2 Tree/Rootwad	7 Beaver Dam
218	44	40	4	1	0	3	4	8,2		3 Boulder	8 Bank
219	16	N/A	2	1	0	3	4	8		4 Meander	9 Log step
220	19	13	4	1	0	3	4	8,3		5 Bar	10 Burial in bed
221	19	24	4	1	0	3	4	8,2			0 none
222	44	9	5	1	1	1	4	8,2			
223	15	6	5	2	1	1	4	2,8		**Function**	
224	11.5	5	1	1	0	3	4	8		0 Drift	2 Collapsed Brid
225	165	15	2	1	0	3	4	8		1 Bridge	3 Ramp
233	20	10	2	1	0	3	4	1			4 Incorporated
245	25	15	2	1	0	3	5	1,8			
244	31	15	2	1	1	3	5	1,2,8		**Channel Type**	
251	14	5	2	1	0	3	5	1,8		1 Pool	5 step/pool
246	43	13	2	1	0	1	5	1,8		2 Riffle	6 Cascade
248	12	10	2	0	0	4	5	1,10,9		3 Glide	7 Other
242	23	17	2	0	0	0	4	3		4 Rapid	
249	14	11	2	0	0	4	5	1,10,9			
247	22	19	2	1	0	4	5	1,10,9			
252	17	10	2	1	0	3	5	8			
253	27	21	2	1	0	3	5	8			
254	19	16	2	1	0	3	5	8			
255	26	14	1	1	0	4	5	10,8			
256	27	24	1	1	0	3	5	8			
257	39	32	2	1	1	3	5	3,8			
258	19	17	2	1	0	3	5	3,8			
259	27	26	2	1	0	3	5	3,8			
260	30	23	1	1	0	3	5	3,8,10			
261	36	11	5	2	1	4	5	2,8,9,10			
262	26	25	1	0	0	0	5	1			
263	19	18	2	1	0	4	5	1,3,8			
264	16	13	2	0	0	0	5	1			
265	13	7	2	0	0	0	5	1			
266	15	11	2	0	0	0	5	1,9			
267	30	17	1	1	0	0	5	1			
268	24	22	2	1	0	0	5	1			
269	28	27	2	1	0	3	5	1,8			
270	17	13	1	1	0	4	5	9,10			

[illegible]	[illegible]	[illegible]	[illegible]	[illegible]	[illegible]	[illegible]	[illegible]	[illegible]			
271	75	11	3	2	1	1	5	8			
272	14	7	3	1	1	3	5	1,8			
273	15	6	3	1	0	3	5	1,8			
274	13	4	4	1	0	3	5	1,8			
275	15	14	4	1	0	3	5	1,8			
276	25	4	4	1	1	3	5	1,8			
277	18	21	2	1	0	4	5	1,8			
278	20	12	1	1	0	4	5	1,8			
279	33	14	1	1	0	0	5	1,8			
280	24	23	0	2	0	1	5	2			
226	21	3	3	0	1	0	4	8,10			
237	21	18	2	1	0	0	4	5,10			
234	16	17	1	1	0	0	4	8			
235	27	14	1	1	0	3	4	8			
236	21	20	0	1	0	3	4	1			
232	15	10	5	1	1	3	4	1,8			
228	19	4	3	0	0	0	4	9,8			
229	20	14	3	1	0	3	4	10,8			
239	20	8	3	2	0	4	4	5			
238	20	18	2	1	0	4	4	8			
241	20	16	2	0	0	0	4	1			

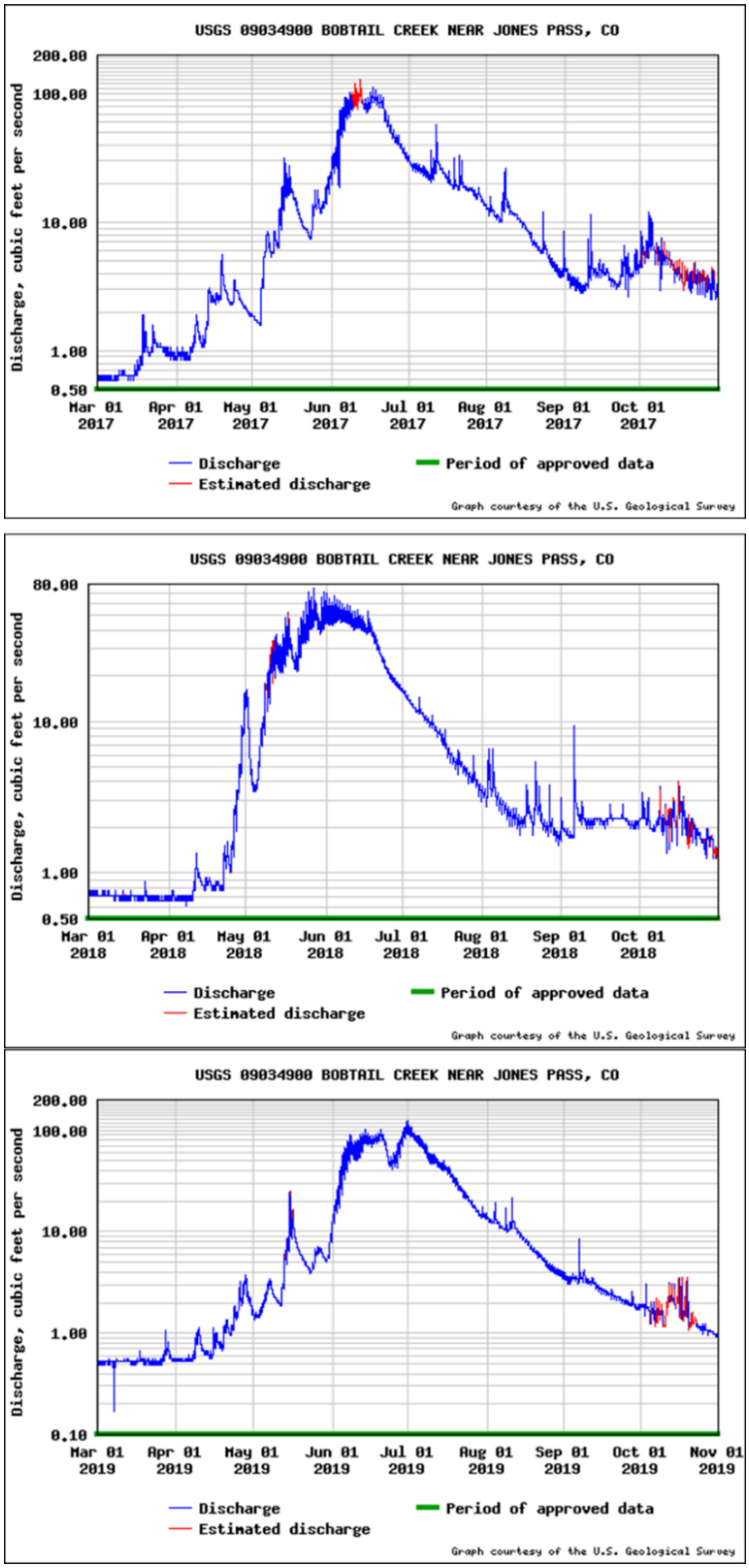

Appendix A.2: *Discharge data from Bobtail Creek for 2017-2019, showing peak flow during summer following snowmelt, which aligns with peak flow at St Louis Creek (as shown in Figure 3). The site was selected for its proximity, similar forest cover, and matching altitude to the study site (US Geological Survey, 2019).*

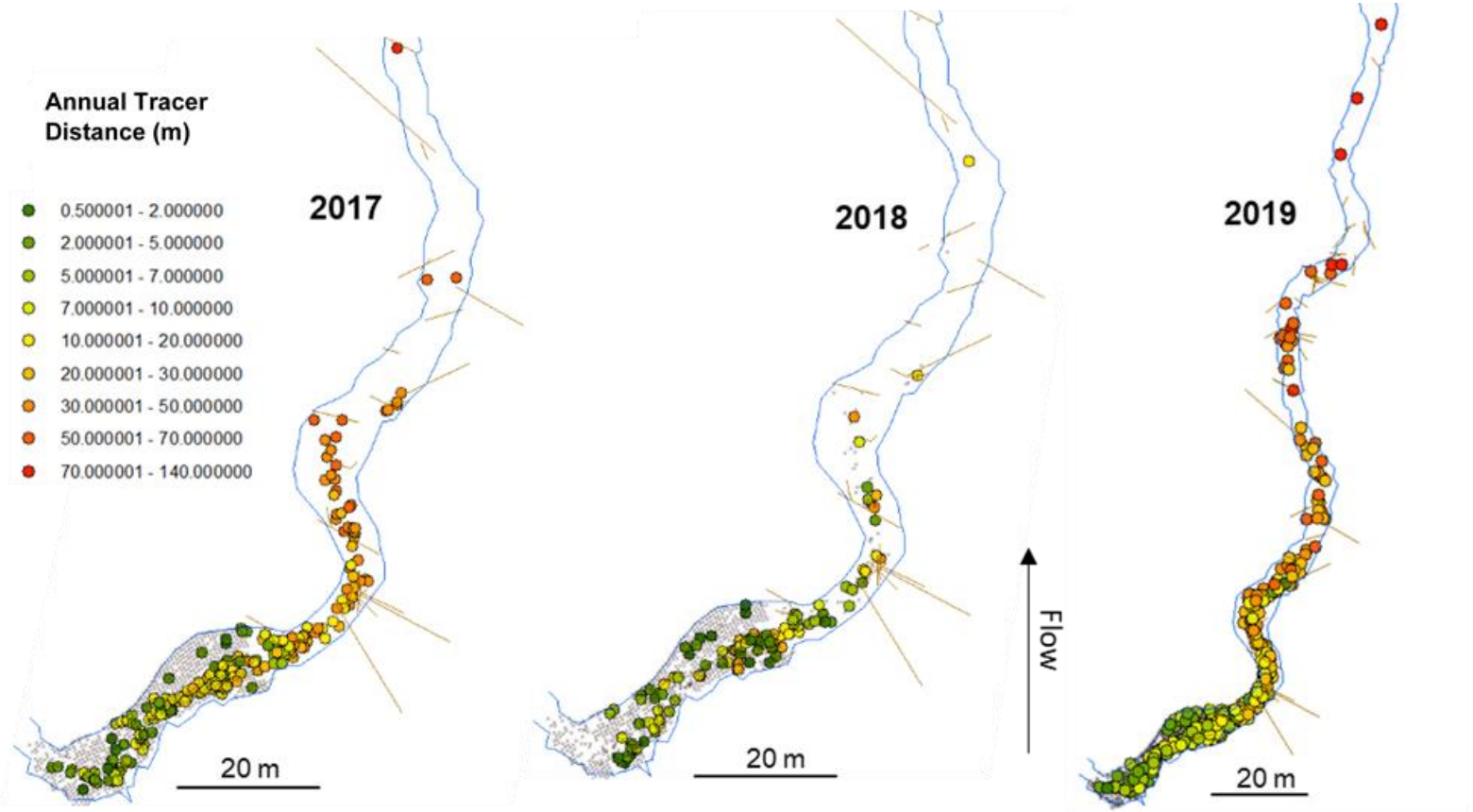

Figure A.3: *Annual tracer transport distance progression from 2017 to 2019 with grey dots representing unmoved cobbles from the previous year. Colour represents distance moved over the last year of the study.*

Table A.4: *Linear mixed model output data for the likelihood of tracer sediment entrainment (Binomial) within the wooded reach, and tracer sediment transport distances (Gamma), including the coefficient, standard error, z-value and p-value for distance to steps. All P values are below the 95% confidence interval and are considered insignificant*

2017 Binomial	**Coefficient**	**Standard Error**	**Z**	**P**
Distance to Step	0.01763	0.08712	0.202	0.83961
2018 Binomial				
Distance to Step	-0.004752	0.089074	-0.053	0.95745
2019 Binomial				
Distance to Step	0.0537	0.05293	1.015	0.3103

2017 Gamma	**Coefficient**	**Standard Error**	**Z**	**P**
Distance to Step	0.03952	0.07072	0.559	0.5763
2018 Gamma				
Distance to Step	0.02087	0.07589	0.275	0.7833
2019 Gamma				
Distance to Step	-0.014925	0.022476	-0.664	0.50724

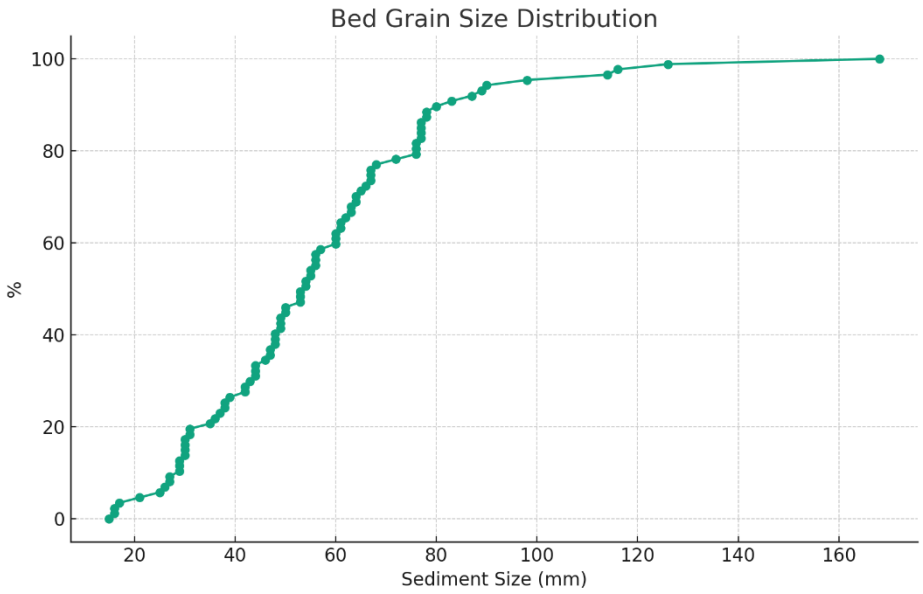

Figure A.5: Bed grain size distribution of measured natural surface particles at St. Louis Creek deriving the D50 of the reach.

Appendix B

Supplementary material for chapter three

Appendix B.1: *Standard deployment settings for Nomad LoRaWAN IMU devices*

AT+SERIAL=3737333151377201

AT+VERFW=5.6.2

AT+VERGIT=959b28215c435d9a016d258a8932e538ea3ba90d

AT+DEVEUI=10ce45fffe0077a4

AT+APPEUI=41db0a44d4979de9

AT+APPKEY=AT_NO_ACCESS

AT+DADDR=d1a00008

AT+NWKSKEY=AT_NO_ACCESS

AT+APPSKEY=AT_NO_ACCESS

AT+NWKID=0x0800A1A5

AT+ADR=1

AT+DR=0

AT+DCS=0

AT+NJM=1

AT+AUTONJM=0

AT+JOINED=0

AT+ABPON=1

AT+REQJOIN=1

AT+JOINCYC=120000

AT+JOINATT=10

AT+JOINSTRAT=0

AT+LORAFAIL=0

AT+FLASH=

AT+FLASHSETFF=

AT+FLASHWRITE=

AT+PWRMODE=1

AT+PWRCYC=300000

AT+LORAEN=1

AT+LORAMODE=2

AT+LORATX=60000

AT+LORATXF=1800000

AT+PLDDELTA=0

AT+PLDCYC=300000

AT+BUFMODE=0

AT+GPSEN=1

AT+GPSSIM=0

AT+GPSTRIG=3

AT+GPSCYC=86400000

AT+GPSHOLD=300000

AT+GPSHOLDFAIL=300000

AT+GPSTO=120

AT+GPSEA=1

AT+GPSNMEA=0

AT+GPSFAIL=1

AT+GPSMAXDOP=500

AT+GPSDISCARD=0

AT+ACCEN=1

AT+ACCRNG=0

AT+ACCTHD=24

AT+ACCDUR=1

AT+ACCAVG=32

AT+ACCANGEN=1

AT+ACCANGCYC=5000

AT+ACCANGTHD=5000

AT+ACCTIME=0

AT+ACCSE=0

AT+ACCSC=32

AT+ACCSF=0x30

25 Hz

AT+ACCSA=4

AT+GYREN=1

AT+MAGEN=1

AT+GYREXPERT=0

AT+GYRFREQ=14.9 Hz

AT+MAGFREQ=5 Hz

AT+GYRSCALE=2000 DPS

AT+GYRASCALE=16g

AT+MAGSCALE=16 G

AT+GYRSTOP=1

AT+GYRSAMPLES=38527

AT+GYRTIME=10000

AT+GYRHOLD=0

AT+STAEN=1

AT+STACYC=3600000

AT+AUXEN=0

AT+AUXCYC=15000

AT+AUX=21710

102240

176

-880

432

AT+LED=1

AT+LOG=1

AT+DEVTYPE=1

AT+DEVSUBTYPE=1

AT+BAT=3003

AT+BATTYPE=0

AT+SUPTYPE=0

AT+HWCFG=95

0x5F

AT+TESTCW=0

AT+TIME=101822

AT+RTC=010100,000219

AT+TIMESYNC=3

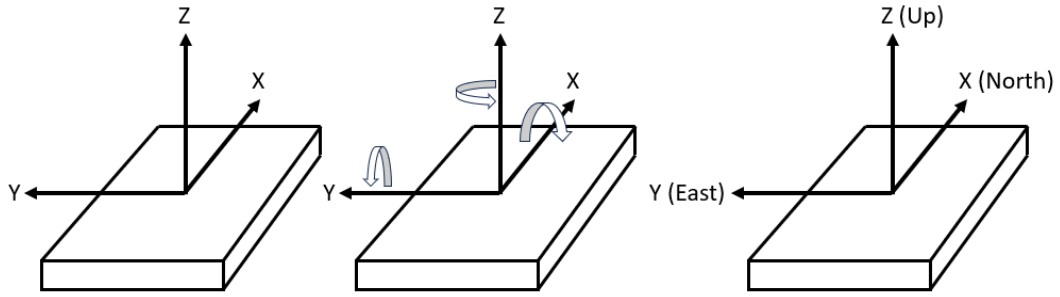

Figure B.2: *IMU sensor schematic demonstrating the distinction between the accelerometer, gyroscope, and magnetometer X, Y and Z axis.*

Appendix C
Supplementary material for chapter four

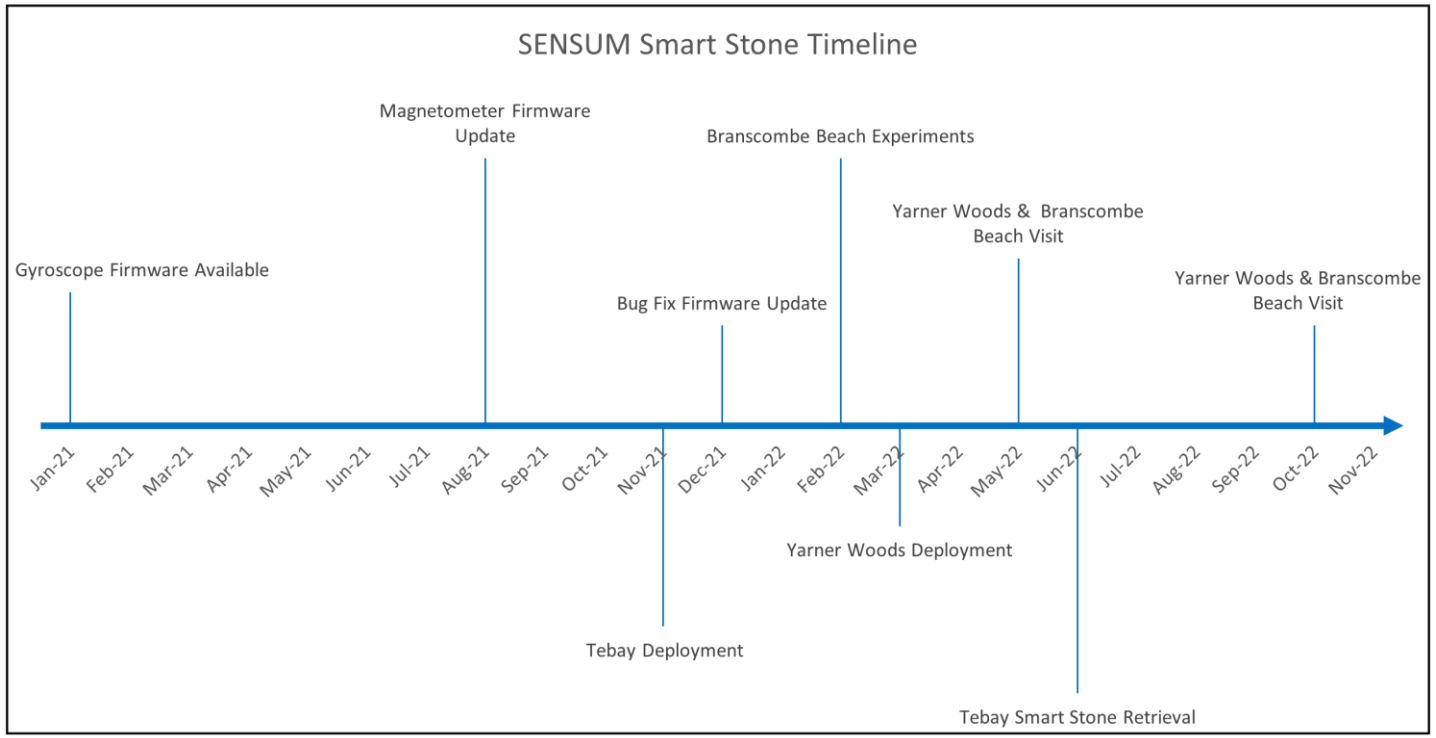

Figure C.1: *Timeline of Miromico firmware update availability in relation to the range of field deployments and experiments.*

Appendix D
Supplementary material for chapter five

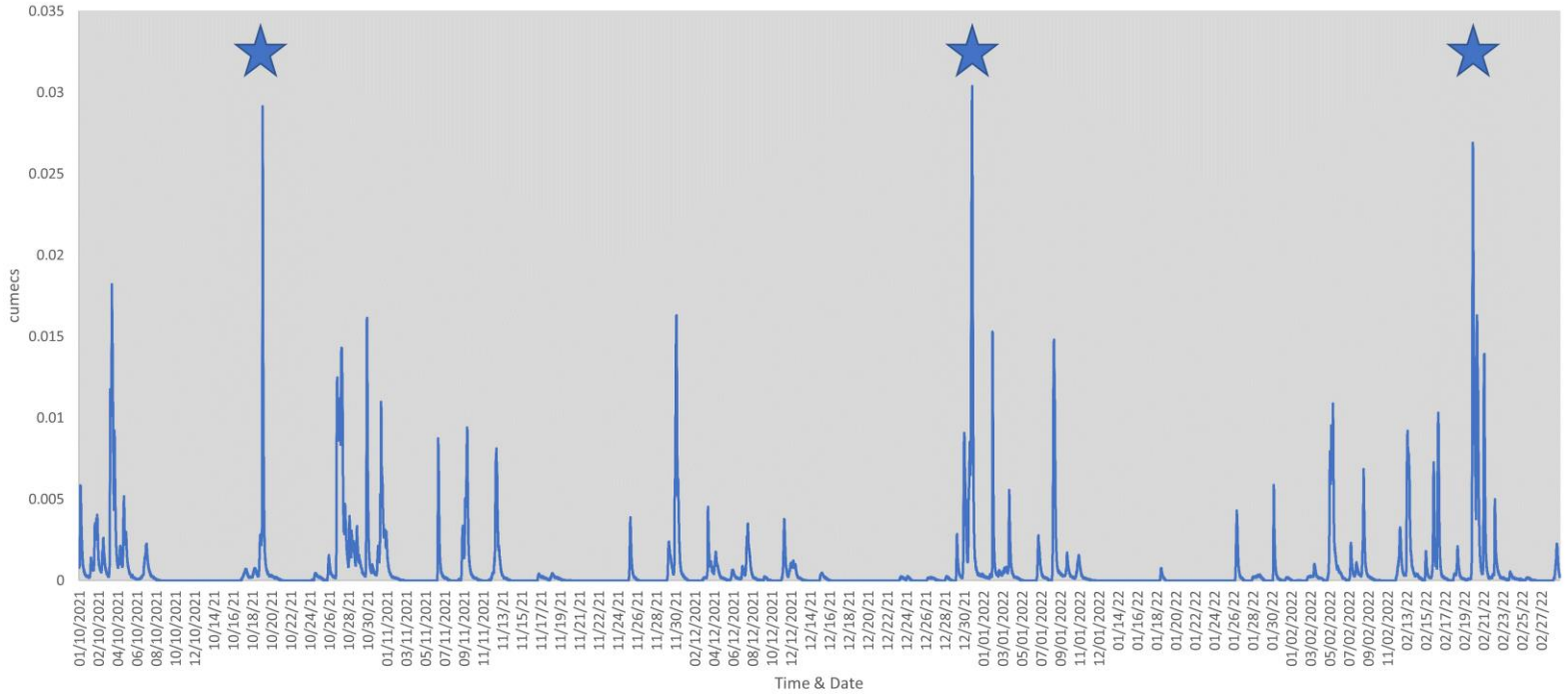

Figure D.1: *Discharge measured at Tebay field site covering the peak flows during the winter months of 2021 – 2022, with the peak flow events suspected to initiate movement highlighted using blue stars (adapted from Chappell and Page, 2020).*

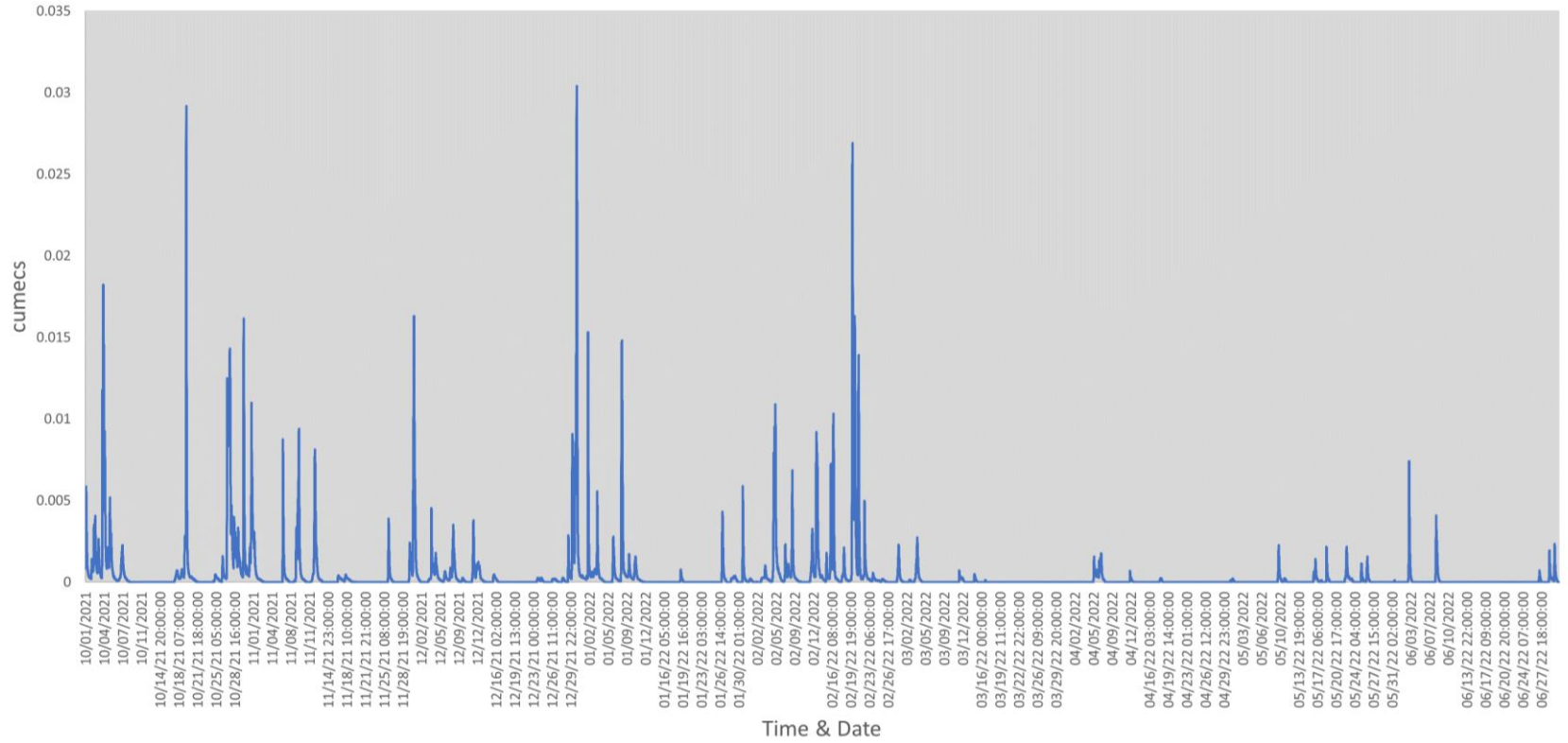

***Figure D.2**: Discharge measured at Tebay field site covering the deployment period of the smart stones (adapted from Chappell and Page, 2020).*

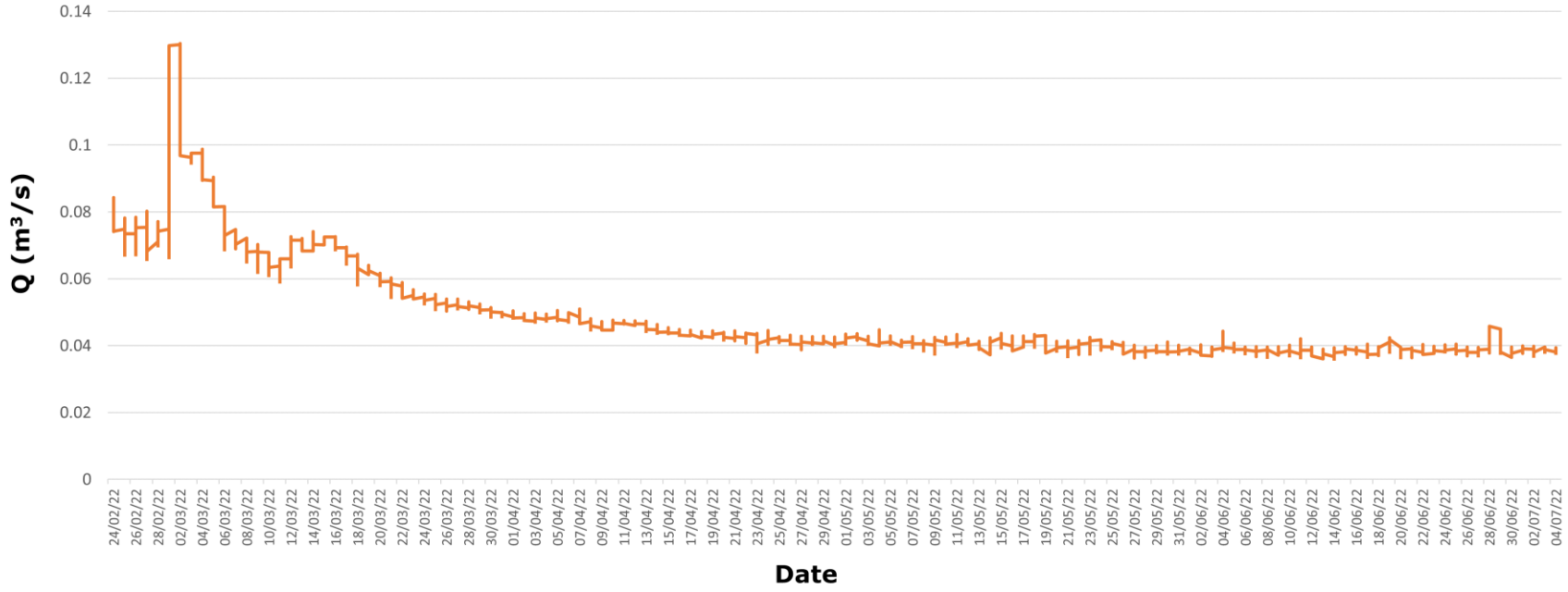

Figure D.3: *Discharge data from the Yarner Wood field site's discharge gauge, which began operation at the end of the winter period (late February 2022). Note the peak in the data matches that of the nearby River Bovey data series.*

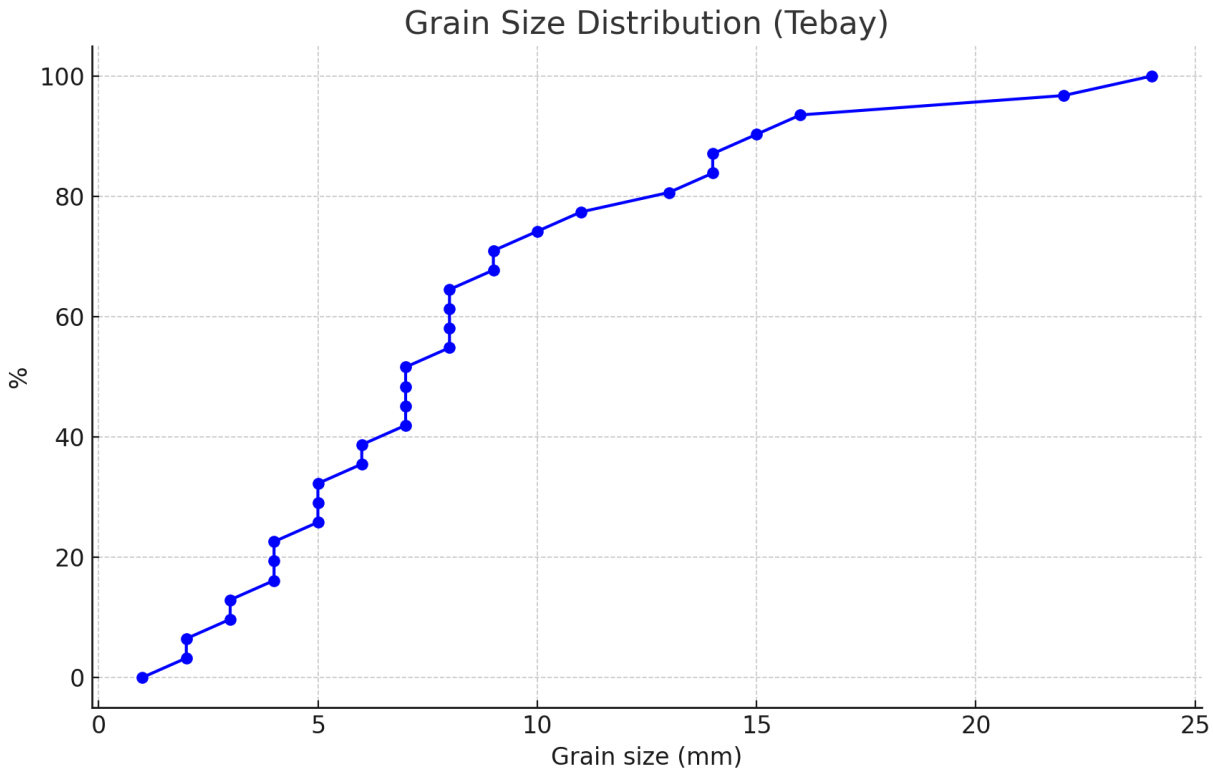

Figure D.4: *Grain size distribution of measured sediments of the surface of the Tebay catchment demonstrating the range of natural sediment sizes in the reach.*

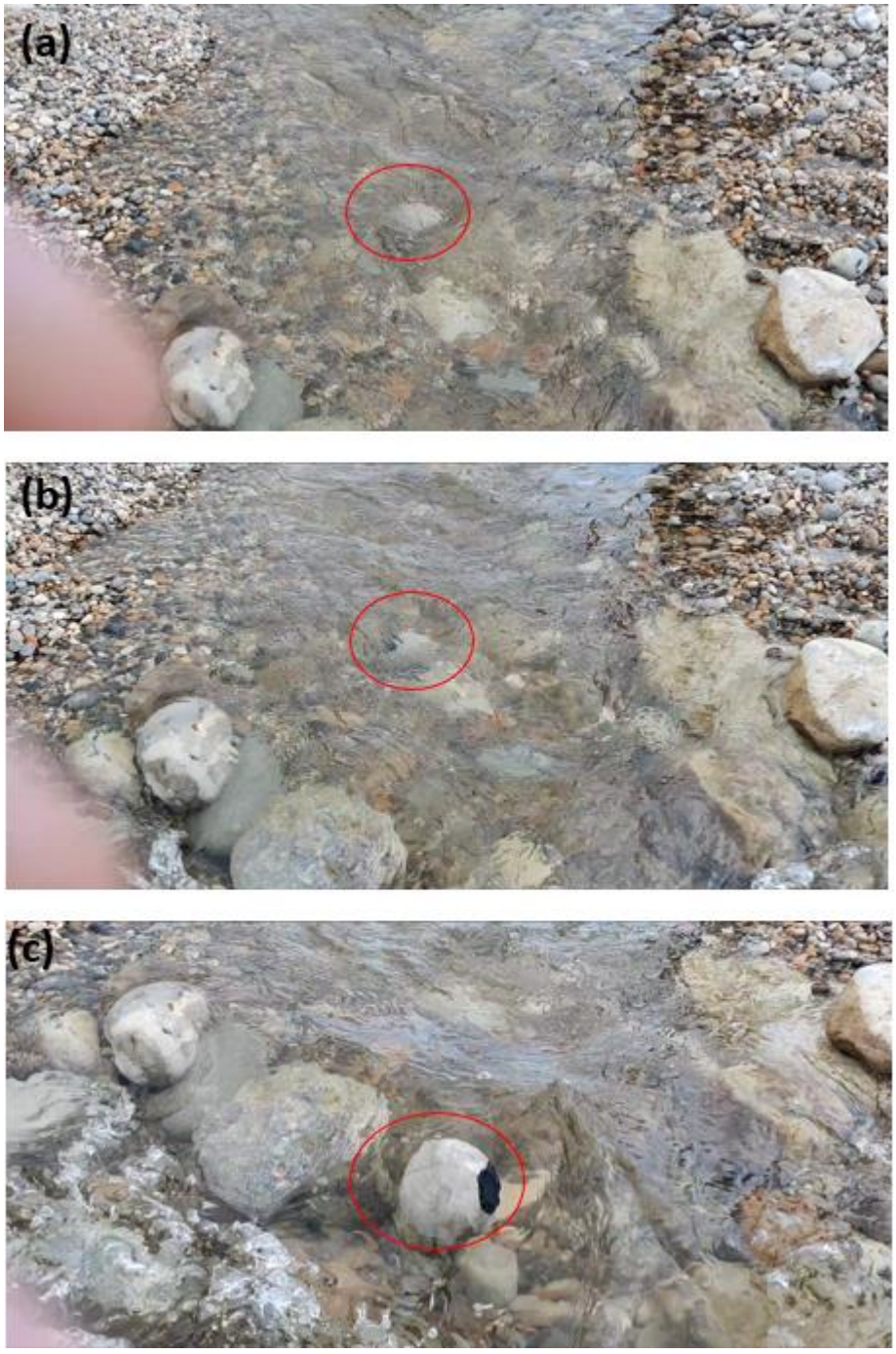

Figure D.5: *Video stills from Branscombe experiments in May. Demonstrating step and rest behaviour of the tracer sediments where: (a) captures the period of tracer movement during initial step; (b) captures the resting period of the tracer where movement ceased and; (c) captures the movement period during the following tracer movement step.*

Bibliography

Abbe, T. B., & Montgomery, D. R. (2003). Patterns and processes of wood debris accumulation in the Queets river basin, Washington. *Geomorphology*, *51*(1-3), 81-107.

Abeywardana, D. K., Hu, A. P. and Kularatna, N., (2012) IPT charged wireless sensor module for river sedimentation detection, *IEEE Sensors Applications Symposium Proceedings,* 1-5, doi: 10.1109/SAS.2012.6166324.

Acácio, M., Catry, I., Soriano-Redondo, A., Silva, J. P., Atkinson, P. W., & Franco, A. (2022). Timing is critical: consequences of asynchronous migration for the performance and destination of a long-distance migrant. Movement Ecology, 10(1), 1-16.

Adelantado, F., Vilajosana, X., Tuset-Peiro, P., Martinez, B., Melia-Segui, J., & Watteyne, T. (2017). Understanding the limits of LoRaWAN. *IEEE Communications magazine*, *55*(9), 34-40.

Akeila, E., Salcic, Z. and Swain, A. (2010) Smart pebble for monitoring riverbed sediment transport, *IEEE Sensors Journal*, 10, 1705–1717.

Allan, J. C., Hart, R., & Tranquili, J. V. (2006). The use of Passive Integrated Transponder (PIT) tags to trace cobble transport in a mixed sand-and-gravel beach on the high-energy Oregon coast, USA. *Marine Geology*, 232(1-2), 63-86.

Allen, J. (2012). *Principles of physical sedimentology*. Springer Science & Business Media.

Ancey, C. & Bohorquez, P. (2018) Stochastic streams bedload transport in mountain, *E3S Web of Conferences,* 40, 05046.

Ancey, C. (2020). Bedload transport: a walk between randomness and determinism. Part 1. The state of the art. *Journal of Hydraulic Research*, *58*(1), 1-17.

Ancey, C., Bohorquez, P., Bardou, E. (2014) Sediment Transport in Mountain Rivers, *ERCOFTAC Bulletin,* 100, 37-52.

Ancey, C., Davison, A., Bohm, T., Jodeau, M., Frey, P. (2008) Entrainment and motion of coarse particles in a shallow water stream down a steep slope, *Journal of Fluid Mechanics*, 595, 83–114.

Anthony, R. E., Aster, R. C., Ryan, S., Rathburn, S., & Baker, M. G. (2018). Measuring mountain river discharge using seismographs emplaced within the hyporheic zone. *Journal of Geophysical Research: Earth Surface*, *123*(2), 210-228.

Apitz, S., & White, S. (2003). A conceptual framework for river-basin-scale sediment management. *Journal of Soils and Sediments*, *3*(3), 132-138.

Arnaud, F., Piégay, H., Vaudor, L., Bultingaire, L. and Fantino, G., 2015. Technical specifications of low-frequency radio identification bedload tracking from field experiments: Differences in antennas, tags and operators. Geomorphology, 238, pp.37-46.

Ashworth, P.J., Ferguson, R.I. (1989) Size-selective entrainment of bed load in gravel bed streams. *Water resources Research.* 25(4), 627-634.

Augustin, A., Yi, J., Clausen, T., & Townsley, W. M. (2016). A study of LoRa: Long range & low power networks for the internet of things. *Sensors*, *16*(9), 1466.

Bark, R. H., Martin-Ortega, J., & Waylen, K. A. (2021). Stakeholders' views on natural flood management: Implications for the nature-based solutions paradigm shift?. *Environmental Science & Policy*, *115*, 91-98.

Batalla, R. J., Vericat, D., Gibbins, C. N., & Garcia, C. (2010). Incipient bed-material motion in a gravel-bed river: Field observations and measurements. *US Geol. Surv. Sci. Investig. Rep*, *5091*, 15.

Bates, D., Mächler, M., Bolker, B., & Walker, S. (2015). Fitting Linear Mixed-Effects Models Using lme4*. Journal of Statistical Software*, 67(1). doi:10.18637/jss.v067.i01

Bendix J. and Cowell, M. (2010) Fire, floods and woody debris: Interactions between biotic and geomorphic processes, *Geomorphology*, 116(3-4), 297-304.

Benelli, G., Pozzebon, A., Bertoni, D., & Sarti, G. (2012). An RFID-based toolbox for the study of under-and outside-water movement of pebbles on coarse-grained beaches. *IEEE Journal of Selected Topics in Applied Earth Observations and Remote Sensing*, *5*(5), 1474-1482.

Benelli, G., Pozzebon, A., Raguseo, G., Bertoni, D., & Sarti, G. (2009, June). An RFID based system for the underwater tracking of pebbles on artificial coarse beaches. In *2009 Third International Conference on Sensor Technologies and Applications* (pp. 294-299). IEEE.

Bennett, S. J., Ghaneeizad, S. M., Gallisdorfer, M. S., Cai, D., Atkinson, J. F., Simon, A., Langendon, E. J. (2015) Flow, turbulence, and drag associated with engineered log jams in a fixed-bed experimental channel, *Geomorphology*, 248 1, 172-184.

Best, J. L. (1988). Sediment transport and bed morphology at river channel confluences. Sedimentology, 35(3), 481-498.

Black, A., Peskett, L., MacDonald, A., Young, A., Spray, C., Ball, T., Thomas, H. and Werritty, A., (2021). Natural flood management, lag time and catchment scale: Results from an empirical nested catchment study. *Journal of Flood Risk Management*, *14*(3).

Bradley, D.N., Tucker, G.E. and Benson, D.A., (2010) Fractional dispersion in a sand bed river. *Journal of Geophysical Research: Earth Surface*, 115(F1).

Bradley, N. & Tucker, G. (2012) Measuring gravel transport and dispersion in a mountain river using passive radio tracers, *Earth Surface Processes and Landforms,* 37(10), 1034-1045.

Bradley, N. (2017) Direct Observation of Heavy-Tailed Storage Times of Bed Load Tracer Particles Causing Anomalous Superdiffusion, *Geophysical Research Letters,* 44(24), 12,227-12,235.

Bridge, J. S., & Best, J. L. (1988). Flow, sediment transport and bedform dynamics over the transition from dunes to upper-stage plane beds: implications for the formation of planar laminae. *Sedimentology*, *35*(5), 753-763.

Brookes, P. C., Wigston, D. L., & Bourne, W. F. (1980). The dependence of Quercus robur and Q. petraea seeding on cotyledon potassium, magnesium, calcium and phosphorus during the first year of growth. *Forestry: An International Journal of Forest Research*, *53*(2), 167-177.

Brousse, G., Arnaud-Fassetta, G., Liébault, F., Bertrand, M., Melun, G., Loire, R., & Borgniet, L. (2020). Channel response to sediment replenishment in a large gravel-bed river: The case of the Saint-Sauveur dam in the Buëch River (Southern Alps, France). *River Research and Applications*, *36*(6), 880-893.

Buffington, J. M., & Montgomery, D. R. (1997). A systematic analysis of eight decades of incipient motion studies, with special reference to gravel-bedded rivers. Water resources research, 33(8), 1993-2029.

Buffington, J. M., Montgomery, D. R. (1999) Effects of sediment supply on surface textures of gravel-bed rivers, *Water Resources Research,* 35, 3523 – 3530.

Bunte, K., Swingle, K.W. and Abt, S.R., (2010) Necessity and Difficulties of Field Calibrating Signals from Surrogate Techniques in Gravel-Bed Streams: Possibilities for Bedload Trap Samplers. *U.S. Geological Survey Scientific Investigations Report,* 2010-5091. Available from: http://pubs.usgs.gov/sir/2010/5091/papers/

Cain, A., & MacVicar, B. (2020). Field tests of an improved sediment tracer including non-intrusive measurement of burial depth. *Earth Surface Processes and Landforms*, *45*(14), 3488-3495.

Candia, A., Represa, S. N., Giuliani, D., Luengo, M. Á., Porta, A. A., & Marrone, L. A. (2018, November). Solutions for SmartCities: proposal of a monitoring system of air quality based on a LoRaWAN network with low-cost sensors. In *2018 Congreso Argentino de Ciencias de la Informática y Desarrollos de Investigación (CACIDI)* (pp. 1-6). IEEE.

Cassel, M., Dépret, T. and Piégay, H., 2017. Assessment of a new solution for tracking pebbles in rivers based on active RFID. Earth Surface Processes and Landforms, 42(13), pp.1938-1951.

Cassel, M., Navratil, O., Perret, F., & Piégay, H. (2021). The e-RFIDuino: An Arduino-based RFID environmental station to monitor mobile tags. *HardwareX*, 10.

Cassel, M., Piégay, H., Fantino, G., Lejot, J., Bultingaire, L., Michel, K., Perret, F. (2020) Comparison of ground-based and UAV a-UHF artificial tracer mobility monitoring methods on a braided river, *Earth Surface Processes and Landforms,* 45, 1123 – 1140.

Chappell, N. and Page, T. 2020. Measuring NFM effectiveness. *NERC NFM programme webinar series,* 3rd December 2020, Available at: www.lancaster.ac.uk/lec/sites/qnfm/

Chappell, N., Beven, K., Lamb, R., Haygarth, P., Quinton, J., Page, T., Kretzschmar, A., Hankin, B. and McShane, G., 2017, Q-NFM : Quantifying the likely magnitude of nature-based flood mitigation effects across large catchments, Retrieved from http://www.lancaster.ac.uk/lec/sites/qnfm.

Chapuis, M., Bright, C.J., Hufnagel, J. and MacVicar, B., 2014. Detection ranges and uncertainty of passive Radio Frequency Identification (RFID) transponders for sediment tracking in gravel rivers and coastal environments. *Earth Surface Processes and Landforms*, 39(15), 2109-2120.

Chapuis, M., Dufour, S., Provansal, M., Couvert, B. and de Linares, M., 2015. Coupling channel evolution monitoring and RFID tracking in a large, wandering, gravel-bed river: Insights into sediment routing on geomorphic continuity through a riffle–pool sequence. Geomorphology, 231, pp.258-269.

Clark, M. J., Bennett, G. L., Ryan-Burkett, S. E., Sear, D. A., & Franco, A. M. (2022). Untangling the controls on bedload transport in a wood-loaded river with RFID tracers and linear mixed modelling. *Earth Surface Processes and Landforms*. 47(9), 2283-2298.

Clauset, A., Shalizi, C., Newman, M.E.J. (2009) Power-law distributions in empirical data, *SIAM Review*, 51(4), 661-703.

Cooper, M. M., Patil, S. D., Nisbet, T. R., Thomas, H., Smith, A. R., & McDonald, M. A. (2021). Role of forested land for natural flood management in the UK: A review. *Wiley interdisciplinary reviews: Water*, *8*(5), e1541.

Cui, Y., Parker, G., Lisle, T. E., Gott, J., Hansler-Ball, M. E., Pizzuto, J. E., Allmendingern N. E., & Reed, J. M. (2003). Sediment pulses in mountain rivers: 1. Experiments. *Water Resources Research*, 39(9).

Dadson, S. J., Hall, J. W., Murgatroyd, A., Acreman, M., Bates, P., Beven, K., ... & Wilby, R. (2017). A restatement of the natural science evidence concerning catchment-based 'natural'flood management in the UK. *Proceedings of the Royal Society A: Mathematical, Physical and Engineering Sciences*, *473*(2199), 20160706.

Davidson, S. (2011). *Modelling channel morphodynamics associated with large wood in an intermediate-sized stream* (Doctoral dissertation, University of British Columbia).

Deane, A., Norrey, J., Coulthard, E., McKendry, D. C., & Dean, A. P. (2021). Riverine large woody debris introduced for natural flood management leads to rapid improvement in aquatic macroinvertebrate diversity. *Ecological Engineering*, *163*, 106197.

Department for Environment Food and Rural Affairs. (2021) *Flood and coastal erosion risk management. An investment plan for 2021 to 2027.* https://assets.publishing.service.gov.uk/government/uploads/system/uploads/attachment_data/file/1006447/Flood_coastal_erosion_investment_plan_2021.pdf

Dey, S. (1999) Sediment threshold, *Applied Mathematical Modelling*, 23, 399–417.

Dey, S., & Ali, S. Z. (2017). Mechanics of sediment transport: Particle scale of entrainment to continuum scale of bedload flux. *Journal of Engineering Mechanics*, *143*(11), 04017127.

Dhont, B., and Ancey, C. (2018) Are Bedload Transport Pulses in Gravel Bed Rivers Created by Bar Migration or Sediment Waves?. *Geophysical Research Letters.* 45(11). 5501-5508.

Dini, B., Bennett, G. L., Franco, A., Whitworth, M. R., Cook, K. L., Senn, A., & Reynolds, J. M. (2021). Development of smart boulders to monitor mass movements via the Internet of Things: a pilot study in Nepal. *Earth Surface Dynamics*, *9*(2), 295-315.

Diplas, P., Dancey, C. L., Celik, A. O., Valyrakis, M., Greer, K., & Akar, T. (2008). The role of impulse on the initiation of particle movement under turbulent flow conditions. Science, 322(5902), 717-720.

Dodd, J.A., Newton, M & Adams, C.E. (2016) The effect of natural flood management in-stream wood placements on fish movement in Scotland, CD2015_02. Available online crew.ac.uk/publications

Dolphin, T., Lee, J., Phillips, R., Taylor, C.J. and Dyer, K.R., 2016. Velocity of RFID tagged gravel in a non-uniform longshore transport system. Journal of Coastal Research, (75 (10075)), pp.363-367.

Dost, B., Gronz, O., Casper, M., Krein, A. (2020) The Potential of Smartstone Probes in Landslide Experiments: How to Read Motion Data. *Natural Hazards and Earth System Sciences.* 20, 3501–3519, https://doi.org/10.5194/nhess-20-3501-2020.

du Boys, P. (1879). Le Rhône et les rivières à lit affouillable – Étude du régime du Rhône et de l'action exercée par les eaux sur un lit à fond de graviers indéfiniment affouillable. *Annales des Ponts et Chaussées,* 49, 141–195.

Dunnink, J., Hartley, R., Rutina, L., Alves, J., & Franco, A. (2019) A socio-ecological landscape analysis of human–wildlife conflict in northern Botswana. *Oryx,* 1-9. doi:10.1017/S0030605318001394

East, A.E., Pess, G.R., Bountry, J.A., Magirl, C.S., Ritchie, A.C., Logan, J.B., Randle, T.J., Mastin, M.C., Minear, J.T., Duda, J.J., Liermann, M.C., McHenry, M.L., Beechie, T.J., Shafroth, P.B. (2015) Large-scale dam

removal on the Elwha River, Washington, USA: River channel and floodplain geomorphic change. *Geomorphology* 228, 765–786.

Einstein, H. A. (1950). *The bed-load function for sediment transportation in open channel flows* (No. 1026). US Department of Agriculture.

Einstein, H., (1937) Bedload transport as a probability problem, Ph.D. thesis, Mitt. Versuchsanst. Wasserbau Eidg. Tech. Hochsch, Zürich.

Faustini, J. M., & Jones, J. A. (2003). Influence of large woody debris on channel morphology and dynamics in steep, boulder-rich mountain streams, western Cascades, Oregon. *Geomorphology*, 51(1-3), 187-205.

Fenton, J. D., & Abbott, J. E. (1977). Initial movement of grains on a stream bed: The effect of relative protrusion. *Proceedings of the Royal Society of London. A. Mathematical and Physical Sciences*, *352*(1671), 523-537.

Ferguson, R. I., & Hoey, T. B. (2002). Long-term slowdown of river tracer pebbles: Generic models and implications for interpreting short-term tracer studies. Water Resources Research, 38(8), 17-1.

Ferguson, R. & Wathen, S. (1998) Tracer-pebble movement along a concave river profile: virtual velocity in relation to grain size and shear stress. *Water Resources Research,* 34, 2031–2038.

Ferguson, R., Church, M., Rennie, C., Venditti, G. (2015) Reconstructing a sediment pulse: Modeling the effect of placer mining on Fraser River, Canada*. Journal of Geophysical Research: Earth Surface*, 120, 1436–1454.

Ferguson, R.I., (2005). Estimating critical stream power for bedload transport calculations in gravel-bed rivers. Geomorphology, 70(1-2), 33-41.

Finkenzeller, K. (2010). RFID handbook: fundamentals and applications in contactless smart cards, radio frequency identification and near-field communication. John wiley & sons.

Floyd, R.E. (2015) RFID in Animal-Tracking Applications, *IEEE,* 5, 32-33.

Frank, D., Foster, D., Sou, I. M., Calantoni, J., & Chou, P. (2015). Lagrangian measurements of incipient motion in oscillatory flows. Journal of Geophysical Research: Oceans, 120(1), 244-256.

Gaeuman, D., Stewart, R., Schmandt, B., Pryor, C. (2017) Geomorphic Response to Gravel Augmentation and High-Flow Dam Release in the Trinity River*. Earth Surface Processes and Landforms.* 42(15), 2523–2540.

Gambiroža, J. Č., Mastelić, T., Šolić, P., & Čagalj, M. (2019, June). Capacity in LoRaWAN networks: challenges and opportunities. In *2019 4th International Conference on Smart and Sustainable Technologies (SpliTech)* (pp. 1-6). IEEE.

Garcia, C., Cohen, H., Reid, I., Rovira, A., Úbeda, X., & Laronne, J. B. (2007). Processes of initiation of motion leading to bedload transport in gravel-bed rivers. Geophysical research letters, 34(6).

Gilbert, G. K. and Murphy, E. C., (1914) The transportation of debris by running water, *US Government Printing Office*, Washington, D.C., USA, 86.

Gimbert, F., Fuller, B. M., Lamb, M. P., Tsai, V. C., & Johnson, J. P. (2019). Particle transport mechanics and induced seismic noise in steep flume experiments with accelerometer-embedded tracers. *Earth Surface Processes and Landforms*, *44*(1), 219-241.

Gintz, D., Hassan, M. A., & Schmidt, K. H. (1996). Frequency and magnitude of bedload transport in a mountain river. *Earth Surface Processes and Landforms*, *21*(5), 433-445.

Gippel C.J., O'Neill I.C., Finlayson B.L., Schnatz I. (1996) Hydraulic guidelines for the re-introduction and management of large woody debris in lowland rivers, *Regulated Rivers: Research & Management,* 12, 223–236.

Golly A., Turowski J.M., Badoux A., Hovius N. (2019) Testing models of step formation against observations of channel steps in a steep mountain stream, *Earth Surface Processes and Landforms,* 44, 1390-1406.

Gomez, B. (1991). Bedload transport. *Earth-Science Reviews*, 31(2), 89-132.

Gomez, B., & Church, M. (1989). An assessment of bed load sediment transport formulae for gravel bed rivers. *Water Resources Research*, *25*(6), 1161-1186.

Grabowski, R., Gurnell, A., Burgess-gamble, L., England, J., Holland, D., Klaar, M., Morrissey, I., Uttley, C., Wharton, G. (2019) The current state of the use of large wood in river restoration and management. *Water and Environment Journal.* 33(3), 366-377.

Gray, J. R., Laronne, J. B., & Marr, J. D. (2010). Bedload-surrogate monitoring technologies (p. 37). US Department of the Interior, US Geological Survey.

Green, G.N. (1992) The Digital Geologic Map of Colorado in ARC/INFO Format. Open-File Report 92-0507, U.S. Geol Sur, Denver, CO. available on-line (04/08/2020): http://pubs.usgs.gov/of/1992/ofr-92-0507/.

Greig, S. M., Sear, D. A., & Carling, P. A. (2005). The impact of fine sediment accumulation on the survival of incubating salmon progeny: implications for sediment management. *Science of the total environment*, *344*(1-3), 241-258.

Grewal, M. S., Weill, L. R., & Andrews, A. P. (2007). *Global positioning systems, inertial navigation, and integration*. John Wiley & Sons.

Gronz, O., Hiller, P. H., Wirtz, S., Becker, K., Iserloh, T., Seeger, M., ... & Ries, J. B. (2016). Smartstones: A small 9-axis sensor implanted in stones to track their movements. *Catena*, 142, 245-251.

Grottoli, E., Bertoni, D., Pozzebon, A., & Ciavola, P. (2019). Influence of particle shape on pebble transport in a mixed sand and gravel beach during low energy conditions: Implications for nourishment projects. *Ocean & Coastal Management*, *169*, 171-181.

Habersack, H. (2001) Radio-tracking gravel particles in a large braided river in New Zealand: a field test of the stochastic theory of bed load transport proposed by Einstein. *Hydrological Processes* 15, 377–391.

Harris, N., & Curry, J. (2018). Development and range testing of a LoRaWAN system in an urban environment. *International Journal of Electronics and Communication Engineering*, *12*(1).

Hart, J. K., & Martinez, K. (2015). Toward an environmental Internet of Things. *Earth and Space Science*, *2*(5), 194-200.

Hassan, M. A. and D. N. Bradley (2017). Geomorphic controls on tracer particle dispersion in gravel-bed rivers. Gravel-Bed Rivers: Process and Disasters: 159-184.

Hassan, M. A., Church, M., & Schick, A. P. (1991). Distance of movement of coarse particles in gravel bed streams. *Water Resources Research*, *27*(4), 503-511.

Hassan, M.A. & Ergenzinger, P. (2003) Use of tracers in fluvial geomorphology. In Tools in Fluvial Geomorphology, Kondolf GM, Piégay H (eds). John Wiley & Sons: Chichester, 397–423.

Hassan, M.A., Voepel, H., Schumer, R., Parker, G., Fraccarollo, L. (2013) Displacement characteristics of coarse fluvial bed sediment. Journal of Geophysical Research: Earth Surface, 118, 155-165.

Helley, E. J., & Smith, W. (1971). *Development and calibration of a pressure-difference bedload sampler*. US Department of the Interior, Geological Survey, Water Resources Division.

Hodge, R. A., Hoey, T. B., & Sklar, L. S. (2011). Bed load transport in bedrock rivers: The role of sediment cover in grain entrainment, translation, and deposition. *Journal of Geophysical Research: Earth Surface*, *116*(F4).

Hodge, R., Voepel, H., Leyland, J., Sear, D., Ahmed, S. (2020) X-ray computed tomography reveals that grain protrusion controls critical shear stress for entrainment of fluvial gravels, *Geology,* 48(2): 149–153.

Howerton, J. M., & Schenck, B. L. (2020, April). The deployment of a LoRaWAN-based IoT air quality sensor network for public good. In *2020 Systems and Information Engineering Design Symposium (SIEDS)* (pp. 1-6). IEEE.

Hsu, L., Finnegan, N. J., & Brodsky, E. E. (2011). A seismic signature of river bedload transport during storm events. *Geophysical Research Letters*, *38*(13).

Hubbell D. and Sayre W., (1964) Sand transport studies with radioactive tracers. *Journal of the Hydraulics Division*, American Society of Civil Engineers 90, 39–68.

Hubbell, D. W. (1964) Apparatus and Techniques for Measuring Bedload. U.S. Geological Survey, *Water Supply Paper,* 1748.

Hubbell, D. W., Stevens Jr, H. H., Skinner, J. V., & Beverage, J. P. (1985). New approach to calibrating bed load samplers. *Journal of Hydraulic Engineering*, 111(4), 677-694.

Ibrahim, D. M. (2019). Internet of Things technology based on LoRaWAN revolution. In *2019 10th International Conference on Information and Communication Systems (ICICS)* (pp. 234-237). IEEE.

Ikpehai, A., Adebisi, B., Rabie, K. M., Anoh, K., Ande, R. E., Hammoudeh, M., ... & Mbanaso, U. M. (2018). Low-power wide area network technologies for Internet-of-Things: A comparative review. *IEEE Internet of Things Journal*, *6*(2), 2225-2240.

Keller, E. A., & Tally, T. (1979). Effects of large organic debris on channel form and fluvial processes in the coastal redwood environment. In *Adjustments of the fluvial system* (pp. 169-197). Routledge.

Keller, E.A. (1970) Bedload movement experiments, Dry Creek, California. *Journal of Sedimentary Petrology*, 40, 1339-1344.

Kelsey, H, Lamberson R, Madej M. (1987) Stochastic model for the long-term transport of stored sediment in a river channel. *Water Resources Research.* 23. 1738–1750.

Khutsoane, O., Isong, B., & Abu-Mahfouz, A. M. (2017). IoT devices and applications based on LoRa/LoRaWAN. In *IECON 2017-43rd Annual Conference of the IEEE Industrial Electronics Society* (pp. 6107-6112). IEEE.

Kinzel, P. (2009) *Channel Morphology and Bed Sediment Characteristics Before and After Habitat Enhancement Activities in the Uridil Property, Platte River, Nebraska, Water Years 2005–2008*, USGS Open-File Report 2009–1147.

Klaar, M.J., Hill, D.F., Maddock, I., Milner, A.M. (2011) Interactions between instream wood and hydrogeomorphic development within recently deglaciated streams in Glacier Bay National Park, Alaska. *Geomorphology* 130, 208–220.

Kok, M., Hol, J. D., & Schön, T. B. (2017). Using inertial sensors for position and orientation estimation. *arXiv preprint arXiv:1704.06053*.

Komar, P. D., & Miller, M. C. (1973). The threshold of sediment movement under oscillatory water waves. *Journal of Sedimentary Research*, *43*(4).

Krein, A., Schenkluhn, R., Kurtenbach, A., Bierl, R., & Barrière, J. (2016). Listen to the sound of moving sediment in a small gravel-bed river. *International Journal of Sediment Research*, *31*(3), 271-278.

Kularatna, N., Melville, B. & Kularatna, D. (2006). Implementation aspects and offline digital signal processing of a smart pebble for river bed sediment transport monitoring. *In Proceedings of Sensors*, 2006 IEEE, EXCO, Daegu, Korea, October 22-25, 1093-1098, Washington, DC, USA: IEEE.

Lamarre, H., and A. G. Roy (2008), The role of morphology on the displacement of particles in a step–pool river system, Geomorphology, 99(1), 270–279.

Lamarre, H., MacVicar, B. and Roy, A.G., 2005. Using passive integrated transponder (PIT) tags to investigate sediment transport in gravel-bed rivers. Journal of Sedimentary Research, 75(4), pp.736-741.

Lane, P. and Sheridan, G. (2002) Impact of an unsealed forest road stream crossing: waterquality and sediment sources. *Hydrological Processes.* 16, 2599 –2612.

Langford T., Langford J., Hawkins S. (2012) Conflicting effects of woody debris on stream fish populations: implications for management. *Freshwater Biology,* 57, 1096–1111.

Laronne, J. & Carson, M. (1976) Interrelationships between bed morphology and bed-material transport for a small, gravel-bed channel. *Sedimentology*, 23, 67–85.

Lavelle, J. W., & Mofjeld, H. O. (1987). Do critical stresses for incipient motion and erosion really exist?. *Journal of Hydraulic Engineering*, *113*(3), 370-385.

Lee, H. Y., You, J. Y., & Lin, Y. T. (2002). Continuous saltating process of multiple sediment particles. *Journal of hydraulic engineering*, *128*(4), 443-450.

Legleiter, J.C. & Kyriakidis, P.C. (2006) Forward and Inverse Transformations between Cartesian and Channel-fitted Coordinate Systems for Meandering Rivers, *Mathematical Geology,* 38(8), 927-958.

Lehpamer, H. (2012). RFID Design Principles (2nd ed.). Norwood, MA: Artech House.

Liébault, F., Bellot, H., Chapuis, M., Klotz, S. and Deschâtres, M., 2012. Bedload tracing in a high-sediment-load mountain stream. Earth Surface Processes and Landforms, 37(4), pp.385-399.

Loveland, P. J., & Clayden, B. (1987). A hardpan podzol at Yarner Wood, Devon. *Journal of soil science*, *38*(2), 357-367.

Ma, Y. W., & Chen, J. L. (2018, April). Toward intelligent agriculture service platform with lora-based wireless sensor network. In *2018 IEEE International Conference on Applied System Invention (ICASI)* (pp. 204-207). IEEE.

MacKenzie, L. G., Eaton, B. C., & Church, M. (2018). Breaking from the average: Why large grains matter in gravel-bed streams. Earth Surface Processes and Landforms, 43(15), 3190-3196.

MacVicar, B.J. and Roy, A.G., 2011. Sediment mobility in a forced riffle-pool. Geomorphology, 125(3), pp.445-456.MacVicar, B. J. and

Papangelakis, E., (2022) Lost and found: Maximizing the information from a series of bedload tracer surveys. *Earth Surface Processes and Landforms*, 47(2), 399-408.

Malmon D. V. (2005) Influence of sediment storage on downstream delivery of contaminated sediment. *Water Resources Research*. 41.

Malmon, D. V., Dunne, T., & Reneau, S. (2003) Stochastic theory of particle trajectories through alluvial valley floors. *The Journal of Geology*, 111(5), 525–542.

Manchev, N. P., Angelov, K. K., Kogias, P. G., & Sadinov, S. M. (2019). Development of Multichannel LoRaWAN Gateway for Educational Applications in Low-Power Wireless Communications. In *2019 IEEE XXVIII International Scientific Conference Electronics (ET)* (pp. 1-4). IEEE.

Maniatis, G. (2016). *Eulerian-Lagrangian definition of coarse bed-load transport: theory and verification with low-cost inertial measurement units* (Doctoral dissertation, University of Glasgow).

Maniatis, G. (2021). On the use of IMU (inertial measurement unit) sensors in geomorphology. *Earth Surface Processes and Landforms*, *46*(11), 2136-2140.

Maniatis, G., Hoey, T. B., Hassan, M. A., Sventek, J., Hodge, R., Drysdale, T., & Valyrakis, M. (2017). Calculating the explicit probability of entrainment based on inertial acceleration measurements. *Journal of Hydraulic Engineering*, *143*(4), 04016097.

Maniatis, G., Hoey, T., & Sventek, J. (2013). A New Method for Rapid Prototyping of Purpose-Specific Sensor Enclosures: Example Application and Implications for Data Coherence. *Journal of Sensor and Actuator Networks*, *2*(4), 761-779.

Maniatis, G., Hoey, T., Hodge, R., Rickenmann, D., & Badoux, A. (2020). Inertial drag and lift forces for coarse grains on rough alluvial beds measured using in-grain accelerometers. *Earth Surface Dynamics*, 8(4), 1067-1099.

Martin, R. L., Jerolmack, D. J., Schumer, R. (2012) The physical basis for anomalous diffusion in bed load transport. *Journal of Geophysical Research Earth Surface*. 117.

Matheson, A., Thoms, M., & Reid, M. (2017). Does reintroducing large wood influence the hydraulic landscape of a lowland river system?. Geomorphology, 292, 128-141.

McDermott Long, O., Warren, R., Price, J., Brereton, T.M., Botham, M.S. and Franco, A.M., (2017) Sensitivity of UK butterflies to local climatic extremes: which life stages are most at risk? *Journal of Animal Ecology*, 86(1), 108-116.

McFee, J. E., Ellingson, R. O., & Das, Y. (1994). A total-field magnetometer system for location and identification of compact ferrous objects. *IEEE transactions on instrumentation and measurement*, *43*(4), 613-619.

McNamara, J. P., & Borden, C. (2004). Observations on the movement of coarse gravel using implanted motion-sensing radio transmitters. Hydrological Processes, 18(10), 1871-1884.

Megahan, W. F. (1982). Channel Sediment Storage Behind Obstructions in Forested Drainage Basins. *Sediment budgets and routing in forested drainage basins*, *141*, 114.

Mikhaylov, K., Petaejaejaervi, J., & Haenninen, T. (2016, May). Analysis of capacity and scalability of the LoRa low power wide area network technology. In *European Wireless 2016; 22th European Wireless Conference* (pp. 1-6). VDE.

Milhous, R.T., 1973. Sediment Transport in a Gravel-Bottomed Stream. PhD Thesis, Oregon State University, Corvallis, Oregon, 232 pp.

Miller, I.M., Warrick, J.A. and Morgan, C., (2011). Observations of coarse sediment movements on the mixed beach of the Elwha Delta, Washington. Marine Geology, 282(3-4), pp.201-214.

Miller, M. C., McCave, I. N., & Komar, P. (1977). Threshold of sediment motion under unidirectional currents. *Sedimentology*, *24*(4), 507-527.

Montgomery, D. R., Massong, T. M., & Hawley, S. C. (2003b). Influence of debris flows and log jams on the location of pools and alluvial channel reaches, Oregon Coast Range. *Geological Society of America Bulletin*, *115*(1), 78-88.

Montgomery, D., Collins, B., Buffington, J., Abbe, T. (2003a) Geomorphic effects of wood in rivers. *The Ecology and Management of Wood in World Rivers, Symposium.* 37, 21-47.

Mutz, M., Kalbus, E., & Meinecke, S. (2007). Effect of instream wood on vertical water flux in low-energy sand bed flume experiments. *Water Resources Research*, *43*(10).

Nelson, J. M., Shreve, R. L., McLean, S. R., & Drake, T. G. (1995). Role of near-bed turbulence structure in bed load transport and bed form mechanics. *Water resources research*, *31*(8), 2071-2086.

Nichols, M.H., 2004. A radio frequency identification system for monitoring coarse sediment particle displacement. Applied engineering in agriculture, 20(6), p.783.

Nikora, V., H. Habersack, T. Huber and I. McEwan (2002). "On bed particle diffusion in gravel bed flows under weak bed load transport." Water Resources Research 38(6): 17-11-17-19.

Niño, Y., & García, M. (1998). Using Lagrangian particle saltation observations for bedload sediment transport modelling. *Hydrological Processes*, *12*(8), 1197-1218.

Nunavath, V., Johansen, S., Johannessen, T. S., Jiao, L., Hansen, B. H., Berntsen, S., & Goodwin, M. (2021). Deep Learning for Classifying Physical Activities from Accelerometer Data. *Sensors*, *21*(16), 5564.

Olinde, L., & Johnson, J. P. (2015). Using RFID and accelerometer-embedded tracers to measure probabilities of bed load transport, step lengths, and rest times in a mountain stream. *Water Resources Research*, *51*(9), 7572-7589.

Oregon RFID, 2021, "Oregon RFID: Fish and Wildlife Tracking PIT Tags" https://www.oregonrfid.com/products/hdx-long-range-readers/mobile-reader-kit/

Packman, A. I., & Jerolmack, D. (2004). The role of physicochemical processes in controlling sediment transport and deposition in turbidity currents. *Marine Geology*, *204*(1-2), 1-9.

Pähtz, T., Clark, A. H., Valyrakis, M., & Durán, O. (2020). The physics of sediment transport initiation, cessation, and entrainment across aeolian and fluvial environments. *Reviews of Geophysics*, *58*(1), e2019RG000679.

Papangelakis, E., Muirhead, C., Schneider, A., & MacVicar, B. (2019). Synthetic radio frequency identification tracer stones with weighted inner ball for burial depth estimation. *Journal of Hydraulic Engineering*, *145*(12).

Papanicolaou, A. N., Diplas, P., Evaggelopoulos, N., and Fotopoulos, S. (2002). Stochastic incipient motion criterion for spheres under various bed packing conditions. *Journal of Hydraulic Engineering*, *128* (4), 369-380.

Parsons, A. J., Cooper, J., & Wainwright, J. (2015). What is suspended sediment?. *Earth Surface Processes and Landforms*, 40(10), 1417-1420.

Parsons, A. J., Onda, Y., Noguchi, T., Patin, J., Cooper, J., Wainwright, J., & Sakai, N. (2014). The use of RFID in soil-erosion research. *Earth Surface Processes and Landforms*, *39*(12), 1693-1696.

Petajajarvi, J., Mikhaylov, K., Roivainen, A., Hanninen, T., & Pettissalo, M. (2015, December). On the coverage of LPWANs: range evaluation and channel attenuation model for LoRa technology. In *2015 14th international conference on its telecommunications (itst)* (pp. 55-59). IEEE.

Petajajarvi, J., Mikhaylov, K., Roivainen, A., Hanninen, T., & Pettissalo, M. (2015, December). On the coverage of LPWANs: range evaluation and channel attenuation model for LoRa technology. In *2015 14th*

international conference on its telecommunications (itst) (pp. 55-59). IEEE.

Petit, F. (1987) The relationship between shear stress and the shaping of the bed of a pebble-Ioaded river (La Rulles-Ardenne). Catena 14(5), 453-468.

Petit, F., Gob, F., Houbrechts, G. and Assani, A.A., 2005. Critical specific stream power in gravel-bed rivers. Geomorphology, 69(1-4), 92-101.

Phillips, C. B., Martin, R. L., & Jerolmack, D. J. (2013). Impulse framework for unsteady flows reveals superdiffusive bed load transport. *Geophysical Research Letters*, *40*(7), 1328-1333.

Pickup, G., Higgins, R., Grant I. (1983) Modelling sediment transport as a moving wave — The transfer and deposition of mining waste. *Journal of Hydrology.* 60(1–4), 281-301.

Piégay, H., Gregory, K. J., Bondarev, V., Chin, A., Dahlstrom, N., Elosegi, A., ... & Zawiejska, J. (2005). Public perception as a barrier to introducing wood in rivers for restoration purposes. *Environmental Management*, *36*(5), 665-674.

Powell, J.A., Logan, J.A. (2005) Insect seasonality: circle map analysis of temperature- driven life cycles. *Theoretical Population Biology*, 67, 161–179.

Pretzlav, K. L., Johnson, J. P., & Bradley, D. N. (2021). Smartrock transport from seconds to seasons: Shear stress controls on gravel diffusion inferred from hop and rest scaling. *Geophysical Research Letters*, *48*(9),

Puttock, A., Graham, H. A., Carless, D., & Brazier, R. E. (2018). Sediment and nutrient storage in a beaver engineered wetland. *Earth Surface Processes and Landforms*, *43*(11), 2358-2370.

Pyrce, R. S. and P. E. Ashmore (2003). "Particle path length distributions in meandering gravel-bed streams: Results from physical models." Earth Surface Processes and Landforms 28(9): 951-966.

Raffa, K.F, Aukema, B.H, Bentz, B.J, Carroll, A.L, Hicke, J. A, Turner, M.G, Romme, W.H. (2008) Cross-scale Drivers of Natural Disturbances Prone to Anthropogenic Amplification: The Dynamics of Bark Beetle Eruptions, *BioScience,* 56(6), 501-517.

Ramson, S. J., León-Salas, W. D., Brecheisen, Z., Foster, E. J., Johnston, C. T., Schulze, D. G., ... & Málaga, M. P. (2021). A self-powered, real-time, LoRaWAN IoT-based soil health monitoring system. *IEEE Internet of Things Journal*, *8*(11), 9278-9293.

Ravindra, G. H., Gronz, O., Dost, J. B., & Sigtryggsdóttir, F. G. (2020). Description of failure mechanism in placed riprap on steep slope with unsupported toe using smartstone probes. Engineering Structures, 221, 111038.

Recking, A. (2012). *Bedload transport in rivers: from the flume to the field* (Doctoral dissertation, HDR mécanique, Université de Grenoble).

Reneau, S. L., Drakos, P. G., Katzman, D., Malmon, D. V., McDonald, E. V., & Ryti, R. T. (2004). Geomorphic controls on contaminant distribution along an ephemeral stream. *Earth Surface Processes and Landforms*, 29(10), 1209-1223.

Rickenmann, D., Turowski, J. M., Fritschi, B., Klaiber, A., & Ludwig, A. (2012). Bedload transport measurements at the Erlenbach stream with geophones and automated basket samplers. *Earth Surface Processes and Landforms*, *37*(9), 1000-1011.

Rosgen, D. L. (1994). A classification of natural rivers. Catena, 22(3), 169-199.

Roskilly, K., Bennett, G., Curtis, R., Egedusevic, M., Jones, J., Whitworth, M., Dini, B., Luo, C., Manzella, I. and Franco, A., (2022). *SENSUM project, Smart SENSing of landscapes Undergoing hazardous hydrogeomorphic Movement* (No. EGU22-10289). Copernicus Meetings.

Roth, D. L., Doane, T. H., Roering, J. J., Furbish, D. J. and Zettler-Mann, A. (2020). Particle motion on burned and vegetated hillslopes. *PNAS*. 117(41). 25335-25343.

Ryan, S., Bishop, E.L., Daniels, J.M. (2014) Influence of large wood on channel morphology and sediment storage in headwater mountain streams, Fraser Experimental Forest, Colorado, *Geomorphology*, 217, 73-88.

Sayers, P. B., Hall, J. W., & Meadowcroft, I. C. (2002). Towards risk-based flood hazard management in the UK. In *Proceedings of the Institution of Civil Engineers-Civil Engineering* 150 (5), 36-42, Thomas Telford Ltd.

Schenk, E. R., Moulin, B., Hupp C. R. Richte, J.M. (2013) Large wood budget and transport dynamics on a large river using radio telemetry, *Earth Surface Processes and Landforms.* 39 (4), 487-498.

Schmidt, K. H., & Ergenzinger, P. (1992). Bedload entrainment, travel lengths, step lengths, rest periods—studied with passive (iron, magnetic) and active (radio) tracer techniques. *Earth surface processes and landforms*, *17*(2), 147-165.

Schneider, J., Hegglin, R., Meier, S., Turowski, J. M., Nitsche, M., & Rickenmann, D. (2010). Studying sediment transport in mountain rivers by mobile and stationary RFID antennas. *River flow 2010*, 1723-1730.

Sear, D. A. (1994). River restoration and geomorphology. *Aquatic Conservation: Marine and Freshwater Ecosystems*, *4*(2), 169-177.

Sear, D. A., Damon, W., Booker, D. J., & Anderson, D. G. (2000b). A load cell based continuous recording bedload trap. *Earth Surface Processes and Landforms*, *25*(6), 659-672.

Sear, D. A., Lee, M. E., Oakey, R. J., Carling, P. A., & Collins, M. B. (2000a). Coarse sediment tracing technology in littoral and fluvial environments: a review. In *Tracers in geomorphology* (pp. 21-55).

Sear, D. A., Lee, M. W. E., Carling, P. A., Oakey, R. J., & Collins, M. B. (2003). An assessment of the accuracy of the Spatial Integration Method (SIM) for estimating coarse bed load transport in gravel-bedded streams using tracers. *Iahs Publication*, 164-171.

Sear, D.A., Thorne, C.R. and Newson, M.D. (2004) *Guidebook of applied fluvial geomorphology: Defra/Environment Agency Flood and Coastal Defence R&D Programme* (R&D Technical Report, FD1914), London. Defra Flood Management Division, 256pp.

Shields, A., (1936) Application of similarity principles and turbulence research to bed-load movement, *Hydraulic Engineering Reports*, Soil Conservation Service, Pasadena, California.

Short, C., Clarke, L., Carnelli, F., Uttley, C., & Smith, B. (2019). Capturing the multiple benefits associated with nature-based solutions: Lessons from a natural flood management project in the Cotswolds, UK. *Land degradation & development*, *30*(3), 241-252.

Slater, L. J., Singer, M. B., Kirchner, J. W. (2015) Hydrologic versus geomorphic drivers of trends in flood hazard. *Geophysical Research Letters,* 42, 370-376.

Šolc, T., A. Stefanovska, T. Hoey, and M. Mikoš (2012), Application of an instrumented tracer in an abrasion mill for rock abrasion studies, Strojniški vestnik- *Journal of Mechanical Engineering*, 58(4), 263–270.

Soriano-Redondo, A., Franco, A. M., Acácio, M., Martins, B. H., Moreira, F., & Catry, I. (2021). Flying the extra mile pays-off: Foraging on anthropogenic waste as a time and energy-saving strategy in a generalist bird. *Science of The Total Environment*, *782*, 146843.

Spazzapan, M., Petrovčič, J., and Mikoš, M., (2004) New tracer for monitoring dynamics of sediment transport in turbulent flows, *Acta Hydrotech*, 22, 135–148.

Spreitzer, G., Schalko, I., Boes, R. M., & Weitbrecht, V. (2022). Towards a non-intrusive method employing digital twin models for the assessment of complex large wood accumulations in fluvial environments. *Journal of Hydrology*, *614*, 128505.

Steeb, N., Rickenmann, D., Badoux, A., Rickli, C. and Waldner, P., 2017. Large wood recruitment processes and transported volumes in Swiss

mountain streams during the extreme flood of August 2005. *Geomorphology,* 279, 112-127.

Sullivan, K., Lisle, T. E., Dolloff, C. A., Grant, G. E., & Reid, L. M. (1987). Stream channels: the link between forests and fishes. In *Chapter Three, In: Ernest O. Salo and Terrance W. Cundy (eds.), Streamside Management: Forestry and Fishery Interactions, Proceedings of a Symposium held at University of Washington, 12-14 February 1986. Contribution no. 57, Institute of Forest Resources, Seattle, Washington. p. 39-97.*

Sutherland, D., Ball, M., Hilton, S., Lisle, T. (2002) Evolution of a landslide-induced sediment wave in the Navarro River, California. *Geological Society of America Bulletin*, 114(8), 1036–1048.

Taraldsen, G., Reinen, T. A., & Berg, T. (2011). The underwater GPS problem. In *OCEANS 2011 IEEE-Spain* (pp. 1-8). IEEE.

Thompson, D. M. (1995). The effects of large organic debris on sediment processes and stream morphology in Vermont. *Geomorphology*, *11*(3), 235-244.

Tsakiris, A. G., Papanicolaou, A. T. N., & Lauth, T. J. (2014). Signature of bedload particle transport mode in the acoustic signal of a geophone. *Journal of Hydraulic Research*, 52(2), 185-204.

Turowski, J. M., Yager, E. M., Badoux, A., Rickenmann, D., & Molnar, P. (2009). The impact of exceptional events on erosion, bedload transport and channel stability in a step-pool channel. Earth Surface Processes and Landforms, 34(12), 1661-1673.

Umazano, A., Melchor, R. (2020) Volcaniclastic sedimentation influenced by logjam breakups? An example from the Blanco River, Chile. *Journal of South American Earth Sciences.* 98.

Valyrakis, M., Diplas, P., Dancey, C. L., Greer, K., & Celik, A. O. (2010). Role of instantaneous force magnitude and duration on particle entrainment. *Journal of Geophysical Research: Earth Surface*, *115*(F2).

Walling, D. E., Russell, M. A., & Webb, B. W. (2001). Controls on the nutrient content of suspended sediment transported by British rivers. Science of the Total Environment, 266(1-3), 113-123.

Wang, S., Fu, B., Piao, S., Lü, Y., Ciais, P., Feng, X., & Wang, Y. (2016). Reduced sediment transport in the Yellow River due to anthropogenic changes. *Nature Geoscience*, *9*(1), 38-41.

Weeks, E., Swinney, H. (1998) Anomalous diffusion resulting from strongly asymmetric random walks. *Physical Review E,* 57(5), 4915–4920.

Wiberg, P. L., & Smith, J. D. (1985). A theoretical model for saltating grains in water. *Journal of Geophysical Research: Oceans*, *90*(C4), 7341-7354.

Wiberg, P. L., & Smith, J. D. (1987). Calculations of the critical shear stress for motion of uniform and heterogeneous sediments. *Water resources research*, *23*(8), 1471-1480.

Wilcock, P. R., & Crowe, J. C. (2003). Surface-based transport model for mixed-size sediment. Journal of hydraulic engineering, 129(2), 120-128.

Wohl, E., Bledsoe, B. P., Fausch, K. D., Kramer, N., Bestgen, K. R., & Gooseff, M. N. (2016). Management of large wood in streams: an overview and proposed framework for hazard evaluation. *JAWRA Journal of the American Water Resources Association*, *52*(2), 315-335.

Wohl, E., Cenderelli, D.A., Dwire, K.A., Ryan-Burkett, S.E., Young, M.K., Fausch, K.D. (2010) Large in-stream wood studies: a call for common metrics. Earth Surface Processes and Landforms. 35, 618–625.

Wohl, E., Scott, D. (2017). Wood and sediment storage and dynamics in river corridors. *Earth Surface Processes and Landforms.* 42, 5-23.

Wolman, M. G., & Miller, J. P. (1960). Magnitude and frequency of forces in geomorphic processes. *The Journal of Geology*, *68*(1), 54-74.

Woodland Trust, W. (2016). Natural flood management guidance: Woody dams, deflectors and diverters.

Xie, Y., Melville, B. W., Shamseldin, A. Y., Whittaker, C. N., & Yang, Y. (2022). Smart Sediment Particle: A novel approach to investigating fluvial bed entrainment using instrumented sensors. International Journal of Sediment Research.

Yalin, M. S., (1963) An expression for bed-load transportation, *Journal of the Hydraulics Division* 89, 221–250.

Yang C., and Sayre W., (1971) Stochastic model for sand dispersion, *Journal of the Hydraulics Division*, 97, 265–288.

Zhao, J. (2018). A review of wearable IMU (inertial-measurement-unit)-based pose estimation and drift reduction technologies. In *Journal of Physics: Conference Series* (Vol. 1087, No. 4, p. 042003). IOP Publishing.